Optimising cancer therapeutics: an *in vitro* and *in silico* approach.

He Yu
Doctor of Philosophy

Aston University
September 2023

Aston University

Optimising cancer therapeutics: an *in vitro* and *in silico* approach

He Yu

Doctor of philosophy

September 2023

Thesis summary

Cancer is a major global health challenge, causing millions of new cases and deaths each year. It's complex, influenced by genetics, environment, and lifestyle, with the tumour microenvironment playing a key role. Treatments like surgery, radiation, and chemotherapy have limitations and side effects, due to the complexity and influence of genetics, environment, and lifestyle, with the tumor microenvironment playing a key role. Moreover, addressing disparities in cancer rates among ethnic groups is crucial for equitable healthcare. There are two pharmacokinetics principles that were utilised in this project: “Top-down” and “Bottom up”.

For the “Top-down”- physiologically based pharmacokinetic modelling (PBPK) work, two tyrosine kinase inhibitors (TKIs) were investigated based on clinical studies: gefitinib and imatinib.

Gefitinib can inhibit the epidermal growth factor receptor (EGFR) to treat non-small cell lung cancer (NSCLC), and it is removed by CYP 2D6 and 3A4. The ethnic differences between Caucasian and Chinese cancer populations were assessed. To explore the impacts of CYP 2D6’s phenotypes on Chinese cancer population group, a virtual Chinese cancer population group was developed, and multiple dose regimens were conducted and compared with the Caucasian cancer population group. CYP 2D6 phenotypes' effects on gefitinib plasma concentrations in Chinese cancer population was evaluated and demonstrated that for the two most prominent CYP 2D6 phenotypes within the Chinese population, namely EM and IM, a dose increase to 500 mg once daily would better target a suggested target trough concentration.

Imatinib can inhibit BCR-ABL activity to treat gastrointestinal stromal tumours (GIST) and chronic myeloid leukaemia (CML). The normal trough plasma concentrations for imatinib in cancer patients is 750-1500 ng/mL. Due to the CYP 2D6 polymorphism, to receive better clinical outcomes within Chinese cancer patients, therapeutic drug monitoring (TDM) strategy was utilised to adjust imatinib trough plasma concentrations to observe the application results post adjustment, through implementation of the developed virtual Chinese cancer population. The commonly used dosing regimen for imatinib is 400–600 mg daily, for advanced disease, it can be used as 600-800 mg daily. Unlike Caucasian patients, Chinese patients are recommended with lower doses (600 mg/day) in clinical treatment to achieve effective plasma concentrations.

For the “Bottom up”- the research focused on improving brain cancer treatment at the cellular level, exploring the inhibition effects of flavonoids on human brain tumour cells. The blood brain barrier (BBB) has been seen as the main obstacle for the treatment of brain cancers, because of its ability to prevent the entry and accumulation of the chemotherapeutic drugs.

Firstly, the cytotoxic properties of selected flavonoids as natural compounds were evaluated by the 3-(4,5-dimethylthiazol-2-yl)-2,5-diphenyl-2H-tetrazolium bromide (MTT) assay. Secondly, the modulating ability of selected flavonoids were tested by the H33343 and mitoxantrone intracellular accumulation assay, and the inhibition effects on the invasion and migration LN 229 cells were assessed by cellular migration assay. Through accumulation assay, 7-aminoflavone, 5-methoxyflavone showed better inhibition effects than KO143; harmine, trihydroxyethylrutin and rotenone indicated similar inhibition effects with KO143. Based on the migration assay, the impacts of these flavonoids on reactive oxygen species (ROS) level and the activation of caspases in LN 229 cells were evaluated to observe the ability associated with apoptosis. The migration increase level of harmine, and rotenone is below 10%, and the migration increase level of 7-methoxyflavanone is over 20%. Furthermore, 100 μM rotenone and 100 μM harmine are detected as the largest detection through ROS assay. Harmine and rotenone are considered as the promising compounds among the selected eight flavonoids, they had demonstrated their potential in their inhibition effects on LN229 cells, ability to regulate BCRP efflux function, induce ROS level increasing and the apoptosis.

Keywords: CNS system; BBB; BCRP; Flavonoids; Gefitinib; Imatinib; PBPK; CYP 2D6 polymorphism; TKI.

Acknowledgements

This thesis is the culmination of a long and arduous journey-one that I have only been able to make because of the dedicated support I have received from so many people along the way. Without you, I could not make it happen.

My deepest and sincerest gratitude goes to my supervisor, Dr. Raj Badhan, he is the best supervisor in this world, and I am blessed by the universe to have him as my supervisor. It is a great honour and privilege that I was given the opportunity to work under his supervision. I would like to thank him for his support, patience, humble, empathy, and great sense of humour. I not only benefited from his broad knowledge, but also his character. Dr Badhan inspires me to have the confidence to continue the research even after the PhD, the motivation for me is to become a researcher like him in the future.

I would like to express my sincerest gratitude to Aston University for giving me the scholarship and the PGR student support fund during the pandemic, sponsoring my postgraduate studies, and supporting me financially during covid- the hardest time for my family.

Sincerest gratitude and deepest thanks to my referees: Dr. Yongping Han, thank you for your encouragement and support throughout these years since I was pursuing my bachelor's degree, I greatly appreciate it and I wish I can make you proud in the future. Dr. William Fraser, thank you for your support and patience, I greatly appreciate it.

Deepest thanks to all the lab technicians, especially Rachel and Daniel, for their patience, technical help, and support. Deepest thanks to all the academics and associated staff: Dr. Afzal-Ur-Rahman Mohammed, my associate supervisor: Dr. Ali Al-Khattawi, Dr. Affiong Iyire, Dr. Daniel Kirby, Dr. Craig Russell, Emma Smith, Noshin Haque, Gillian Cook, Catherine Jarrett.

I am also thankful to all my colleagues and friends at the Aston pharmacy school. Abdul Ershad, Abdulkhaliq, Aminah, Alfredo Shital, Anas, Annsar, Anthony, Anwar, Carlo, Dania, Dilawar, Kyprianos, Manveer, Ola, Rhys, Rodrick, Ruba, Thu, Tu, Shoag, Zakia. Thank you all for your encouragement, friendship, and support during these years.

Deepest thanks to my friends: Dr. Zhongyuan Sun and Dr. Jian Zhou. Thank you for your friendship and support during the hardest time of my family, I really appreciate it.

I am extremely grateful to my parents: my mother Xiaojing Zhu, thank you for your unlimited love and support since I was born; and my father: Lei Yu, thank you for being a good father and always being there for me. My greatest thanks for their love, care and patience during my education and life journey.

Deepest love and gratitude for all my family, and my greatest gratitude and love go to my grandfather, Hailong Yu, thank you for being a great grandpa and supported my dream even during uncertainties.

My sincerest apology that I cannot mention each of you individually, but please know that your contributions have been truly appreciated.

List of Publications

List of published peer reviewed articles

Yu, H. & Badhan, R. K. S. 2021. The Pharmacokinetics of Gefitinib in a Chinese Cancer Population Group: A Virtual Clinical Trials Population Study. Journal of Pharmaceutical Sciences, 110, 3507-3519.

Yu, H. & Badhan, R. K. S. 2023. The Application of Virtual Therapeutic Drug Monitoring to Assess the Pharmacokinetics of Imatinib in a Chinese Cancer Population Group. Journal of Pharmaceutical Sciences, 112, 599-609.

List of contents

List of abbreviations

AA	Amino acid transporters
AAFE	Absolute average fold error
AAG	Alpha-1 acid glycoprotein
ABC transporter	ATP-binding cassette transporter
AChE	Acetylcholinesterase
AD	Alzheimer's disease
ADC	Antibody-drug conjugate
ADME	Absorption, distribution, metabolism, and excretion
AFE	Average fold error
AIF	Apoptosis-inducing factor
AJs	Adheren junctions
Apaf-1	Apoptotic protease activating factor-1
AUC	Area Under the Curve
AUC0-24	Area under the curve for a 24-hour period on the specific dosing period
AUC0-∞	Area under the curve from 0 to infinity
AUCinf	Area under the curve to infinity
BAB	The brain arachnoid barrier
BBB	Blood brain barrier
BBTB	Blood-brain tumour barrier
BCECs	Brain capillary endothelial cells
BCRP	Breast cancer resistance protein
BCSFB	Blood-cerebrospinal fluid barrier
BMI	Body mass index

BSA	Body surface area
CCyR	Cytogenetic response
Cinf	Concentration at the end of the infusion
CL	Clearance
C_{max}	Peak plasma concentrations
C_{min}	Trough plasma concentration
CML	Chronic myeloid leukaemia
CML-CP	In chronic phase is a daily dosage of 400 mg imatinib
CMT	Carrier-mediated transport
CNS	Central nervous system
COX	Cyclooxygenase
CSF	Cerebrospinal fluid
CYP450	Cytochrome P450
CyR	Cytogenetic response
Cyt c	Cytochrome c
DCF	2' 7' dicholoroflouresciene
DCF-DA	2',7'-dichlorofluorescin diacetate
DDIs	Drug-drug interactions
DFMO	Difluoromethyl ornitine
DMEM	Dulbecco's modified Eagle's medium
ECs	Endothelial cells
EGF	Epidermal growth factor
EGFR	Epidermal growth factor receptor
EM	Extensive metabolisers

EMA	European Medicines Agency
Endo G	Endonuclease G
ErbB	Erythroblastosis oncogene B
EUTOS	The European CML Treatment and Outcome Study
FaSSIF	Fasting simulated small intestinal fluid
FBS	Fetal Bovine Serum
FcRn	Neonatal Fc receptor
FDA	Food and Drug Administration
FeSSIF	Fed simulated small intestinal fluid
fm_{2D6}	Fraction of drug metabolised by CYP 2D6
fm_{3A4}	Fraction of drug metabolised by CYP 3A4
fMRI	Functional MRI
FTC	Fumitremorgin C
Fu	The free fraction or the fraction unbound
fu_{plasma}	Plasma protein binding
FUS	Focused ultrasound
GBM	Glioblastoma
GBM	Glioblastoma multiforme
GFR	Glomerular filtration rate
GI	Gastrointestinal tract
GIST	Gastrointestinal stromal tumours
GLUT	Glucose transporter
H33342	Hoescht-33342
HBA	Hydrogen bond acceptor groups
HBD	Hydrogen bond donor groups

HER	Human epidermal growth factor receptor
HIF	Human intestinal fluid
HSCs	Hematopoietic stem cells
IC	Inhibitory concentration
IC_{90}	The concentration of a drug needed to inhibit by 90%
IM	Intermediate metabolisers
ISF	Interstitial fluid
Itra	Itraconazole
IV	Intravenous
JAMs	Junctional adhesion molecules
JNK	C-Jun N-terminal kinase
LDLR	Low-density lipoprotein receptor
MCT	Monocarboxylate lactate transporter
MDR	Multiple drug resistance
MEUS	Microbubble-enhanced ultrasound
MHLW	Japan's Ministry of Health Labour and Welfare
MHRA	Medicines and Healthcare Products Regulatory Agency
MR	Molecular response
MRP	Multidrug resistance protein
MTX	Methotrexate
MX	Mitoxantrone
NBDs	Nucleotide-binding domains
NCCN	National Comprehensive Cancer Network
NOS	Not otherwise specified

NSCLC	Non-small cell lung cancer
OMM	The outer mitochondrial membrane
OS	Overall survival
PBPD models	Physiology-based pharmacodynamic models
PBPK	Physiologically based pharmacokinetics
PBS	Phosphate buffered saline solution
PFS	Progression-free survival
P-gp	P-glycoprotein
Ph chromosome	Philadelphia chromosome
PIR	Polymorph interaction ratio
PK/PD	Pharmacokinetic/pharmacodynamic
pKa	Acid dissociation constant
PM	Poor metabolisers
PR	Polymorph ratios
QSP	Quantitative systems pharmacology
RMT	Receptor-mediated transcytosis
RTK	Receptor tyrosine kinases
SD	Standard deviation
SDratio	Standard deviation ratio
SGF	Simulated gastric fluid
SGLTs	Sodium-coupled glucose transporters
SLC	Solute carrier superfamily
SMIs	Small molecule inhibitors
smTKIs	Small molecule tyrosine kinase inhibitors

SNPs	Single Nucleotide Polymorphisms
t1/2	Elimination half-life
TDM	Therapeutic drug monitoring
T-DM1	Ado-trastuzumab emtansine
TfR	Transferrin receptor
TJs	Tight junctions
TKIs	Tyrosine kinase inhibitors
TM	Transmembrane
T_{max}	Time to maximum plasma concentration
TMS	Transcranial magnetic stimulation
UM	Ultrarapid metaboliser
Vd	Volume of distribution
Ve-cadherin	Vascular endothelium cadherin
VPC	Visual predictive checking strategy
ZO-1	Zonula occludens protein 1

List of Figures

List of Supplementary Figures

List of Tables

List of Supplementary Tables

Chapter 1 Introduction

1.1 Cancers

As a major health-threatening disease worldwide and the largest public burden affecting people's quality of life, the Global Cancer Observatory has been collecting and monitoring statistics on cancer for thirty years [1]. Recent research indicates that cancer has caused over 19.3 million new incidences and 10 million deaths by 2020 worldwide [2, 3].

Cancer is a multifaceted and diverse illness characterised by uncontrolled cell growth and proliferation, which results in the development of malignant tumours [4]. Many factors, including genetic, environmental, and lifestyle factors, contribute to the development of cancer [5]. Cancer is produced by mutations or abnormalities in the genetic material of cells at the molecular level [6]. These mutations can occur naturally or be caused by external causes such as: radiation, chemicals, or viruses [6]. Moreover, cancer-causing mutations may be passed from parents [7]. Accumulating mutations in critical genes can result in the activation of oncogenes, which accelerate cell growth and division, and the inactivation of tumour suppressor genes, which typically regulate cell development and prevent the formation of tumours. This imbalance in cell growth and division regulation results in uncontrolled cell development and the formation of a tumour [7].

In addition, the tumour's microenvironment has a significant impact on the genesis and progression of cancer. Its microenvironment is made up of neighbouring cells, blood vessels, and extracellular matrix [8]. Cancer cells can recruit and manipulate these cells and chemicals to enhance their growth and survival, avoid the immune system, and promote angiogenesis, the development of new blood vessels that nourish and oxygenate the tumour [9]. In addition to genetic and microenvironmental variables, lifestyle factors including food, physical exercise, and smoking may contribute to the development of cancer [10]. These variables can cause DNA damage and raise the chance of mutations within the microenvironment of a tumour, as well as disrupt the equilibrium of immune cells and cytokines [11].

Cancer is commonly treated with a range of options including surgery, radiation therapy, and chemotherapy, all of which target different cancer cell components and the tumour's microenvironment [12]. These treatments can be useful in shrinking or eradicating tumours, but they can also cause severe side effects and are typically not curative [13].

Interestingly, there exist disparities in the incidence of cancer between ethnic groups and utilising these disparities rationally can contribute to the promotion of equitable public health management [14]. Clinic visits and treatment regimens are often modified according to ethnicity in order to minimise variations in diagnostic paths between ethnic groups [15]. The systematic treatment procedure aims to help all disease-affected groups, and those with a

greater incidence of cancer receive more screenings; therefore, theoretically, the treatment effect should be enhanced [16].

1.1.1 Type of tumours

Tumours can be loosely described as a collection of abnormal cells growing in an uncontrolled way and do not have apoptosis as normal cells in the human body [17]. Tumours can almost start from anywhere in the human body, and can be categorised into benign tumours, malignant tumours and premalignant conditions [18].

Benign tumours can be defined as non-cancerous tumours, and it is different from malignant tumours in a number of respects [19, 20]: Benign tumours usually grow slowly, and do not invade other tissues or organs, they may be easily removed from the human body after surgery, and once they are removed, they may not relapse [21]. Furthermore, they normally have a smooth covering, and the cells in the benign tumours are quite similar to normal cells [22]. Therefore, benign tumours will only be noticed when they grow large, cause pain [23] constrict tissues or organs such as brain tumours, or have the secretion of chemicals to affect the human body [24].

On the contrary, malignant tumours grow much faster than benign tumours [25], they invade and spread into nearby cells or tissues or organs to induce the formation of blood vessels to support its growth, they may relapse after the surgery, but the surface of the covering is usually composed of normal cells [26]. Furthermore, the site in the human body where the tumours start from the beginning is called primary tumours [27], if the tumours spread into other parts of the body, the new collection of tumours is called secondary tumours [28], which is also called metastases, and the original tumours is named as metastatic cancer [27].

Moreover, regardless of benign and malignant tumours, there are premalignant conditions which are also related to tumours. Premalignant cells can be considered as the prophase of cancer cells [29], and they have the potential to divide and differentiate into mature cancer cells. During the period of time which premalignant transform into cancer cells, there are varying degrees of changes in premalignant cells happening, and these changes can usually be classified as hyperplasia, atypia, metaplasia, dysplasia and carcinoma *in situ* [30]. Hyperplasia indicates that there are some abnormal cells which have the same appearance of normal cells, but their speed of dividing and growth is much faster than regular normal cells, and small amounts of hyperplasia cells are premalignant [31].

Furthermore, atypia shows that the morphology of this type of cell can be observed to be different from normal cells, some of atypia cells are premalignant, and sometimes healing and inflammation may cause the atypia [32]. Additionally, metaplasia [33], can be recognised as a handful of cells with normal appearance appearing where they should not in most instances, and there are only small numbers of metaplasia cells are premalignant. Moreover, dysplasia can be regarded as premalignant conditions, and most of this type of cell are abnormal, and some of them may be observed as normal cells [34]. Additionally, this type of cell grows faster than normal cells.

In addition, carcinoma *in situ* can be thought as the severest condition during the period of premalignancy [35]. This type of cell is clearly abnormal and have great potential to turn into mature cancer cells [36], but in this stage, they cannot spread into other tissues or organs [37]. Once the body of the patients are in the premalignant conditions, their body should be monitored regularly to avoid aggravating the conditions [38]. Besides, unlike cancer cells, premalignant cells may disappear without treatment.

1.1.2 Brain cancers

As a global burden of disease, brain cancers are present with a low survival rate and high impact on patients' lives [39], and is ranked in the top-10 leading causes of mortality [39]. The incidence of brain and other CNS cancers has been increasing over the past few decades worldwide. Each year, over 5,000 new cases of primary brain tumours are diagnosed in the United Kingdom [40]. Population-based studies in the United Kingdom have revealed ethnic disparities in the incidence rates of the majority of malignancies, with non-Caucasian populations typically at a lower risk than Caucasian populations [40].

Brain tumours refer to a group of abnormal cells that continually divide and multiply in the brain, with the ability to infect neighbouring brain cells and tissues and expand [41]. Brain tumours fall into two categories: benign and malignant [41]. According to the characteristics of malignant tumours (specifically, brain cancer), malignant brain tumours have a greater propensity to infect neighbouring cells and tissues than benign brain tumours [42]. In the meantime, the proliferation rate of malignant brain tumours will be noticeably faster than that of benign brain tumours [43]. In addition, brain cancer is typically caused by the progression of astrocytoma or oligodendroglioma, whereas the most common benign brain tumours are meningiomas or astrocytomas [41].

The main challenge of brain cancer is the blood- brain barrier (BBB), this is a substantial obstacle in the brain, which functions as a useful boundary between blood and brain to protect

the brain from neurotoxins [44]. This obstacle is seen as the main challenge for chemotherapy for brain cancer, it prevents the entry of many macromolecules and over 98% of small molecules from entering the brain including normal paracellular and diffusion routes [45]. Also, within the BBB, there are many ABC efflux transporters actively efflux exogenous substances. Furthermore, the main transport pathway of the BBB is the passive transport because the brain needs many essential water-soluble nutrients and metabolites to support itself [44].

Alternately, based on the original site of tumours, brain tumours can be classified as either primary or secondary [46]. Secondary brain tumours refer to cancer cells that grow and proliferate from tumours in other regions of the body (the main location is not the brain) and spread through blood or tissue [47], and continue to divide and proliferate in the brain and form a new collection of tumours in the human body [41].

In addition, the World Health Organization (WHO) revised the classification of brain tumours five times between 1979 and 2016 based on four characteristics: mitosis, necrosis, nuclear atypicality, and microvascular hyperplasia [48]. Brain tumours are graded from minimal (I) to severe (IV) [49, 50]. When the grade is lower, so is the severity and destructiveness. Grade I brain tumour cells closely resemble normal cells morphologically and develop slowly [51].

In Grade II, modest morphological abnormalities can be identified in the brain tumour cells, and these cells may be able to penetrate neighbouring tissues or cells. Brain tumour cells are abnormally seen in Grade III, and they can infect adjacent brain tissue and cells. In Grade IV, brain tumour cells grow rapidly and are fully morphologically aberrant in comparison to normal cells [52]; glioblastoma (GBM) normally refers to Grade IV brain tumour.

Glioblastoma is arguably the most prevalent form of brain cancer [53]. Hence, the treatment of glioblastoma can be served as the standard treatment for brain cancer [54].

Primary brain cancers arise in the meninges, neuroepithelial tissue, pituitary gland and associated structures, cranial nerves, germ cells, and haematological organs [55, 56]. Histopathological criteria and immunohistochemistry data were utilised for classification [57]. Headaches and seizures are the most typical symptoms of these brain tumours [58]. Brain imaging and histology are essential for diagnosing a suspected brain tumour [59]. Gadolinium-enhanced magnetic resonance imaging (MRI) was the preferred imaging technique [60]. Imaging, like MRI [61], did not reveal any pathologic characteristics that could identify primary brain tumours from metastatic or non-neoplastic illness [62]. Due to its low sensitivity in discriminating cancers from benign or inflammatory lesions, fluorodeoxyglucose positron emission tomography is not advised for the detection of primary lesions [63]. A multidisciplinary team customizes treatment recommendations depending on tumour kind and location,

possibility of malignancy, patient age, and medical condition [64]. Typically, surgery, radiation therapy, and chemotherapy are utilised in the treatment of cancer.

1.1.3 *In vitro* models for glioblastomas

There are four commonly utilised cell lines for GBM research: LN229, SNB19, U87, and U251 [65]. In 1979, a patient with right frontal parieto-occipital glioblastoma provided the LN229 cell line, which is cultivated in a medium containing 90% Dulbecco's modified Eagle's medium (DMEM) and 10% fetal bovine serum (FBS) at 37°C [66].

The SNB19 cell line was derived from the left parieto-occipital glioblastoma of a 47-year-old man in 1980, and the suggested media is identical to that of the LN229 cell line. In addition, U87 cell line was derived from a female patient with pleomorphic glioma, while U251 cell line was derived from a male patient aged 75 years with pleomorphic glioma [67]. There four cell lines are all originated from neuroepithelial cells [68], thus, they are utilised to develop a useful model system to study the biology of brain tumours and test potential cancer therapies [69]. In addition, the BBB might be viewed as the key to overcoming GBM and other CNS illnesses; hence, the development of BBB models is essential for future research.

1.2 The Central nervous system

The central nervous system (CNS) is a complex network of the brain and spinal cord responsible for receiving, processing, and transmitting information throughout the body [70]. The CNS is crucial for the proper functioning of the body, and any damage to this system can lead to severe consequences, including brain cancer [71]. The CNS is vital for behaviour control and regulating physiological processes. It receives data from sensory receptors, primarily via the spinal cord [72].

The central nervous system governs the body at its core. It is comprised of the brain and spinal cord and is responsible for interpreting sensory data, regulating movement, and coordinating the body's numerous tissues [72]. Neurons in the central nervous system must convey information via electrical and chemical signals, and the accurate transmission of nerve signals requires a stable central nervous system microenvironment [73]. Hence, the blood-brain barrier, the blood-cerebrospinal fluid barrier, and the barrier surrounding the CNS supplied by the avascular arachnoid epithelium are the three primary locations of the CNS barrier [74].

Composed of neurovascular units, junctional complexes, and tight junctions, the blood-brain barrier is widespread in mammals with a healthy central nervous system and serves as a barrier to preserve proper central nervous system function [75]. The neurovascular unit is predominantly made of endothelial cells that create capillaries [76]. The capillaries generated by these endothelial cells have a total surface area of approximately 150-200$cm^2.g^{-1}$ of tissue, constituting the biggest blood-brain interface in the body [77]. In addition to endothelial cells, the neurovascular unit contains astrocytes, pericytes, neurons, and extracellular matrix [75]. Occludins are present in complexes involving ligation. Connecting adhesion molecules to Membrane-associated guanylate kinase-like proteins is Important [78]. Calcium, phosphorylation, and G protein are necessary for the regulation of Tight junction function [79].

1.3 The Blood Brain Barrier

1.3.1 History

In 1878, Paul Ehrlich [80] began injecting coloured dyes into the bodies of animals, excluding the brain [81]. In 1885, he found out all the organs and tissues could be coloured by injected dyes excluding the brain and cerebrospinal fluid (CSF) [80]. Prior research had not addressed why the brain and CSF were not stained, and the initial conclusion was that the CNS may have a low affinity for important dyes [80]. In 1900, Lewandowsky [80] found out when cholic acids or sodium ferrocyanide was given intravenously, neurological symptoms would arise, but CNS would not have connected effects.

Hence, the concept of “blood brain barrier” (BBB) was brought forward by Lewandowsky in 1900, however it could not explain the mechanism of the “barrier”. The anomaly that brain could not be stained was explained by Tschirgi [82], Tschirgi found out some injected dyes could mix with plasma proteins, particularly with albumin [83]. Goldmann [84] utilised Trypan blue to stain animals and found out the brain and CSF still could not be stained while the choroid plexuses were stained. Hence, the affinity between CNS and various colours was not the fundamental basis of the event.

Later the hypothesis of CSF was brought forward by Goldmann in 1913, CSF may transfer chemicals to the brain through the choroid plexuses [85]. In 1921, Stem and Gautier [86] first concluded the concept of the BBB, as follows: There is a barrier between the blood and the brain, substances can be excluded from the brain due to the barrier, and substances must reach the brain tissue in order to gain access to the CSF in order to enter the brain; if they do not appear in the CSF, they cannot enter the brain. If the chemicals cannot penetrate the “barrier”, CSF may transfer them into the brain.

1.3.2 The structure of the BBB

The BBB can be viewed as the systemic microvasculature of the CNS, which is capable of regulating the level of small molecules transferred between the blood and the CNS, hence aiding in the maintenance of CNS homeostasis [71]. The disruption of the BBB can disrupt the brain's homeostasis and prevent immune cells and tiny chemicals from entering the brain, leading to neurodegenerative disorders and other neurological diseases such as stroke [87]. Endothelial cells (ECs) and tight junctions (TJs) based on the capillary wall, pericytes, astrocytes, the basement membrane, and immune cells make up the walls of cerebral capillaries [88] (Figure 1.1). Adult BBB surface area is between 12-18m^2 [89], and accessible brain cells in these capillaries are smaller than 25μm [74].

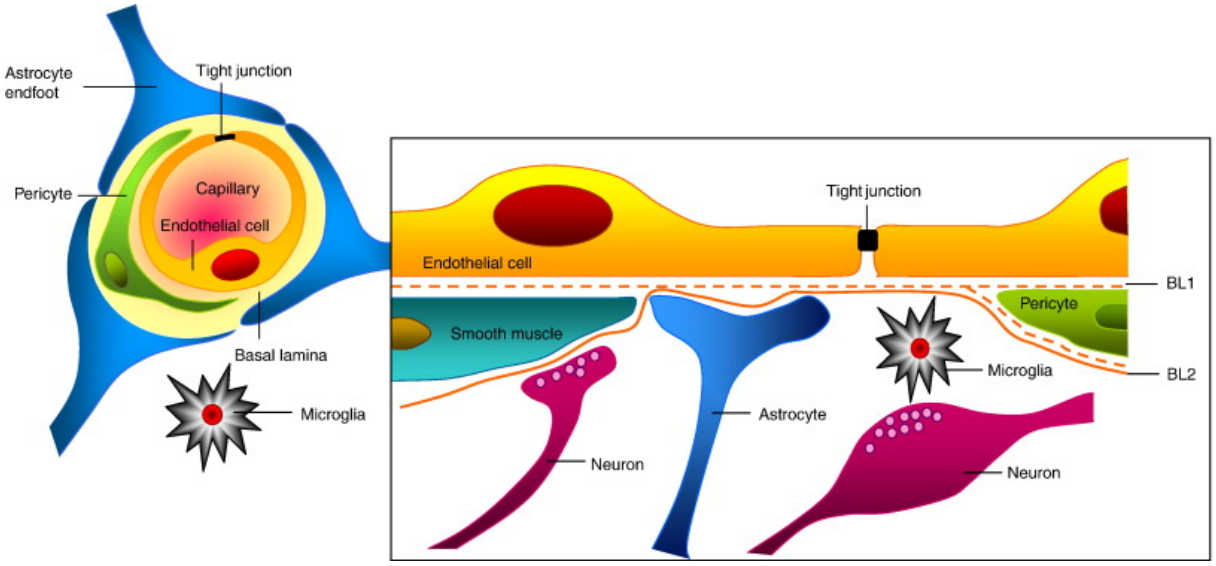

Figure 1.1 The physiology of the blood brain barrier (BBB).

Obtained from [44].

Tight junctions are formed between the edge of endothelial cells; Vasoactive neurotransmitters and peptides are found in the axonal projections of neurons onto arteriolar smooth muscle, which control regional cerebral blood flow; Along the length of the cerebral capillaries, pericytes are randomly distributed and partially surround the endothelium. The cerebral endothelial cells and pericytes are both encompassed by and play a role in the nearby basement membrane, which constitutes a unique perivascular extracellular matrix known as basal lamina 1 (BL1). This matrix differs in composition from the extracellular matrix found in the glial endfeet surrounding the brain parenchyma (BL2). A thick layer of foot processes from astrocytes surrounds the capillaries, and this tight cell association is crucial for producing and maintaining the barrier qualities.

Brain capillary endothelial cells (BCECs) are flat, squamous epithelial cells that form the walls of blood arteries [90]. The role of ECs is to inhibit the free flow of interstitial fluid (ISF) between the brain and blood [91]. In addition, TJs are generated between ECs, and pericytes are

dispersed along brain capillaries, with a portion surrounding ECs (Figure 1.1) [92]. Further, the ECs and pericytes are surrounded by the basement membrane and this matrix is generally named perivascular extracellular matrix (basal lamina 1, BL1) [78]. Unlike BL1, BL2 is composed of the extracellular matrix of glial endfeet and brain parenchyma [93].

The endfeet of astrocytes can stimulate the construction of a network to maintain the barrier, and microglia are the immune cells which are situated in the brain [94]. Additionally, TJs are located on the apical plasma membrane, and they are constituted of three key transmembrane proteins- claudins, occludin and junctional adhesion molecules (JAMs) (Figure 1.2) [95]. The C-terminal region of occludins can be employed to bind with zonula occludens protein 1 (ZO-1), ZO-2 and ZO-3 (Figure 1.2) in endothelial cells [96], while JAMs are from immunoglobulin superfamily [97].

Adheren junctions (AJs) can maintain the TJs and junctional complex, and the main composition of AJs is vascular endothelium cadherin (Ve-cadherin), which can drive the growth and production of adhesive complexes between the neighbouring cells [97].

Regarding the function of the BBB, it is able to exclude external substances (toxins and waste), maintain ion homeostasis and a low level of protein to ensure brain communication and connectivity, and have minimum immune cell damage to continue immune response and surveillance [98].

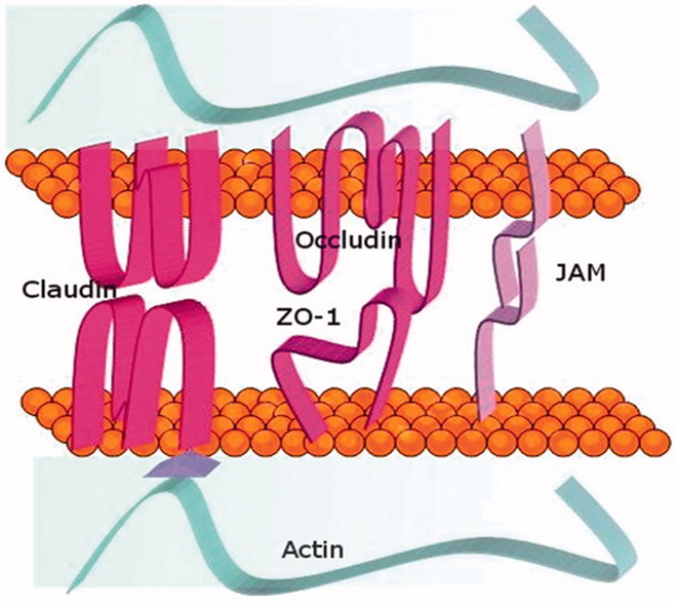

Figure 1.2 The structure of the tight junctions (TJs).

Obtained from [99].

They are proteins consisting of tight junctions, which contain intracellular domains that attach to the cytoskeleton and extracellular domains that mediate physical interactions.

1.3.3 Molecular transport pathways at the BBB

The ECs, astrocytes, pericytes, and microglia are interconnected with TJs and AJs to form a functional barrier within the BBB. The BBB transport pathways can be classified as either transcellular or paracellular [87]. Lipophilic agents can be delivered through transcellular channels, and hydrophilic compounds can cross by paracellular pathways [100]. Transmembrane diffusion, carrier-mediated transport (influx and efflux), transcytosis, and nasal administration are the four major routes for drug transport via the BBB [100]. Many chemical substances with low molecular weight and lipid solubility can be transferred by transmembrane diffusion, and high lipid solubility may result in increased BBB permeability [100]. Typically, the elements that determine lipid solubility are charge, protein binding, and molecular weight [100]. Moreover, carrier mediated transport (influx and efflux) is primarily influenced by transporter proteins in the BBB [101]. These transporters can be classified as influx and efflux transporters; influx transporters such as glucose transporter (GLUT1), monocarboxylate lactate transporter (MCT1), and sodium-coupled glucose transporters (SGLTs) [100] can increase the absorption of the drugs, whereas eff [102]. In addition, transcytosis can transport substances using receptors including Transferrin receptor (TfR) [103], low-density lipoprotein receptor (LDLR), and neonatal Fc receptor (FcRn) [104].

1.3.4 The function of BBB in drug delivery

Numerous studies have demonstrated that the BBB is a substantial obstacle in the context of medication delivery, preventing over 98% small molecules and all large molecule drugs from transversing [105]. The unique function of the BBB is effluxion or impeding exogenous substances entering the brain to maintain the homeostasis [106].

Lipinski's rule of five “Ro5” was developed in 1997 and is considered as a general guideline for assessing if a chemical molecule had qualities that would make it likely to be an orally active medicine in humans or determines whether a chemical compound has a certain pharmacological or biological activity [107]. The Ro5 is as follows [107]: the molecular weight (<500), hydrogen bond acceptor groups (HBA, sum of single bond -O and single bond -N, <10), hydrogen bond donor groups (HBD, sum of single bond -OH and single bond -NH groups, <5), and finally, calculated partition coefficient (log P) not greater than 5. According to Lipinski, the Rule of 5 only applies to substances that aren't substrates for active transporters [107].

The physical and chemical properties of drugs will affect their entry to the brain. Currently, the main ways for drugs entering into the brain can be classified as 4 categories as follows [108, 109]: A) For passive diffusion, including paracellular and transcellular, the properties of drugs can be optimised, and paracellular drug transport may be conducted by interrupting BBB permeability; B) carrier-mediated transport (CMT) mechanisms expressed on the BBB are utilised; C) absorptive transcytosis: cationic molecules have the ability to be transported nonspecifically throughout the cell via adsorptive transcytosis and endocytosis; D) receptor-mediated transcytosis: by binding to receptors, particular ligands are endocytosed and transported within the cell via receptor-mediated transcytosis.

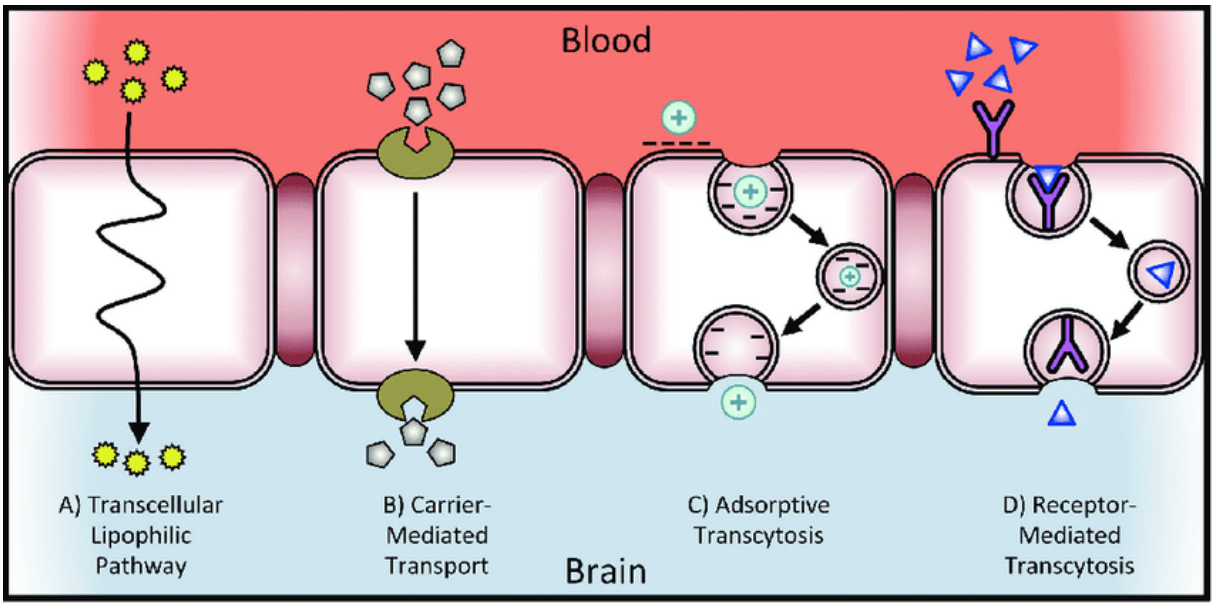

Figure 1.3 The BBB transport pathways.

Obtained from [109]

(A) The transcellular lipophilic pathway enables small lipophilic molecules to enter the brain via passive diffusion across the BBB. (B) Carrier-mediated transport (CMT) is a form of facilitated transport in which molecules are transported from the environment into and through the cell via the action of specific proteins. C) absorptive transcytosis: cationic molecules can be transported nonspecifically throughout the cell via adsorptive transcytosis and endocytosis; D) receptor- mediated transcytosis: by binding to receptors, particular ligands are endocytosed and transported within the cell via receptor-mediated transcytosis.

The exclusion of chemicals from the brain is typically attributed to their restricted paracellular permeability, which is a result of the presence of tight junctions that impede them into the BBB [110]. Adsorptive transcytosis is a mechanism that facilitates the internalization of locally abundant plasma proteins, such as albumin, which are often transported with difficulty, through the process of cationization [110]. Transporters are observed within endothelial cells and play a crucial role in mediating the transportation of diverse substances, including choline, amino

acids, glucose, purine bases, nucleosides. Specific transporters, such as P-gp and BCRP, mediate the translocation of molecules across cellular membranes by an energy-dependent mechanism [110]. These proteins function as efflux transporters.

Receptor-mediated transcytosis is a process characterized by the specific internalization and transportation of particular proteins, such as insulin and transferrin, via receptor-mediated endocytosis followed by transcytosis [110]. Occasionally, medications have the capacity to traverse the BBB because of their atypical permeability, which is attributed to their water solubility [105]. Cationic molecules have a greater inclination to traverse the BBB, potentially as a result of their interaction with the negatively charged EC membrane and proteoglycans situated in the basement membrane [110].

1.3.5 Current formulation strategies to deliver drugs across the BBB

Various strategies have been proposed to improve penetration, including the manipulation of drug properties, leveraging endogenous transporters or receptors at the BBB, and the adoption of nanoparticulate drug carriers or antibodies specifically targeting BBB receptors through receptor-mediated transcytosis (RMT) [111].

It is noteworthy that the BBB primarily permits the entry of lipophilic molecules with low molecular weights, specifically those under a threshold of approximately 400-500 Da [111]. This restrictive nature poses difficulties in treating neurological disorders. Further complicating the landscape is the fact that a scant proportion, less than 10%, of potential therapeutic agents with CNS indications progress to clinical trials, predominantly due to challenges associated with brain penetration [111].

A range of strategies exist aimed at enhancing the delivery of drugs to the brain. One prominent method entails the use of nanoparticles and liposomes—minuscule particles that can be tailored to transport drugs across the BBB [112]. These carriers can be precisely engineered to target specific neural cells or tissues, potentially optimising drug efficacy. Nonetheless, the capability of nanoparticles to autonomously traverse the BBB remains a topic of debate, with some positing the necessity of active targeting [112]. Furthermore, research has also explored alternative avenues such as leveraging the permeability of the BBB under pathological scenarios or adopting non-invasive procedures like microbubble-enhanced ultrasound (MEUS) and transcranial magnetic stimulation (TMS) to transiently disrupt the BBB, thus facilitating drug penetration [112].

Additionally, intranasal administration capitalises on the nasal cavity's direct conduits to the cerebrum through the olfactory and trigeminal pathways, offering another potential solution [113]. Furthermore, ligand conjugation involves affixing particular ligands to nanocarriers, allowing these ligands to subsequently adhere to specific BBB receptors and aid in barrier traversal [113].

Also, membrane coating, in which nanocarriers are wrapped in organic or artificial substrates like erythrocyte membranes or polymers, is a novel method [113]. This not only improves biocompatibility, but it also makes immunological clearing less effective. On the other hand, stimuli-induced BBB disturbance uses agents like ultrasound or changes in osmotic pressure to temporarily break down the BBB's tight junctions, which makes it easier for drugs to get into the brain [113].

Besides these strategies, there are numerous drug delivery systems to deliver drugs to specific places in the brain [113].

Liposomes, which have a double layer of lipids, are promising. These vesicular structures can put drugs inside them and guide them to specific cells or tissues. By adding ligands to improve targeting accuracy, their natural biocompatibility can be further increased [113].

Dendrimers, which have complex dendritic topological structures, are another option because they can be made in a way that can be carefully controlled and may have therapeutic applications [113].

The ability of nanoparticles and liposomes to interact with the BBB supports their potential for application for the delivery of drugs to the brain [112]. While some studies imply that nanoparticles may penetrate the BBB through a process known as receptor-mediated transcytosis, in which they bind to particular receptors on brain endothelial cells and then move across, other studies raise the possibility of an alternative mechanism known as adsorptive-mediated transcytosis, which depends on electrostatic interactions between the particles and the cellular surface [112]. These lipid-based structures can be designed to wrap particular medications and then guided towards chosen brain cells or tissues, a technique that can both increase the efficacy of drug delivery and reduce side effects [112].

The BBB serves as a selective interface enveloping the microvasculature of the CNS [113]. Constituted of endothelial cells with intricate TJs, the BBB meticulously restricts the passage of numerous chemical pharmaceuticals and biopharmaceutical agents [113]. As a result, therapeutic management of CNS ailments becomes intricate, as drugs frequently fail to access their designated cerebral targets. This impediment can lead to diminished therapeutic outcomes and augmented adverse effects [113].

To address these challenges, several strategies have emerged to bolster drug transport to the cerebral region [113]. Noteworthy among these is passive transcytosis, which leverages nanocarriers, such as liposomes or nanoparticles. This strategy facilitates drug transit across the BBB, encompassing the nanocarrier's absorption by ECs, followed by its release beyond the BBB confine [113].

1.4 The role of drug transporter protein at the BBB

There are a few transporters located at the BBB, such as glucose transporters, amino acid (AA) transporters, monocarboxylate transporters, ATP-binding cassette (ABC) transporters and the solute carrier superfamily (SLC) [114]. Glucose transporters are responsible for the transport of glucose- the necessary nutrients for the brain, eg: GLUT 1, especially expressed at the BBB [114]. The AA proteins are the ones transporting necessary substances- amino acids for the protein synthesis, the rate of brain proteins synthesis is not limited by the availability of amino acids, eg: LAT1 (SLC7A5)- the main AA transporter at the BBB [114]. Glycolysis occurs during the brain's absorption of glucose, and the lactic acid produced is transferred to Interstitial fluid (ISF) by Monocarboxylate transporters or used as an energy source during neuronal development, eg: MCT1- may avoid the accumulation of lactic acid in the BBB [114]. Instead of anticipating the ATP hydrolysis, SLCs can mediate transport of solutes as secondary active transporters, eg: SLCO2B1 (OATP2B1) transporter is highly expressed in the endothelial cells of brain capillaries, suggesting its potential role in facilitating the transportation of several neuropeptides and neurosteroids across the BBB [115].

The ATP-binding cassette (ABC) transporter superfamily is one of the largest membrane protein families [116]. Two ATP-binding domains, also known as nucleotide-binding domains (NBDs), and two transmembrane domains (TMDs) are often present in ABC transporters [117] (Figure 1.4). The two NBDs consist of NBD1 and NBD2, whereas the two TMDs consist of TMD1 and TMD2 [118] (Figure 1.4). In many organisms, the combination of ABC transporters may vary [119]. For instance, the ABC transporters in bacteria can be individually combined or a combination of NBDs and TMDs [120]. The ABC transporters in eukaryotes mostly are a combination of NBDs and TMDs, and they are combined by a polypeptide, and there may be some combinations of ABC transporters that are homodimeric or heterodimeric [121].

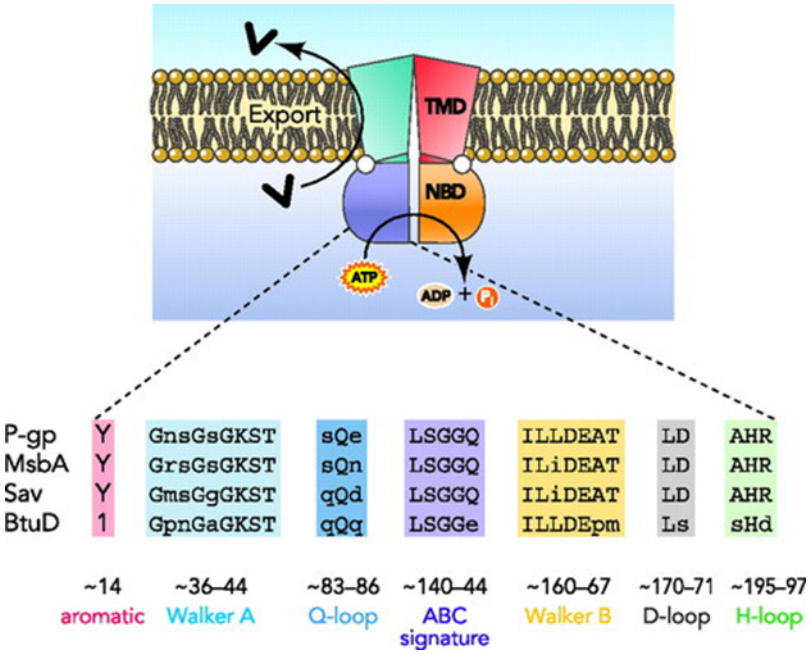

Figure 1.4 The structure of a minimal ABC transporter with four domains.

Obtained from [120].

The binding of ligands is facilitated by two transmembrane domains (TMDs), while the transportation process is powered by the binding and hydrolysis of ATP through the two nucleotide binding domains (NBDs). The transmembrane domains (TMDs) found in various subfamilies of ABC transporters may not exhibit homology. The nucleotide-binding domains (NBDs) exhibit homology across the whole family. Every nucleotide-binding domain (NBD) is composed of seven motifs that are highly conserved, although they are not completely unchanging.

In addition, A, Q, D, and H loops, Walker A and B conserved motifs, and the trademark C motif are classed as NBDs [122]. The functional ATP site is formed by the Walker A and B motifs (NBD1) and the signature region (NBD2), which bind ATP in the interspace of NBDs [123]. Typically, the two TMDs conjugate with 6–11 membrane-spanning -helices, and the helices dictate the substrate specificity. The primary function of ABC transporters is to inflow and efflux endogenous and xenobiotic chemicals, and the link between ABC transporters and multiple drug resistance (MDR) results from this function.

There are currently 48 ABC genes in the human genome, and more than 20 ABC transporters have been linked to human diseases, including cancer, cystic fibrosis, CNS disorders, and gout [124]. Importantly, the MDR phenomenon is mediated by a group of phosphoglycoproteins (mostly ABC transporters); these phosphoglycoproteins employ the energy of ATP hydrolysis to perform active transport to pump out the anticancer medicines of the tumour cells, in order to decrease the potential toxicity of these anticancer agents to the tumour cells [125].

Three major ABC transporters are associated with the MDR phenomenon: P-gp, MRP, and BCRP [125].

1.4.1 P-glycoprotein (P-gp)

P-glycoprotein (P-gp) was initially discovered in the ovary cell membranes of Chinese hamster in 1976. It is a glycosylated approximately 170 kDa transmembrane protein that is encoded by ABCB1 (also known as MDR1)- a MDR gene [126]. P-gp's primary role is to efflux poisons and xenobiotics, and this active efflux transporter is frequently overexpressed in cancer cells [127]. Active transport is facilitated by P-gp through the utilisation of ATP hydrolysis energy. Relative to cancer cells without P-gp expression, the concentration of anticancer medication is lower in these cells.

P-gp has already demonstrated the capacity to generate drug resistance prior to exposure to chemotherapeutic drugs for anticancer treatment [127]. In addition to being expressed in the luminal membranes of the endothelium of brain capillaries, P-gp is broadly expressed in the plasma membranes of numerous organs, including the liver, kidney, and intestine, as well as other human body tissues [128]. P-gp's structure consists of two homologous halves, each of which contains six putative transmembrane domains and hydrophilic N- and C-terminal portions [129]. The C-terminal regions contain nucleotide-binding sequences, which are employed to bind and hydrolyse ATP [129].

Inhibition of P-gp can also improve the efficacy of anticancer medications [130]; therefore, the regulation of P-gp must be investigated. In addition, numerous P-gp efflux substrates exist, such as anticancer drugs Mithramycin, Taxol (paclitaxel, docetaxel), and Actinomycin D; cytotoxic agents Puromycin, Calcium channel blocker, and Verapamil [129]; HIV protease inhibitors such as Ritonavir; hormones such as Testosterone and other agents such as Digoxin [131]; and HIV protease inhibitors such as Ritonavir [129].

1.4.2 Multidrug resistance protein (MRP)

Multidrug resistance proteins (MRPs) are derived from the subfamily C of the ABC transporter, and the human body contains nine MRPs derived from the same subfamily [132]. These nine MRPs are denoted by the designations MRP1, MRP2, MRP3, MRP4, MRP5, MRP6, MRP7, MRP8, and MRP9 [133]. Several transmembrane (TM) helices are located in the TMDs of these MRPs, which have NBDs for ATP binding and hydrolysis [134]. Being members of the ABC transporter family, MRP4, 5, 8, and 9 contain two NBDs and two TMDs as well as other

typical ABC transporters; these four MRPs are referred to as "short MRPs" [135]. The remaining human MRPs are referred to as "long MRPs" because their structures contain an extra NH2-proximal MSD0 [135]. In addition, as the only known MRP that is relevant to tumour multidrug resistance [136], MRP1 is encoded by ABCC1, which is predominantly expressed in the BBB, and it can be related to inflammatory responses and mediation with numerous anticancer drugs such as methotrexate (MTX) and vincristine, with MK-571 being the typical MRP1 inhibitor [137]. The precise mechanism of MRP1 is unknown [138].

1.4.3 Breast cancer resistance protein (BCRP)

1.4.3.1 Breast cancer resistance protein structure and function

The human breast cancer resistance protein (BCRP/ABCG2) is a member of the subfamily G of the ABC transporter superfamily [139]. The BCRP gene was cloned and isolated from the highly doxorubicin-resistant MCF7 breast cancer cell line (MCF-7/AdrVp) due to its overexpression [140]. Moreover, BCRP is a transporter with a molecular weight of around 72kDa and 655 amino acids [141]. This protein has a single N-terminal linked to six putative transmembrane regions[142] (Figure 1.5). BCRP consists of 1 NBD and 1 MBD and is therefore known as "half transporters" [143]. Otherwise, "complete transporters" like ABCB1 consist of 2 NBDs and 2 MBDs [144], but "full transporters" like ABCC1 include an additional MSD attached to the amino acid's terminal [145].

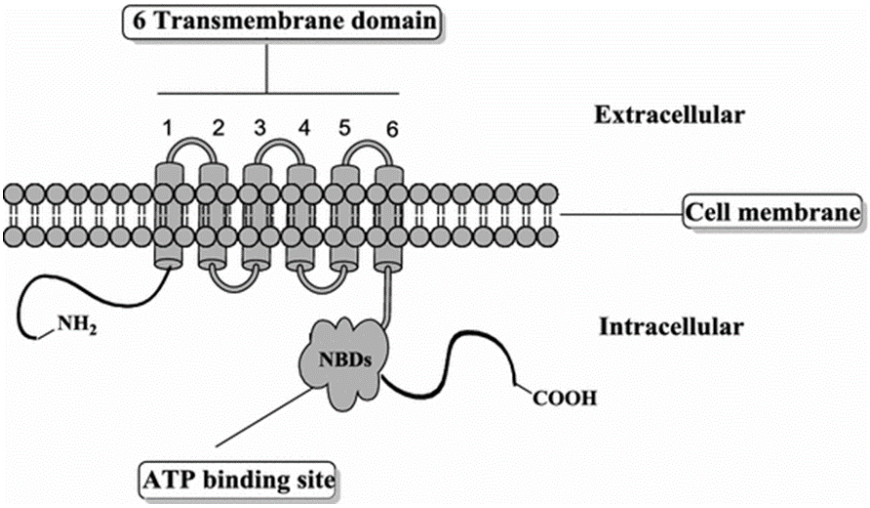

Figure 1.5 The structure of the BCRP.

Obtained from [146].

Breast Cancer Resistance Protein (BCRP) is classified as a half-ABC transporter, compared to P-gp, BCRP is characterised by six transmembrane domains and a single ATP-binding site, while P-gp possesses twelve transmembrane domains and two ATP-binding sites.

Moreover, BCRP has been found to be expressed in several organs, such as the brain, liver, and kidney, with the highest level found in the placenta [147]. Since the mechanism and function of BCRP are similar to those of P-gp, the high expression of BCRP in placenta may reduce the danger of chemotherapeutic drug exposure to the foetus [148]. Due to BCRP's mechanism, the ability to cause MDR can also be considered a part of BCRP's function [149]. As a distinct member of the ABC transporter family, BCRP's substrates are not restricted to chemotherapeutic medicines such as gefitinib, mitoxantrone, methotrexate, and other medications, but also include non-chemotherapeutic pharmaceuticals such as dipyridamole and statins [150]. P-gp cannot transport hydrophilic conjugated organic anions, although BCRP can, whereas P-gp can transport hydrophobic molecules [150]. Hence, once P-gp and BCRP can be produced simultaneously, they may induce a synergistic effect that strengthens the tissue barrier's (e.g., the BBB) ability to restrict drug permeability [150].

1.4.4 ABC transporters on the BBB and brain tumour

ABC transporters play a pivotal role in modulating drug delivery within gliomas by inducing multidrug resistance in neoplastic cells and hampering the effective delivery of chemotherapeutic agents to the cerebral domain [151]. Central to the functions of these transporters is their involvement in drug efflux mechanisms, which expel therapeutic agents from the brain and subsequently curtail their access to intended intracerebral targets [151]. Their expression is ubiquitous across various anatomical barriers, prominently including the BBB, the blood-cerebrospinal fluid barrier (BCSFB), the arachnoid barrier (BAB), and the blood-brain tumour barrier (BBTB) [151]. Notably, within glioma contexts, the manifestation of ABC transporters in oncogenic cells presents an added impediment, operating as an auxiliary barrier to chemotherapeutics. These transporters possess the capability to extrude drugs from intracellular environs, conferring a heightened resistance to chemotherapeutic regimens [151]. This multidrug resistance phenomenon significantly undermines the efficacy of chemotherapeutic interventions, culminating in the frequently observed suboptimal prognoses in patients afflicted with glioblastoma multiforme (GBM) [151]. As such, delving deeper into the intricate dynamics of ABC transporters and their implications for cerebral drug delivery emerges as imperative for forging breakthrough therapeutic strategies for glioma management [151].

Additionally, prior studies have shown significant alterations in the expression levels of ABC transporters at the blood-brain barrier in relation to neurological disorders., including

Parkinson's disease, stroke, epilepsy, and Alzheimer's disease [152]. For instance, it has been observed that the expression of P-gp is elevated in animal models of epilepsy and stroke. Nevertheless, the processes responsible for generating these alterations are intricate and encompass multiple signalling pathways [152]. However, it is important to acknowledge that the chemotherapy drugs may also be subjected to efflux via ABC transporters. As an illustration, it has been observed that certain anticancer medications, including doxorubicin, vinblastine, vincristine, and etoposide, are subject to efflux via ABC transporters, resulting in lower than anticipated concentrations within the brain. Various drugs, including immunosuppressive agents such as cyclosporine A, corticoids, analgesics like morphine, antibiotics such as erythromycin, tetracyclines, and fluoroquinolones, antiepileptic drugs like phenytoin, cardiac glycosides such as digoxin, and antiemetics like domperidone and ondansetron, have been identified as substrates for different ABC transporters [152]. Several studies have demonstrated that the upregulation of certain ABC transporters in the BBB might lead to the emergence of resistance to anticonvulsant medications [152].

1.4.5 Current inhibitors of ABC transporters

The majority of P-gp inhibitors are small molecule inhibitors, which can be categorised into the first, second, and third generations [153].

First-generation P-gp inhibitors including Verapamil (a Ca^2+ channel blocker), trifluoperazine (a calmodulin antagonist), and quinidine, reserpine, and yohimbine (antihypertensives) failed because their working doses for inhibition reached hazardous levels [154].

Second generation P-gp inhibitors, such as PSC 833 (valspodar) [153], were developed from the first-generation inhibitors with modifications, including alterations in chirality aimed at minimizing toxicity [155]. However, they were unsuccessful because their effectiveness of inhibition exceeded the tolerant level, and this effect had a negative impact on the therapeutic effect of the chemotherapeutic drugs.

The third generation of inhibitors were highly focused and overcame the deficiencies of the second generation. In contrast to the second generation, they did not interact with Cytochrome P450 (CYP450) 3A4 [153], and the typical therapeutic effect was unaffected by the third-generation inhibitors. However, this generation exhibited unexpected toxicity, therefore it too was unsuccessful [153].

For BCRP, recent inhibitors include fumitremorgin C (FTC) and Ko143[156], are effective and safer than previous inhibitors, such as GF120918 [156], but FTC is neurotoxic and cannot

inhibit P-gp and MRP-1 [156]. Ko143 has a similar structure to FTC, although it is more selective than FTC[157]. Yet, both FTC and Ko143 can only block the activity of BCRP ATPase[156], hence their limitations are evident.

Furthermore, for the current *in vitro* studies of BCRP modulators, as natural drugs, flavonoids have shown potential for the promising treatment of MDR. For example, a dimer of flavonoids known as Ac15(Az8)2, has been found to exhibit significant potency, safety, and selectivity as a BCRP inhibitor [158]. The findings demonstrate a substantial reversal of drug resistance mediated by BCRP both *in vitro* and *in vivo*, as evidenced by human colon cancer xenograft trials [158]. The compound AC15(Az8)2 has been found to effectively inhibit the ATPase activity of the BCRP, leading to a reduction in drug efflux and an increase in intracellular drug accumulation [158]. Hence, it can be inferred that Ac15(Az8)2 exhibits several characteristics that make it a promising candidate for further exploration in the context of combination therapy for the treatment of BCRP-overexpressing malignancy.

Moreover, there is the other flavonoid compound- 5,7-dimethoxyflavone (5,7-DMF), which is extracted from black ginger, has been found to enhance drug absorption by inhibiting the efflux of drugs mediated by P-gp and BCRP [159]. This mechanism leads to an increase in drug absorption inside the Caco-2 cell monolayer [159]. Hence, it is advisable to take into account the co-administration of health products containing black ginger with medicinal medications that serve as substrates for BCRP or P-gp, considering of a positive impact on their pharmacokinetic properties [159]. The findings of this study indicate that the administration of 5,7-DMF, has the potential to enhance the absorption of paclitaxel in Caco-2 cell monolayers [159]. As an anticancer drug, paclitaxel is typically provided intravenously to patients due to its limited oral bioavailability, thus the co-administration of 5,7-DMF and paclitaxel may have potential importance for the development of oral dosage discovery of paclitaxel [159].

1.5 Flavonoids as a novel class of ABC transporter modulators

Flavonoids, a major class of naturally occurring compounds, are plentiful in plants, vegetables, fruits, rhizomes, flowers, and even wine [160]. Furthermore, flavonoids have shown promised inhibition effects on ABC transporters. Numerous flavonoids have been demonstrated to interact with efflux transporters, particularly P-gp and BCRP, in *in vitro* studies, and the potential consequences of flavonoid–drug interactions owing to flavonoid modulation of these efflux transporters have been reported [161]. The significance of these flavonoid–efflux transporter interactions in pharmacokinetic interactions has not been demonstrated conclusively [161].

As a class of natural substances with a polyphenol structure, flavonoids cannot be ignored for their benefits [162]. Certain flavonoids employed as therapeutic enzyme inhibitors, such as cyclooxygenase (COX), have anti-inflammatory, antioxidant, and anti-cancer properties [163]. According to studies, flavonoid derivatives may decrease coronary heart disease mortality. Moreover, flavonoids such as phosphoinositide 3-kinase and xanthine oxidase (XO) can efficiently regulate human enzymes [164]. Meanwhile, as antioxidant, flavonoids can affect diseases such as cancer and atherosclerosis, and due to antioxidant action, flavonoids are now widely employed in many health goods, pharmaceuticals, and even cosmetics [165].

Dietary flavonoids are flavonoids found in foods such as vegetables, fruits, and beverages [166]. Furthermore, flavonoid derivatives are likewise physiologically active. Being a secondary metabolite derived mostly from plants, it can play a significant role in the plant growth process [167]. The subgroup of flavonoids is determined by the carbon numbers, unsaturation, and oxidation of the C ring, which is regarded to be the basis for flavonoids' classification [168]. Moreover, C ring is connected to B ring [168].

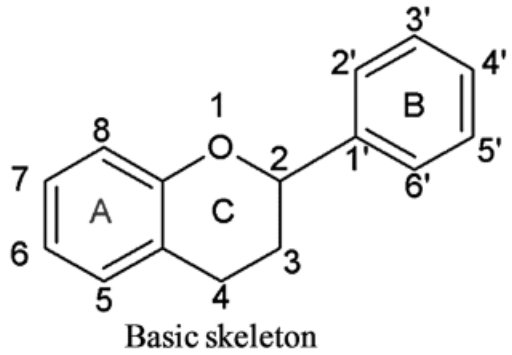

Figure 1.6 Basic structure of flavonoids.

Obtained from [168].

Flavonoids possess a fundamental chemical structure characterised by a 15-carbon framework, in which two benzene rings are linked together by a 3-carbon link. Thus, these compounds are shown as C6-C3-C6 structures.

Additionally, the flavonoids can be broadly categorised into 6 types, anthocyanin, chalcone, flavanones, flavones, flavonols and isoflavonoids [168].

1.5.1 The chemical structure and classification of flavonoids

The basic structure of flavonoids is a diphenylpropane skeleton with a C6-C3-C6 structure [169]. There are two benzene rings (Rings A and B) joined by three carbon chains and one pyran ring closed by a benzyl A ring (Ring C) [170]. In addition, flavonoids are typically categorised according to their distinct chemical structures [171]. Anthocyanins, chalcones, flavanones, flavones, flavonols, and isoflavonoids are the most prevalent subgroups of flavonoids [172]. Anthocyanins are the sole category of flavonoids that can be responsible for plant colour, and position 3 of the C ring is typically coupled to sugar units [173]. Common anthocyanins include cyanidin, malvidin, and peonidin, and their natural sources include fruits, vegetables, nuts, and dried fruits, as well as medicinal herbs [172]. However, chalcone, such as arbutin and phlioridzin, can be referred to as open-chain flavonoids due to their distinct chemical structures, and the natural sources of chalcone are nearly identical to those of anthocyanins, with the exception of nuts and dried fruits [174]. Moreover, there is a double bond between positions 2 and 3 in flavonols and flavones and isoflavonoids [172]. The C ring is therefore saturated, and it is also known as dihydroflavones [168, 172]. There is a double bond between positions 2 and 3 for flavones, and a ketone in position 4 of the C ring [172].

The majority of flavones may have a hydroxyl group at position 5 of the A ring [172]. Typical flavones include apigenin and tangeretin, and the most common natural sources include fruits, medicinal herbs, and other sources [172]. Moreover, for flavonols such as quercetin, rutin, and morin [172], there is typically a hydroxyl group in position 3 of the C ring [172], and the most common natural sources of flavonols are fruits, vegetables, medicinal plants, and others [168]. Moreover, the B ring of isoflavonoids is frequently connected to position 4 of the C ring [175]. Common isoflavonoids include genistin, genistein, and glycitein; their natural sources include legumes and medicinal herbs [168].

Moreover, flavanones and flavones are present in fruits, medicinal herbs, and other plant sources [168]. Moreover, anthocyamin can be found in nuts and dried fruits in addition to fruits, vegetables, medicinal plants, and other sources, it is responsible for producing colours such as red and blue, and its potential advantages are providing antioxidant power and protection for vitamins [168]. In addition, each subgroup contains typical flavonoid medications. For instance, malvidin and peonidin are both anthocyanin [176]; arbutin and phlorizin belong to the chalcone subgroup [177]; flavanones have naringin, hesperitin and hesperidin as classic molecules [178]; apigenin, baicalein and rhoifolin are flavones [179]; quercetin, myricetin, rutin are flavonols [180]; glycitein and daidzin can be considered as isoflavonoidsin [168].

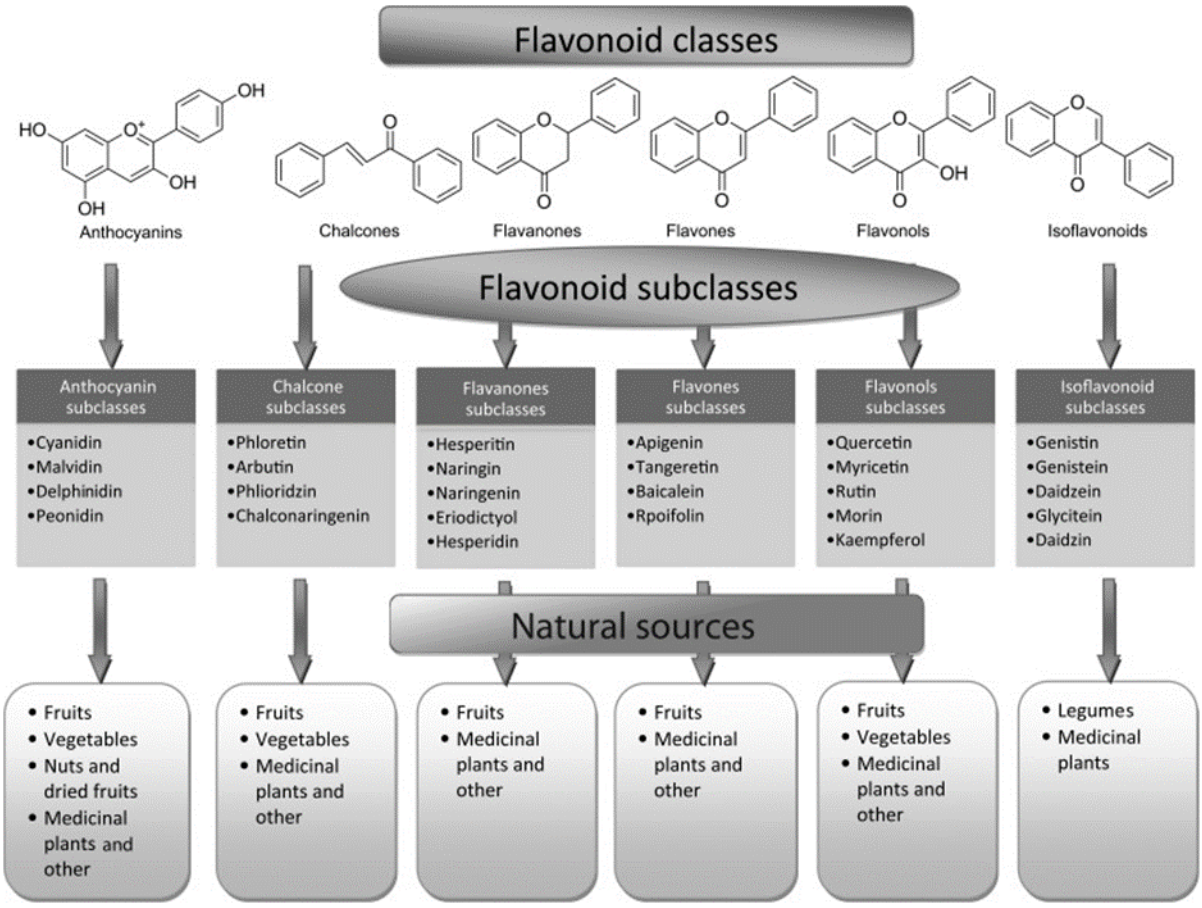

Figure 1.7 Subgroups of flavonoids.

Obtained from [181].

General classes, subclasses, and natural sources of flavonoids.

1.5.2 The impacts of flavonoids on health and cellular function

Numerous prospective health benefits have been attributed to their antioxidant [182] and anti-inflammatory properties [183]. On the effects of flavonoids on human health, a growing body of research has emerged in recent years, with studies focusing on their cardiovascular benefits [184], anti-inflammatory effects [183], anti-cancer [185], antiviral [186], antibacterial [187], vasodilatory [188], and anti-ischemic [189].

1.5.2.1 Antioxidant properties

The primary antioxidant effect of flavonoids is to prevent free radical-related chemical reactions from damaging cells [190], and the antioxidant capacity of many flavonoids is greater than that of vitamins C and E [191]. Flavonoids have multiple protective mechanisms against free radical-induced cellular injury [192]. Flavonoids, which are abundant in nature, may have a role in preventing coronary heart disease [193]. There are approximately eight known mechanisms for flavonoids to prevent free radical-induced injury [194]. In addition to directly scavenging reactive oxygen species, flavonoids can also activate metal chelating compounds and antioxidant enzymes, inhibit NAPDH oxidase, and boost the antioxidant properties of low-molecular-weight antioxidants [195]. In addition to the mentioned above, flavonoids can increase the levels of -tocopherol free radicals and uric acid and reduce oxidative stress caused by NO [196].

1.5.2.2 Cardiovascular benefits

Prior research has demonstrated that flavonoid consumption may reduce the risk of cardiovascular disease[197], and in addition to French red wine [198], consuming tea may also reduce the risk of cardiovascular disease [184]. Studies in both the United States and Europe have investigated the relationship between tea consumption and cardiovascular disease [199]. To clarify the potential influence of tea type on the research effect, multiple studies have demonstrated that green tea has a positive effect on the heart's health [184], although this result is presently limited to the Asian population. Additionally, both black and green tea have the potential to reduce the risk of ischemic stroke [184]. In addition, eating fresh fruits and vegetables has long-term benefits as well [200]. As dietary active constituents, flavonoids will also have noticeable effects on berries [201].

A study demonstrated that fresh cranberry juice can efficiently increase the blood's antioxidant capacity [202]. From the perspective of inhibiting inflammation and scavenging free radicals, it can be linked to cardiovascular protection [203]. Flavonoids (such as kaempferol, and quercetin) can exert their antihypertensive effects by activating the cAMP/protein kinase A cascade, which is implicated in the mechanism of action of NO in endothelial cells [204]. Flavonoids can activate NO synthase in vascular smooth muscle cells by stimulating kinases, thereby increasing the concentration of NO in endothelial cells [205]. Meanwhile, the activation of cGMP-protein kinase G cascade will stimulate potassium channel, reduce vascular smooth muscle contraction, and induce vasodilation. This mechanism of action effectively lowers blood

pressure and is responsible for anti-inflammatory effects that reduce the incidence of cardiovascular disease [206].

In addition, flavonoids have been linked to reduced blood pressure and cholesterol levels, both of which are risk factors for cardiovascular disease [207]. Flavonoids have been shown to reduce the risk of stroke by increasing the production of nitric oxide in the blood, which relaxes and dilates blood vessels, thereby enhancing blood flow and decreasing the risk of stroke [208]. Finally, flavonoids may also reduce the risk of atherosclerosis [209], a condition characterized by the accumulation of plaque in the arteries, which increases the risk of heart attack and stroke [210]. In addition, flavonoids can reduce arterial plaque, thereby lowering the risk of atherosclerosis and other forms of cardiovascular disease [211].

1.5.2.3 Anti-Inflammatory effects

By inhibiting the production of pro-inflammatory molecules, such as cytokines and chemokines, and by activating anti-inflammatory pathways, flavonoids are believed to reduce inflammation [212]. In addition to possessing anti-allergy properties, flavonoids are capable of inhibiting the release of histamine, a chemical emitted during an allergic reaction [213].

Flavonoids reduce inflammation in animal models of rheumatoid arthritis and other inflammatory conditions [214], according to investigations on animals. Flavonoids have been found to reduce inflammation in asthma and other allergic conditions in humans [215]. In addition, flavonoids have been shown to reduce allergic rhinitis symptoms and the risk of developing asthma [216]. Furthermore, it is believed that flavonoids exert their anti-inflammatory and anti-allergy effects by inhibiting the activity of certain enzymes, such as cyclooxygenase and lipoxygenase [217]. Flavonoids can reduce inflammation by inhibiting the activity of these enzymes, which are involved in the production of pro-inflammatory molecules.

1.5.2.4 Neuroprotective effects

Flavonoids may have neuroprotective effects and help to protect against neurological disorders [218]. Flavonoids can help protect neurons from damage, reduce inflammation, and even help to repair damaged neurons [219]. The most promising results have been seen in studies focusing on Alzheimer's disease, Parkinson's disease, and multiple sclerosis [220].

Flavonoids were found to be effective in reducing the oxidative stress associated with Alzheimer's disease [221]. This is significant because oxidative stress has been linked to the

formation of amyloid plaques, which are one of the major causes of cognitive decline in patients with Alzheimer's disease [222]. The flavonoids were also found to improve memory and cognitive function, suggesting that they may be a potential treatment for Alzheimer's disease [223].

Flavonoids have also been studied for their potential to reduce the risk of Parkinson's disease [224]. Flavonoids can help protect the brain from oxidative damage and reduce inflammation, both of which are factors in the development of Parkinson's disease [225]. Furthermore, flavonoids have been found to help reduce symptoms of Parkinson's disease such as tremors, bradykinesia, and rigidity [226]. This suggests that flavonoids may be a promising treatment option for those suffering from this debilitating disorder [227].

1.5.2.5 Anti-cancer effects

The specific mechanisms by which some flavonoids inhibit or prevent cancer have not been fully elucidated. Catechins have been regarded as advantageous constituents in tea; yet their underlying mechanism remains unclear [228]. Daidzein and genistein are widely recognized isoflavones due to their capacity to induce estrogenic effects in animal models [228].

Certain flavonoids have been discovered to possess the ability to impede cancer processes. Flavones have been extensively investigated as potential anticancer medicines due to their ability to inhibit tumour growth in cancer cells through the mechanism of apoptosis [228]. Luteolin has been observed to inhibit the activity of the epidermal growth factor (EGF) breast cancer cell line in people [228]. The induction of apoptosis in breast cancer cells is triggered by luteolin through the suppression of fatty acid production, a crucial lipogenic enzyme that is frequently upregulated in several types of human malignancies [228].

There is evidence to suggest that flavonols possess the ability to impede the development of breast cancer. Quercetin, a glycoside mostly present in onions, apples, and garlic, has been observed to induce DNA damage in cancer cells [228]. Three mechanisms exist for anthocyanins to inhibit the growth of cancer cells [228]: 1) Inhibition of signal pathways to prevent signal transduction; 2) The regulation of antioncogenes; 3) By influencing the Notch pathway and beta-catechin.

Flavonoids can regulate many cellular processes and trigger programmed cell death, cell cycle arrest, and autophagy, thereby inhibiting the proliferation and invasion of cancer cells. They have been proved to decrease reactive oxygen species (ROS) production and initiate apoptosis.

Caspases are a group of intracellular proteins that are widely believed to function as the main triggers of apoptosis, they can be classified into two different categories: initiators, namely Caspase-8, -9, and -10, and executors, namely Caspase-3, -6, and -7 [229]. Proteins are cleaved during apoptosis by caspases, among which caspase-3 has been demonstrated to be more effective than caspase-7 [229]. The extrinsic and intrinsic pathways are two well-known methods by which the caspase activation cascade occurs. The activation of the initiator caspase-8 and cleavage of the downstream effector caspase-3 occur in the extrinsic pathway in response to stimulation of death receptors like Fas/Apo1 or TRAIL [229]. The release of cytochrome c (Cyt c) into the cytoplasm from the mitochondrial intermembrane gap is a unique action of the intrinsic pathway that involves mitochondria [229]. The released cytochrome c attracts and activates caspase-9 by binding to the Apaf-1 docking protein and form a caspase-9 holoenzyme complex, which also includes Apoptotic protease activating factor-1 (Apaf-1) and Cyt c, activates caspase-3 and results in cell death [229].

Reactive oxygen species (ROS) are a kind of free radical; these small molecules function as intracellular messengers and can have adverse impacts on the integrity of DNA, RNA, and proteins when present in large amounts [230]. The intrinsic pathway, also known as the mitochondrial pathway, is a crucial mechanism involved in the regulation of apoptosis. ROS can activate p53 and/or c-Jun N-terminal kinase (JNK), this activation subsequently leads to the activation of the pro-apoptotic Bcl-2 protein, resulting in the inhibition of anti-apoptotic protein function [231]. Simultaneously, ROS induces the oxidation of cardiolipin, resulting in the cleavage of Cyt c and its subsequent release into the cytoplasm [231]. Furthermore, the presence of ROS leads to the depolarization of the mitochondrial membrane and/or the activation of Bax/Bak channels located on the outer mitochondrial membrane (OMM) [231]. This process subsequently results in the release of apoptosis-inducing factor (AIF), endonuclease G (Endo G), cytochrome c, and Smac/Diablo from the mitochondria into the cytoplasm [231].

Flavonoids can increase p53 and inhibit the Bcl-2 protein to release Cyt C, thus inducing the activation of caspase-9, then starting apoptosis by the activation of caspase-3 and 7; they can initiate caspase-8, thereby inducing the apoptosis of cancer cells [232]. The pro-oxidative effect of flavonoids triggers DNA fragmentation, consequently elevating reactive oxygen species (ROS) production in cancer cells and ultimately inducing apoptosis [233].

1.5.3 The inhibition effects of flavonoids as modulators on ABC transporters

P-gp, MRP, and BCRP are the three most prevalent human ABC transporters linked with MDR [234], and studies have shown that flavonoids can decrease the action of these ABC transporters to alleviate MDR [235]. Flavonoids can interact with P-gp by influencing the rate of ATP hydrolysis [236], and certain functional groups of flavonoids, such as the 5-hydroxyl group, the 3-hydroxyl group, and the 2,3-double bond, may be the key to modulating flavonoids for the ABC transporters [237].

Quercetin can inhibit Hoechst 33342 by reducing the activity of ATPase [238]. Nevertheless, not all flavonoids can inhibit P-gp; Genistein (an isoflavone) has been found to have no obvious inhibitory effect on the MDR mediated by P-gp [239]. In addition, several flavonols, such as myricetin and robinetin, have an inhibitory impact on the MDR owing to MRP2 [240], and the phase II metabolites of quercetin are regarded as a potent MRP2 inhibitor [239]. Several flavonoids, including genistein, hesperetin, kaempferol, naringenin, and phloretin, as well as quercetin, have been shown to inhibit the BCRP-associated MDR [239]. The preceding examples demonstrate that flavonoids have the capacity to inhibit human ABC transporters [235], which can aid in inhibiting BBB-located transporters to improve the treatment of chemotherapeutic medicines for brain tumours.

1.6 The role of pharmacokinetics in supporting improved CNS drug delivery

The most difficult task in treating CNS tumours is to apply findings from preclinical research to the clinic. Surgery and medical treatment will be impacted by the CNS's varied tumour microenvironment [241]. Traditional pharmacokinetic models, on the other hand, are unable to assess plasma drug concentrations in the CNS and forecast drug-plasma concentrations in brain tissue from blood sampling [241]. Anticancer drug absorption is a contentious topic, and there are not enough tools to measure the duration of drug in the brain or how the continual flow of cerebrospinal fluid (CSF) affects this sensitive organ [241].

1.6.1 Principles of pharmacokinetics

Physiologically based pharmacokinetic (PBPK) modelling is a mechanistic technique that uses mathematical equations, mass transport concepts, fluid dynamics, and biological data to predict the reactions of a chemical within the human body [242]. Compartments are usually defined by grouping organs or tissues with similar blood perfusion rate and lipid content of the human body, and organs are divided into sub-compartments [243]. Each compartment model

is associated with its own mass-energy balance equation, and blood functions as a link that connects these compartment models [244]. The complete PBPK model functions based on the principles of absorption, distribution, metabolism, and excretion (ADME) [245].

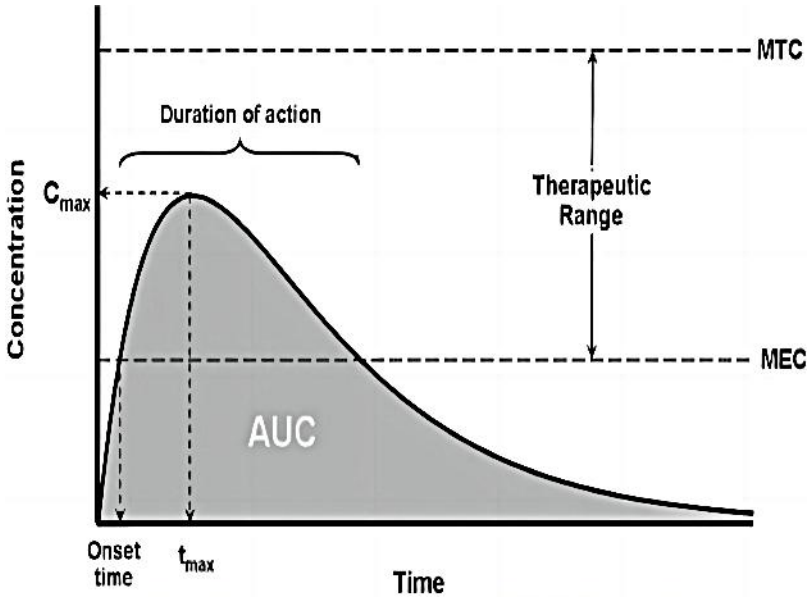

Figure 1.8 Plasma Concentration Vs Time Profile.

Obtained from [246].

The plasma-concentration profile shows common pharmacokinetic parameters [247]: T_{max}: the peak time when the drug's plasma concentration reaches the top in the human body; C_{max}: the corresponding maximum concentration recorded; AUC: a measure of the exposure to the drug; MEC: the minimal effective concentration; MTC: the minimal toxic concentration. Therapeutic range: the drug-plasma concentration range between MEC and MTC.

Absorption is the absorption of a medication molecule into the bloodstream, which can occur following parenteral (but not intravenous) or enteral administration [245].

Distribution refers to the movement of a drug molecule throughout the body, including its attachment to plasma proteins and accumulation in different tissues [245].

Metabolism is defined by the biotransformation of a drug molecule by enzymes in the liver and other organs, which might impact its pharmacological efficacy and toxicity.

Excretion refers to the removal of a drug molecule from the body, which might occur by urine, faeces, or breath [245].

1.6.2 Physiologically based pharmacokinetic (PBPK) modelling

PBPK modelling provides a framework for the cointegration of pharmacological activities and physiological parameters to determine the physiological changes during drug disposal [248]. The development of PBPK modeling originated from the idea proposed by a few scientists regarding variations in drug parameters within the human body, which was documented in 1937 [249]. Pharmacokinetics refers to the physiological responses of the human body to the effects of a medicine after it has been absorbed [250].

PBPK models provide an opportunity to assess intricate clinical circumstances, including the administration of drugs to specific populations such as pregnant women and paediatric patients, genetic variations in individuals, and drug-drug interactions (DDIs) [251]. The PBPK model is a fundamental tool for developing specific prescription plans in the medical field, it has the potential to predict prescriptions for various demographic groups, such as gender, ethnicity, age, and illness status [251]. Therefore, it improves the management and evaluation of prescriptions across diverse populations. Besides their broad application in commercial software like Simcyp® Population-based simulator, PBPK models can be applied in other areas such as novel drug development, government regulatory evaluation, and preclinical investigations [251]. The PBPK model provides a cost-effective and time-efficient approach, allowing for an evaluation of drug safety and efficacy prior to its clinical usage [251].

1.6.3 General physiologically based pharmacokinetic (PBPK) modelling building process

The creation of PBPK models depends on the collection of a significant number of drug-related data and the system parameters of people and preclinical experimental animals, which are provided by a huge number of clinical and published data [252]. Included in a drug's physicochemical qualities are its acidity and alkalinity, molecular weight, solubility, permeability, and capacity to bind to plasma proteins [253]. In addition, different ethnicities will be factored into the crucial analytical portion to establish distinct test groups that will replicate the population. The mentioned pharmacokinetic parameters will be described as four sections step by step followed the corresponding physiological changes happened in the human body-namely ADME: absorption, distribution, metabolism, and elimination [254].

In order to build a PBPK model, it is necessary to comprehend the PBPK model's cognition, which is the process of merging drug knowledge and biological changes caused by medications [255]. Through the plasma concentration-time curve, the changes of the medication within the human body and their interaction can be expressed [256]. Various tissues and organs in the human body will participate in the drug distribution process, and the

drug concentration of each tissue and organ during and after processing can be used as an empirical reference in the study [257]. Thus, a substantial quantity of clinical data is required to develop the physiological parameters of numerous organs and tissues for the PBPK model [258].

While the development of the PBPK model must take into account the features of the drug and the organs and tissues involved in the human body, the emphasis is generally placed on these two aspects: drug parameters and body parameters, when developing the model [257]. Initially, drug properties can be categorised into these followed major groups: permeability and partition coefficient, drug conjugation process, and metabolic transporters [259]. The permeability and partition coefficient of pharmaceuticals can be determined by prediction models and experimental assessment, as the physicochemical parameters of drugs can be regarded as the parameters of distribution in the human body [260]. Although this step will be evaluated by *in vitro* tests, this passive process will not be applied to all scenarios, thus while this step can play a role in quantifying organ and tissue balance, this passive process will not be applicable to all situations [261]. The body's parameters are utilised as a reference for the internal environment to participate in the development of the model, and the body's principal organs will participate in the ADME process of the drug [261]. Organ characteristics include organ surface area and volume, blood flow rate, protein-bound abundance [262], and tissue composition of body-participating organs. Some examples are the heart, lungs, brain, stomach, spleen, pancreas, intestine, liver, kidney, gonads, thymus, adipose tissue, muscle, bone, and skin [261]. The tissues are connected via the arterial and venous blood compartments, and each tissue has its own blood-flow rate, volume, tissue-partition coefficient, and permeability [263]. A significant advantage of PBPK modelling is the availability of a thorough structural representation of an organism's physiology [264]. The model's many parameters are derived either from compilations of prior information or from formulas that have been rigorously tested [264].

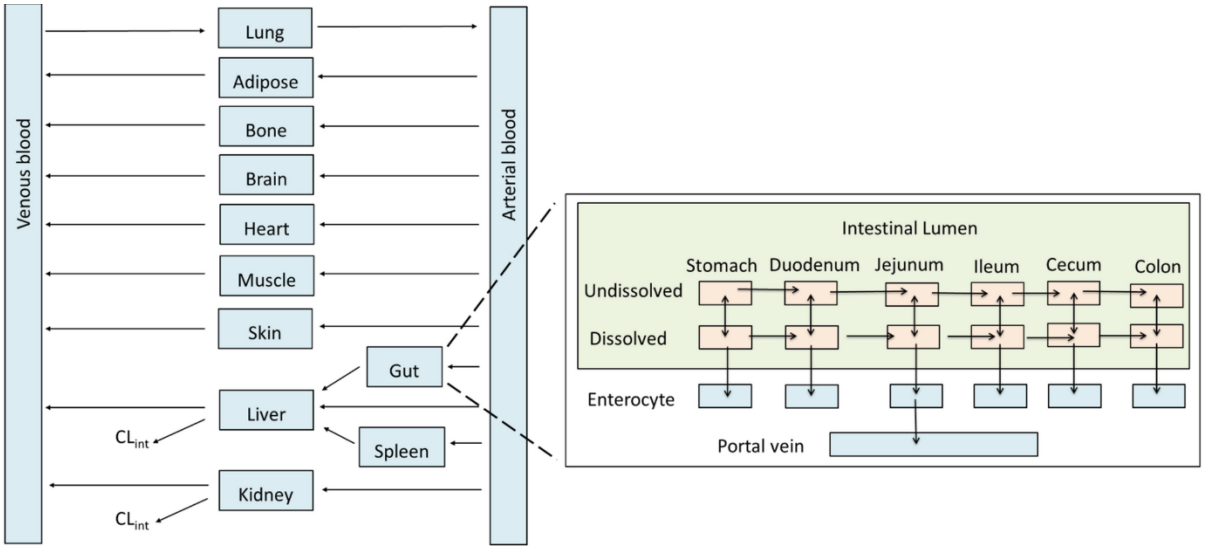

Figure 1.9 Involved organs for physiologically based pharmacokinetic (PBPK) modelling modelling.

Obtained from [265].

The basic structure of PBPK models consists of blood vessels connecting compartments that represent various human parts. (A detailed representation of the gut is shown in the insert) Species-specific tissue volume (or weight) and tissue blood flow rate are used to define each compartment. Adipose, bone, brain, gut, heart, kidney, liver, lung, muscle, skin, and spleen are among the major body tissues/organs that are regarded as separate compartments. The inset includes a detailed illustration of the gut as a representative example. CLint: intrinsic clearance.

The development techniques for PBPK models can be loosely categorised into three groups [266]. The first group represents the "top-down" development method, which combines clinical data with conventional models [266, 267]. This is also called Pop-PK, this method can use DDIs performance of drugs to describe and analyze the source of abnormal factors, but this method cannot predict the overview of DDIs' outcomes of drugs [268]. The second category is "bottom-up," which is just the reverse of the first group, which relies on the combination of computer and *in vitro* data [266, 267], this method uses organs/tissues as compartments and the blood flow connected them. Furthermore, this method can be able to predict the drugs' performance, the common software with this method are: SimCYP, Monolix and R, et cetera [268]. Obviously, this development strategy is formed during the initial phases of drug development [266]. "Middle out" is the third group, which incorporates both *in vivo* and *in vitro* data. This development strategy for continuous optimization also includes model optimization and clinical data feedback [266].

In the "top-down" development method, the classic empirical models have the advantage of being safe to research populations, but the disadvantages are quite apparent, as the sources of these models are the literature, although the number of the data is sufficient, but the system

parameters of the organs are not known [269]. While the majority of drug-related system metrics refer to average persons, with minimal or no data collection for particular populations or populations with various diseases [269, 270]. Hence, as the complexity of the demand for the PBPK model increases, even though the system parameters of the medication are determined *in vitro* by the “bottom-up” development method, the *in vitro* experiment is uncertain, and it is difficult to make timely and effective adjustments. Based on the restrictions of the first two PBPK creation approaches, the "middle out" method takes both of their benefits into account. When it comes to data processing, however, it is evident that the optimization of computer processing data will have a significant effect on the development of models [269].

There is an example which targeted the improvement of anticancer drugs in the CNS through PBPK modelling. To investigate the impact of the combination of focused ultrasound (FUS) and microbubbles on the transportation of two chemotheraputic drugs often used in the treatment of brain metastases, namely doxorubicin and ado-trastuzumab emtansine (T-DM1), were utilised to conduct a comprehensive study [271]. Trastuzumab emtansine is an anticancer drug commonly used in the treatment of non-specific cancers, and T-DM1 is an antibody-drug conjugate (ADC) [271]. The PBPK model demonstrates that the combination of FUS with microbubbles can diminish the vascular barrier of the patients’ brains, enhance interstitial convective transport within solid tumours, and significantly improve the absorption of small chemotherapeutic medicines by endothelial cells [271].

1.6.4 The current application of physiologically based pharmacokinetic (PBPK) modelling

Before the end of 2015, the European Medicines Agency (EMA) assessed the impact of PBPK modeling adoption in drug development, noting its rising use for simulating drug effects in diverse populations, yet with limited government disclosure. The potential influence of PBPK model outcomes on medication development and market surveillance was recognized. EMA's review covered 97 reports, of which 79 were publicly accessible official documents. Among 22 procedures related to MA, 3 explicitly referenced the PBPK paradigm, and 25 programs linked to the new MA explicitly cited PBPK models. Notably, most references to PBPK models were absent from public publications in the majority of the 51 programs identified from 67 PBPK models submitted by pharmaceutical companies [272]. In 2014, the US FDA seminar titled "Application of Physiologically-based Pharmacokinetic (PBPK) Modelling to Support Dose Selection" addressed PBPK's current application in academia and industry, along with challenges in dose regulation for specific population groups, taking into consideration safety and effectiveness concerns [273]. The substantial potential of PBPK models for investigating

drug safety and development in specific populations was emphasized. Analysis of FDA-submitted PBPK models revealed a focus on drug interactions, particularly predictions concerning CYP3A and 2D6 enzyme activities. It was noted that when drugs are CYP enzyme substrates, the impact of CYP enzyme inhibitors should be considered. However, a gap in PBPK model development remains, particularly for breakthrough drugs. Importantly, the US FDA, EMA, and Japan's Ministry of Health Labour and Welfare (MHLW) endorse PBPK modeling for DDI assessment and hepatic impairment studies. Additionally, both the FDA and the Medicines and Healthcare Products Regulatory Agency (MHRA) of the United Kingdom have organized PBPK workshops [274].

Furthermore, individual variations in the pharmacokinetics and pharmacodynamics of molecular targeted therapies, such as small molecule tyrosine kinase inhibitors (smTKIs), exist to ethnicity [275]. Variations in treatment efficacy and side effects may result from these distinctions, consequently impacting patient survival and quality of life.

Research has indicated that administering an equivalent dosage of smTKIs to individuals of diverse ethnic backgrounds may lead to varying systemic exposures, levels of effectiveness, and toxicity [275]. Extrinsic and intrinsic factors contribute to these variations. Intrinsic factors include body size, weight, and inheritance. Extrinsic factors include smoking, medicinal use, and diet habits. Variations in gene expression or activity among ethnic groups have the potential to impact drug-metabolizing enzymes and transporters, consequently influencing the drug's pharmacokinetics [275]. Furthermore, variations in pharmacodynamics may result from variations in sensitivity or resistance to drug target proteins due to genetic variation.

By recognising these distinctions, it is possible to identify ethnic groups that are particularly vulnerable to treatment resistance or adverse reactions. Prescribers can enhance dosage selection and identify patients who require drug concentration monitoring to optimise treatment efficacy while minimising adverse effects by considering ethnicity as an important consideration [275]. This improves the quality of life for patients, increases treatment success, and facilitates the individualization of treatment plans.

Drug-drug interactions (DDIs) are an additional major concern in the field of anticancer treatments [276]. Inducers of specific drug-metabolizing enzymes have the potential to elevate the clearance rate of anticancer medications, consequently impacting their clinical effectiveness [276]. To ensure optimal treatment outcomes, potential DDI must be closely monitored throughout treatment and adjusted in accordance with the patient's ethnicity and other unique characteristics.

1.6.5 Software applications for PBPK modelling: the Simcyp simulator

The utilisation of PBPK software approaches is advantageous due to the general acceptance of compartment models within the scientific field for their ability to predict drug dose and outcomes of different dose administrations [244]. The physiologically based pharmacokinetic (PBPK) model has the capability to assess the disease or damage condition of vulnerable populations by utilising pharmacokinetic (PK) data, such as clearance [244]. It is currently challenging to accurately estimate in clinical practice when administering medications to these vulnerable population groups. Predictions of toxicology can provide the evaluation of potential threats to human health. The utilisation of the PBPK modellings offers notable advantages in terms of saving time and cost, and integrating machines and artificial intelligence can further enhance the development of a more robust model [244].

Simcyp simulator is a computer- based software using designed programmes based on a series of inference methods and algorithms to conduct the prediction of drugs' ADME process in the human body [277]. As a reference for predicting the changes of drugs in the human body in response to physiological changes, PBPK models must integrate organ volume and tissue composition as physiological properties of the human body [278]. When considering the physicochemical properties of the drug, its permeability, plasma protein stability, and enzyme activity must be taken into consideration [253]. By simulating virtual populations, Simcyp is primarily used to investigate the absorption, distribution, metabolism, and excretion of pharmaceuticals in a specific population [279]. The results of PBPK modelling will be used to evaluate the impact of physiological information of different populations, such as ethnicities, age, sex, and disease, and to combine drugs to have an impact on drug development, such as modifying drug design or exploring drug interactions [280]. For instance, cancer patients have higher levels of alpha-1 acid glycoprotein (AAG) than healthy volunteers [281], indicating that the demographic distribution of the population is crucial to the effect of drug PK. To modify the specific physiological parameters of the virtual population, it is necessary for the establishment of a new model of PBPK to synthesize a large quantity of clinical data, as well as to synthesize the correlation between patients [282].

The advantages of the application of Simcyp are obvious. Simcyp can replace or accelerate the preparation of clinical trials through modelling, which is one motivation for utilising it [283]. In the early stages of drug discovery, dosage assessment can be carried out on virtual humans using Simcyp, including testing the dosing regimens; thus, Simcyp can participate in the decision-making process during drug discovery [283]. Simcyp can save expenses and offer suggestions for clinical trials. Multiple populations including sensitive populations can benefit from the application of Simcyp [283].

1.7 Basis for this research project

1.7.1 Aims

The overall aim of this research project is to promote cancer treatment and improve the current cancer therapies for specific population groups by utilising two perspectives to explore the depth of the project- pharmacokinetics and pharmacology.

For PBPK modelling, the ethnic differences caused by CYP 2D6 phenotype frequencies is the focus to target different populations. The PBPK research in this thesis focuses on the Chinese cancer population group. The first generation of tyrosine kinase inhibitors (TKIs)- gefitinib and imatinib - were selected for investigation in PBPK research due to their widespread clinical use in cancer treatment.

For gefitinib study, the main goal was to build a virtual Chinese cancer population model utilising gefitinib and its clinically relevant dose regimen using the principles of mechanistic pharmacokinetic modelling and virtual clinical trials. Additionally examined and noted for future therapeutic application were the effects of DDIs and CYP 2D6 polymorphism.

For imatinib study, the main goal of this study was to utilise the established therapeutic drug monitoring (TDM) approach and virtual clinical trials to develop a dosing adjustment strategy that is clinically applicable for virtual Chinese cancer populations. The strategy aims to ensure the maintenance of optimal plasma imatinib levels. Additionally, the study investigated the influence of various ethnic groups on TDM.

For brain tumour, the research focused on exploring specified flavonoids' impact on brain tumour cells and investigate the influenced level of BCRP located in the BBB. BBB is a permeability barrier that restricts the delivery of anticancer drugs to brain lesions. Passive drug diffusion and active transport via a BBB-expressed drug efflux transporter protein are required for drug transport. This study seeks to investigate the potential of flavonoids as natural drugs to modulate the BCRP function towards human glioblastoma LN 229 cells. This involved cultured cells and fundamental molecular techniques and quantitative analysis.

Therefore, to achieve the aims, the overall objectives were listed below.

1.7.2 Objectives

To achieve the aims, the overall objectives were:

- Develop the gefitinib Chinese cancer population model by validating the previously single dose studies in Caucasian subjects and optimizing this model with multiple studies. Validate the developed Chinese cancer population model by multiple dose regimens. Assess the impacts of DDIs using CYP inhibitors (3A4 and 2D6) and inducer (3A4) and explore the impacts of 2D6 inhibitors for different CYP2D6 phenotypes' patients.
- Validate the previously developed imatinib PBPK model using published single and multiple dose studies in Caucasian population and validate the imatinib model in a virtual Chinese cancer population. Observe TDM dosing regimen and compare the different imatinib TDM outcomes between Caucasian and Chinese cancer populations. To explore a virtual-TDM dosing regimen of imatinib in Chinese cancer population group, and to assess the differences of TDM strategies caused by multiple ethnic groups.
- Assess the cytotoxicity of flavonoids on LN 229 cells, the effect of flavonoids to modulate the expression of BCRP, the effect of flavonoids on cellular migration, the effect of flavonoids as anti-cancer agents on reactive oxygen species generation and the effect of flavonoids as anti-cancer agents on the activation of caspases.

Chapter 2 The pharmacokinetics of gefitinib in a Chinese Cancer population group: a virtual clinical trials population study

Disclaimer

Elements of this chapter have been published as follows:

YU, H. & SINGH BADHAN, R. K. 2021. The Pharmacokinetics of Gefitinib in a Chinese Cancer Population Group: A Virtual Clinical Trials Population Study. Journal of Pharmaceutical Sciences, 110, 3507-3519.

2.1 Introduction

Lung cancers are a common cause of cancer related deaths worldwide [284] with non-small cell lung cancer (NSCLC) comprising approximately 85 % of lung cancers [284, 285]. Lung cancer can be classified as four main subgroups: squamous cell carcinoma, large cell carcinoma, adenocarcinoma and small cell carcinoma [286]. The first 3 subgroups are normally seen as the most common lung cancer-non-small lung cancer. In NSCLC, adenocarcinoma is the predominant type of NSCLC, which is 32-40% of incidence, followed by squamous in 25-30% of cases and large cell carcinoma in 8-16% of cases [287, 288]. Squamous and SCLC cancers develop primarily in the central airways [289], whereas adenocarcinomas (including bronchioloalveolar cancer) develop in the periphery [290, 291]. Large cell carcinoma is a less differentiated version of the other types of NSCLC. The normal lung lacks squamous epithelium, and these tumours develop as a result of metaplastic alterations caused by smoking [292, 293]. SCLCs have neuroendocrine characteristics and develop from cells that have been instructed to specialise along these lines. Adenocarcinoma develops from bronchiole progenitor cells (Clara cells) or alveolar progenitor cells (Type II pneumocytes) or mucin generating cells [291]. The widely accepted standard for identifying non-small cell lung cancer is histopathology study by skilled pathologists, which specifies the cancer kinds [294]. However, there are other types of lung cancer which are not normal as above mentioned. A limited fraction of tumours with mixed (sarcomatoid and adenosquamous carcinomas) or not otherwise specified (NOS) histologies and clinical features are indistinguishable from other subtypes [292].

In terms of the definition of NSCLC, it is any epithelial type of lung cancer excluding small cell carcinoma. NSCLC is difficult to treat and the survival rates are poor, ranging from 68 % in patients with stage 1B disease to up to 10 % in patients with stage 4A/B disease [295]. Currently, non-small cell lung cancer (NSCLC) accounts for 30% of all cancer-related deaths within the Chinese population [296], and its prevalence is projected to rise to approximately 40% by 2030 [297].

Treatment is stage dependant, and tyrosine kinase inhibitors (TKIs) are a commonly used group of agents which target the epidermal growth factor receptor (EGFR), a key receptor implicated in the growth and proliferation of the cancers. The cell surface and transmembrane receptors are essential components of the signalling pathways and are involved in signal transduction. At the cellular level, a large class of receptors involved in the daily signalling pathways of cells are receptor tyrosine kinases (RTK) located on the cell surface [298]. Epidermal growth factor (EGF) is a family member for erythroblastosis oncogene B (ErbB) family of RTK [298]. As the first discovered member of ErbB family in 1978, EGFR(ErbB1,

HER1) is a 170-kDa monomeric glycoprotein [299], when it combines with epidermal growth factor (EGF), the complex can normally show physiological activities in cells. Meanwhile, there are other receptors with similar chemical structures, ErbB2 (neu, HER2), ErbB3 (HER3) and ErbB4 (HER4) [300, 301]. ErbB is the term obtained from the resemblance between these receptors and avian ErbB, a viral oncogene. Human epidermal growth factor receptor (HER) is the alternative name for this group's receptors. In addition, ErbB2 is sometimes referred to as neu since it was produced from a mouse glioblastoma cell line, which is a kind of neural tumour [298]. ErbB receptors are found in the basolateral membrane of epithelial cells, where they interact with their ligands in the stroma to mediate communication between the epithelium and the extracellular matrix [298].

EGFR is a trans-membrane protein which contains both an extracellular epidermal growth factor domain and an intracellular tyrosine kinase domain. As a tyrosine kinase receptor, EGFR is associated with the occurrence and progression of NSCLC by gene mutation or amplification [302], and the activating mutation of EGFR typically occurs in the tyrosine kinase domain [303], which can activate the following signalling pathways in the absence of contact with EGFR ligends, for example, EGF. In the case of ligand binding, downstream signalling pathways are triggered, whereas EGFR, which normally binds to ligands (e.g. EGF), can form phosphorylated dimers to activate downstream signalling pathways (e.g. RAS/RAF/MAPK, JAK/STAT) [304], which is the key during cell proliferation, survival, and apoptosis.

TKIs can be classified into first, second and third generation inhibitors and targeting the EGFR has been the primary focus in clinical oncology. Uncommon EGFR mutation (termed a “complex” or “compound” mutation) can be seen as the most frequent reason that occurred in lung cancer patients, and based on clinical research, different EGFR mutations may have different sensitivities to TKIs [305]. The past two decades have focussed on two orally administered EGFR-TKI agents, gefitinib and erlotinib [306]. However, gefitinib was the first agent granted approval by the Food and Drug Administration (FDA) for the treatment of lung cancer [307]. Gefitinib is known as N-(3-chloro-4-fluorophenyl)-7-methoxy-6-(3-morpholin-4-ylpropoxy)quinazolin-4-amine (shown in Figure 2.1), its formula is $C_{22}H_{24}ClFN_4O_3$ and molecular weight is estimated as 446.9g/mol. Additionally, erlotinib’s name is N-(3-ethynylphenyl)-6,7-bis(2-methoxyethoxy)quinazolin-4-amine and formula is $C_{22}H_{23}N_3O_4$, and its molecular weight is similar to gefitinib’s, which is 393.4g/mol [308]. Furthermore, gefitinib and erlotinib possess similar chemical structures. However, their pharmacokinetic and pharmacodynamic features resulting from their distinct molecular architectures and binding capacities. Significantly more hazardous than gefitinib, erlotinib may induce rash, nausea, vomiting, tiredness, and stomatitis [309]. Despite the fact that it may not shorten the patients’ survival time, a number of research indicate that it will diminish their quality of life [310, 311].

There are two causes behind these outcomes: Firstly, their gap between oral dose and maximum tolerable dosage are different: erlotinib oral dose 150mg/day; maximum tolerable dosage, 150 mg/day. Meanwhile, gefitinib oral dose 250mg/day; maximum tolerable dosage, 600 mg/day; Secondly, the pharmacokinetics of the two EGFR TKIs are distinct. Gefitinib accumulates more in tumour tissue than in plasma after absorption, while erlotinib does the converse [309]. The anticancer effectiveness of gefitinib and erlotinib was almost same in the subset of patients with EGFR mutation status. In addition, in one research of advanced cancer patients with solid tumours, a single 100 mg IV dosage of erlotinib was well tolerated and was associated with very mild side effects [312].

Gefitinib is known to be slowly absorbed orally, with a bioavailability of approximately 60 % and time to maximum plasma concentration (T_{max}) of 3-7 hours, unaffected by dose nor food intake [313]. As a lipophilic dibasic molecule, gefitinib possesses a free base during medication administration, which slows its absorption. This suggests that gefitinib has the clear pH-independent property. When the pH is low, the solubility will be high, but in terms of the absorption process in the stomach environment, the pH will be about 5, resulting in a considerable drop in absorption [314]. In addition, the solubility of gefitinib changes in various simulated human body environments with varying pH values. Gefitinib's solubility in human intestinal fluid (HIF) and fasting simulated small intestinal fluid (FaSSIF) (both with a pH of around 7) is almost identical to 0.08 mg/mL, which is very low. When the solubility is simulated in the fed simulated small intestinal fluid (FeSSIF), it is somewhat more than in the HIF and FaSSIF, at 1.950mg/mL. In simulated gastric fluid (NaCl 2 g/L + 65.75 mL/L 1 M HCl) (SGF), however, the solubility may exceed 9.5 mg/mL at a final pH of around 1.6 [314].

Its volume of distribution is high, in excess of 1000 L and with a long half-life of approximately 48 hours and is highly protein bound ($fu_{plasma} < 0.05$) [313, 315]. Gefitinib elimination is primarily mediated through hepatic biotransformation through primarily CYP 3A4 and 2D6 [316, 317] with less than 4 % being eliminated renally [318]. The therapeutic range is thought to be wide, ranging from 10-5000 ng/mL [319], however pharmacodynamic target endpoints are suggested to require a trough concentration of > 200 ng/mL [320-322].

Interindividual variability in TKIs is common, for a variety of reasons. Many TKIs are neutral or weak bases and their acid dissociation constant (pKa) is therefore associated with pH dependant solubility, which could contribute towards interindividual variability in subjects taking acid-supressing agents [323], a phenomena contributing to the reduced peak plasma concentrations (C_{max}) and area under the curve (AUC) for gefitinib. Gefitinib is accessible as a free base and has pKa values of 5.4 and 7.2, thus it ionises in solution when pH drops. Gefitinib is sparingly soluble at pH 1, but essentially insoluble at pH 7, with a rapid decrease in solubility

between pH 4 and 6 [324]. Further, although most TKIs are low clearance drugs [325], interindividual variability associated with drug metabolism is often associated with changes in hepatic exposure (governed by the unbound fraction in plasma) and the intrinsic hepatic clearance and associated enzyme abundance [325].

When comparing East Asian and non-East Asian populations for the influence of racial differences on TKI treatment, a demographic analysis of 384 NCSLC patients indicated that survival outcomes were comparable between the two groups [326], and that racial differences had no significant effect. A history of non-smoking, on the other hand, had a beneficial effect on treatment outcomes. According to this study, non-smoking patients were more likely to have a normal body mass index (BMI) in a retrospective investigation utilizing the Glans-look lung cancer database [327], and Asians were as diagnostically beneficial prognostic factors as non-smoking history. Asians represent a distinct subset within the population with an EGFR mutation, and associated study is critical for furthering our understanding of NSCLC. It is worth noting that even within the Asian population, when NSCLC patients were compared for ethnic differences, the EGFR mutation results of Xinjiang Uygur and Han people were significantly different [328], demonstrating that even within the Asian population, ethnic differences can result in different EGFR mutations. The mechanism of EGFR mutation consequently influences clinical therapy outcomes. As a result, studies targeting specific subgroups are critical while undertaking research in Asian populations, particularly with regard to EGFR-TKI therapy.

Physiological and biochemical changes in the oncology populations compared to healthy populations can influence pharmacokinetics. The cause of this is multifactorial but can be attributed to impaired hepatic [329] and renal function [330], lower albumin/higher α-one acid glycoprotein and altered functional metabolic capacity of the liver [331]. Furthermore, prominent physiological differences are evident when comparing Chinese population groups to Caucasian population groups, namely revolving around body weight, liver size, functional metabolic capacity of the liver and variations in polymorphic frequencies of CYP-isozymes [332, 333].

Previously Chen *et al* (2018) [334] described a pharmacokinetic model for gefitinib exploring change in plasma levels within Caucasian CYP 2D6 ultrarapid metabolisers (UM) and extensive metabolisers (EM) populations following drug-drug interactions. They demonstrated that CYP 2D6 UM phenotypes presented with significantly reduced AUC when compared to EM phenotypes, however concluded that such a change would have limited impact as this reduction is still above gefitinib's *in-vitro* IC_{90} for *EGFR* activating mutations in NSCLC patients. Given the fact that CYP 2D6 is highly polymorphic and possess frequencies which differ between Caucasian (UM: < 5 %; intermediate metabolisers (IM): <2 % ; poor metabolisers

(PM):<10 %) and Asian patients (UM: ~1 %; IM: 30-50 %; PM: ~1-3 %) [335, 336], assessing the impact of such differences in phenotype frequencies on gefitinib pharmacokinetics is warranted. Furthermore, given the paucity of information comparing the clinical pharmacokinetics of gefitinib in Chinese cancer population groups, we applied the principals of mechanistic physiologically based pharmacokinetic modelling to: (i) develop a Chinese cancer population group; (ii) compare gefitinib between Caucasian vs Chinese cancer groups and (iii) assess the impact of CYP 2D6 phenotypes on gefitinib plasma concentrations.

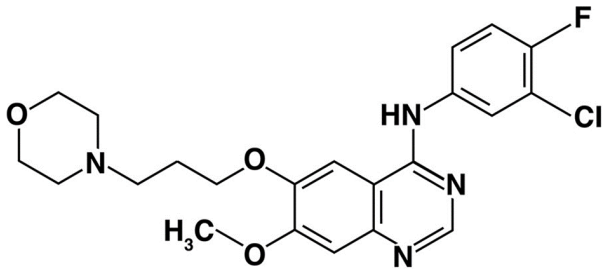

Figure 2.1 Chemical structure of gefitinib.
Obtained from [337].

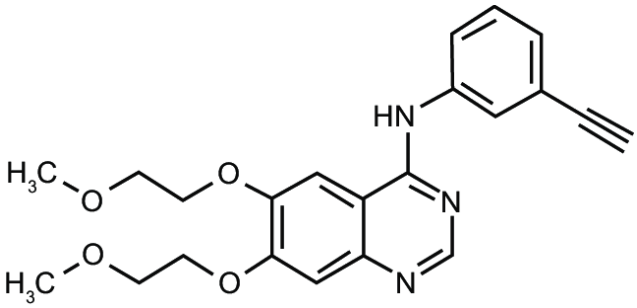

Figure 2.2 Chemical structure of erlotinib.
Obtained from [338].

2.2 Aims and objectives

The primary aim of this study was to use the principles of mechanistic pharmacokinetic modelling and virtual clinical trials to develop a virtual Chinese cancer population model using gefitinib and its clinically relevant dosing regimen. The impacts of DDIs and CYP 2D6 polymorphism were also investigated and observed for further clinical usage.

To achieve the aims, the overall objectives were:

- To validate the previously single dose studies to validate a gefitinib model in Caucasian subjects.
- To optimize and develop the gefitinib model using multiple studies.
- To validate the established Chinese cancer population model by multiple dose regimens.
- To assess the impact of DDIs using CYP inhibitors (3A4 and 2D6) and inducer (3A4) within this virtual Chinese cancer population model on gefitinib plasma concentration.
- To explore the impacts of 2D6 inhibitor for different CYP2D6 phenotypes' patients using this developed Chinese cancer population model.

2.3 Methods

All simulations were carried out using the physiologically-based pharmacokinetic (PBPK) modelling tool Simcyp to conduct virtual clinical trials simulations in subjects (Simcyp Ltd, a Certara company, Sheffield, UK, Version 19). Unless otherwise stated, mixed genders (50:50) were incorporated into all simulations. We adopted a workflow model with four stages (Figure 2.2).

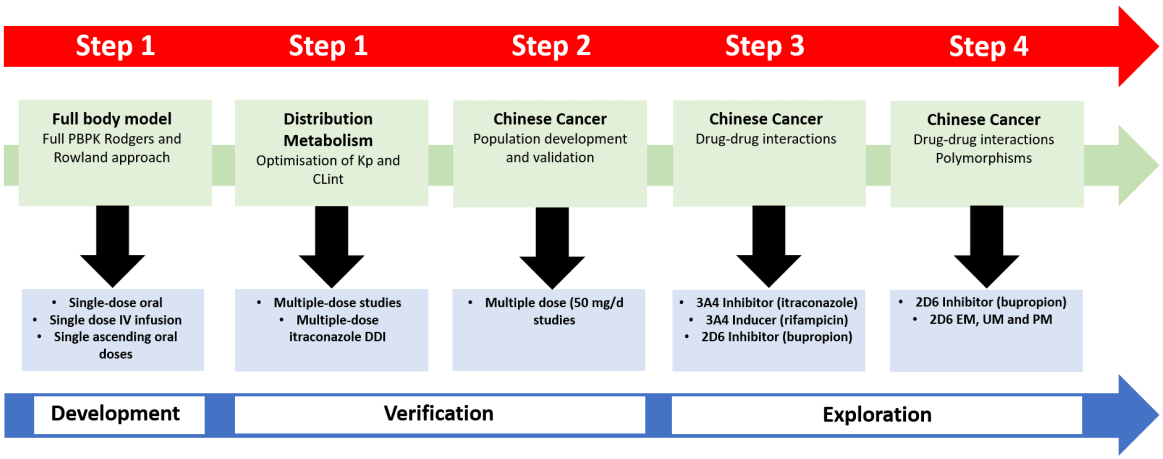

Figure 2.3 The workflow model for model development, validation, and exploration.

2.3.1 Step 1: Validation of a gefitinib model in Caucasian subjects

We utilised a previously developed model of gefitinib [334] and expanded upon existing validation attempts by considering 5 studies within healthy Caucasian populations: (i) 24 healthy Caucasian male volunteers (18-62 years old) received a single dose of gefitinib 250 mg orally on day 4 alone or in the presence of itraconazole 200 mg/day for 12 days [339]; (ii) 8 healthy Caucasian volunteers (aged 18-65 years old) receiving an intravenous infusion of gefitinib 50 mg or 100 mg [313]; (iii) 17 patients with advanced solid tumours (over 18 years old) administered a single 50 mg gefitinib intravenous infusion over 5 minutes [313]; (iv) 5 healthy Caucasian volunteers receiving 100 mg once daily for 3 days [340]; (v) 4 healthy Caucasian volunteers receiving ascending single doses (10, 25, 50 and 75 mg) [340].

2.3.2 Step 2: Development and validation of a virtual Chinese cancer population

To assess the applicability of the model within a specific Chinese cancer population, we adapted the existing Chinese population to account for the physiological alterations previously reported [329] to occur in the oncology population group, namely reduced haematocrit, increased α-1 acid glycoprotein and decreased albumin and reduced glomerular filtration rate (GFR) [341]. The Simcyp Healthy Volunteer (Caucasian) and Cancer (Caucasian) population groups were compared in order to assess the degree of change in the aforementioned physiological parameters and associated variances, and these changes were altered within the Simcyp Chinese (healthy volunteers) population group to establish the Chinese cancer population. Thereafter, the simulated patient demographic data, namely simulated weight, height, body surface area (BSA), haematocrit, albumin, AAG, GFR and serum creatinine, were graphically examined as a function of age in 2000 simulated subjects (1000 males and 1000 females). In order to evaluate if the adapted population model could adequately describe the Chinese cancer population, we assessed the simulated demographic parameters with those reported within the literature [342-351] for Chinese (all parameters) or Japanese (AAG) populations.

In order to validate the adaptations, the pharmacokinetics of gefitinib in the virtual Chinese cancer population was compared to reported studies in Chinese cancer patients where gefitinib was dosed to: (i) 11 patients at 250 mg gefitinib once daily for 15 days [352]; (ii) 58 NSCLC patients dosed 250 mg once daily and where steady state trough plasma concentration were reported [353]; (iii) 22 NSCLC patients dosed 250 mg once daily and where steady state trough plasma concentrations were reported [354].

For all subsequent simulations, an age range of 40–50-year-old was selected, reflecting the abundant age ranges identified from this section.

2.3.3 Step 3: Comparison of the impact of drug-drug interactions on gefitinib pharmacokinetics between Caucasian and Chinese cancer populations

Drug-drug interactions are common with TKIs [355], and clinically relevant DDIs have been reported for gefitinib [339, 356] due to its primary metabolic routes being governed by CYP 3A4 and CYP 2D6 [316, 317]. However CYP 2D6 is highly polymorphic and the use of inhibitors of 2D6 in poor metaboliser (PM) phenotypes is suggested to warrant close monitoring for safety and toxicity due to the possibility of raised plasma concentrations [357].

To assess the impact of DDI we assessed the role of three perpetrator agents, itraconazole (3A4 inhibitor), rifampicin (3A4 inducer) and bupropion (2D6 inhibitor) on gefitinib (as a victim drug) pharmacokinetics in the virtual Chinese cancer population (n=100), aged 40-50 years with 50 % female. A 250 mg once daily gefitinib dose was administered for 28 days for inhibitor studies with 200 mg once daily (itraconazole) or 150 mg once daily (bupropion). For inducer studies, rifampicin was dosed throughout the study at 600 mg once daily for 60 days with gefitinib dosed on days 28-56.

2.3.4 Step 4: The impact of drug-drug interactions on gefitinib pharmacokinetics in CYP 2D6 polymorphic Chinese cancer subjects

To assess the impact of DDIs on gefitinib pharmacokinetics in individuals entirely polymorphic for CYP2D6, we utilised the virtual Chinese cancer population group comprising EM, PM, IM or UM populations in a study involving bupropion. A 250 mg once daily gefitinib dose was administered for 28 days with coadministration of 150 mg once daily (bupropion) to 100 subjects aged 40-50 years with 50 % female, with the resulting pharmacokinetics assessed on the final dosing day.

2.3.5 Predictive performance

In order to confirm the predictive performance of model simulations during the validation steps for Section 2.1 and 2.2, we utilised a prediction of pharmacokinetic metric to within two-fold

(0.5-2.0 fold) of that published clinical data as being generally accepted [358-360], supported by a standard deviation ratio (SDratio) calculated as follows:

$$\text{SDratio} = \sqrt{\left(\frac{\text{SD observed}}{\text{Mean observed}}\right)^2 + \left(\frac{\text{SD predicted}}{\text{Mean predicted}}\right)^2} \times \frac{\text{Mean predicted}}{\text{Mean observed}} \quad (1)$$

where SD observed and SD predicted are the SD of observed and predicted values; Mean observed and mean predicted are the arithmetic mean of observed and predicted values. Model performance was finally graphically considered by comparing the mean ratio and SDratios.

2.3.6 Visual predictive checks

In addition, a visual predictive checking (VPC) strategy was utilised where the predicted mean and 5th and 95th percentiles of the concentration–time profiles were visually compared with retrospective observed data, with the prediction assumed to be valid when the predicted data points overlapped with the observed data sets [361-363].

2.3.7 Data and statistical analysis

All the observed data acquired from published studies was extracted by WebPlotDigitizer v.3.10 (http://arohatgi.info/WebPlotDigitizer/). Statistical analysis was conducted with GraphPad Prism version 8.0 for Windows (GraphPad Software, La Jolla, CA, USA, www.graphpad.com) and statistical significance determined as $P < 0.05$.

2.4 Results

2.4.1 Step 1: Validation of a gefitinib model in Caucasian subjects

The model simulated plasma concentration-time profiles and pharmacokinetic parameters were consistent with observed data and ranges (Figure 2.3) and broadly within 2-fold for the geometric mean C_{max}, T_{max} and AUC, for both oral and IV infusion administered under single and multiple dose regimens (Figure 2.4) (2.7.2 Section 2).

Dosing		PK Parameters	Observed	Predicted
Single	Segura *et al* (2003) [364]	$AUC_{(0\text{-}24\ h)}$	96.50 (65.90)	156.83 (138.69)
		C_{max}	8.60 (5.50)	11.10 (8.87)
		t_{max}	5 (3-5)	3.9 (1.72)
	Yasui-Furukori *et al* (2007) [365]	$AUC_{(0\text{-}48\ h)}$	127 (67)	230.3 (222.34)
		C_{max}	6.5 (2.4)	11.10 (8.87)
		t_{max}	5 (4-10)	3.9 (1.71)
	Massaroti *et al* (2005) [366]	$AUC_{(0\text{-}120\ h)}$	225.04 (291.91)	312.34 (347.90)
		C_{max}	9.02 (8.82)	11.10 (8.87)
		t_{max}	5.03 (1.91)	3.89 (1.71)
Multiple	Segura *et al* (2005)[367]	$AUC_{(0\text{-}8\ h)}$ [Day 1]	53.8 (26.7)	65.37 (53.52)
		$AUC_{(0\text{-}8\ h)}$ [Day 8]	159.8 (49.8)	205.76 (104.80)
		C_{max} [Day 1]	10.4 (4.8)	11.09 (8.87)
		C_{max} [Day 8]	26.1 (7.1)	31.61 (15.18)
		t_{max} [Day 1]	3 (3–5)	3.87 (1.62)
		t_{max} [Day 8]	8 (3–8)	4.15 (0.83)

Table 2.1 Summary of pharmacokinetics parameters from the single and multiple-dose studies.

AUC, area under the curve; C_{max}, maximum plasma concentration and t_{max}, time at maximum plasma concentration. Data represent mean (standard deviation). AUC: ng/ml h; C_{max}: ng/ml; and t_{max}: h.

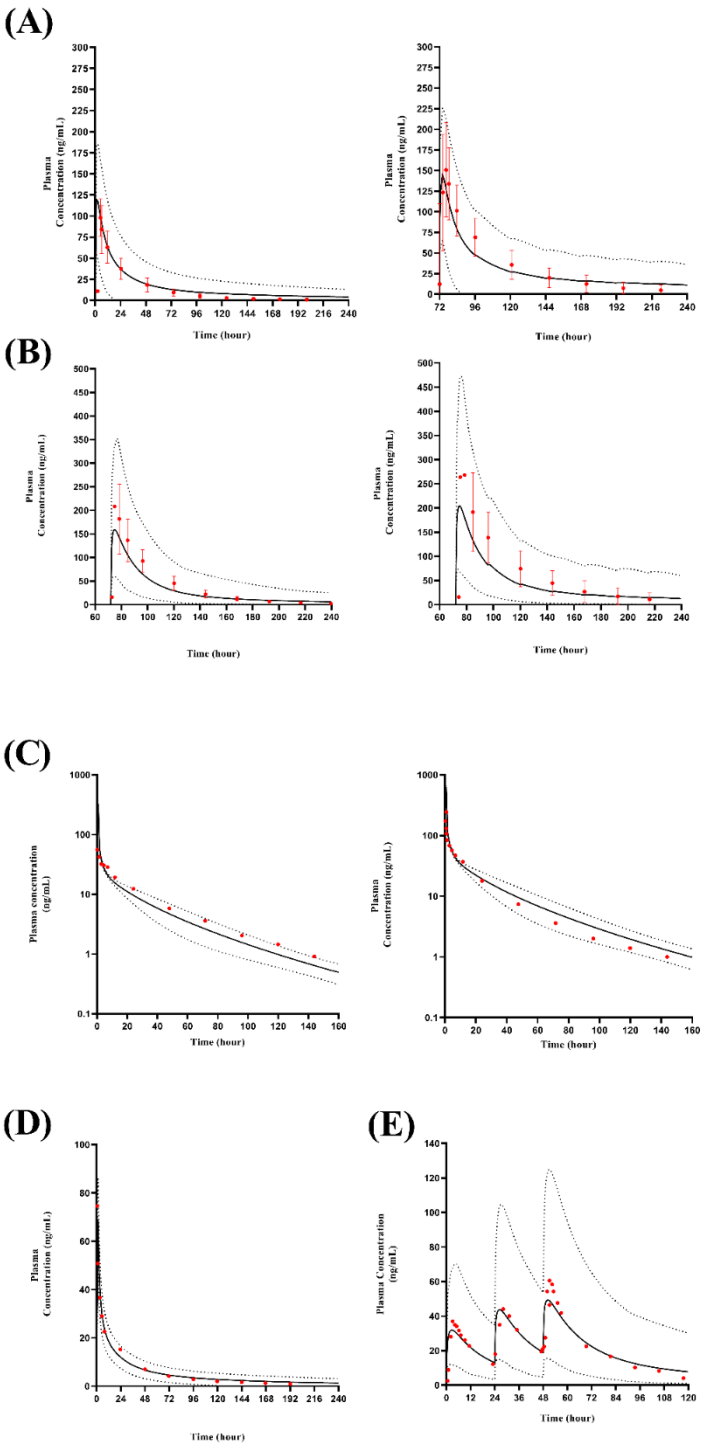

Figure 2.4 Simulated plasma concentration-time profiles of gefitinib in Caucasian subjects.

Single oral dose administration of 250 mg (A) or 500 mg (B) gefitinib on day 4 alone or in the presence of 200 mg once daily itraconazole (left and right panels, respectively) [368]; (C) intravenous gefitinib infusion of a 50 mg (left) and 100 mg (right) dose in healthy Caucasian subjects [369]; (D) a 50 mg single intravenous infusion dose (5 min duration) administered to Caucasian Cancer patients; (E) a 100 mg once daily dose for three days in healthy Caucasian subjects [370].

Filled red circles and associated vertical lines indicate the observed mean and standard deviation from clinical data; solid black lines indicated predicted population mean plasma concentration profile and dotted lines indicate the corresponding 5th and 95th percentile range of the predicted mean.

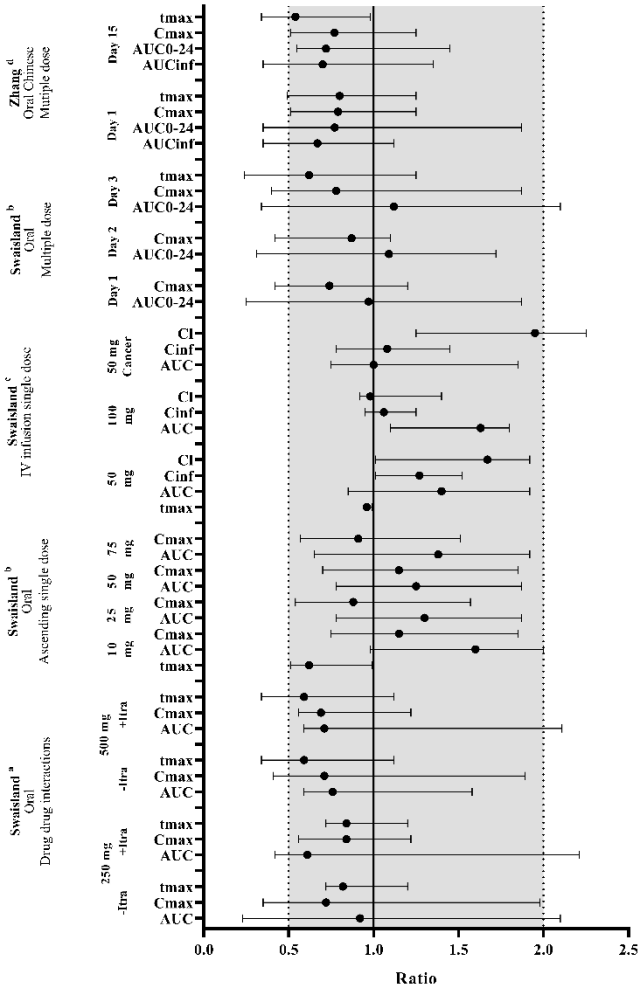

Figure 2.5 Model validation summary.

Forest plot showing the predicted mean ± SD over the observed ratio of pharmacokinetic parameters in subjects, with the dotted and shaded area representing the 2-fold range [0.5 to 2] and solid black line the line of unity. Caucasian: [a] [368]; [b] [370]; [c] [369]; Chinese: [d] [371]. Itra: itraconazole; AUC: area under the curve, C_{max}: peak plasma concentration; t_{max}: time to maximum plasma concentration; Cinf: concentration at the end of the infusion; Cl: Clearance; AUC_{0-24}: area under the curve for a 24-hour dosing period; AUC_{inf}: area under the curve to infinity.

2.4.2 Step 2: Development and validation of a virtual Chinese cancer population

The adaptation of the existing Simcyp Chinese population with elements of the pre-defined Simcyp Cancer population, was successfully confirmed with clinical patient demographic parameters being broadly within 90 % CI of the simulated values (Figure 2.5) without requiring optimisation.

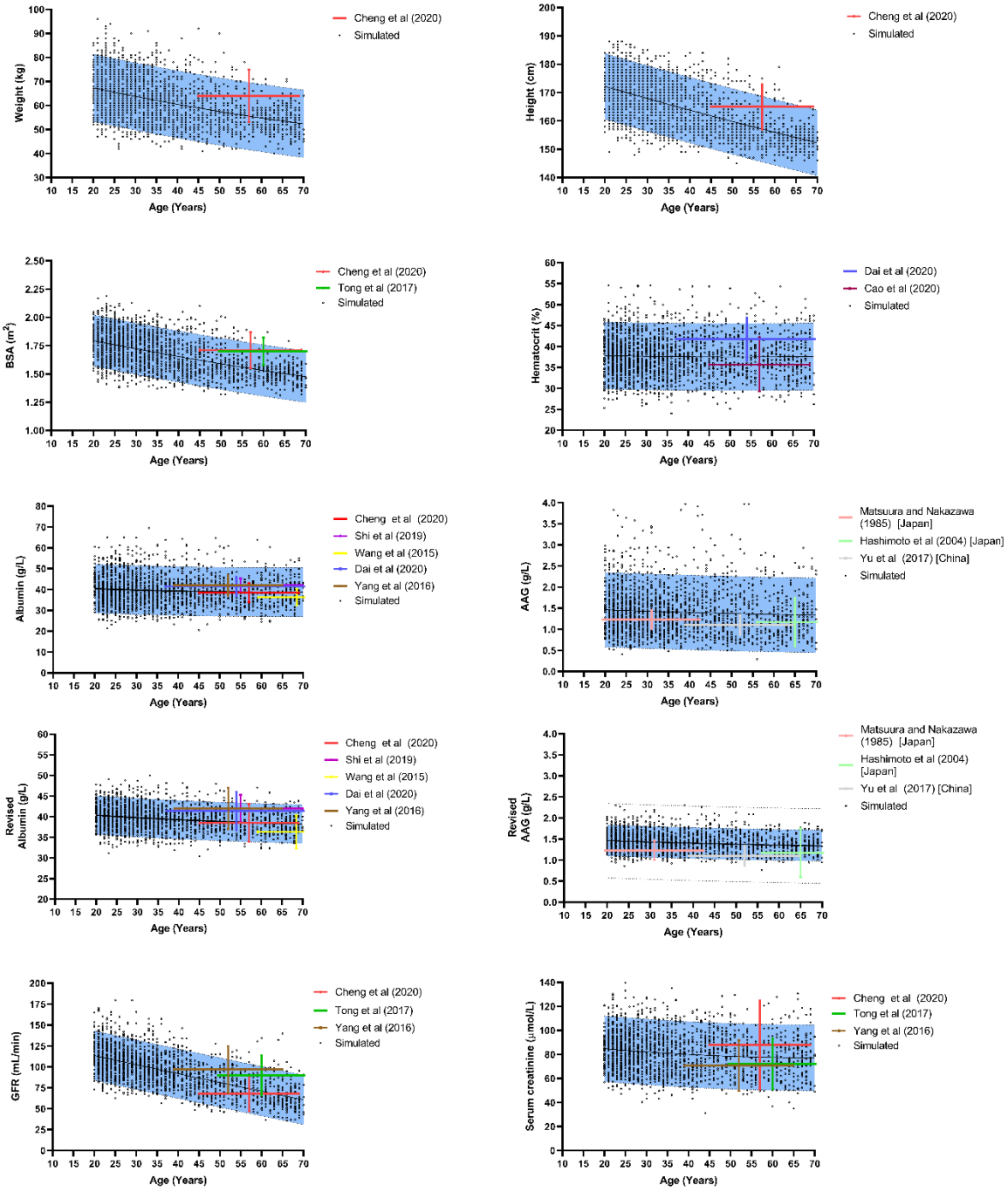

Figure 2.6 Validation of the Chinese cancer population.

The simulated weight, height, body surface area (BSA), haematocrit, albumin, alpha-1-acid glycoprotein (AAG), glomerular filtration rate (GFR) and serum creatinine as a function of age within the Chinese cancer (mixed gender) population. Blue shaded regions represent a 90% confidence interval from 2000 virtual individuals simulated (black circles) using Simcyp and the solid black line represents the mean values. The coloured bars represent mean and standard deviations obtained from literature studies. [372-381]

For albumin and AAG, a second population was simulated with a 50% reduction in% CV.

Model simulated plasma concentration-time profiles and pharmacokinetic parameters in the virtual Chinese cancer population were consistent with observed data and ranges for those reported [371] (Figure 2.6A) and were within 2-fold of the observed data (Figure 2.4) (Table S 2.6).

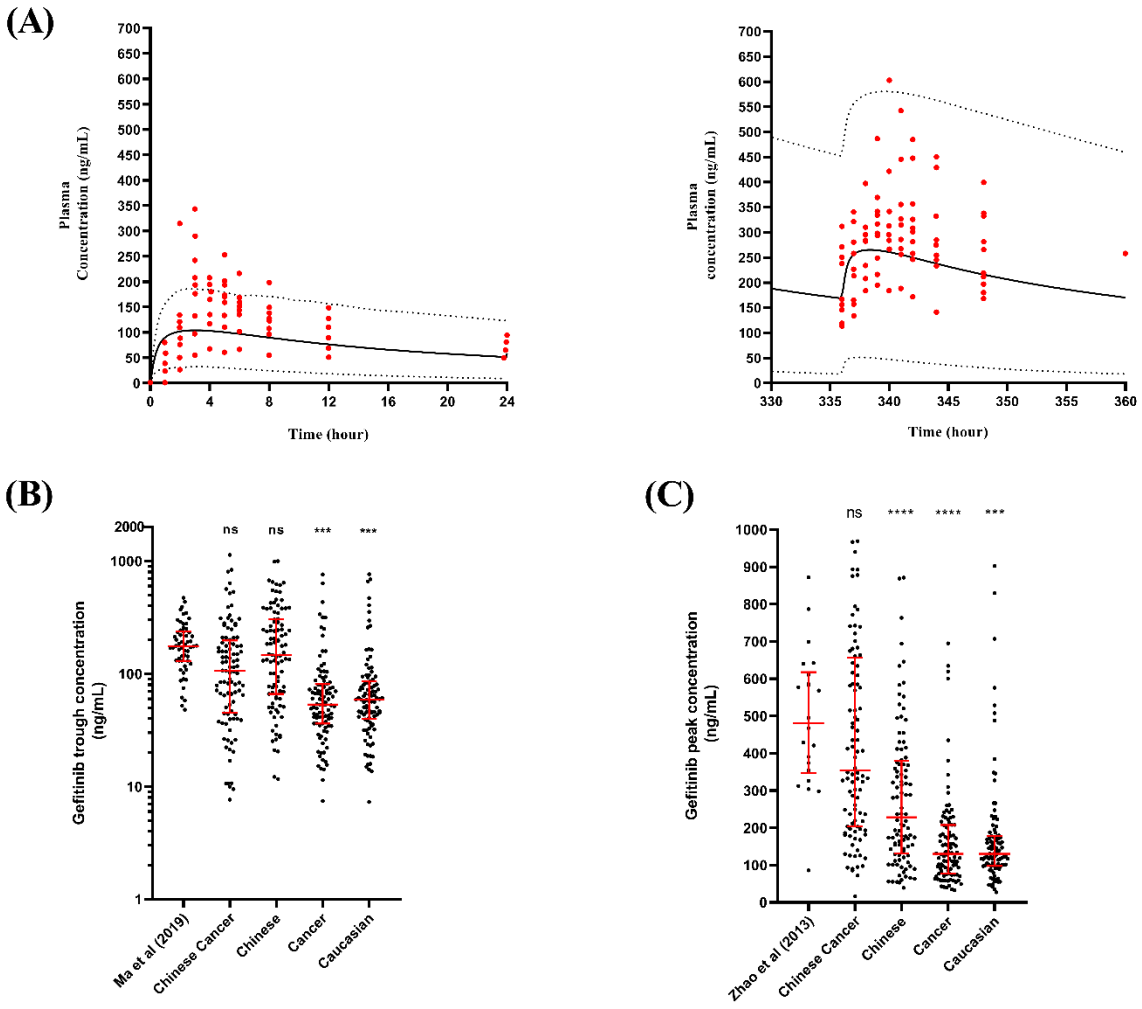

Figure 2.7 Gefitinib pharmacokinetics in Chinese cancer patients.

(A) Multiple oral 250 mg dose once daily for 15 days on day 1 (left panel) and day 15 (right panel) [5]; (B) Trough plasma concentration from 55 NSCLC patients dosed 250 mg once daily [382]; (C) Steady state peak plasma concentration from 22 NSCLC patients dosed 250 mg once daily [354].

(A) and (B): filled circles indicate the observed clinical data and dotted lines indicate the corresponding 5th and 95th percentile range of the predicted mean; (C) and (D): solid black circles indicate observed clinical concentrations for Ma et al. or Zhao et al. and simulated concentrations for other populations, with vertical red lines indicate interquartile range and horizontal lines indicated the observed or predicted median.

Simulated median trough plasma concentration in Chinese cancer (113.2 ng/mL) or Chinese (146.5 ng/mL) populations were not significantly different from those reported from 55 NSCLC

patients dosed 250 mg once daily [353], 175.5 ng/mL (Figure 2.6 B). However, statistically significant differences were demonstrated in the Simcyp Caucasian and Cancer population groups ($P < 0.05$) (Figure 2.6B) (Table S 2.7).

Similarly, predicted median peak plasma concentrations in Chinese cancer populations (299.7 ng/mL) were not significantly different from those reported concentrations from 22 NSCLC patients dosed 250 mg once daily (481 ng/mL) [354], but were significantly different in Simcyp Caucasian, Cancer and Chinese populations (Figure 2.6 C) (Table S 2.8).

2.4.3 Step 3: Comparison of the impact of drug-drug interactions on gefitinib pharmacokinetics between Caucasian and Chinese cancer populations

To address the potential impact of ethnicity on gefitinib use across oncology population groups, we assessed the extent of drug-drug interactions (DDIs) using a CYP 3A4 inhibitor (itraconazole), CYP 3A4 inducer (rifampicin) and a CYP 2D6 inhibitor (bupropion), in both Caucasian cancer and Chinese cancer groups.

For inhibitor studies with both itraconazole (Figure S 2.1 A) and bupropion (Figure S 2.1 C), the interaction resulted in an approximate 1.5-fold increase in AUC. The AUC Ratio and trough plasma concentration (C_{min}) ratio were greater for CYP 2D6 inhibition with bupropion compared to itraconazole but not statistically significantly different. However, the C_{max} ratio was statistically significantly higher for bupropion (1.59 ± 0.48) when compared to itraconazole (1.45 ± 0.31) ($P < 0.001$) (Table S 2.9). When compared to Caucasian cancer patients, the AUC ratio was not significantly different for itraconazole but was significantly different for bupropion (Caucasian: 1.34 ± 0.21; Chinese: 1.55 ± 0.34) ($P<0.001$). Furthermore, the C_{min} ratio was significantly different for bupropion (Caucasian: 1.42 ± 0.25; Chinese: 1.75 ± 0.62) ($P<0.001$) (Table S 2.10). Further, the inhibition of CYP 3A4 reduces fm_{3A4} (fraction of drug metabolised by CYP 3A4) by approximately 50 % in Chinese but 30 % in Caucasian subjects, with inhibition of CYP 2D6 reducing fm_{2D6} (fraction of drug metabolised by CYP 2D6) by approximately 12 % in Chinese and 7 % in Caucasian subjects (2.7.4 Section 4). C

In the presence of an inducer, rifampicin (Figure S 2.1B), the interaction resulted in an approximate 3.3-fold decrease in AUC ($P < 0.001$) with 2.5- and 4-fold decreases in C_{max} ratio and C_{min} ratio respectively (Table S 2.9). When compared to Caucasian Cancer patients, the AUC, C_{max} and C_{min} ratios were not significantly different (Table S 2.10). The induction of CYP 3A4 increased fm_{3A4} by approximately 2.2-2.4-fold in both Chinese and Caucasian and reduced fm_{2D6} by approximately 2-fold in both populations (2.7.4).

2.4.4 Step 4: The impact of drug-drug interactions on gefitinib pharmacokinetics in CYP 2D6 polymorphic Chinese cancer subjects

Following multiple dosing simulations, the presence of bupropion resulted in an increase in the plasma concentrations of gefitinib in all but the PM phenotype (Figure 2.10A) (Table 2.2). Furthermore, compared to EM subjects, UM phenotypes resulted in the largest decrease in plasma concentrations and PM the largest increase in plasma gefitinib concentrations (Figure 2.10A) (Table 2.2). When compared to EM, the changes in C_{max}, C_{min} and AUC were statistically significantly different in both the absence ($P < 0.001$) and presence ($P < 0.010$) of the interaction (Table 2.2) (Figure 2.11).

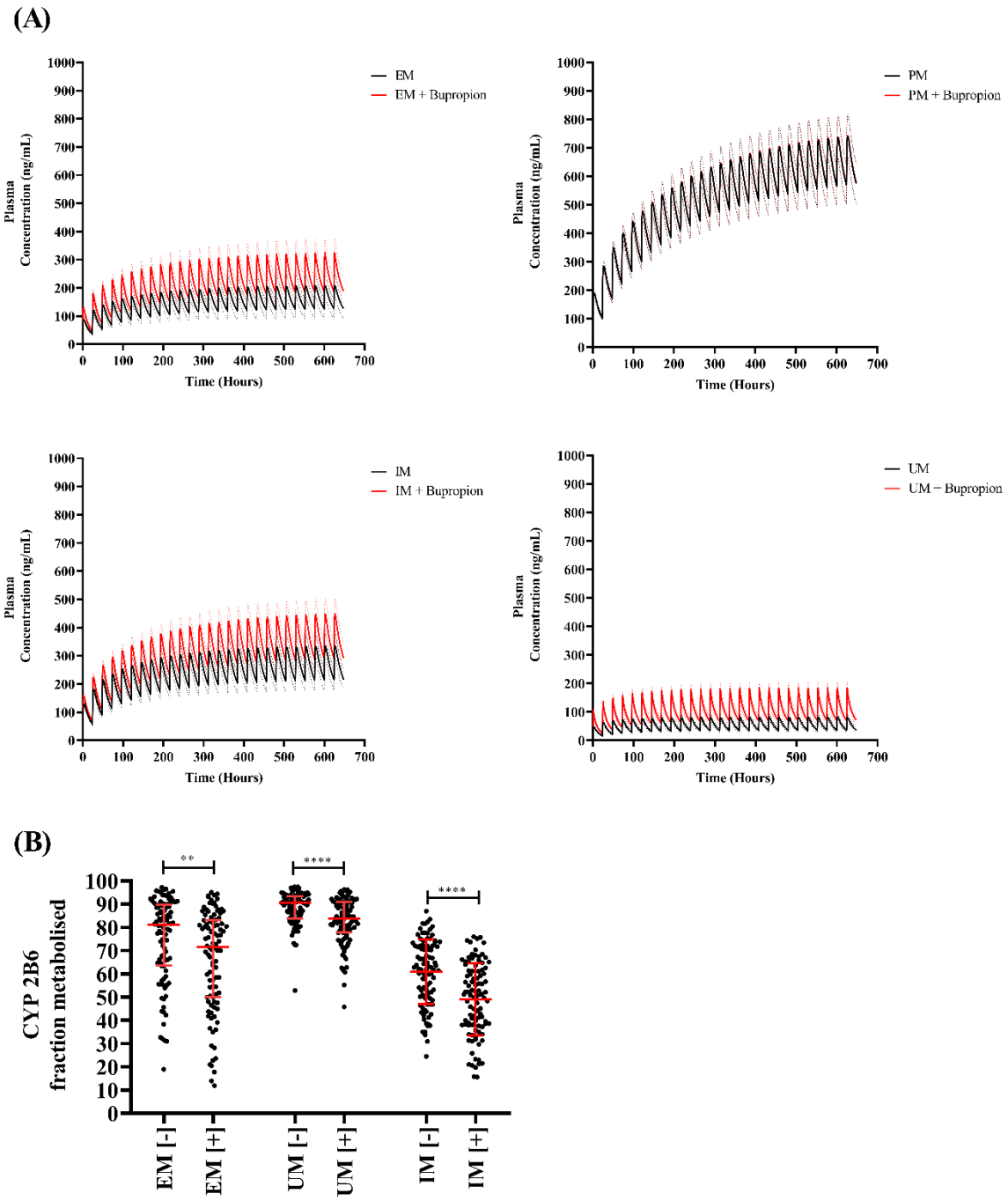

Figure 2.8 Gefitinib pharmacokinetics in Chinese cancer CYP 2D6 polymorphic patients.

The pharmacokinetics of gefitinib following multiple 250 mg once daily oral doses for 28 days dose in the absence (black) or presence (red) of bupropion, for (A) extensive metabolizers [EM], poor metabolizers [PM], ultrarapid metabolizers [UM] and intermediate metabolizers [IM], dotted lines indicate the corresponding 5th and 95th percentile range of the mean (solid line). (B) CYP2D6 fraction metabolized for EM, UM and IM (PM = 0). Solid circles represent simulated values with horizontal red lines representing media and 5th and 95th percentiles. ** $P < 0.01$; *** $P < 0.001$; **** $P < 0.0001$. Stars above data points indicates statistical testing between the control (EM) and phenotypes with matching study design (i.e., all [-] or all [+] bupropion).

		CYP 2D6 Polymorphism			
		EM	**PM**	**UM**	**IM**
Absence	AUC (ng/mL.h)	3991.14 (4563.97)	15809.15 (8943.55)	1356.2 (1069.29)	6589.44 (4823.40)
	T_{max} (h)	2.09 (0.81)	3.15 (0.63)	1.55 (0.6)	2.57 (0.73)
	C_{max} (ng/mL)	210.04 (200.08)	740.87 (382.92)	81.83 (53.74)	336.5 (207.89)
	C_{min} (ng/mL)	131.97 (181.21)	572.37 (356.23)	35.83 (34.09)	214.95 (187.99)
	CL (L/h)	154.7 (163.2)	22.60 (15.63)	311.6 (237)	58.64 (42.2)
	fm_{3A4}	25.28 (18.4)	100	11.59 (7.1)	39.09 (14)
	fm_{2D6}	81.15 (19.40)	0	90.41 (8.04)	60.91 (14)
Polymorph [a] ratio	AUC Ratio	-	3.96	0.34	1.65
	C_{max} Ratio	-	3.52	0.39	1.60
	C_{min} Ratio	-	4.33	0.27	1.63
Presence	AUC (ng/mL.h)	5941.38 (6076.58)	15810.32 (8944.2)	2666.34 (2261.09)	8786.03 (6574.28)
	T_{max} (h)	1.78 (0.76)	3.14 (0.63)	1.21 (0.46)	2.26 (0.71)
	C_{max} (ng/mL)	330.77 (255.86)	740.91 (382.95)	188.28 (107.66)	452.66 (274/81)
	C_{min} (ng/mL)	187.62 (235.02)	572.41 (356.28)	69.96 (73.4)	289.33 (256.07)
	CL (L/h)	93.2 (93.08)	22.60 (15.63)	166.8 (133)	45.11 (33.61)
	fm_{3A4}	28.23 (21.7)	100	17.16 (9.75)	50.93 (15.47)
	fm_{2D6}	71.98 (21.70)	0	83.85 (9.8)	49.07 (15.47)
Interaction summary [b]	AUC Ratio	1.61 (0.35)	1 (0)	1.95 (0.49)	1.33 (0.17)
	C_{max} Ratio	1.83 (0.49)	1 (0)	2.48 (0.6)	1.36 (0.17)
	C_{min} Ratio	1.51 (0.32)	1 (0)	2.05 (0.52)	1.33 (0.19)
Polymorph interaction ratio [c]	AUC Ratio	-	2.66	0.45	1.48
	C_{max} Ratio	-	2.24	0.57	1.37
	C_{min} Ratio	-	3.1	0.39	1.55

Table 2.2 The impact of CYP 2D6 polymorphisms on the extent drug interactions with bupropion for a 250 mg gefitinib dose.

AUC: area under the curve; C_{max}: maximum plasma concentration; C_{min}: minimum (trough) plasma concentration; T_{max}: time to maximum plasma concentration; CL: total clearance; fm_{3A4}: fraction of drug metabolised by CYP 3A4; fm_{2D6}: fraction of drug metabolised by CYP 2D6; Data reported as geometric mean and (standard deviation). [a] Ratio of each polymorph against EM for each pharmacokinetic parameter (C_{max}, C_{min} or AUC) in the absence of a drug interaction. [b] Ratio of each pharmacokinetic parameter (C_{max}, C_{min} or AUC) in the presence and absence of a drug interaction. [c] Ratio of each polymorph against EM for each pharmacokinetic parameter (C_{max}, C_{min} or AUC) in the presence of a drug interaction.

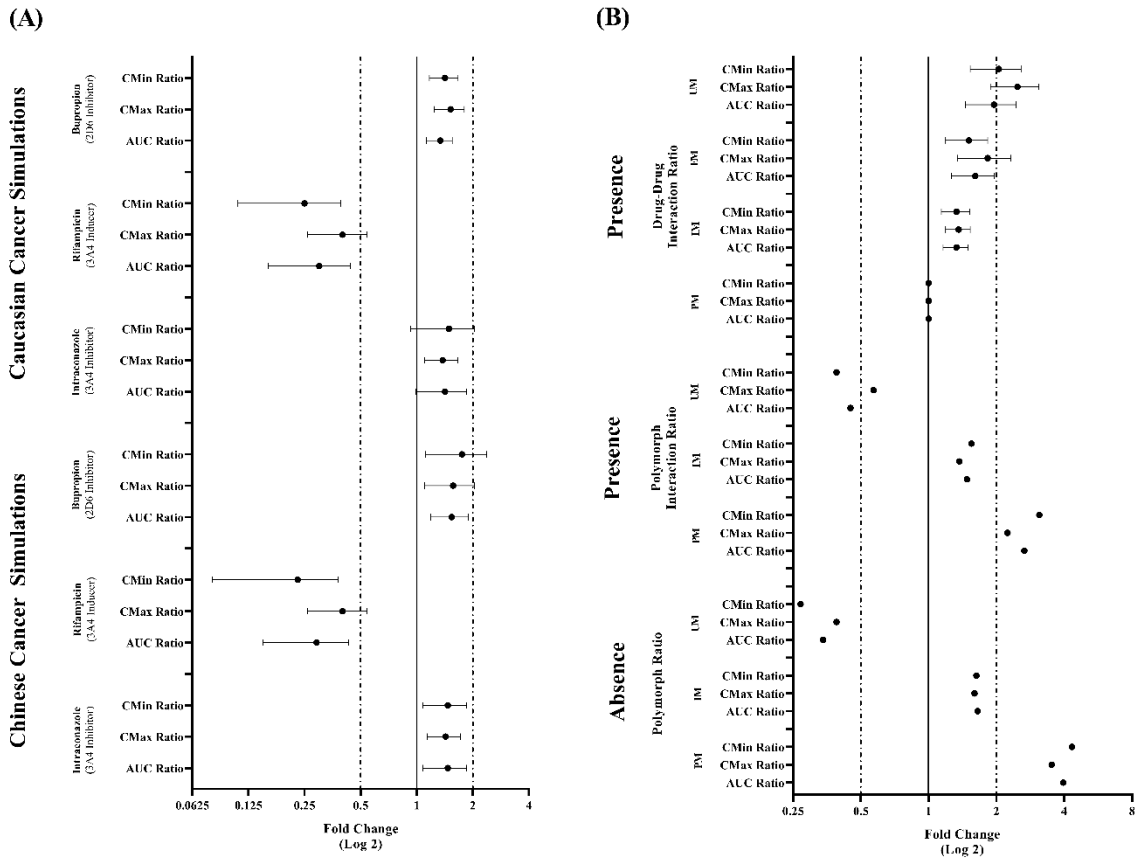

Figure 2.9 Forrest plot summary of the impact of drug-drug interaction simulations on gefinitib pharmacokinetics, conducted in Chinese and Caucasian simulated cancer popualtions.

Forest plots showing the predicted gefitinib mean ± SD ratios of area under the curve (AUC), peak plasma concentration (C_{max}) and trough plasma concentration (C_{min}). (A) Drug-drug interaction simulations in Chinese cancer and Caucasian cancer populations. (B) Drug-drug interaction simulations between gefitinib and bupropion in the Chinese cancer population for each CYP 2D6 polymorph (PM: poor metabolizer; IM: intermediate metabolizer; UM: ultrarapid metabolizer; EM: extensive metabolizer).

Polymorph ratio: the pharmacokinetic parameter in each polymorph relative to EM phenotype in the absence of a drug interaction; Polymorph interaction ratio: the pharmacokinetic parameter in each polymorph relative to EM phenotype in the presence of a drug interaction; Drug-drug interaction ratio: the pharmacokinetic parameter in the presence of the interaction relative to the absence for each polymorph.

The dotted line represents a 2-fold range [0.5 to 2] and solid black line the line of unity.

In the absence of bupropion, the impact of CYP 2D6 polymorphisms was assessed by comparing the 'polymorph ratios' (PR), (C_{max}, C_{min} and AUC for each phenotypes vs EM, all in the absence of the interaction). The predicted PR were broadly consistent for changes in AUC, C_{max} and C_{min}, ranging from 2.7-3.18 (PM), 0.25-0.34 (UM) and 1.23-1.58 (IM) for (Table 2.2). When compared to EM, the fraction metabolised by CYP 3A4 (fm_{3A4}) decreased by 63 % for UM and increased by 46 % for IM (Figure 2.11). Whereas the fraction metabolized by CYP

2D6 (fm_{2D6}) increased by 27 % for UM and decreased by 19 % for IM (Figure 2.10B) (Figure 2.11). As expected, phenotypes demonstrated statistically significant lower (PM and IM) or higher (UM) clearances in the absence of bupropion ($P < 0.001$) (Table 2.2).

In the presence of bupropion, the impact of the DDI on each polymorph was assessed by comparing the C_{max}, C_{min} and AUC ratios (presence vs absence of bupropion). These were broadly consistent, ranging from 1.48-1.79 (EM), 1 (PM), 1.92-2.40 (UM) and 1.29-1.32 (IM) (Table 2.2) (Figure 2.11). In the presence of bupropion, fm_{3A4} decreased by 35 % for UM and increased by 21 % for IM, compared to EM (Table 2.2) (Figure 2.11). Whereas fm_{2D6} increased by 5 % for UM and decreased by 15.6 % for IM, compared to EM (Table 2.2) (Figure 2.10B) (Figure 2.11).

In the presence of bupropion, phenotypes demonstrated statistically significant differences in clearance ($P < 0.001$) (Table 2.2), which decreased by 39 % (EM), 18 % (IM) and 50 % (UM).

The impact of CYP 2D6 polymorphisms in the presence bupropion, was assessed by comparing the 'polymorph interaction ratio' (PIR) (C_{max}, C_{min} and AUC for each phenotypes vs EM, all in the presence of the interaction). The PIR was broadly higher for PM and IM phenotypes but lower for UM phenotypes (Table 2.2), with decreases reported for trough concentrations (C_{min}) PIR for PM (22 %) and IM (16 %) but an increase for UM (48 %) (Figure 2.11).

When assessing the percentage of subjects with trough concentrations below 200 ng/mL for a 250 mg daily dose, the interactions resulted in only a moderate decrease, approximately 10 %, in EM and UM groups and 22 % decrease for IM (Table 2.3). Furthermore, subjects possessing trough concentration below 50 ng/mL were high both in the absence (80 %) and in the presence (56 %) of an interaction for UM (Table 2.3). Whereas for IM this was 8 % and 5 % (Table 2.3).

When this dose was increased to 500 mg once daily, for EM and PM subjects the percentage of subjects with trough concentrations below 200 ng/mL decreased both in the absence and presence of bupropion (Table 2.3). However, for UM these remained high (absence: 95 %; presence: 80 %), with IM phenotypes presenting with lower numbers of subjects, 25 % (absence) and 17 % (presence) (Table 2.3).

	Trough concentration (ng/mL)	*CYP 2D6 Polymorphism*							
		EM		**PM**		**UM**		**IM**	
		250 mg	**500 mg**	**250 mg**	**500 mg**	**250 mg**	**500 mg**	**250 mg**	**500 mg**
Absence	*≤200*	83	60	14	3	99	95	62	25
	100-199	23	20	11	3	4	11	37	17
	50-99	21	20	3	0	14	29	17	7
	<50	39	20	0	0	80	55	8	1
Presence	*≤200*	72	49	14	3	92	80	48	17
	100-199	27	25	11	3	13	24	31	12
	50-99	21	12	3	0	23	26	12	4
	<50	24	12	0	0	56	30	5	1

Table 2.3 Percentage of subjects with trough concentrations below a pharmacodynamic cut-off in polymorphic subjects.

Percentage of subjects with gefitinib trough concentrations, following a 250 mg or 500 mg once daily dose, below the therapeutic window, in the absence of presence of bupropion, demarking for CYP2D6 phenotype (EM: extensive metabolizer; PM: poor metabolizer: UM: ultrarapid metabolizer).

2.5 Discussion

Globally, lung cancers are a common cause of cancer related deaths [284], with NSCLC contributing to approximately 85 % of all lung cancers [284, 285]. Furthermore, the prevalence of lung cancer is high across China and is expected to increase by approximately 40 % by 2030 [297]. A common anticancer agent used to treat NSCLC is gefitinib, an inhibitor of the EGFR TK domain. Gefitinib significantly improves the survival of patients with advanced lung adenocarcinoma [383]. However, confounding treatment is the uncertainly of the impact of CYP 2D6 polymorphisms on the potential requirement for dose titrations, which may be necessary to optimise anticancer activity in addition to reducing the occurrence of adverse drug reactions such as, rash, liver dysfunction and diarrhoea [384, 385].

This study built upon existing studies reporting a PBPK model for gefitinib [334, 386], by conducting an extensive validation with a variety of single and multiple dose studies, with oral and IV-infusion dosing routes. In validation studies with both healthy Caucasian and Chinese subjects, predicted gefitinib plasma concentrations were within the range reported in clinical studies (Figure 2.3) and mean predicted pharmacokinetics parameters were all within 2-fold of those reported (Figure 2.4). T_{max} tended to be underpredicted but within the 2-fold boundary. This may be a result of the wide inter-subject variability in oral absorption pharmacokinetics [339, 340, 387-390], with a similar underprediction reported by Chen *et al* (2018) [318]. This is likely to be a result of typical inter-subject variability in GI physiology or the result of variation in gastric emptying in addition to precipitation/dissolution of gefitinib in the GI tract [387, 388, 390]. In addition, the post-prandial increase in stomach pH could alter the dissolution/solubility of gefitinib, however this would be balanced against the increased gefitinib solubility offered by the increased bile salts and volume expansion in the small-intestine, which together may contribute to this wide variability [313].

Furthermore, for the IV-infusion validation studies (Table S 2.4), all pharmacokinetic parameters were predicted to within 2-fold of those reported, however an overprediction was noted for the prediction of clearance from these studies [313], albeit still within the 2-fold criterion. This may, in part, be due to the approach at estimating an appropriate intrinsic clearance by Chen at al [318], and given the polymorphic nature of CYP 2D6, the prediction of clearance could be improved through better *in-vitro* estimates for each polymorph.

Having confirmed the robustness of the model in a wider range of retrospective clinical studies when compared to previous attempts by others [318, 386], we next combined both the Simcyp Cancer (based on Caucasian subjects) and Simcyp Chinese populations (Figure 2.5). We adapted the existing Chinese population to account for the physiological alterations previously reported [329] to occur in the oncology population group, namely reduced haematocrit,

increased α-1 acid glycoprotein and decreased albumin and reduced GFR [341]. Parameters describing the mean and % CV for these changes were taken from the Simcyp Chinese population. Chinese cancer patients tended to be older, typically > 40 years old (Figure 2.5). However, a population of 2000 subjects aged 20-70 year old were simulated, and demographic parameters were compared with reported variances for key changes within the adapted population (Figure 2.5) [342, 344, 346-348]. The resulting analysis demonstrated that the mean and 90 % prediction intervals were within the range (mean and standard deviation) reported in studies (Figure 2.5). To further validate the adaptions to the population, we utilised three reports of gefitinib plasma concentrations in Chinese cancer patients. Simulations were able to recapitulate the spread of observed gefitinib plasma concentrations (Figure 2.6A), with calculated parameters within 2-fold of those reported (Figure 2.3) (2.7.3) (Figure 2.6B and 6C). Higher AUC and trough concentrations have been reported previously in Chinese vs Caucasian healthy subjects and Chinese cancer vs Caucasian cancer subjects [391, 392]. The peak and trough plasma concentrations between Caucasian and Chinese (in both healthy volunteer and cancer) subjects showed clear differences, with Chinese subjects demonstrating higher predicted plasma concentrations in all cases when compared to Caucasian subjects (Figure S2.7 and Figure S 2.8). Such difference may be driven by physiological and biochemical differences between the ethnicities and between their health status (healthy or cancer), and may include changes such as impaired hepatic [329] and renal function [330], lower albumin/higher α-1-acid glycoprotein and altered functional metabolic capacity of the liver [331], in addition to more direct prominent physiological differences when comparing Chinese population groups to Caucasian population groups, such as differences in body weight, liver size, functional metabolic capacity of the liver and variations in polymorphic frequencies of CYP-isozymes [332, 333].

The prevalence of drug-drug interactions is significant in cancer chemotherapy. Cytotoxic agents are often administered in combination to achieve maximum therapeutic outcomes, which can often lead to significant interpatient variability as a result of drug interactions [393, 394]. Given that the primary metabolism pathways for gefitinib are CYP 3A4 (fm_{3A4} ~30-40 %) and CYP 2D6 (fm_{2D6} ~60-70 %) [316, 317], and that the former may contribute to the wide inter-individual variability [325, 395, 396] and the latter a cause of potential phenotype based variations in plasma levels [397], we considered DDIs for CYP 3A4 inhibition (itraconazole) and 3A4 induction (rifampicin) and a CYP 2D6 inhibition (bupropion).

For inhibition studies, the C_{max} ratio for bupropion was significantly different when compared to itraconazole, suggesting gefitinib plasma concentrations are more susceptible to CYP 2D6 inhibition than CYP 3A4 inhibition (Figure 2.11). When compared with Caucasian cancer subjects, only bupropion demonstrated a statistically significant difference in C_{min} ratio and

AUC ratio (Figure 2.11). The cause of this difference may be related the more prevalent CYP 2D6 polymorphic frequencies in Chinese patients and is further discussion in subsequent sections.

In the presence of rifampicin, a potent CYP 3A4 inducer, deceases in AUC, C_{max} and C_{min} were similar to those reported by Swaisland *et al* (2005) [339] in healthy Caucasian subjects (Figure 2.11). Further, the extent of the interaction was similar in both Caucasian and Chinese cancer subjects, with no statistically significant differences. As expected, the presence of the CYP 2D6 phenotypes within the Chinese population (EM: 59.7 %; PM: 3 %; IM: 39 %; UM: 1 %) may have contributed to a differential outcome for DDIs compared to Caucasian population (EM: 86.5 %; PM: 8.2 %; IM: 0 %; UM: 5.3 %) and this was further assessed in specific CYP 2D6 phenotypes with drug interactions with bupropion (Table 2.2) (Figure 2.11).

In the absence of a drug interaction, PM and UM expectedly demonstrated opposing effects on AUC, C_{max} and C_{min} (Table 2.2) (Figure 2.11). The inhibitor effects of bupropion on CYP 2D6 expectedly reduced fm_{2D6} for all phenotypes (except PM), with a concomitant increase in fm_{3A4} with IM demonstrating also equivalent contributions from each isozyme.

When attempting to translate the complexities associated with DDI affecting polymorphic CYP isozymes, we finally compared the number of subjects with predicted trough concentration either (i) < 50 ng/ml, (ii) 50-99 ng/mL, (iii) 100-199 ng/mL and (iv) ≤200 ng/mL (Table 2.3). The therapeutic range is thought to be wide, ranging from 10-5000 ng/mL [319] however pharmacodynamic trough concentration are suggested to be > 200 ng/mL [320-322].This is primary based around assessment of median overall survival (OS) metrics, in wild-type and EGFR-mutated NSCLC [321, 398].

At the dose studied, 250 mg once daily, a high proportion of subjects (>70 %) demonstrated trough concentrations < 200 ng/mL in both the absence and presence of bupropion, for EM and UM phenotypes. For UM phenotypes, in the absence of an interaction 80% of subjects possess though concentration of < 50 ng/mL, which decreased to 56 % in the presence of the interaction (Table 2.3). However, given that the frequency of UM within the Chinese population is low (~1 %), this may be less relevant than compared to the IM frequency (30-50 %), where higher doses, 500 mg once daily, resulted in the 25 % and 17 % of subjects with trough concentrations below 200 ng/mL (Table 2.3).

For EM phenotypes, the high percentage of subjects with trough levels below 200 ng/mL would indicate the possibility of subtherapeutic levels. However, steady state trough levels following a 250 mg dose in a Chinese cancer population have been reported to span a range of approximately 40-500 ng/mL [353], with over 60 % of their reported subjects have trough

concentrations lower than 200 ng/mL. When considering the range reported by Ma *et al* [353], we simulated a similar range (39 %) of subjects demonstrated trough concentration less than 50 ng/mL. However, a dose increase to 500 mg results in a 28 % (absence) and 32 % (presence) decrease in the number of subjects with trough levels below 200 ng/mL.

The UM phenotype demonstrated nearly all subjects (99 %) possessed trough levels below 200 ng/mL and 80 % below 50 ng/mL. There is currently a paucity investigating the pharmacokinetics of gefitinib in UM phenotypes, and the importance of assessing its impact on gefitinib has been previously indicated by regulators [399]. This may partly be a result of the complexity associated with relating genotype to specific phenotypes [400]. Furthermore, in the context of the Chinese population group, the frequency is low (~1 %). Nevertheless, further work is necessary to investigate the impact of UM phenotype of the need for dose adjustments, given the higher frequency of the UM phenotypes in both African, Middle East and Caucasian population groups (5-8 %) [401]. Furthermore, the availability of more specific intrinsic clearances for each CYP 2D6 polymorph, may improve the application of the model in the Chinese population.

For CYP 2D6 PM phenotypes, trough plasma concentrations were simulated to be almost 3 times higher than the suggested target trough of 200 ng/mL. Whilst this may be beneficial for therapy, NSCLC patients with activating epidermal growth factor receptor (EGFR) mutants tend to be highly responsive for gefitinib [385, 402], and potentially up to 50 times as sensitive [403]. Furthermore, a common adverse reaction is a gefitinib-induced rash which can occur at frequency of between 30 % - 87 %, with a severe form having an incidence of 7 %−22 %, and which can result in treatment cessation [402, 404]. For PM subjects, at such increased trough gefitinib plasma concentrations, the incidence of skin rashes may be high [321], albeit it with a lower risk within the Chinese population due to low frequencies of the PM phenotype. More commonly however are IM phenotype, was in the absence and presence of bupropion, a 250 mg dose resulted in trough levels broadly in-excess of the 200 ng/mL cut-off and within a range reported by other studies [320-322].

Whilst the requirement for TDM for gefitinib is currently not mandatory, at a standard dose of 250 mg once daily, a significant number of subjects possess maintenance trough levels below 200 ng/mL. Furthermore, the contribution of CYP3A4 to gefitinib metabolism may add to the wide inter-individual variability simulated within our studies and also reported in clinical studies [395, 396]. Current clinical guidelines advocate the 250 mg once daily rather than a higher dose of 500 mg once daily due to a lack of a clinical difference at the higher doses [405, 406]. However our results demonstrate that a dose increase to 500 mg once daily may be warranted to increase trough concentrations and prolong response to treatment [398], particularly in EM

and IM phenotypes. However, for the UM phenotype, further research is required to clinically explore the relationships between resultant lower gefitinib trough concentrations and a pharmacodynamic response.

The polymorphisms associated with CYP 2D6 are well characterised, however surprisingly the potential impact of these polymorphisms on gefitinib dosing is sparse and further research is required to examine this. Furthermore, given the differences in CYP 2D6 polymorph frequencies in Chinese subjects compared to Caucasian subjects, the model presented could be updated in the future to address the paucity in current knowledge surrounding the metabolism pathway fractions (i.e., $fm_{CYP\ 2D6}$ and $_{3A4}$) in relation to how clearance is influenced by CYP 2D6 polymorph frequencies in Chinese cancer subjects.

PBPK modelling, as demonstrated by our study and others [318], provides the potential to investigate the complexity associated with CYP isozyme related polymorphism in complex pathophysiological states such as Cancer, where the risk of drug-drug interactions are common, particularly where the polymorphic frequencies are not examined in detail due to low frequencies. Furthermore, although TDM is not formally part of gefitinib dosing, further clarity on the proposed plasma concentration dosing window is required to fully exploit clinical outcomes.

2.6 Conclusion

This study developed and validated a Chinese Cancer population group using the Simcyp Simulator, with which the impact of CYP 2D6 polymorphism and CYP 2D6 inhibition (by bupropion) were investigated to assess the need for dose titrations. The model demonstrated that for the two most prominent CYP 2D6 phenotypes within the Chinese population, namely EM and IM, a dose increase to 500 mg once daily would better target a suggested target trough concentration. However, further work is required to better define the target plasma concentrations.

2.7 Supplementary materials

2.7.1 Section 1

Parameters	Gefitinib	Notes
Compound type	Weak Base	
Molecular weight (g/mol)	446.9	
Log P	4.15 [a]	
fu	0.089 [b]	
pKa 1	5.42	
B/P	0.8	
Vss (L/kg)	24.4	Full PBPK model with optimised Kp scalar of 0.41
k_a (h^{-1})	0.15	Optimised
fa	1	
$CLint_{3A4}$ (µL/min/pmol)	0.42	Optimised
$CLint_{2D6}$ (µL/min/pmol)	25	Optimised
Absorption Model	First Order	
Distribution Model	Full PBPK	

Table S 2.1 Gefitinib model parameters.

Unless otherwise stated, data obtained/adapted from Chen *et al* (2017) [318]. B/P, ratio of concentration of drug in blood to that in plasma; C_{Lint}, intrinsic metabolic clearance for each CYP isozyme; 2D6, cytochrome P450 2D6; 3A4, cytochrome P450 3A4; fa, fraction of dose absorbed; fu, unbound fraction of drug in plasma; ka, first-order absorption rate constant; Log P, partition coefficient; pKa, acid dissociation constant; Vss, volume of distribution at steady state; Optimised, model parameters were optimised to produce parameters with better certainty, and which best recovered published clinical drug profiles during stages 1 and 2 (see Methods). Parameter optimisation was conducted with the Weighted Least Square (WLS) approach and the Nelder-Mead minimisation method on Simcyp®.

2.7.2 Section 2: Validation

		-Itraconzaole		+Itraconzaole	
	Parameters	**Observed**	**Predicted**	**Observed**	**Predicted**
250 mg	$AUC_{(0-\infty)}$ (ng/mL.h)	2968 (1310-7140)	2716.39 (672.30-27120.30)	5348 (2060-18400)	3266.12 (728.50-38187.54)
	C_{max} (ng/mL)	103.3 (51.5-194)	70.22 (29.13-172.84)	155.9 (69-400)	130.78 (38.09-348.15)
	T_{max} (h)	5.0 (3.0-7.0)	4.08 (1.96-8.31)	5.0 (3.0-7.0)	4.38 (1.97-8.32)
500 mg	$AUC_{(0-\infty)}$ (ng/mL.h)	6921 (4790-14200)	5289.45 (1346.48-54299.42)	10919 (4090-27100)	7645.46 (800.07-73688.74)
	C_{max} (ng/mL)	227.8 (70.1-638)	162.29 (38.26-461.69)	301.8 (117-654)	210.80 (46.19-696.30)
	T_{max} (h)	5.0 (3.0-24.2)	2.94 (1.65-6.62)	5.0 (3.0-7.0)	2.94 (1.65-6.62)

Table S 2.2 Pharmacokinetics parameters for single dose studies of gefitinib in the absence and presence of 200 mg itraconazole daily.

$AUC_{(0-\infty)}$: area under the curve from time 0 to infinity, C_{max}: maximum concentration; T_{max}: time to maximum concentration.

Geometric means (range): AUC and C_{max}; Median (range): T_{max}. Observed data obtain from Swaisland *et al* (2005) [339].

Dose (mg)	Parameters	Observed	Predicted
10	$AUC_{(0-24)}$ (μg/L.h)	34.9 (22.2-53.0)	57.45 (13.54-130.27)
	C_{max} (μg/L)	2.6 (1.5-4.2)	3.05 (0.64-8.05)
	T_{max} (h)	5.5 (5.0-7.0)	3.4 (1.75-9.11)
25	$AUC_{(0-24)}$ (μg/L.h)	78.8 (52.5 -118)	104.28 (28.86-315.68)
	C_{max} (μg/L)	6.8 (4.0 - 11.8)	6.09 (1.09-17.63)
	T_{max} (h)	5.0 (3.0 - 7.0)	3.4 (1.75-9.11)
50	$AUC_{(0-24)}$ (μg/L.h)	171.6 (97.6-246.4)	214.16 (67.71-851.36)
	C_{max} (μg/L)	13.1 (9.4-16.8)	15.45 (3.19-45.26)
	T_{max} (h)	5.5 (5.0-7.0)	3.4 (1.75-9.11)
75	$AUC_{(0-24)}$ (μg/L.h)	291.9 (179.9-392)	397.91 (86.57-1027.04)
	C_{max} (μg/L)	24.9 (15.8-33.3)	22.68 (4.28-62.89)
	T_{max} (h)	5.0 (5.0-5.0)	3.4 (1.75-9.11)

Table S 2.3 Summary pharmacokinetics parameters for different single dose studies of gefitinib in the purpose of validation in healthy male subjects.

AUC: area under the curve determined over a 24-hour period; C_{max}: maximum concentration; T_{max}: time to maximum concentration. Geometric means (range): AUC and C_{max}; Median (range): T_{max}. Observed data obtain from Swaisland *et al* (2001) [340].

	PK Parameters	Observed	Predicted
50 mg	AUC $_{(0-24)}$ (ng/mL.h)	601 (548-727)	859.5 (556.12-1482.49)
	C_{inf}	115 (97-143)	140.2 (96-157.21)
	T_{max} (h)	1.0 (1.0-1.1)	0.96 (0.95-1.05)
	Cl (mL/min)	693 (471-885)	1004 (555-1466)
100 mg	AUC $_{(0-24)}$ (ng/mL.h)	1050 (917-1330)	1718 (1112.24-2564.97)
	C_{inf} (ng/mL)	223 (190-301)	238.2 (192.2-314.34)
	T_{max} (h)	1.0 (1.0-1.1)	0.96 (0.95-1.05)
	Cl (mL/min)	1020 (759-1250)	1004 (555-1466)
50 mg Cancer	AUC $_{(0-24)}$ (ng/mL.h)	791 (447-1230)	792.06 (545.31-1516.50)
	C_{inf} (ng/mL)	2231 (823-4300)	2424.8 (1983-3078)
	T_{max} (h)	na	na
	Cl (mL/min)	514 (194-1460)	1004 (555-1466)

Table S 2.4 Pharmacokinetics parameters following an intravenous infusion of single doses in healthy male subjects and cancer patients.

$AUC_{0-\infty}$: Area under the curve from 0 to infinity; AUC_{0-24}: area under the curve for a 24 hours period on the specific dosing period; T_{max}: time to maximum plasma concentration. Geometric means (range): AUC, C_{inf}, Cl; Median (range): T_{max}. Observed data obtain from Swaisland *et al* (2005) [313].

Parameter	Days	Observed	Predicted
AUC_{0-24} (μg/L.h)	Day 1	502 (217-818)	490.39 (95.95-1873.14)
	Day 2	737 (342-1194)	808.15 (108.66-1358.40)
	Day 3	994 (482-1663)	1114.11 (128.51-4296.27)
$AUC_{0-\infty}$ (μg/L.h)	Day 3	2236 (917-4731)	2322.27 (705.01-5279.45)
C_{max}(μg/L)	Day 1	39.5 (16.7-71.0)	29.54 (5.97-89.45)
	Day 2	47.1 (22.6-79.4)	41.68 (19.74-76.20)
	Day 3	63.6 (33.3-97.5)	49.79 (7.9-203.40)
T_{max} (h)[b]	Day 1	5.0 (3.0-7.0)	3.1 (1.58-6.91)
	Day 2	5.0 (3.0-8.0)	3.1 (1.58-6.91)
	Day 3	6.0 (5.0-7.0)	3.1 (1.58-6.91)

Table S 2.5 Pharmacokinetics parameters following multiple doses of gefitinib in healthy male subjects.

$AUC_{0-\infty}$: Area under the curve from 0 to infinity; AUC_{0-24}: area under the curve for a 24 hours period on the specific dosing period; C_{max}: maximum plasma concentration; T_{max}: time to maximum plasma concentration. Geometric means (range): AUC and C_{max}; Median (range): T_{max}. Observed data obtain from Swaisland *et al* (2001) [313].

2.7.3 Section 3: Validation in Chinese cancer patients

Parameters	Day 1		Day 15	
	Observed	Predicted	Observed	Predicted
$AUC_{0-\infty}$ (ng/mL.h)	6397 (35)	3951.92 (48)	18101 (62)	12752 (51)
AUC_{0-24} (ng/mL.h)	3436 (20)	2648.11 (20)	7978 (29)	5812.18 (36)
C_{max} (ng/mL)	272 (31)	212.82 (39)	465 (28)	359.78 (42)
T_{max} (h)	3 (3-6)	2.41 (0.51-11.41)	4 (3-6)	2.16 (0.51-4.82)

Table S 2.6 Pharmacokinetics parameters for a single and a multiple dose study of gefitinib in Chinese cancer subjects.

$AUC_{0-\infty}$: Area under the curve from 0 to infinity; AUC_{0-24}: area under the curve for a 24 hours period on the specific dosing period; C_{max}: maximum plasma concentration; T_{max}: time to maximum plasma concentration. Geometric means (% CV): AUC, C_{max}. Median (range): t_{max}. Observed data obtain from Zhang *et al* (2020) [371].

	Trough plasma concentration (ng/mL)			
	Geometric mean	**Median**	**25% Percentile**	**75% Percentile**
Ma *et al* (2019)	170.3	175.5	130.3	237.5
Chinese cancer	97.75	106.5	45.04	197.1
Chinese	138.7	146.5	66.14	302.7
Cancer	57.2	53.44	36.12	80.76
Caucasian	61.53	59.1	39.66	85.71

Table S 2.7 Steady state trough plasma concentration from 58 NSCLC patients dosed 250 mg once daily.

Trough plasma concentrations reported from Ma *et al* (2019) [353] and simulated in the Chinese cancer, Chinese Healthy Volunteer, Cancer and Caucasian Healthy Volunteer Simcyp populations.

	Peak plasma concentration (ng/mL)			
	Geometric mean	**Median**	**25% Percentile**	**75% Percentile**
Zhao et al (2011)	449.7	481	347	617.5
Chinese cancer	293.1	295.2	169.3	546.6
Chinese	222.1	228.4	131.4	380.1
Cancer	131.9	130.0	76.65	207.6
Caucasian	137.6	130.1	97.50	177.7

Table S 2.8 Steady state peak plasma concentration from 22 NSCLC patients dosed 250 mg once daily.

Trough plasma concentrations reported from Zhao *et al* (2011) [354] and simulated in the Chinese cancer, Chinese Healthy Volunteer, Cancer and Caucasian Healthy Volunteer Simcyp populations.

2.7.4 Section 4: Drug-drug interactions

		3A4		2D6
		[Inhibitor]	*[Inducer]*	*[Inhibitor]*
		Itraconazole	**Rifampicin**	**Bupropion**
Absence	AUC (ng/mL.h)	17304.51 (22474.71)	14080.86 (17088.67)	17304.51 (22474.71)
	T_{max} (h)	2.34 (0.76)	2.33 (0.75)	2.34 (0.76)
	C_{max} (ng/mL)	278.97 (237.16)	279.01 (237.21)	278.97 (237.16)
	C_{min} (ng/mL)	55.59 (99.72)	80.95 (129.48)	55.59 (99.72)
	fm_{3A4}	31.67 (19.4)	31.67 (19.4)	31.67 (19.4)
	fm_{2D6}	68.3 (19.41)	68.3 (19.41)	68.3 (19.41)
Presence	AUC (ng/mL.h)	32167.55 (54824.08)	3291.85 (3581.58)	24822.14 (30438.71)
	T_{max} (h)	2.59 (0.91)	1.57 (0.44)	1.95 (0.73)
	C_{max} (ng/mL)	453.97 (505.16)	99.59 (75.64)	389.14 (294.19)
	C_{min} (ng/mL)	113.59 (257.45)	12.55 (17.94)	85.23 (143.02)
	fm_{3A4}	17.62 (14.20)	72.17 (19.23)	41.06 (22.13)
	fm_{2D6}	82.38 (14.2)	27.83 (19.23)	59.94 (22.13)
Interaction Summary [a]	AUC Ratio	1.47 (0.36)	0.29 (0.14)	1.54 (0.35)
	C_{max} Ratio	1.43 (0.29)	0.4 (0.14)	1.57 (0.47)
	C_{min} Ratio	1.47 (0.39)	0.23 (0.15)	1.75 (0.63)

Table S 2.9 The impact of drug-drug interactions on gefitinib pharmacokinetics in Chinese cancer populations.

AUC: area under the curve; C_{max}: maximum plasma concentration; C_{min}: minimum (trough) plasma concentration; T_{max}: time to maximum plasma concentration. Data reported as geometric mean and (standard deviation). [a] Ratio of each pharmacokinetic parameter (C_{max}, C_{min} or AUC) in the presence and absence of a drug interaction. fm_{3A4}: fraction of drug metabolized by CYP 3A4; fm_{2D6}: fraction of drug metabolised by CYP 2D6. Data reported as geometric mean and (standard deviation).

		3A4		2D6
		[Inhibitor]	*[Inducer]*	*[Inhibitor]*
		Itraconazole	**Rifampicin**	**Bupropion**
Absence	AUC (ng/mL.h)	8495.96 (13117.16)	8495.96 (13117.16)	8495.96 (13117.16)
	T_{max} (h)	2.07 (0.68)	2.07 (0.68)	2.07 (0.68)
	C_{max} (ng/mL)	165.15 (150.8)	165.15 (150.8)	165.15 (150.8)
	C_{min} (ng/mL)	28.29 (63.16)	28.29 (63.16)	28.29 (63.16)
	fm_{3A4}	29 (23.5)	29 (23.5)	29 (23.5)
	fm_{2D6}	71 (24)	71 (24)	71 (24)
Presence	AUC (ng/mL.h)	17132.67 (42322.1)	1916.77 (2165.25)	10495.63 (13328.4)
	T_{max} (h)	2.16 (0.8)	1.39 (0.36)	1.59 (0.6)
	C_{max} (ng/mL)	261 (369.26)	60.13 (47.01)	225.92 (150.83)
	C_{min} (ng/mL)	73.39 (244.97)	4.3 (7.09)	33.92 (63.85)
	fm_{3A4}	20.65 (24.4)	69.75 (16)	33.8 (23.3)
	fm_{2D6}	79.35 (24.4)	30.25 (16)	66.2 (23.2)
Interaction Summary	AUC Ratio	1.42 (0.43)	0.3 (0.14)	1.34 (0.21)
	C_{max} Ratio	1.38 (0.28)	0.4 (0.14)	1.52 (0.28)
	C_{min} Ratio	1.49 (0.56)	0.25 (0.14)	1.42 (0.25)

Table S 2.10 The impact of drug-drug interactions on gefitinib pharmacokinetics in Caucasian cancer populations.

AUC: area under the curve; C_{max}: maximum plasma concentration; C_{min}: minimum (trough) plasma concentration; T_{max}: time to maximum plasma concentration. Data reported as geometric mean and (standard deviation). [a] Ratio of each pharmacokinetic parameter (C_{max}, C_{min} or AUC) in the presence and absence of a drug interaction. fm_{3A4}: fraction of drug metabolised by CYP 3A4; fm_{2D6}: fraction of drug metabolised by CYP 2D6. Data reported as geometric mean and (standard deviation).

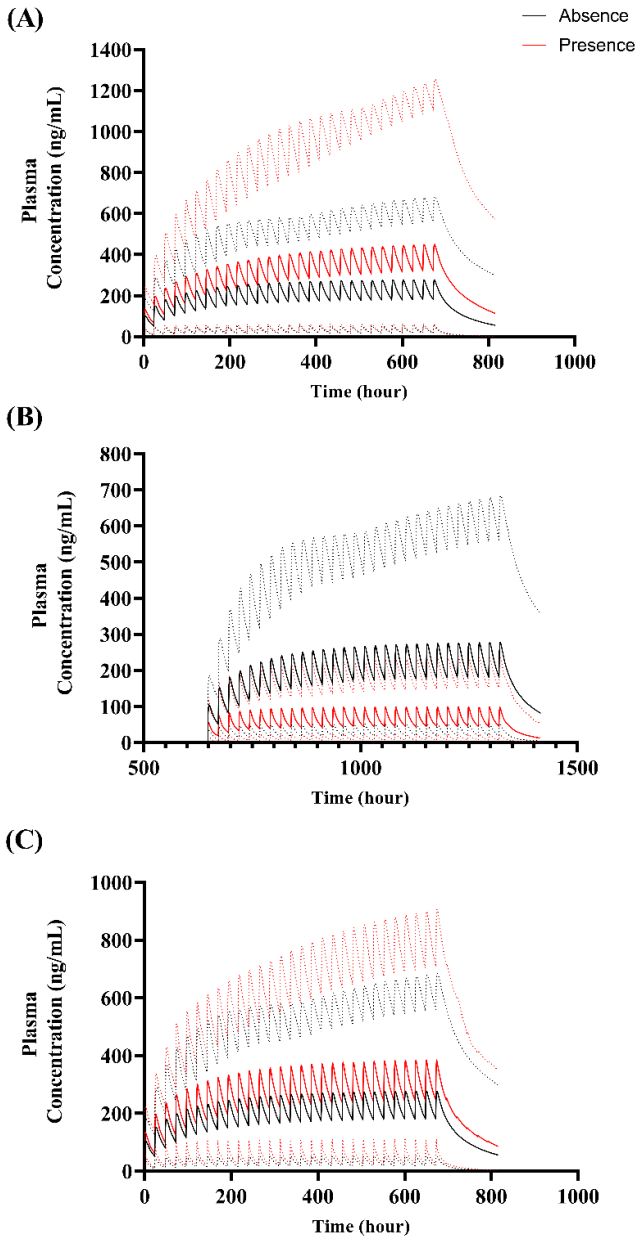

Figure S 2.1 Gefitinib pharmacokinetics in Chinese cancer patients.

Multiple oral 250 mg dose once daily for 28 days, dosed in the absence (black) or presence (red) of (A) 200 mg once daily itraconazole (3A4 inhibitor); (B) rifampicin (3A4 inducer) dosed throughout the study at 600 mg once daily for 60 days with gefitinib dosed on days 28-56; (C) bupropion (2D6 inhibitor) dosed at 150 mg once daily. Studies were conducted in Chinese Cancer population (n=100). Dotted lines indicate the corresponding 5th and 95th percentile range of the mean (solid line).

Chapter 3 The application of virtual therapeutic drug monitoring to assess the pharmacokinetics of imatinib in a Chinese Cancer population group

Disclaimer

Elements of this chapter have been published as follows:

YU, H. & BADHAN, R. K. S. 2023. The Application of Virtual Therapeutic Drug Monitoring to Assess the Pharmacokinetics of Imatinib in a Chinese Cancer Population Group. Journal of Pharmaceutical Sciences, 112, 599-609

3.1 Introduction

Tyrosine kinase inhibitors (TKIs) have revolutionised the treatment of several cancers [407], but there still remains a need to consider optimising dosing to ensure personalised anticancer treatment in a range of patient groups [408]. Imatinib, which inhibits BCR-ABL activity, has gained attention as one candidate which would benefit from TDM approaches [409-411], particularly in gastrointestinal stromal tumours (GIST) and chronic myeloid leukaemia (CML). As a member of the first generation of TKIs, imatinib was the first TKI to be used to treat chronic myeloid leukaemia (CML) [412].

The BCR-ABL oncoprotein is a result of mutations in the BCR/ABL fusion gene, which is the most prevalent genetic variant in chronic myeloid leukaemia, accounting for nearly 95% of cases [413-415]. The BCR-ABL oncoprotein's tyrosine activity facilitates the uncontrolled transmission of various downstream signalling pathways, which results in uncontrolled cell proliferation. Hematopoietic stem cells (HSCs) altered with BCR-ABL mutant genes are unable to differentiate normally or undergo apoptosis, and hence change into leukaemia stem cells (LSCs) [413, 416]. Unpolished stem cells continue to grow and amass in the bone marrow, eventually resulting in leukaemia. The BCR-ABL oncoprotein contains a tyrosine kinase domain [417], and when this domain interacts with ATP, thus, CML develops. Thus, inhibiting the binding of the two with a TKI prevents the BCR-ABL oncoprotein from activating its tyrosine kinase activity to achieve the goal of CML treatment [413, 418]. Imatinib is a type of TKI that is classified as an ATP-competitive inhibitor, it is also the first TKI approved to use in EU and USA in 2001 for clinical treatment [412, 419]. It suppresses the growth of cells expressing the BCR-ABL gene and promotes apoptosis by competing with ATP for binding sites [413].

Gastrointestinal stromal tumours (GIST) are one of the commonest types of mesenchymal tumour localised to the gastrointestinal tract [420, 421], affecting approximately 7 people per million per year in Western countries [422], 16 people per million per year in Korea [423, 424] and approximately 4 people per million per year in China [425]. Globally, the incidence of GIST is over 10 cases per million individuals, which corresponds to at least 8000 new cases in Europe each year [426, 427]. The most common anatomical site of original tumour in 9747 GISTs was the stomach (55.6%), followed by the small intestine (31.8%), the colon (6.0%), other/various locations (5.5%), and the oesophagus (0.7%) [428]. The majority of GISTs are caused by oncogenic mutations in the tyrosine kinase receptor KIT and/or platelet-derived growth factor receptor- α(PDGFR-α) [429, 430]. Over 80% GIST patients respond to imatinib or achieve persistent stabilisation of tumour development with ongoing therapy can be a daily dosage of 400 to 600 mg imatinib [430]. Whilst surgical resection is the mainstay treatment,

only 70 % of patients attain a 5-year post-operative survival [431] and the economic burden of therapeutic interventions is high, at over $100,000 per patient per year [432]. Furthermore, a large study in Chinese patient identified a steep rise in cases after 50 years old, with males being more predisposed than females. This phenomenon could potentially be attributed to mutations in the expression of the Escape from X-Inactivation Tumour Suppressor gene on chromosomal Y and its severe downregulation. Additionally, alcohol use and smoking, particularly among males, can be responsible as cancer risk factors as well [425]. Furthermore, chronic myeloid leukaemia (CML) is a myeloproliferative neoplasm defined by the Philadelphia (Ph) chromosome and driven by the BCR-ABL1 tyrosine kinase [433]. Chronic myeloid leukaemia (CML) accounts for approximately 20 % of all cases on leukaemia within adults [434]. Approximately 33 % of patients with CML treated with imatinib demonstrate a lack of complete cytogenetic response (CCyR) or present with drug resistance/toxicity [435-437]. Additionally, the standard of therapy for individuals newly diagnosed with chronic myeloid leukaemia (CML) in chronic phase is a daily dosage of 400 mg imatinib (CML-CP) [438]. However, greater doses of imatinib may increase response in patients with CP-CML taking imatinib. Patients receiving 800 mg per day for 12 months attained cytogenetic and major molecular responses more rapidly than those receiving 400 mg per day [439]. Imatinib dosage escalation to a daily dose of 600 mg or 800 mg has showed potential efficacy in individuals with a sluggish or poor response and disease progression [438, 440].

In both cases, a key in the paradigm of treatment is imatinib, which has revolutionised treatment outcomes and improved survival times [441, 442]. Imatinib is well absorbed with an absolute bioavailability of > 98 % [443, 444], which is not dose or dosage form dependant [445, 446]. Its half-life is approximately 18 hours, and multiple dosing often leads to target plasma concentration in-excess of the 0.5 μM required for TKI in-vitro [445, 447]. Furthermore, it is highly protein bound (>95 %) [448] and has a large volume of distribution (Vd) > 400 L [444]. The elimination of imatinib is governed by CYP 2C8 (primary role) [449] and 3A4 [450-452], with other CYP isozymes (CYP1A2, CYP2D6, CYP2C9 and CYP2C19) playing a minor role (< 3 % contribution in total) [450-453]. Furthermore, being a low extraction drug, the elimination of imatinib is highly sensitive to protein binding and intrinsic clearance. Confounding the pharmacokinetics of imatinib, is its wide inter-individual variability with steady-state trough concentrations varying by over 20-fold in CML patients [454, 455], although this is thought to be a result of the intracellular site of action. It is often utilised at a fixed daily dose of 400 mg, which can be increased to 600 mg in accelerated disease phases.

Oncology patients tend to demonstrate altered physiology which may influence a drugs pharmacokinetics, with key changes including reduced haematocrit, increased α-1 acid glycoprotein and decreased albumin and reduced glomerular filtration rate (GFR) [329, 341].

Furthermore, racial and weight differences between Chinese and Caucasian patient demographics have a direct role in current Chinese guidelines for treatment. Furthermore, the tolerance of Chinese patients to higher doses (> 400 mg/day) is often lower than that of Caucasian patients, with the (United States) National Comprehensive Cancer Network (NCCN) guidelines recommending 800 mg/day [456-458] for those who show limited improvement at the standard dose (400mg/daily) (originating from Caucasian studies), whereas in Chinese studies doses are recommended at 600 mg/day [459, 460].

Given the long-term use of imatinib, appropriate steady-state levels are critical in limited side effects and toxicity such as myelosuppression, nausea, diarrhoea, hypophosphatemia, musculoskeletal symptoms, rash, fatigue, and headaches [461]. For both CML and GIST, a target trough concentration of 1000 ng/mL and 1100 ng/mL has been suggested, respectively [462, 463]. Whilst these are often drive around pharmacodynamic endpoints (e.g. hematologic, cytogenetic and molecular responses), some groups have advocated the use of such concentrations as pharmacokinetic predictors of response [464, 465]. Furthermore, given the wide inter-individual variability reported in trough concentration (50-100 %) [466], sub- or supra- therapeutic dosing is possible [466, 467].

In order to address the clinical consequences of this variability, Gotta *et al* (2014) coined the term “rescue TDM” to refer to ‘corrective’ dosing based on therapeutic drug monitoring (TDM) for specific cases to support optimal imatinib plasma concentrations [411]. Recently, Buclin *et al* (2020) [409] utilised the work by Gotta *et al* [411] to emphasize the need for TDM for imatinib, providing a structured approach to accomplish this. In the approach originally developed by Gotta *et al* (2014) [411], dose adjustments were support for subtherapeutic patients (500-800 mg once daily) and supratherapeutic patients (200-400 mg once daily).

C_{min} was the preferred imatinib pharmacokinetic indicator when performing TDM. Usually C_{max} and AUC can also be used as indicators, but for imatinib, the intra-patient variability is much smaller than the inter-patient variability [468], so the C_{min} is obtained 5 to 7 days after the first dose of the drug reaches a steady state in the body of patients, just before the second dose is administered. When C_{min} is utilised as an indication, it can also be viewed as the difficulty and opportunity presented by imatinib-specific TDM. TDM can effectively reduce the cost of clinical application of imatinib, but the difficulty of obtaining clinical data is significantly greater than the difficulty of laboratory monitoring [427, 468]; therefore, the formation of a true standard framework TDM must be continuously enhanced to be suitable for different patient populations. To confirm that TDM can perform the anticipated regulatory role in the treatment of GIST with imatinib, a study evaluated whether patients with advanced GIST could obtain longer progression-free survival (PFS) with defined C_{min} values for imatinib was performed in

2016 [469]. The experimental results demonstrate that when the specified control concentration of imatinib is 760ng/ml, the PFS obtained in GIST patients is favourably associated with the concentration, validating the viability of TDM. Furthermore, there were 28 clinical studies considered in a 2019 study of the treatment results of imatinib in chronic myeloid leukaemia(CML) TDM [470]. The findings of the investigation demonstrate that TDM can predict the efficacy of imatinib with absolute certainty. The suggested therapeutic range is between 1000 and 1500ng/ml, and larger trough concentrations will not enhance the drug's effectiveness.

Higher plasma concentrations have been reported in Chinese cancer patients when compared to Caucasian cancer patients [471, 472]. Given the physiological difference between Chinese and Caucasian cancer patients, particularly changes in alpha-1-acid glycoprotein, the assessment of optimal doses to attain targeted plasma concentrations is warranted and can be pragmatically achieved through the use of mechanistic physiologically-based pharmacokinetic modelling approaches [473].

In this study, we utilise previous work conducted by our group to assess the requirements and approaches towards dose titrations in Chinese cancer patients, with explicit account of the physiological differences encountered in Chinese cancer patients compared to Caucasian cancer patients.

3.2 Aims and objectives

The primary aim of this study was to use the published TDM strategy and virtual clinical trials to provide a clinically relevant dosing adjustment strategy for virtual Chinese cancer populations that could be implemented to maintain effective plasma imatinib levels, the impacts of multiple ethnic groups on TDM were explored.

To achieve the aims, the overall objectives were:

- To validate the previously developed imatinib PBPK model using published single and multiple dose studies in Caucasian population.
- To validate the imatinib model in a virtual Chinese cancer population.
- To observe TDM dosing regimen in the virtual Chinese cancer population.
- To compare the different imatinib TDM outcomes between Caucasian and Chinese cancer populations.

3.3 Methods

In order to conduct virtual clinical trials simulations in subjects, the physiologically based pharmacokinetic (PBPK) modelling tool Simcyp (Simcyp Ltd, a Certara company, Sheffield, UK, Version 19) was utilised. Unless otherwise stated, all simulations utilised mixed genders (50:50). Further, we adopted a workflow model with four stages (Figure 3.1).

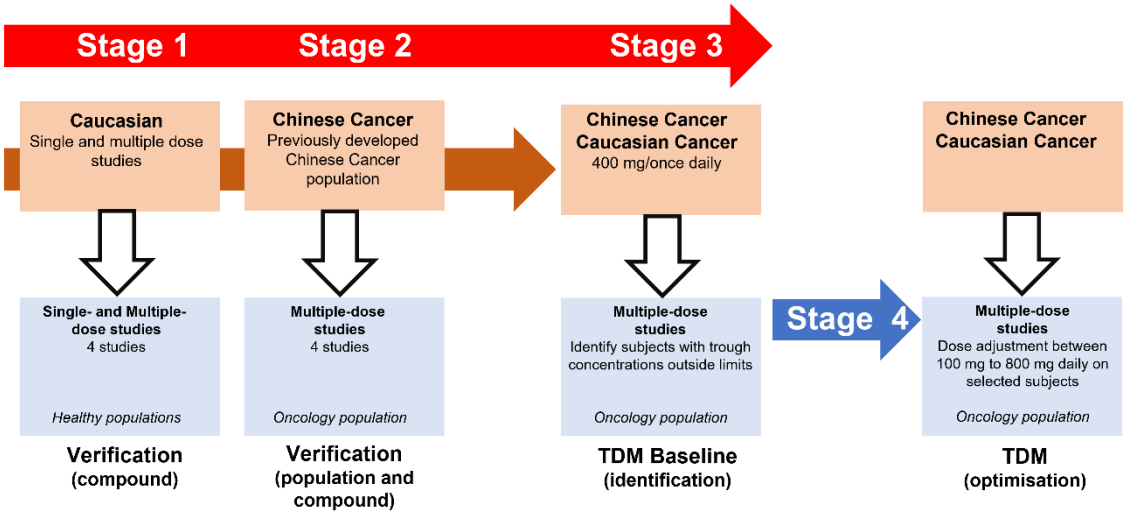

Figure 3.1 The workflow model for model verification and TDM.

3.3.1 Step 1: Validation of imatinib in Caucasian subjects

We utilised a previously developed and validated model of imatinib [474], with some modifications. The validation dataset utilised included 4 studies within Caucasian populations: (i) 12 healthy Caucasian volunteers (2 female) (40-58 years old) who received a single dose administration of imatinib 400 mg [444]; (ii) 34 cancer patients (6 female) (28-84 years old) who received multiple doses of imatinib 400 mg with sampling on days 1 and 15 [475]; (iii) 50 cancer patients (21 female) (39-82 years old) who received multiple doses of imatinib 400 mg/day for 15 days [476]; (iv) 103 patient (83 female) (18-77 years old) who received multiple doses of imatinib 400mg/day for 15 days [477].

3.3.2 Step 2: Validation of imatinib in a virtual Chinese cancer population

In order to assess differences in pharmacokinetics of imatinib in Chinese and Caucasian cancer subjects, we utilised a previously developed virtual Chinese cancer population group [478] in a virtual trial to compare predicted trough imatinib plasma concentration to those

reported at steady state for doses of (i) 100, 200, 250, 300, 400, 600, 600 and 800 mg once daily (36 subjects aged 17-79 years) [479]; (ii) 190 GIST subjects dosed 400 mg once daily (31-85 years) [480] ; (iii) 84 CML subjects dosed 300-600 mg once daily (18-76 years) [481]; (iv) 129 GIST subjects dosed 200-600 mg once daily (29-75 years) [482]. This virtual Chinese cancer population group incorporates physiological alterations previously reported [329] to occur within oncology populations includes reductions in haematocrit, increases α-1 acid glycoprotein and decreases in both albumin and GFR [341].

3.3.3 Step 3: Imatinib TDM in a virtual Chinese cancer population

Although there is no definitive guidance on the need for TDM for imatinib, previous studies have examined approaches to implementing TDM in clinical practice [409-411, 483-486]. Utilising the “rescue TDM” approach coined by Gotta *et al* (2014), we implemented the subsequent structured approach to TDM suggested by Buclin *et al* (2020) [409] (Figure 3.2), in order to assess the need for imatinib TDM in a virtual Chinese cancer population group.

A 10x10 trial design (100 subjects) was implemented (20–50-year-olds, 50 % female) with a dose of 400 mg once daily for 28 days, followed by dose adjustments in 100 mg daily increments to the target dose and maintained for a further 28 days at each specific target dose. At day 28 (before adjustment) and day 56 (after adjustment), subjects were identified who demonstrated trough plasma concentrations below or above the target thresholds, and the impact of the dose adjustment was quantified in relation to ability to target the therapeutic concentration range (750-1500 ng/mL) identified by Buclin *et al* (2020) [409].

As a comparison, an identical trial design was implemented for the Simcyp Cancer (Caucasian) population group.

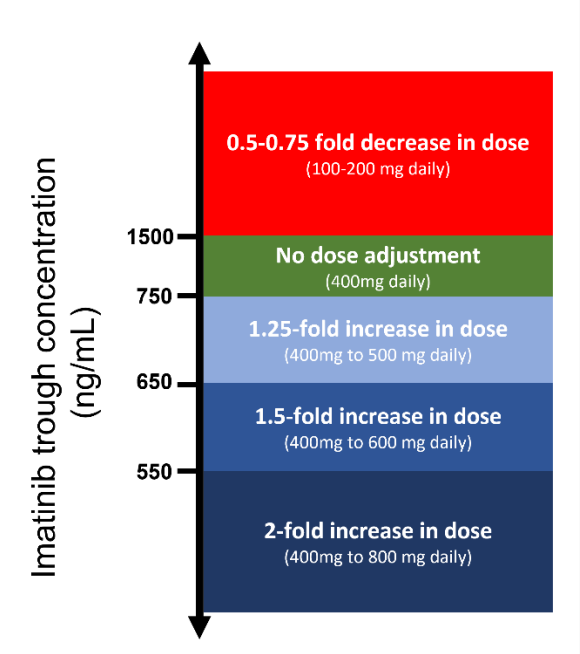

Figure 3.2 TDM-guided dose titrations.

Dose titrations were conducted based on approaches previously described [409]. Subjects with imatinib trough plasma concentration outside of the prescribed target trough window (750-1500 ng/mL), following a 400 mg once daily (to steady state) dosing schedule, were identified and subjected to dose adjustment based on either a dose increase or decrease, dependent upon their trough plasma concentration.

3.3.4 Predictive performance

For the validation steps 1-3, predictive performance was determined within 2-fold (0.5–2.0-fold) range of reported pharmacokinetic parameters [358, 487, 488]. A visual predictive checking (VPC) strategy (U.S. Food and Drug Administration, 2012) [489-491] was also adopted for predicting plasma concentration-time profiles. This checking strategy was performed visually when the predicted plasma-concentration profiles, including the predicted mean and 5th and 95th percentiles, was compared with the observed data which should overlap with the predicted data sets. Furthermore, the prediction accuracy of the simulation profiles was evaluated using average fold error (AFE) (Equation 1) and absolute average fold error (AAFE) (Equation 2) [492-494] were calculated to further validate provide a measure of precision and bias, as follows:

$$AFE = 10^{\frac{1}{n}\cdot\sum log\left(\frac{pred_t}{obs_t}\right)} \quad \textbf{(1)}$$

$$AAFE = 10^{\frac{1}{n}\cdot\sum\left|log\left(\frac{pred_t}{obs_t}\right)\right|} \quad \textbf{(2)}$$

where *n* represents the number of observations, $pred_t$ and obs_t are the predicted and observed concentrations at time *t*. Deviations from unity refer to over-prediction (AFE > 1) or under-prediction (AFE < 1) of the observed data. AAFE measures the absolute error from the true value and inherent determined bias of the profile. AAFE values of ≤2 were considered appropriate [495].

Mean predicted values (e.g., C_{max} or C_{min}) were compared with observed values and the standard deviation ratio (SDratio) calculated (Equation 3) [473] as follows:

$$\text{SDratio} = \sqrt{\left(\frac{\text{SD observed}}{\text{Mean observed}}\right)^2 + \left(\frac{\text{SD predicted}}{\text{Mean predicted}}\right)^2} \times \frac{\text{Mean predicted}}{\text{Mean observed}} \quad \textbf{(3)}$$

where SD observed and SD predicted are the SD of observed and predicted values; Mean observed and mean predicted are the arithmetic mean of observed and predicted values. A criterion of < 2-fold was deemed an acceptable prediction of values [358, 487, 488].

The observed clinical data used in verification studies were extract using WebPlotDigitizer v. 3.10 (https://automeris.io/WebPlotDigitizer/). Statistical significance was confirmed as $p < 0.05$.

3.4 Results

3.4.1 Step 1: Validation

The model was successfully validated against 5 adult imatinib single- and multiple-dosing regimen studies, with the majority of plasma concentrations falling within the 5th and 95th percentiles of the predicted concentrations (Figure S 3.1). Further, in all cases the AFE and AAFE were between 0.85-1.21 and 0.98-1.14, indicating successful model predictions (Table S 3.1).

3.4.2 Step 2: Validation of imatinib in a virtual Chinese cancer population

Simulated median steady-state trough and peak imatinib plasma concentrations in Chinese cancer populations were broadly within 1.5-fold of those reported for a variety of doses from 100 mg – 800 mg (Figure 3.3) with mean prediction ratio and SD-ratio within the 2-fold boundary (Table 3.1).

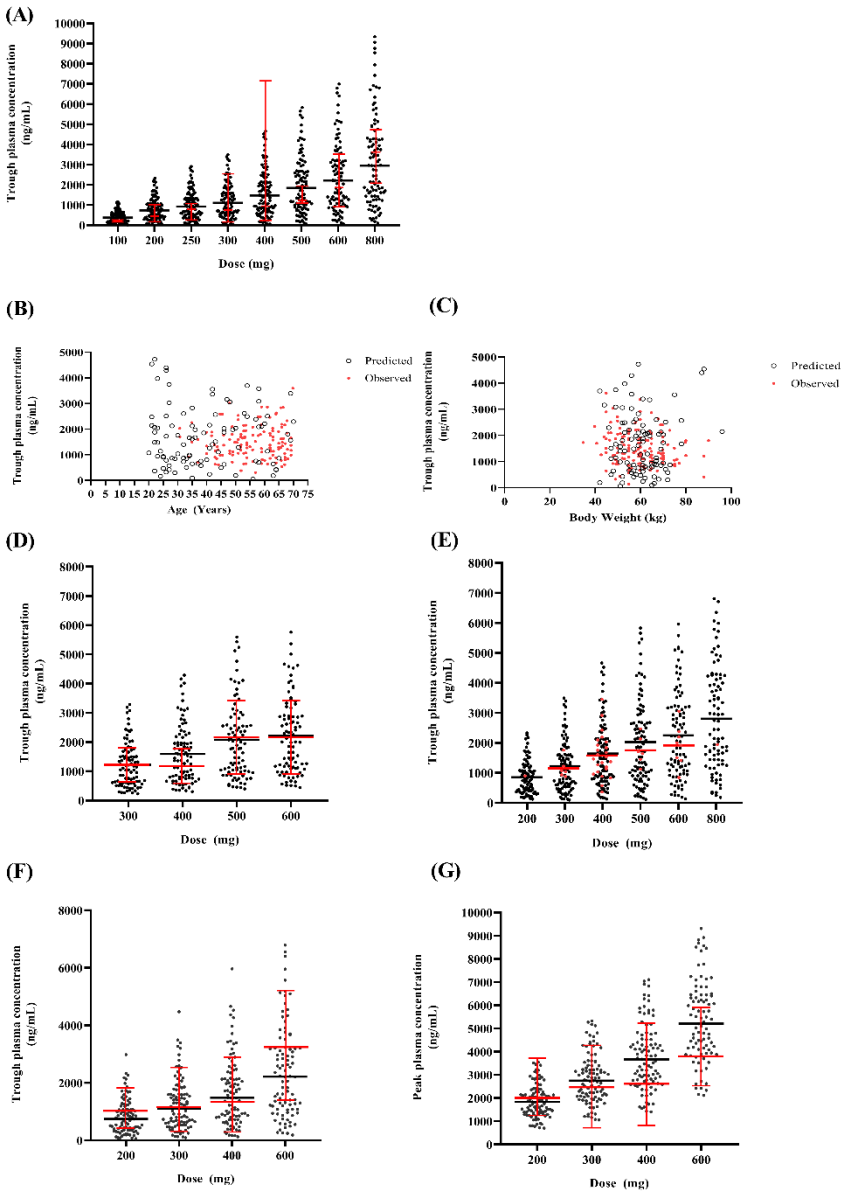

Figure 3.3 Imatinib plasma concentration following oral dose administration in Chinese cancer subjects.

Steady-state trough plasma concentration reported following **(A)** 100, 200, 250, 300, 400, 600, 600 and 800 mg once daily doses (36 subjects aged 17-79 years) [479]; (**B** and **C**) 190 GIST subjects dosed 400 mg once daily (31-85 years) [480] demarked for age and body weight; (**D**) 84 CML subjects dosed 300-600 mg once daily (18-76 years) [481]; (**E** and **F**) 129 GIST subjects dosed 200-600 mg once daily (29-75 years) [482]. Circles indicate the predicted (black) or observed (red) individual data. Where individual concentration observed data was not reported, the reported observed mean and range were used and is represented by red horizontal lines (mean) and range (upper and lower horizontal lines).

		C_{min} (ng/mL)		Comparison	
	Dose (mg)	Predicted	Observed	Mean ratio	SD Ratio[a]
Xia et al (2020)	100	369.11 (82.74-1162.87)	378 (140-334)	0.98	1.08
	200	738.015 (85.46-2327.15)	640 (346-1222)	1.15	1.12
	250	922.41 (111.8-2909.74)	986 (440-1265)	0.94	1.02
	300	1106.8 (138.2-3492.63)	940 (337-2781)	1.18	1.24
	400	1475.37 (150.8-4659.26)	1139 (421-7493)	1.32	1.42
	500	1843.795 (320.49-5827.25)	1422 (1283-2155)	1.31	1.38
	600	2212.075 (76.14-6996.38)	2076 (1103-3775)	1.07	1.08
	800	2948.395 (101.38-9336.94)	3879 (2303-5017)	0.76	1.05
Wu *et al* (2018)	300	1221.7 (756.7)	1564.65 (596.2)	0.80	1.24
	400	1593.4 (987.2)	1521.3 (610.3)	1.07	1.42
	500	2078.9 (1289.9)	2540.3 (1298.1)	0.82	1.38
	600	2208 (1291.3)		0.87	1.08
Zhong et al (2012)	200	849.7 (541.2)	732.6	1.16	nd
	300	1227.2 (828.1)	996 (337.7)	1.23	1.45
	400	1635.8 (1105.6)	1446.2 (757.3)	1.13	1.52
	500	2024.5 (1388.5)	1631.9 (507.1)	1.23	1.24
	600	2246.9 (1440.2)	1802.3 (709.1)	1.24	1.13
	800	2802.7 (1724.1)	1832.7	1.56	nd
	200	738.3 (78.2-2981.1)	960.1 (367.2-1751.2)	0.73	1.26
	300	1107.6 (102.15-4471.9)	1087.5 (253.2-2452.1)	1.02	1.11
	400	1484.3 (143.2-5963.2)	1270.9 (224.7-2809.3)	1.17	1.23
	600	2215.3 (192.4-6788.9)	3162.6 (1327-5112.8)	0.73	1.42
		C_{max} (ng/mL)			
Zhang et al (2018)	200	1832.2 (701.6-3548.2)	1988.5 (1232.2-3699.3)	0.93	1.23
	300	2748.3 (1053.6-5342.6)	2456.3 (701.8-4256.7)	1.11	1.15
	400	3665.7 (1406.2-7102.1)	2604.8 (802.6-5211.9)	1.43	1.33
	600	5205.7 (2113.6-9303.4)	3785.6 (2516.5-5897.3)	1.39	1.23

Table 3.1 Predicted and observed imatinib trough or peak plasma concentrations at in the Chinese cancer population group.

Data represents mean (range) or mean (SD). C_{min}: trough plasma concentration; C_{max}: peak plasma concentration; Mean ratio: ratio of predicted to observed concentration; nd: not determined. [a] SD ratio: ratio of predicted to observed SD ratio. Observed SD was obtained or calculated from original reference source.

3.4.3 Step 3: Imatinib TDM in a virtual Chinese cancer population

In order to examine the requirement for TDM-based dose adjustment, simulations in Chinese and Caucasian cancer populations assessed the changes in trough imatinib plasma concentrations following dose adjustment from a baseline of 400 mg once daily across a range of 200-800 mg once daily. Trough plasma concentrations were higher for Chinese than Caucasian subjects (Figure 3.4A) (Table 3.2) with a standard dose resulting in trough levels of 1816.2 ng/mL (52.85-8257.29 ng/mL) and 1216.6 ng/mL (121.23-4464.89 ng/mL) respectively (Table 3.2) (Figure 3.4B).

	Trough plasma concentration (ng/mL)			
Dose	Chinese		Caucasian	
(mg)	Mean (Range)	SD	Mean (Range)	SD
200	907.79 (26.46-4095.64)	721.56	608.28 (60.66-2231.98)	413.81
300	1361.92 (39.66-6168.77)	1083.70	912.44 (90.96-3348.33)	620.79
400	1816.2 (52.85-8257.29)	1446.70	1216.6 (121.23-4464.89)	827.82
500	2270.62 (66.02-10360.15)	1810.49	1520.77 (151.48-5581.64)	1034.90
600	2725.17 (79.17-12476.44)	2175.04	1824.95 (181.71-6698.57)	1242.03
800	3634.66 (105.42-16745.82)	2906.26	2433.36 (242.1-8933.03)	1656.426

Table 3.2 Predicted imatinib trough plasma concentrations at difference doses in Chinese and Caucasian cancer subjects.

Data represents mean (range) and standard deviation (SD).

In order to engage in virtual-TDM, we considered each simulated subject and sampled the steady-state trough plasma concentration (following 400 mg once daily dosing), prior to dose-titrations. At a 400 mg dose, fewer Chinese subjects possessed trough concentrations within the target range (750-1500 ng/mL) when compared to Caucasian subjects, 26 % and 43 % respectively (Table 3.3). However, a greater number of Chinese subjects possessed trough concentrations in excess of the upper limit of the target range (>1500 ng/mL), 51 %, when compared to Caucasian subjects, 25 % (Table 3.3).

In Chinese and Caucasian populations, 9 % and 13 % of subjects, respectively, possessed sub-therapeutic concentration in the range of 550-750 ng/mL, of which all were recapitulated to the target range, upon the application of the appropriate TMD method (Figure 3.2) (Table 3.3). However, for those with plasma concentration < 550 ng/mL, a dose increase to 800 mg

was only able to recover 50 % (Chinese) and 42.1% (Caucasian) of those subject to within the target therapeutic range (Table 3.3). For subjects with plasma concentration >1500 ng/mL, a dose reduction to 200 mg once daily was able to recover 67 % (Chinese) and 84 % (Caucasian) of those patients of within the target therapeutic range (Table 3.3).

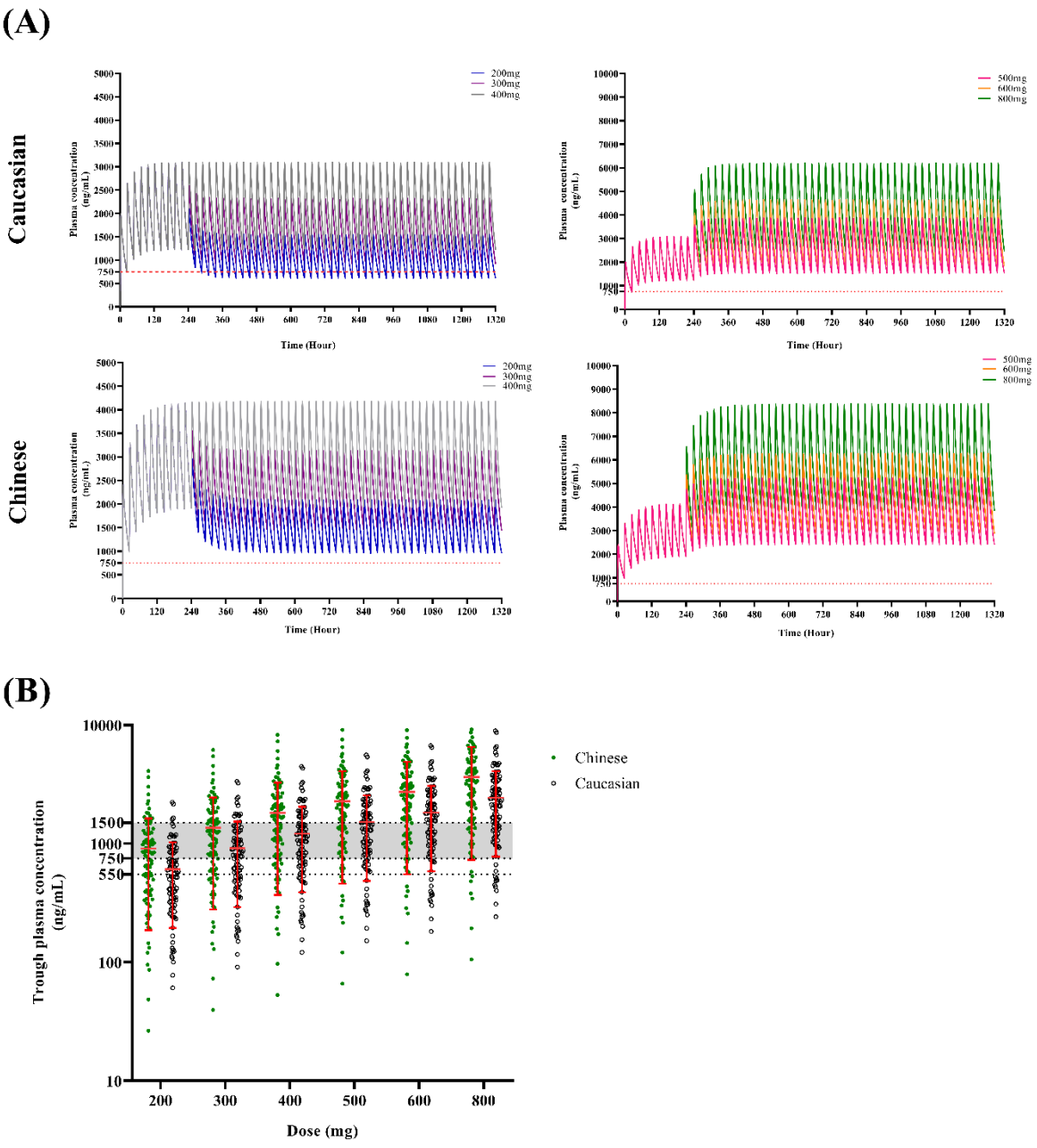

Figure 3.4 Simulated imatinib plasma concentrations in Chinese and Caucasian cancer subjects at different doses.

(A) Simulated plasma concentration in 100 Caucasian (upper panels) or Chinese (lower panels) cancer subjects (20–50-year-olds) following an initial dose of 400 mg once daily to steady-state (10 days) and thereafter dose titrations to between 200-400 mg once daily (left panels) or 500-800 mg once daily (right panels). Horizontal dashed line indicates lower target trough plasma concentration (750 ng/mL). (B) Simulated plasma concentration in 100 Caucasian (open circles) or Chinese (solid green circles) cancer subjects (20–50-year-olds) at steady-state doses of between 200-800 mg once daily Horizontal shaded regions represents target trough plasma concentration (750-1500 ng/mL). Red lines indicate median and 5th- and 95th percentiles.

Population	Trough level [a]	Mean trough concentration (ng/mL)	SD (ng/mL)	Subjects within trough range [b]	Dose Adjustment [c]	Adjusted Dose (mg)	Mean trough concentration (ng/mL)	SD (ng/mL)	Pre-adjustment subjects within target therapeutic range post-adjustment [d]
		Pre-Adjustment				Adjustment			
Chinese	<550	320.99	156.12	14	x2	800	640.61	311.36	50 % (n=7)
	550-650	611.67	16.77	3	x1.5	600	916.79	24.5	100 % (n=3)
	650-750	695.22	30.57	6	x1.25	500	868.64	38.15	100 % (n=6)
	750-1500	1102.7	216.96	26	None	400	1102.7	216.96	na
	>1500	2995.07	1909.81	51	x0.5	200	1496.31	950.81	66.7 % (n=34)
					x0.75	300	2245.4	1429.34	29.4 % (n=15)
Caucasian	<550	336.97	136.91	19	x2	800	673.34	273.68	42.1 % (n=8)
	550-650	593.7	30.84	6	x1.5	600	890.39	46.66	100 % (n=6)
	650-750	683.21	25.01	7	x1.25	500	853.89	31.13	100 % (n=7)
	750-1500	1126.77	223.42	43	None	400	1126.77	223.42	na
	>1500	2338.47	779.16	25	x0.5	200	1169.04	389.53	87.5 % (n=21)
					x0.75	300	1753.71	584.33	44 % (n=11)

Table 3.3 Predicted imatinib trough plasma concentrations at difference doses in cancer subjects following the application of TDM.

100 subjects (20–50-year-olds) were initiated on an initial dose of 400 mg once daily to steady-state (10 days) ('Pre-Adjustment') and thereafter dose titrated to between 200-800 mg once daily ('Adjustment'). [a] Trough levels were demarked for therapeutic range (750-1500 ng/mL) and regions above and below this. [b] Represents the percentage of subjects (n=100 in total) with trough levels within the range indicated. [c] Represents the adjustment made to the initial steady-state dose (400 mg once daily) and below this. [d] Represents the number of pre-adjustment subjects who have a concentration, following the revised dose adjustment, within the target trough range (750-1500 ng/mL). na: not applicable

3.5 Discussion

The management and treatment of patients with CML and GIST have significantly improved since the first TKI, imatinib, was introduced, with similar survival rates to that of control subjects [496]. As a selective inhibitor of the protein tyrosine kinase Bcr-Abl, platelet-derived growth factor receptors (PDGFRα and PDGFRβ) and KIT, imatinib has been demonstrated as part of the treatment of CML and GIST [497, 498].

Monitoring the plasma concentration of imatinib may be beneficial in optimizing treatment strategies [499], particularly given that all tyrosine kinase inhibitors are administered orally and, usually, as fixed doses regardless of the patient's weight, age, or gender, leading to inconsistent bioavailability and individual differences in plasma levels across a population [500].

For adult CML/GIST patients, the current recommended dose is 400 or 600 mg once daily [501], resulting in quite diverse plasma concentrations in different ethnic groups, with the average plasma imatinib concentration in 10 countries (Asia (China, South Korea, Japan, and India), Europe (France, Norway, the Netherlands, Belgium, and Italy), and North America (United States)) ranging from 800-1500 ng/mL [502].

In this study, we utilised virtual-TDM to optimise imatinib therapy in virtual Chinese and Caucasian cancer subjects. The imatinib model was adapted and validated in single and multiple dose studies in Caucasian subjects [444, 475-477] in addition to a being validated using a previously developed virtual Chinese cancer population group [478] with CML/GIST multiple dose studies [479-482]. In these validation studies, the predicted imatinib plasma concentrations were within the range reported in clinical studies (Figure S 3.1) (Figure 3.3) and mean predicted pharmacokinetics parameters were all within 2-fold of those reported (Table 3.1). Some level of under/over-prediction was evident in Figure 3.3F and G, when predicting trough (Figure 3.3F) and peak (Figure 3.3G) plasma concentrations with observed data from 129 GIST subjects dosed 200-600 mg once daily (29-75 years) [503]. However, the observed data recruited a total of 129 patients in an observational phase 4 trial, with patients demarked for imatinib daily dose and hence the observed data for each dose reflect a smaller subset of the total patient number, and this may have contributed to the under/overprediction at the higher doses. Nonetheless, median predictions were within 2-fold of those reported.

Failures in imatinib treatment can be attributed to the resistance mutations of imatinib in the kinase domain of BCRABL1 [504]. In these cases, therapeutic drug monitoring (TDM) may provide clinicians with opportunities for informed dosage decisions. The European CML Treatment and Outcome Study (EUTOS) [505], offered guidance on approaches for TDM with imatinib in addition to identify the relationship between imatinib plasma concentration and response. Using centralised TDM and clinical outcome data including cytogenetic response (CyR) and molecular response (MR), the imatinib plasma concentrations of thousands of CML patients were collected in the registry, and the population PK modelling was used to analyze the data. This model describes pharmacokinetic parameters of imatinib in specific population, quantifies the impact of patient characteristics on the behaviour of imatinib, and provides an individual estimate of C_{min}. Additionally, the observations suggest that due to the lower concentration of imatinib and the slower response rate, early dose optimization of TDM may benefit some patients [505]. This study exemplifies the potential of TDM for different populations and provides theoretical evidence for individual variations. Critically, this study suggested at a defined therapeutic target concentration which was utilise as the basis for this work.

Having confirmed the ability of the model to recapitulate plasma concentrations within both Caucasian cancer and Chinese cancer populations, we subsequently applied TDM-based dose adjustment, using the approach developed by EUTOS [411], in simulations by assessing the changes in trough imatinib plasma concentrations following dose adjustment from a baseline of 400 mg once daily across a range of 200-800 mg once daily (Figure 3.4).

For all doses studied, the trough imatinib plasma concentration was higher than that predicted within Caucasian Cancer subjects, concurring with previous reports which have highlighted that broadly lower doses may be required in Asian versus Caucasian subjects [471, 506-511].

Notability, there was a wide interpatient variability in predicted plasma concentrations in both population groups (Figure 3.4), a feature also reported by others [455, 462, 512]. The cause of this may be attributed to both variability in the abundance of CYP metabolic pathways or transporter expression/function pathways. However, in the context of comparing Chinese and Caucasian cancer population, the differences in both body weight and body surface area may also contribute to this, with our virtual Chinese and Caucasian

cancer populations possessed body weights of 62.21 kg ± 9.45 kg and 74.3 kg ± 14.8 kg and BSA of 1.69 m^2 ± 0.16 m^2 1.85 m^2 ± 0.21 m^2. This difference is the often quoted reason for Chinese cancer population required lower doses to support treatment outcomes broadly lower doses are required in Chinese versus Caucasian subjects [471, 506-511].

For Chinese cancer subjects, at the standard dose of 400 mg once daily, only 26 % of subjects possessed trough concentrations within the expected therapeutic range, with 51 % exceeding 1500 ng/mL (Table 3.3). In applying TDM approaches, whilst a doubling of dose to 800 mg was only able to recapitulate 50 % (n=7) of the subtherapeutic subjects at 400 mg below 550 ng/mL, the equivalent 1.25-fold (500 mg) and 1.5-fold (600 mg) increase in dose was able to recover all subtherapeutic subjects between 550-750 ng/mL into the target range. For trough levels above 1500 ng/mL, a 50 % reduction in dose was able to recover 66% of subtherapeutic subjects into the target window. Similar trends were identified for Caucasian cancer subjects, albeit with dose adjustment for subjects with trough levels above 1500 ng/mL resulting in an increase in the recovery to target concentrations. Drug included adverse effects are likely with high imatinib plasma concentrations, and include, nausea, vomiting, oedema and cutaneous reactions [513]. The latter occurs often at higher doses (400-800 mg/day), although most are mild in nature [514]. Although our study was limited to 200 mg/day as the lowest dose, case reports of 100-200 mg/day have demonstrated to result in improve clinical outcomes [515, 516].

The case for TDM for imatinib has been widely made by many [408, 409, 411], and clear cost-effectiveness with TDM-guided therapy versus fixed dose therapy has been demonstrated with improved in ‘cost per quality-adjusted life year’ [410, 517]. TDM has been applied with imatinib in a number of approaches. Lamkheet *et al* (2017) [484], demonstrated that under standard imatinib dosing, < 40 % of subjects had trough levels within the target range (calculated per individual) which with dose adjustment (400 mg to 800 mg) leading to > 90 % of subjects with adequate trough levels. Similarly, Yoon *et al* (2013) [516], considered dose titrations in toxicity cases in two GIST patients and demonstrated reduced intolerable adverse events through dose reductions to 100 mg/daily.

However, challenges remain. As highlighted by Buclin *et al* (2020) [409], ranging from throughput limitations of current analytic methods for the detection of imatinib, lack of specific anticancer TDM cost-effectiveness studies to support implementation, constrains

of precise trough sampling, and ultimately the unwillingness of prescribers to modify established dosing approaches.

3.6 Conclusion

This study demonstrates the application of physiologically based pharmacokinetic modelling and virtual clinical trials, to engage in virtual-TDM of imatinib in a specific Chinese cancer population. Clear differences are evident between Caucasian and Chinese cancer patients, and this warrants further analysis to fully implement TDM in multiple ethnic groups.

3.7 Supplementary materials

Section 1: Validation results

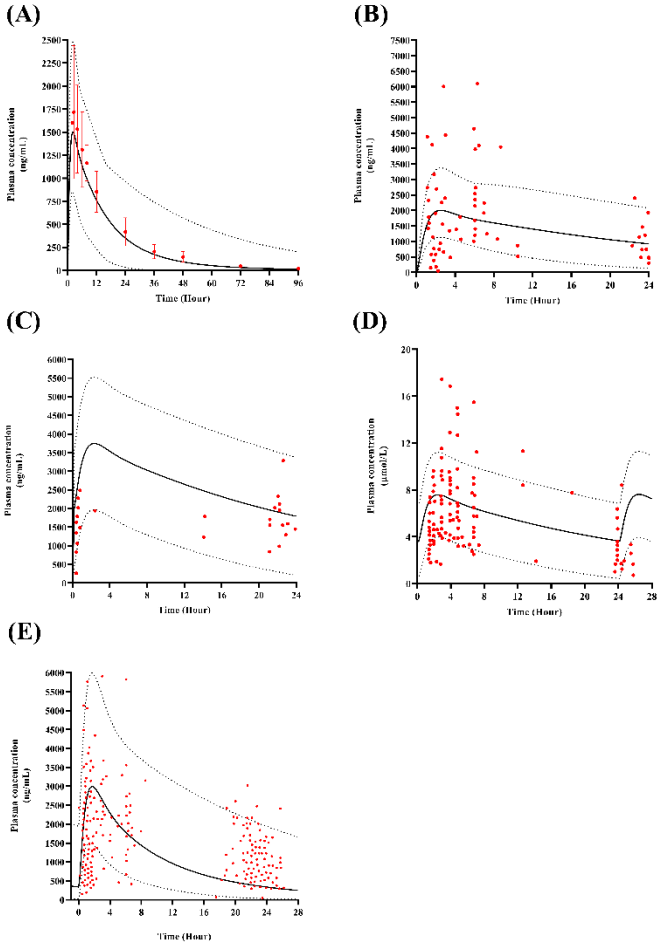

Figure S 3.1 Predicted Imatinib plasma concentration following oral dose administration.

(A) 12 healthy Caucasian volunteers (2 female) (40-58 years old) who received a single dose administration of imatinib 400 mg [444]; 34 cancer patients (6 female) (28-84 years old) who received multiple doses of imatinib 400 mg with sampling on days 1 (B) and 15 (C) [475]; (D) 50 cancer patients (21 female) (39-82 years old) who received multiple doses of imatinib 400 mg/day for 15 days [476]; (E) 103 patient (83 female) (18-77 years old) who received multiple doses of imatinib 400mg/day for 15 days [477]. Filled red circles and vertical lines indicate the observed mean and standard deviation obtain from clinical data; solid black lines are the predicted population mean plasma concentration profile and associated dotted are the corresponding 5th and 95th percentile range of the predicted mean.

Study		PK Parameters	Observed	Predicted
Single	Peng et al (2004)	$AUC_{(0-\infty)}$ (μg.h/mL)	32.6 ± 16.5	38.3 ± 13.9
		C_{max} (μg/mL)	1.8 ± 1.2	1.5 ± 0.5
		t_{max} (h)	2.5 (1-6)	2.3 (1.4-3.2)
Multiple (Day 1)	Petain et al (2008)	$AUC_{(0-24\ h)}$ (μg.h/mL)		49.7 ± 18.2
		C_{max} (μg/mL)		1.8 ± 0.8
		t_{max} (h)		2.5 (1.3-3)
		CL/F (L/h)*	10.9 (19)	11.3 (51)
Multiple (Day 15)	Petain et al (2008)	$AUC_{(0-24\ h)}$		65.1 ± 43.3
		C_{max} (μg/mL)		3.8 ± 1.9
		t_{max} (h)		2.4 (1.5-3.5)
		CL/F (L/h)*	10.9 (19)	10.6 (49)
Multiple (Day 15)	Eechoute et al (2012)	$AUC_{(0-24\ h)}$ (μM.h)		131.6 ± 87.8
		C_{max} (μM)		7.7 ± 3.9
		t_{max} (h)		2.4 (1.5-3.5)
		CL/F (L/h)*	9.5 (50)	10.5 (49)
Multiple (Day 15)	Renard et al (2015)	$AUC_{(0-24\ h)}$ (μg.h/mL)		49.4 ± 19.3
		C_{max} (μg/mL)		3.0 ± 1.9
		t_{max} (h)		2.5 (1.4-3.4)
		CL/F (L/h)*	10.8 (43)	10.3 (51)

Table S 3.1 Predicted and observed imatinib pharmacokinetics in validation datasets.

$AUC_{(0-\infty)}$: area under the plasma concentration-time curve from time zero to infinity; $AUC_{(0-24)}$: area under the plasma concentration-time curve during 24 h after dose; C_{max}: peak plasma concentration; CL/F: apparent clearance; t_{max}: time to maximum plasma concentration. Data presented as mean (SD) or *mean (CV). For t_{max}, data is presented as mean (range).

Parameter	Chinese			
	Healthy		Cancer	
	Male	Female	Male	Female
Haematocrit (%)	45.3 (9.5)	40.5 (10.9)	34.2 (15)	29.2 (14.5)
α-1 acid glycoprotein (g/L)	0.638 923)	0.575 (24)	1.15 (36.4)	1.25 (39.8)
Albumin (g/L)	50.34 (10)	49.38 (10)	39.5 (19.7)	39.2 (15.4)
GFR (mL/min)	106.4 (19)	119.1 (24)	102.7 (18)	92.2 (21)
Creatinine (μmol/L)	76.5 (16)	57 (20.4)	87.8 (16)	69 (17)
Weight (kg)	64.6 (18)	57.5 (19)	67.4 (13)	55.2 (10)

Table S 3.2 Demographic and biochemical changes describing the Chinese Cancer population.

Simcyp population group parameter changes used in the development of the Chinese cancer population group. For a full description of the model development and validation please see Yu et al (2021) [473].

Chapter 4 The modulation effects of flavonoids on breast cancer resistance protein in glioblastomas cells

4.1 Introduction

Glioblastomas multiforme (GBM) is widely acknowledged as an exceptionally aggressive neoplasm and is considered the predominant malignant primary tumour that affects the brain and CNS [518]. It accounts for 48.6% of malignant CNS tumours and for 14.5% of all CNS cancers [518]. Patients with GBM often have a median overall survival (OS) of only 15 months, which is a fairly brief timeframe [518].

The primary challenge in addressing malignant gliomas lies in the presence of the BBB, a barrier consisting of specialised capillary endothelial cells with tight junctions composed of claudins (specifically claudins -1, -3, -5), occludins, and junctional adhesion molecules [519]. The BBB selectively permits the passive diffusion of small molecules with molecular weights less than 500 Da and sizes less than 400 nm, provided they possess lipophilic properties. In contrast, molecules that do not meet these criteria rely on alternative processes to traverse the blood-brain barrier, such as pinocytosis, receptor- or carrier-mediated transcytosis, and solute-carrier-protein pathways [519]. The maintenance of BBB integrity and homeostasis is augmented by ABC transporters, including P-gp, MDR1, BCRP, and various other resistance proteins that are present in the lumen and meninges [519]. Regulating these efflux pumps has mainly been unsuccessful.

Increased active transport efflux of anticancer medications and decreased drug concentration within the cancer cells are seen in multidrug-resistant cancer cells as the primary reasons why cancer treatment fails [520]. The origin of this phenomena is commonly attributed to the upregulation and/or function of ABC transporters within the tumour-brain-barrier and at the BBB itself [520].

The current body of research focuses on the utilisation of third generation P-gp inhibitors, specifically tariquidar, in conjunction with first-line chemotherapy for the management of NSCLC [520]. Furthermore, tariquidar is also known as a BCRP modulator, can inhibit BCRP in a lower concentration (~1 μM) than P-gp (~2.3 μM). However, natural products such as flavonids, have been recently explored for their ability to modulate drug transporter function and impart anti-cancer effects on cellular development/progression.

As candidate natural compounds, several flavonoids have been assessed for cytotoxic effects on BCRP-MDCKII cells as *in vitro* studies [521]. Amentoflavone, apigenin, biochanin A, chrysin, diosimin, genkwanin, hypericin, kaempferol, kaempferide,

licochalcone A, and naringenin have shown substantial suppression on BCRP (over 50%) [521]. This inhibition was accompanied by a notable enhancement in the absorption of mitoxantrone into BCRP-MDCKII cells. The eleven flavonoids that significantly inhibited BCRP are divided into several categories, including flavone, dihydroflavone, flavonol, biflavone, chalcone, isoflavone, and dianthrone [521]. Furthermore, prior research has indicated a positive association between the upregulation of BCRP and an elevated resistance to TMZ [521]. Conversely, the inhibition of BCRP has been found to enhance the ability of TMZ to penetrate the brain and exhibit antitumour effects [521]. Licochalcone A and Genkwanin showed effective inhibition effects when co-utilised with TMZ in U251, U251T and T98G cells [521], the inhibition% of these 2 drugs in U251T and T98G are both over 95%, which indicated as promising BCRP inhibitors, further research is needed.

Given that the practical application of existing BCRP inhibitors (e.g. GF120918, FTC) is hindered due to a range of neurotoxic effects [522], the current study is centred around the identification of suitable inhibitors/modulators of BCRP using flavonoids.

4.2 Aims and objectives

Based on the ability of flavonoids- depressing BCRP function on the glioblastoma cells at the BBB, the aims of this chapter are to determine and estimate the impacts and expression of flavonoids on BCRP function in LN229 cells. The experiments involved the apoptosis and application of reactive oxygen species inducing agents. LN229 cells were used as the test subjects.

The overall objectives as follows:

- To assess the cytotoxicity of flavonoids on LN 229 cells;
- To assess the effect of flavonoids to modulate the expression of BCRP in LN 229 cells;
- To assess the effect of flavonoids on cellular migration of LN 229 cells;
- To assess the effect of flavonoids as anti-cancer agents on reactive oxygen species generation in LN 229 cells;
- To assess the effect of flavonoids as anti-cancer agents on the activation of caspases in LN 229 cells.

4.3 Materials

Drugs: Dulbecco's modified essential media with 4.5 g/L glucose (DMEM), Fetal Bovine Serum (FBS), L-glutamine, Antibiotic-Antimycotic® (100X) were obtained from Biosera (Sussex, UK); 0.25 % w/v trypsin-EDTA; Phosphate buffered saline (PBS) solution; Hoescht-33342 (H33342); ROS assay kit (Ab113851, Abcam Cambridge, UK); A fluorescence Caspase-3/7 assay kit (Cayman Chemicals, 10009135, USA); Ko143, and all other chemicals were sourced from Sigma (Dorset, UK);

For this chapter, the used flavonoids were listed as follows: Harmine, 4-hydroxy-3-methoxycinnamaldehyde, 7-aminoflavone, rotenone, trihydroxyethylrutin and 5-methoxyflavone, 6-hydroxyflavanone, 7-methoxyflavanone. The corresponding stock solution were prepared with dimethyl sulfoxide (DMSO), the concentration of all these stock solutions was 10mM and stored at −80 °C for further application.

4.4 Methodology

4.4.1 Culture of LN 229 cells

The LN229 cell line (ATCC: CRL-2611), derived from human glioblastoma, was cultivated in a growth medium consisting of 1% foetal bovine serum (FBS), 1% volume/volume antibiotic-antimycotic, and Dulbecco's Modified Eagle Medium (DMEM).

The cells were added into an uncoated T75 flask and cultivated for a period of 4-5 days until reaching confluency. Subsequently, a volume of 1 mL of trypsin-EDTA solution with a concentration of 0.25% weight/volume was added into the flask and allowed to incubate for a duration of 3 minutes. Following this, the trypsin-EDTA solution was neutralised by adding an equal volume of growth media. The cell suspension was subsequently transferred onto T25, T75 flasks; 24 well-, 96 well-plates for subsequent experimental procedures.

4.4.2 The cellular toxicity of flavonoids on LN 229 cells

As a cell viability assay, a 3-(4,5-dimethylthiazol-2-yl)-2,5-diphenyl-2H-tetrazolium bromide (MTT) assay was used to determine and evaluate the cytotoxicity under the

impacts of our chosen flavonoids. A 96-well plate with 50,000 cells per well was seeded and incubated in the 37 °C constant temperature and humidity (5% CO_2) incubator for 24 hours. Then the medium of cells was removed and were incubated with a 6-fold concentration range of flavonoids (0.001-100 μM) for 24 hours. During the 24 hours, MTT sterile powder was diluted with DMSO until this storage concentration of MTT was 5mg/mL and stored in -20 °C refrigerator. On the day of experiment, MTT storage was diluted as a working concentration of 0.5mg/mL (1:10) using serum-free medium. When the 96-well plate was ready, the medium was removed, and the wells were washed with pre-warmed PBS. Thereafter, the 96-well plate was treated with MTT working concentration, namely 0.5mg/mL. The 96-well plate was covered with foil and incubated in the dark for 4 hours. After 4 hours, MTT working solution was removed and the purple crystals left in the wells were dissolved with 100μL/well DMSO. Then the 96-well plate was wrapped with foil again and shaked gently on an orbital shaker for 15 minutes. After 15 minutes, the absorbance of the wells was measure with a multilabel microplate reader at 362 nm and the cell viability was calculated as follows:

$$\%\ \text{cell viability} = \frac{\text{UV absrobance in drug} - \text{treated cells}}{\text{UV aborbance in control cells}} \times 100$$

4.4.3 Inhibition of efflux function of BCRP in Hochest-33342 and Mitoxantrone intracellular accumulation assay towards LN 229 cells

The accumulation assay is to determine the fluorescence of the accumulated amount of Hoescht-33342 (H33342) and mitoxantrone in the LN229 cells, so as to assess the impacts of the flavonoids on BCRP function. For preparation of this assay, a 96-well plate with 50,000 cells per well was seeded and incubated in the 37 °C constant temperature and humidity (5% CO2) incubator for 24 hours. On the day of this assay, the medium was removed, and the cells were incubated with a 6-fold concentration of flavonoids (0.001-100μM) for 1 hour. Then, the cells were incubated with a 6-fold concentration of flavonoids (0.001-100μM) with 10μM Hoescht-33342 (H33342) or mitoxantrone for 1 hour. Thereafter, all the medium was removed, and this 96-well plate was washed with cold PBS twice and 100μL PBS was added into each well. Then this well plate was frozen in the -80 °C refrigerator for 30 minutes. After 30 minutes, all the cells were scratched and removed from this well plate and transferred into a black 96-well plate. The resulting intracellular

fluorescence group used H33342 was measured by a multilabel microplate reader (Tecan Spark 10M®) at an excitation and emission wavelength of 340 nm and 510 nm, respectively. The resulting intracellular fluorescence group used mitoxantrone was measured by a multilabel microplate reader (Tecan Spark 10M®) at an excitation and emission wavelength of 355 nm and 465 nm, respectively.

4.4.4 Cellular migration assay towards LN 229 cells in the presence of flavonoids

The main features of glioblastomas cells are invasion and migration [523]. As the most common malignant brain tumour, GBM cells can migrate away from the central tumour mass into healthy brain tissues, these growing GBM cells can promote tumour growth in the invaded area [524].

This cellular migration assay is to assess the migration rate of LN 229 cells in the presence of flavonoids. A 24-well plate with 70,000 cells per well was seeded and incubated in the 37 °C constant temperature and humidity (5% CO2) incubator for 24 hours, and the medium was replaced with flavonoids diluted by serum-free medium (concentration: 50 μM) for 24 hours of incubation. Thereafter, vertical and horizontal scratches were made in the middle of each well by a 20 μL pipette tip. The wells were washed with PBS to remove the scratched cells debris. Images were captured after the incubated 24 hours. The closure distance was measured by Image J and used to calculate the percentage of wound closure under the impacts of flavonoids. The percentage of wound closure was calculated using the ImageJ software according to the differences between the initially scratched area and new closure area following the incubation period. To compare effectiveness, a minimum cut-off of 50 % inhibition of cellular migration was utilised.

$$Wound\ closure\ (\%) = \frac{W_0 - W_t}{W_0} \times 100 \quad [525]$$

W_0 = Wound area at 0 h (μm)

W_t = Wound area at Δh (μm)

4.4.5 ROS assay towards LN 229 cells

ROS, a by-product of aerobic metabolism in cells, can activate signaling pathways that promote regular cell growth [526]. By raising ROS levels, anticancer drugs can destroy cancer cells [526]. Due to the features of cancer cells, which make them more vulnerable to oxidative damage, drugs that regulate ROS may improve the efficacy of cancer therapies [526].

ROS assay is to assess the potential for optimal flavonoids to activate ROS pathways in LN229 cells. A fluorescent probe 2',7'-dichlorofluorescin diacetate (DCF-DA) cellular ROS assay kit (Ab113851, Abcam Cambridge, UK) was utilised. Once DCFDA diffuses into a cell, esterase converts it to a nonfluorescent molecule. The intracellular generated ROS is capable of oxidizing this non-fluorescent molecule into the highly fluorescent compound-2' 7' dicholoroflouresciene (DCF).

A dark, clear bottom 96-well plate with 25,000 cells per well was seeded and incubated for 24 hours. On the day of the assay, the media was removed and 100 µL per well of 1×Buffer was added to wash each well. Then, 100 µL per well diluted DCFDA (25µM) was added into the 96 well plate to stain cells and leave this well plate in 37 °C constant temperature and humidity (5% CO2) incubator for 45 minutes' incubation. Thereafter, the cells were treated with the selected flavonoids at 10 µM, 100 µM and 500 µM and positive control TBHP solution at 50 µM, 100 µM for 4 hours' incubation. Furthermore, 30 minutes prior to completion of treatment, 100 µL per well 2×DCFDA dilution was added on top of the treated cells. After the whole 4 hours incubation was completed, the 96 well plate was transferred to the microplate reader (Tecan Spark 10M®) without washing and read end point in the presence of selected flavonoids and DCFDA with an excitation and emission wavelength range between 485 nm and 535 nm.

4.4.6 The activation of Caspase-3/7 assay

A fluorescence Caspase-3/7 assay kit (Cayman Chemicals, 10009135, USA) was utilised to assess the ability of the selected flavonoids to activate apoptosis in LN229 cells. A specific substrate, N-Ac-DEVD-N'-MC-R110, was employed during this assay, which upon cleavage by active caspase-3 or caspase-7, a highly fluorescent product was generated and measured using excitation and emission wavelengths of 485 and 535 nm, respectively.

A 96-well plate at a density of 50,000 cells per well in the appropriate LN229 cells culture media was seeded and incubated for 24 hours. Thereafter the cells were treated with selected flavonoids and active caspase-3 positive control all at 10 μM and 100 μM for 4 hours. Then, the plate was centrifuged in a plate centrifuge at 800×g for 5 minutes and the media was aspirated. Thereafter, 200 μL/well of assay buffer was added into each well and the plate was re-centrifuged at 800×g for 5 minutes. Next, the supernatant was removed and 100 μL/well of cell lysis buffer was added, followed by the incubation under gentle shaking for 30 minutes at room temperature. Thereafter, the plate was centrifuged for an additional 10 minutes at 800 × g followed by the transfer of 90 μL supernatant into the corresponding wells of a new black 96-well plate, each well was added with 10 μL of the caspase-3/7 assay buffer. Then, 100μL of the active caspase-3 positive control were added into corresponding wells, and each well was added with 100 μL caspase-3/7 substrate solution. Then, the plate was incubated for 90 minutes at 37 °C, 5% CO^2. The fluorescence intensity of the well plate was measured with a plate reader (Tecan Spark 10M®) using excitation and emission wavelengths of 485 and 535 nm, respectively.

4.4.7 Statistical Analysis

All data is presented as mean ± standard deviation, with experiments being conducted in at least 3 replicate independent experiment unless otherwise stated.

Where appropriate, statistical analyses was performed in GraphPad Prism 9 (La Jolla, California, USA), with t-tests used to determine differences between the mean values. A significance p-value of <0.05 was considered as statistically significant.

4.5 Results

4.5.1 Assessment of intracellular toxicity of the flavonoids in LN 229 cells.

A MTT cytotoxicity assay was utilised to investigate the cellular toxicity towards LN229 cells, it was conducted across a 6-fold concentration (0.001-100 μM) range of modulators for 24 hours. All the modulators displayed limited toxicity up to 100 μM, with an IC50 determined only for harmine (336.3 ± 2.52 μM), 4-hydroxy-3-methoxycinnamaldehyde (641.2 ± 2.80 μM), 7-aminoflavone (1261 ± 3.1 μM) and 7-methoxyflavanone (968.2 ± 2.98 μM).

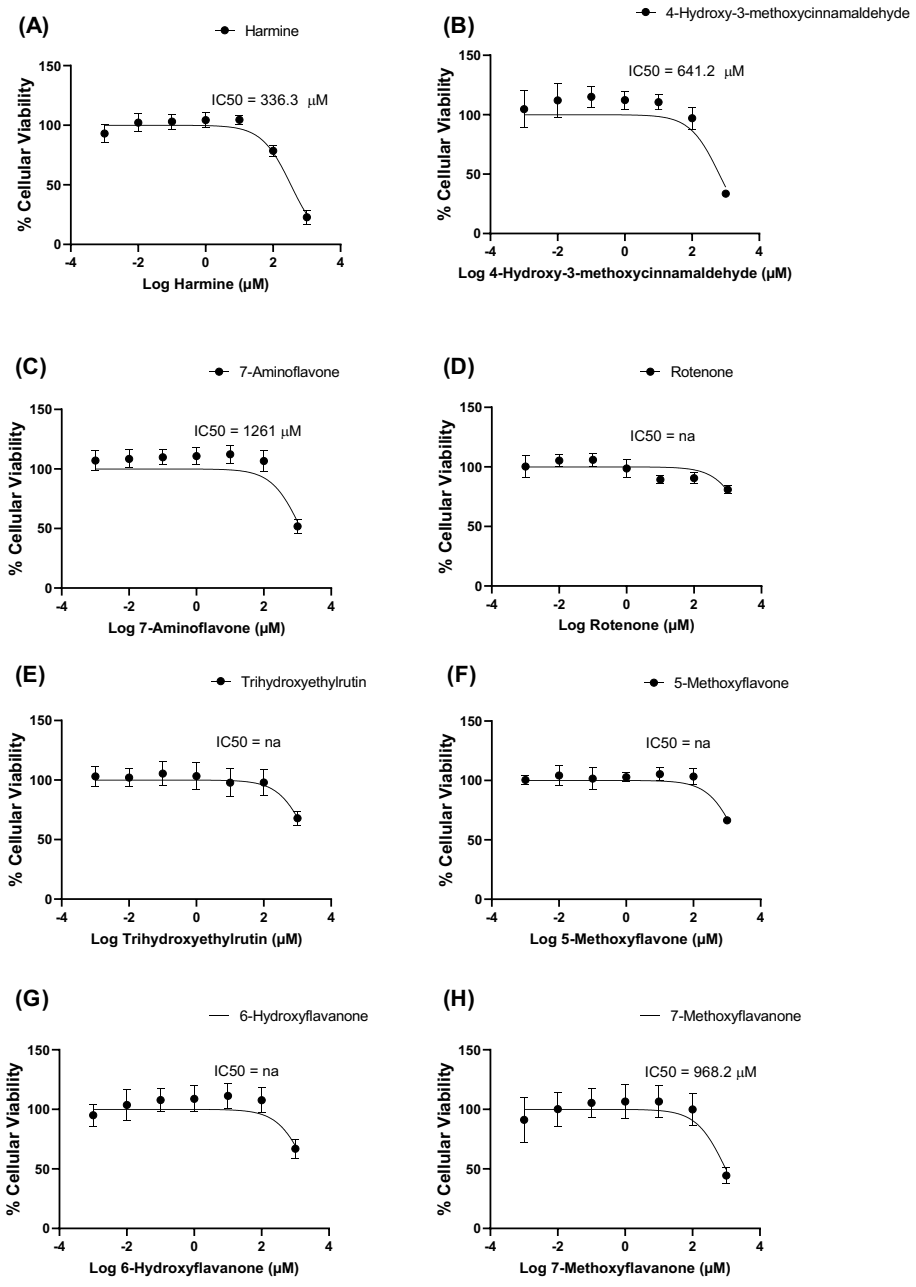

Figure 4.1% Cellular viability under the treatment of selected flavonoids.

LN 229 cells were seeded and grown on 96 well plates for 24 hours, followed by exposure to selected flavonoids over concentration range of 0.001-1000 μM for 24 hours: Harmine (A), 4-Hydroxy-3-methoxycinnamaldehyde (B), 7-Aminoflavone (C), Rotenone (D), Trihydroxyethylrutin (E) and 5-Methoxyflavone (F), 6-Hydroxyflavanone (G), 7-Methoxyflavanone (H), prior to an MTT assay being performed. 20 μl/ well (0.5 mg/mL) of MTT was added and the plates were incubated for additional 24 hours. The media was removed and 100 μL/well of DMSO was added, then the plate absorbance was measured at 570 nm. The output data was reported as IC50. Filled circles and associated vertical lines indicate the observed mean and standard deviation from clinical data; solid black lines indicated predicted % Cellular viability mean verse flavonoids concentration profile in a log scale.

4.5.2 Assessment of modulated BCRP function in Hochest-33342 and Mitoxantrone intracellular accumulation assay towards LN 229 cells

To exclude the effects of fluorescence on the determined results, the fluorescence of PBS, H33342, mitoxantrone and selected flavonoids were examined. The fluorescence of harmine was extremely high, thus it was removed from Figure 4.2. The fluorescence of 7-aminoflavone showed significance when compared to H33342 (* $P \leqslant 0.01$). However, the fluorescence of 7-aminoflavone showed significance when compared to PBS (**** $P \leqslant 0.0001$). Meanwhile, the fluorescence of 5-methoxyflavone also showed significance

when compared to PBS (*** P ⩽ 0.001). Therefore, harmine, 7-aminoflavone, 5-methoxyflavone utilised mitoxantrone during the accumulation assay.

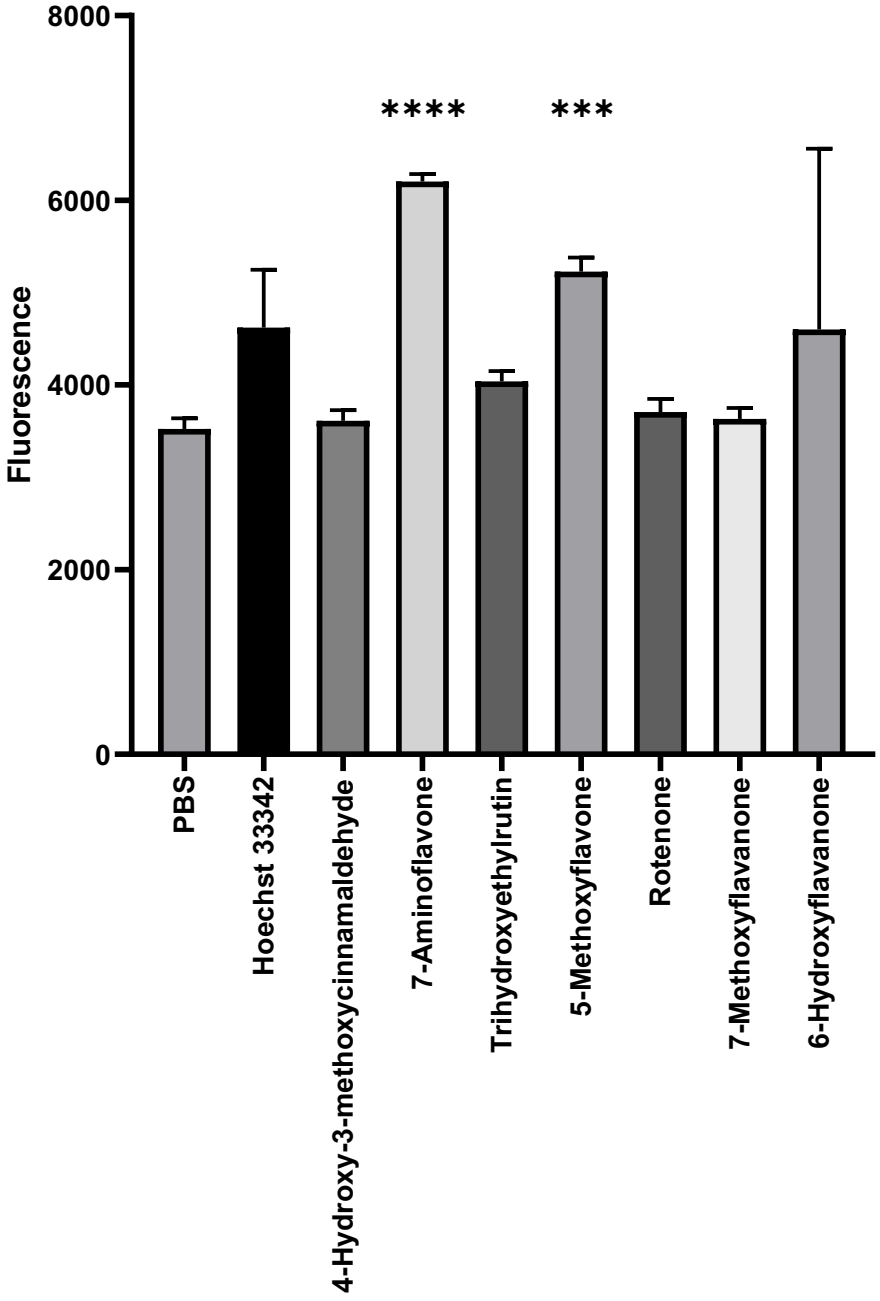

Figure 4.2 The determined fluorescence of the Hoechst 33342, PBS, and flavonoids.

The Hoechst 33342 and flavonoids were diluted with PBS and determined in a 96 well plate, and each compound had 8 replicates. * P ≤ 0.05, ** P ≤ 0.01, *** P ≤ 0.001 and **** P ≤ 0.0001. The resulting intracellular fluorescence was measured by a multilabel microplate reader (Tecan Spark 10M®) at an excitation and emission wavelength of 340 nm and 510 nm, respectively.

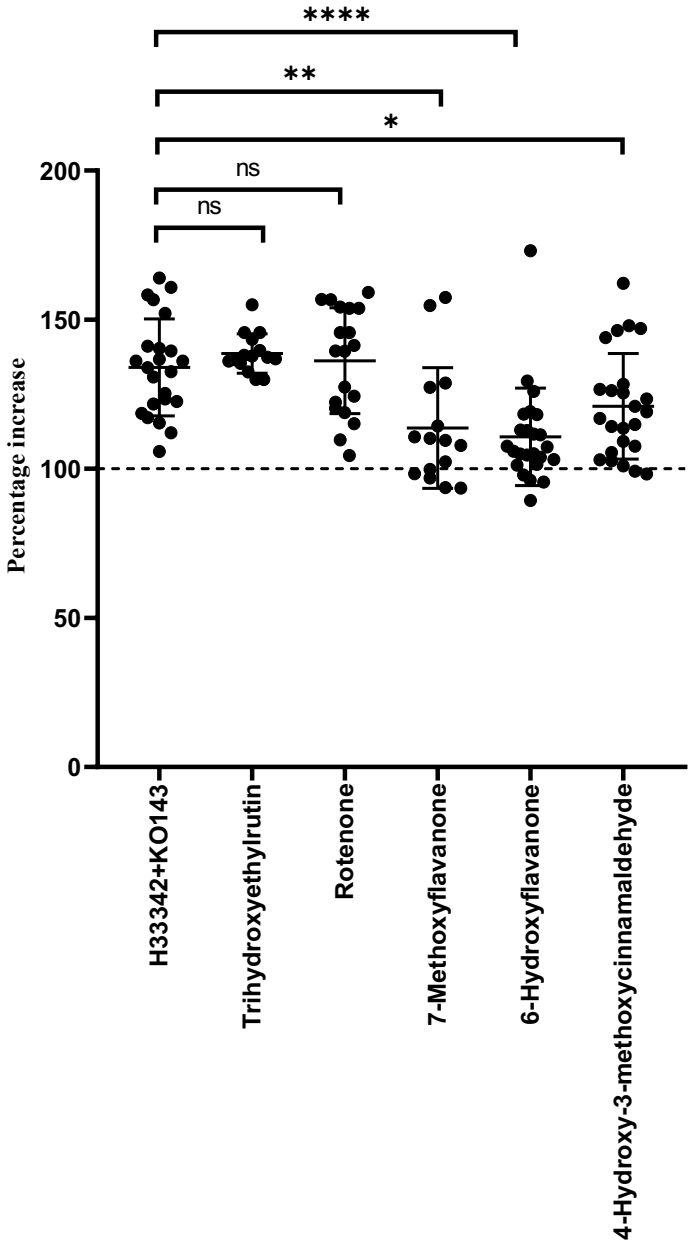

Figure 4.3 Assessment of the intracellular Hoechst 33342 accumulation in the presence of Ko143 and flavonoids.

LN229 cells were cultured in the 96-well plates at 37°C in a humidified atmosphere of 5% CO2 in air for 24 h. The media was prepared, and cells were subsequently incubated with a percentage increase range (1 μM-100 μM) of 7-Methoxyflavanone, 6-Hydroxyflavanone, Trihydroxyethylrutin, Rotenone and 4-Hydroxy-3-methoxycinnamaldehyde, Hoechst 33342 and Ko143. Significant differences between Ko143 and flavonoids are shown above. * P ≤ 0.05, ** P ≤ 0.01, *** P ≤ 0.001 and **** P ≤ 0.0001. The resulting intracellular fluorescence was measured by a multilabel microplate reader (Tecan Spark 10M®) at an excitation and emission wavelength of 340 nm and 510 nm, respectively.

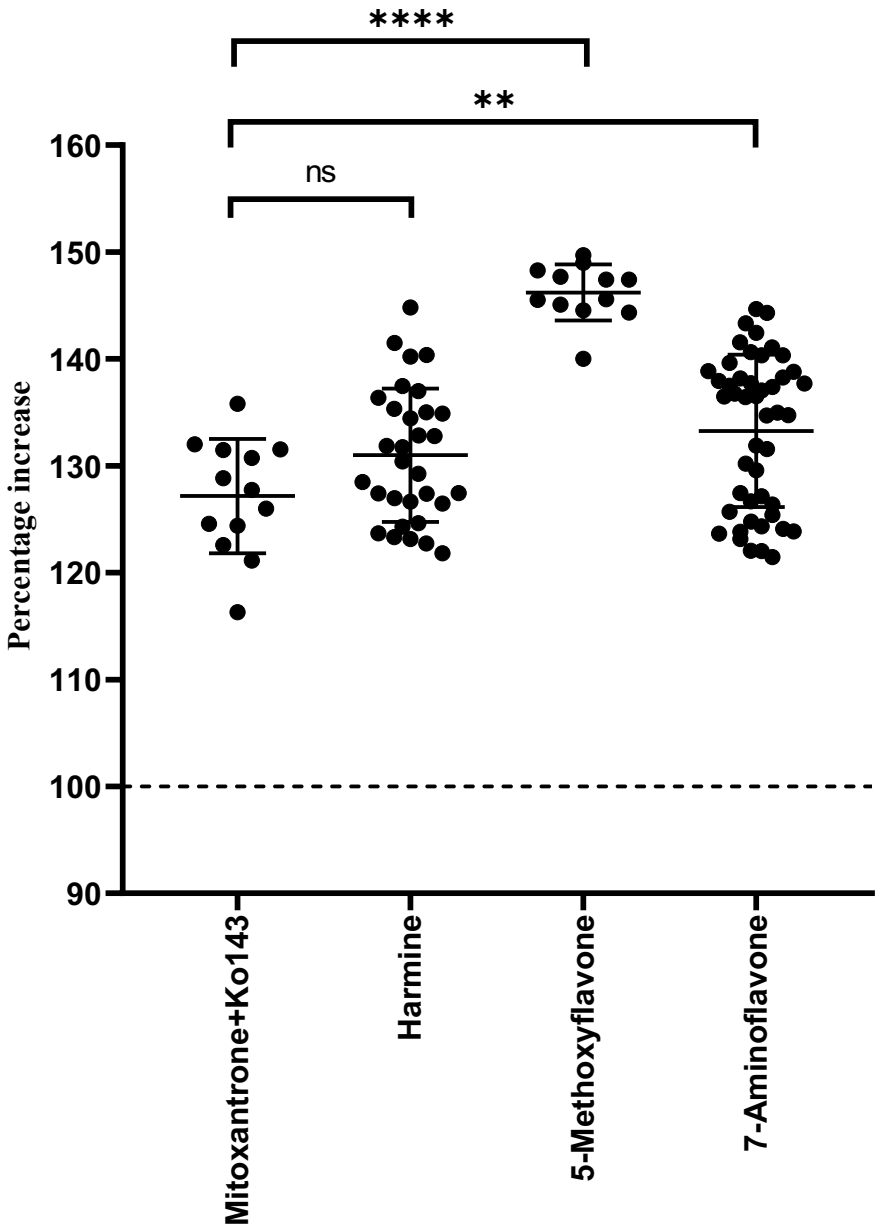

Figure 4.4 Assessment of the intracellular Mitoxantrone accumulation in the presence of Ko143 and flavonoids.

LN229 cells were cultured in the 96-well plates at 37°C in a humidified atmosphere of 5% CO2 in air for 24 h. The media was prepared, and cells were subsequently incubated with a percentage increase range (1 μM-100 μM) of harmine, 5-methoxyflavone, 7-aminoflavone, mitoxantrone and Ko143. Significant differences between Ko143 and flavonoids are shown above. * P ≤ 0.05, ** P ≤ 0.01, *** P ≤ 0.001 and **** P ≤ 0.0001. The resulting intracellular fluorescence was measured by a multilabel microplate reader (Tecan Spark 10M®) at an excitation and emission wavelength of 355 nm and 465 nm, respectively.

4.5.3 Assessment of cellular migration towards LN 229 cells in the presence of flavonoids

In order to examine the ability of the flavonoids to inhibit cellular migration of human glioblastoma cells LN229, a cellular migration assay was conducted where the migration of cells within a scratch was quantified over 24 hours in the presence of 50 μM of the flavonoids (Figure 4.5). Incubation with all modulators resulted in statistically significant decreases in cellular migration compared to control (*** $P \leqslant 0.001$ and **** $P \leqslant 0.0001$), except for 5-methoxyflavone, 7-aminoflavone, 4-hydroxy-3-methoxycinnamaldehyde, trihydroxyethylrutin, 6-hydroxyflavanone (Figure 4.5).

Harmine and rotenone demonstrated < 10 % migration following 24 hours with the overall order of migration (Figure 4.5) being: untreated > 6-hydroxyflavanone > 4-hydroxy-3-methoxycinnamaldehyde > 5-methoxyflavone > 7-aminoflavone > trihydroxyethylrutin > 7-methoxyflavanone > harmine > rotenone (Figure 4.5).

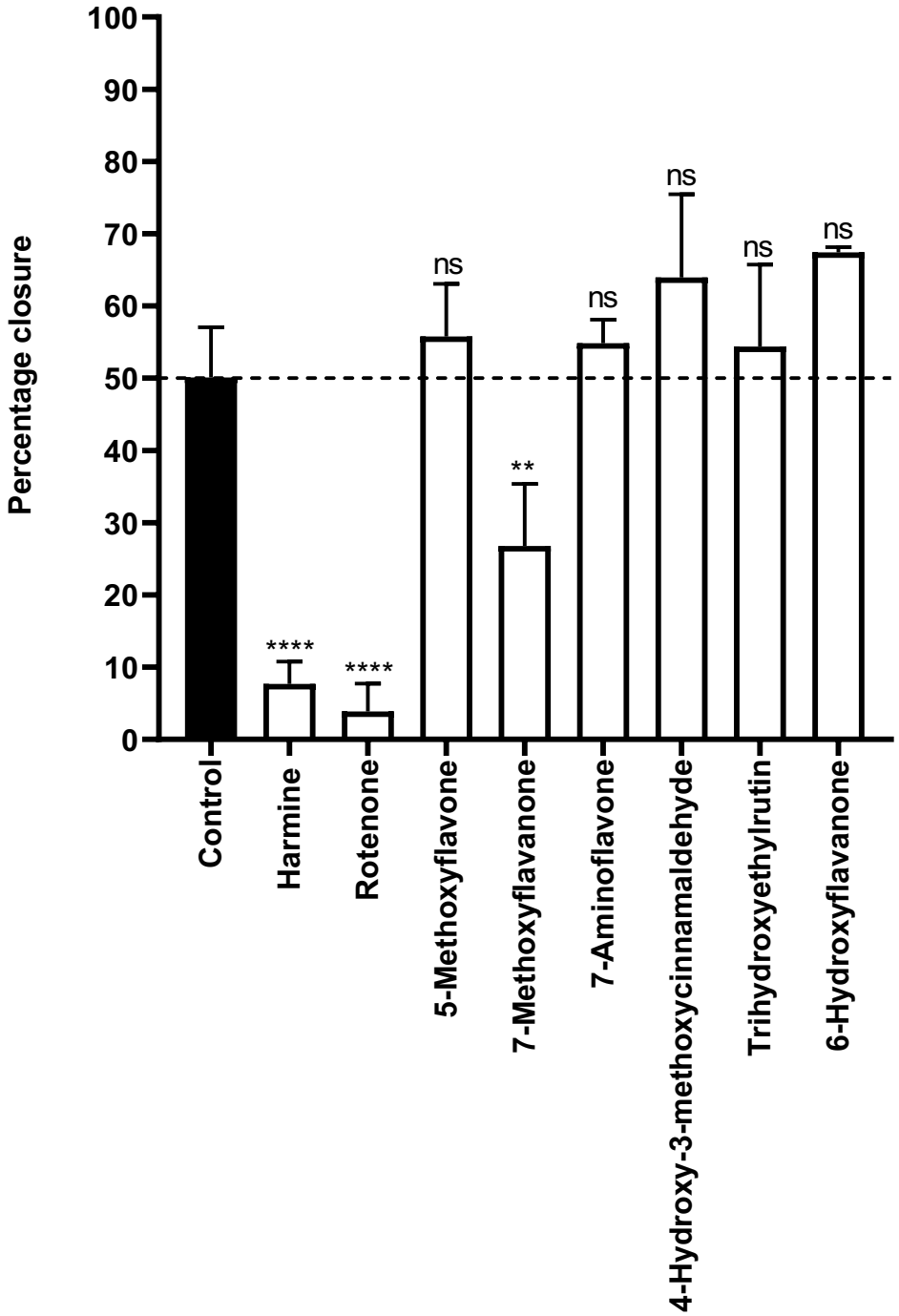

Figure 4.5 Cellular migration assay

Percentage closure of LN229 cells following scratches made to the plate surface. Cells were incubated with serum free media containing 50 μM of the flavonoids for 24 hours within a humidified atmosphere of 5% CO2 in air. Images were taken under the microscope before and after 24 hours of incubation, with the horizontal dashed line representing a 50% closure cut-off. All the flavonoids are shown above. * P ≤ 0.05, ** P ≤ 0.01, *** P ≤ 0.001 and **** P ≤ 0.0001.

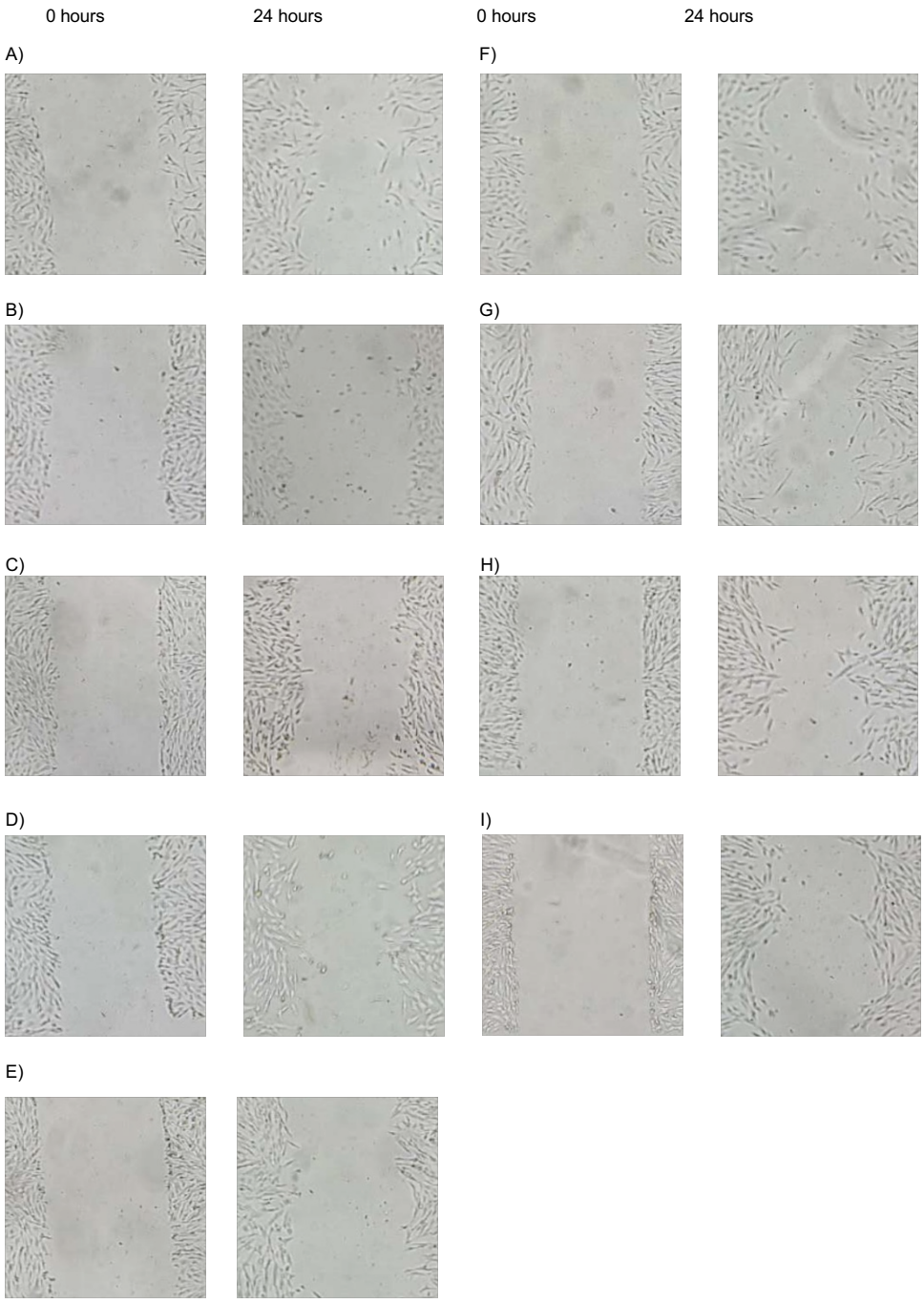

Figure 4.6 Cellular migration assay.

Images of the wound at 0 and 24 hours of LN229 cells following scratches made to the plate surface. Cells were incubated with serum free media containing 50 μM of the modulators for 24 hours within a Cell-IQ incubator. Automated looped images were taken prior to incubation A: Untreated; B: Harmine; C: Rotenone; D: 5-Methoxyflavone; E: 7-Methoxyflavanone; F: 7-Aminoflavone; G: 4-Hydroxy-3-methoxycinnamaldehyde; H: Trihydroxyethylrutin; I: 6-Hydroxyflavanone.

4.5.4 Evaluation of ROS levels towards LN 229 cells in the presence of flavonoids

Based on the results of scratch assay, the harmine, rotenone and 7-methoxyflavanone were selected to assess their ability to ROS pathways in human glioblastomas LN229 cells. A ROS assay was conducted across a concentration range of 10-100 μM.

Among these 3 drugs, rotenone 100 μM showed the largest ROS detection, 269.26 ± 41.82% of the untreated group. It was the only one that showed statistically significant in ROS production when compared to the untreated group.

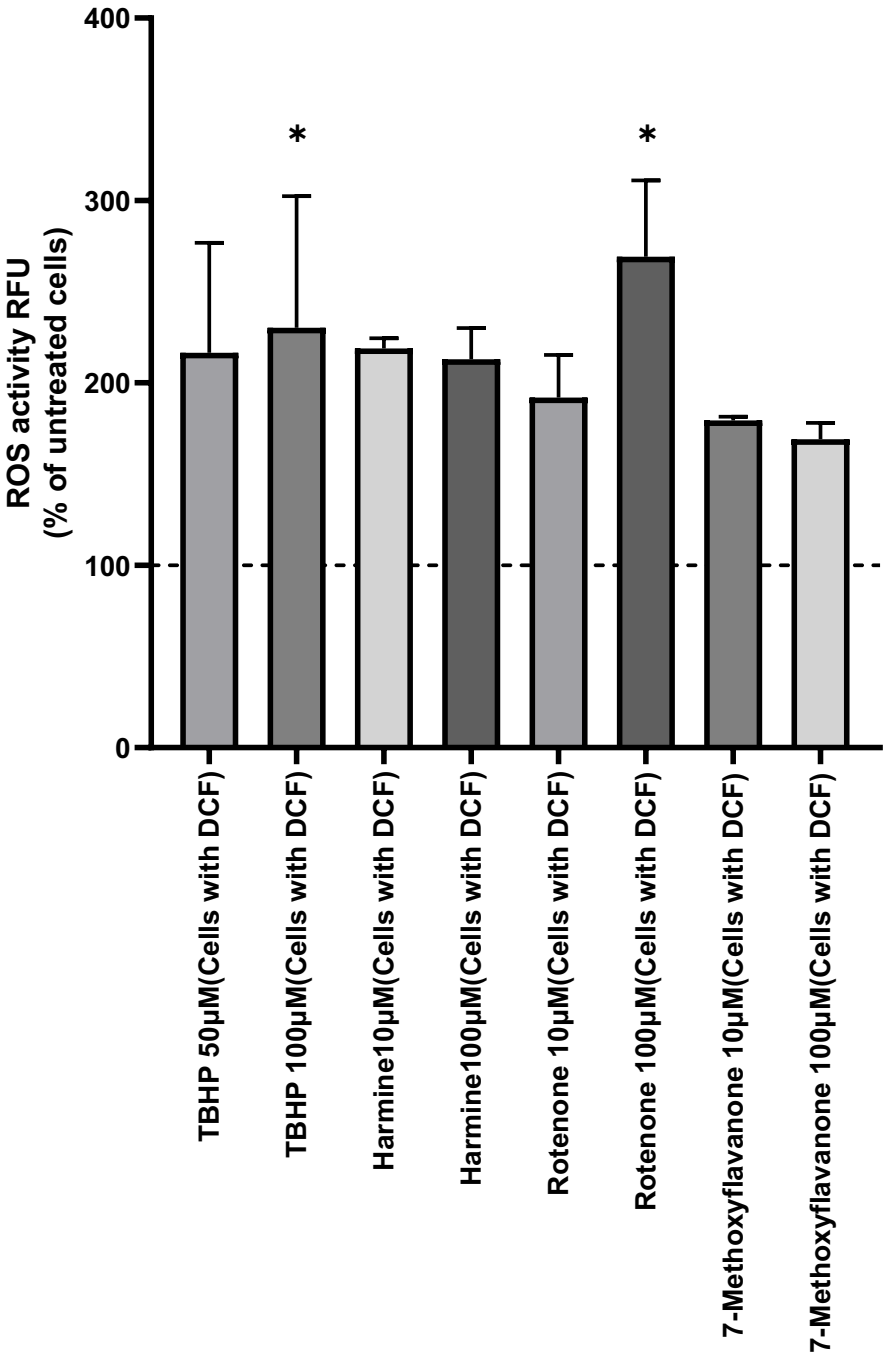

Figure 4.7 Radical oxygen detection assay

LN 229 cells were seeded in a 96-well plate and incubated for 24 hours before being washed by 1×Buffer. Then, the cells were treated with 25μM DCFDA and incubated for 45 minutes. Thereafter, the cells were treated with the selected flavonoids at 10 and 100 μM, and positive control TBHP solution at 50 μM, 100 μM for 4 hours' incubation. The fluorescence of DCFDA was measured with an excitation and emission wavelength range between 485 and 535 nm. Results are presented normalized against untreated cells. * $P \leq 0.05$, ** $P \leq 0.01$, *** $P \leq 0.001$ and **** $P \leq 0.0001$.

4.5.5 Evaluation of the activated caspase-3/7 towards LN 229 cells in the presence of flavonoids

The activation of caspase-3 and -7 serves as the functional and ultimate event in the apoptotic cascade. This activation is utilised as a marker to identify apoptosis and as a therapeutic target for addressing apoptotic resistance in cancer. The Cayman's caspase-3/7 fluorescence assay kit selected a specific substrate, N-Ac-DEVD-N'-MC-R110, which was cleavage by caspase-3 or -7 and produced a fluorescence compound. This compound can be measured within the wavelength range of 485 and 535 nm.

Harmine, rotenone and 7-methoxyflavanone were selected to be assessed at concentrations of 10 and 100 μM for each drug (Figure 4.7).

At 10 μM, no statistically significant differences were observed in Caspase activity when compared to untreated controls. At 100 μM, only harmine demonstrated a statistically significant ($P \leq 0.001$) increase in Caspase activity when compared to the untreated group.

For 10 μM of each drug, none of them showed statistically significance compared to the untreated group. Furthermore, the results, RFU- % of untreated group are similar, 97.01± 2.55 % for harmine, 97.32± 0.95 % for rotenone and 98.95± 1.20 % for 7-methoxyflavanone.

For 100 μM of each drug, there was no statistically significance of rotenone and 7-methoxyflavanone, and the RFU results are similar to the results of 10 μM of the corresponding drugs, 97.61± 3.54 for rotenone and 98.08± 2.17 % for 7-methoxyflavanone. However, with the 100 μM concentration of harmine, it demonstrated statistically significance ($P \leq 0.001$) compared to the untreated group. Unlike the other 2 drugs, the RFU of 100 μM harmine was 109.62± 4.09 % compared to the untreated group.

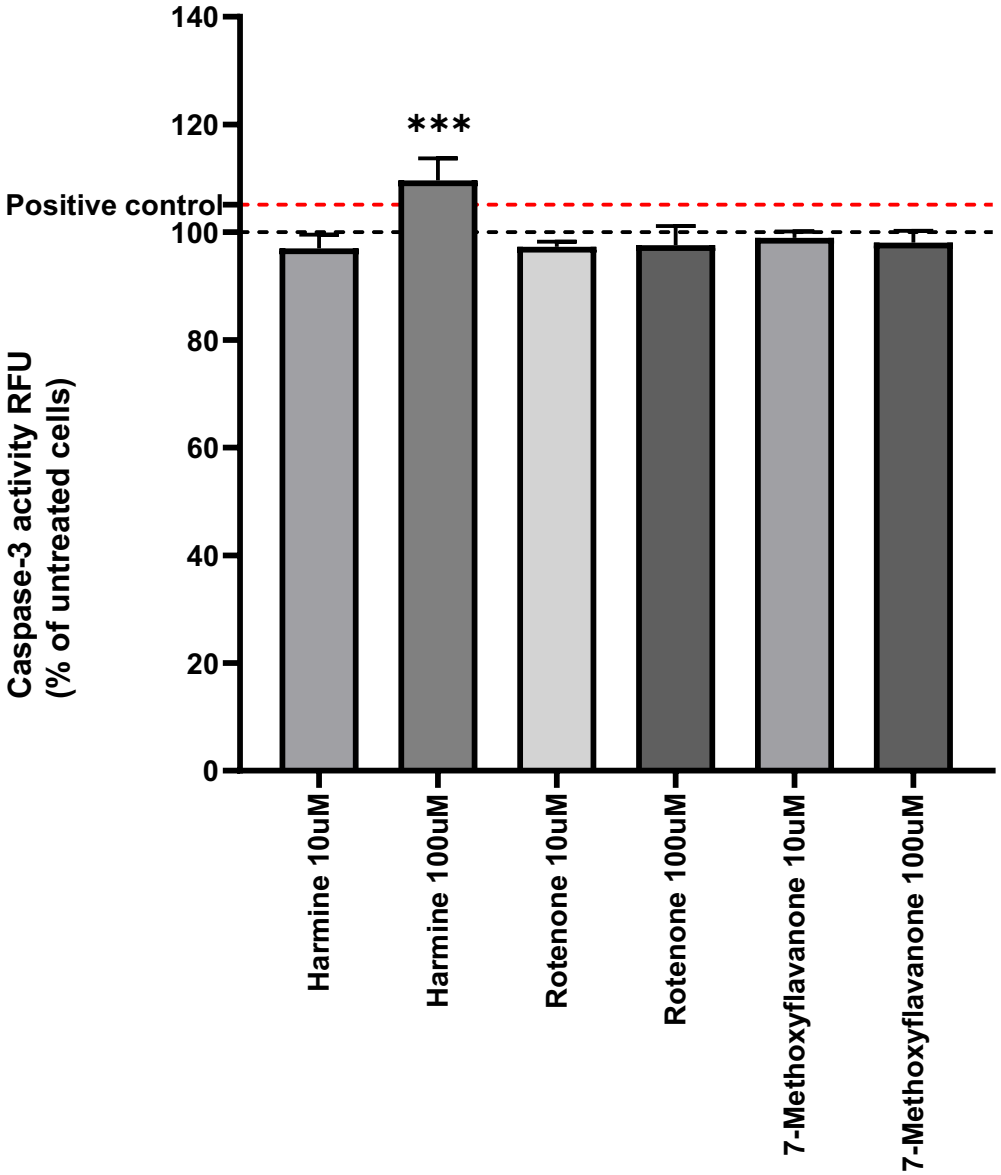

Figure 4.8 Caspase-3/7 assay

LN 229 cells were seeded in a 96-well plate and incubated for 24 hours before being incubated by 3 selected flavonoids (harmine, rotenone and 7-methoxyflavanone) for another 4 hours, and concentrations of 10 and 100 μM for each drug were used during the incubation. Caspase-3 or -7 cleaved the substrate, N-Ac-DEVD-N'-MC-R110, and the generated fluorescent compound was detected at the wavelength of excitation and emission wavelengths of 485 and 535 nm, respectively. Results are presented normalized against untreated cells. * $P \leqslant 0.05$, ** $P \leqslant 0.01$, *** $P \leqslant 0.001$ and **** $P \leqslant 0.0001$.

4.6 Discussion

As natural drugs, flavonoids are famous for its low toxicity, thus, MTT assay was utilised to assess the intracellular toxicity of the selected flavonoids at first. Additionally, the potential of flavonoids as BCRP inhibitor may cause the increasing accumulation of drugs towards the cancer cells. To explore the ability of flavonoids' BCRP inhibition effects on human glioblastomas LN 229 cells, this chapter used the accumulation assay. To evaluate the potential of flavonoids' ability to inhibit the migration of cancer cells, cellular migration assay was utilised. Furthermore, ROS assay was selected to assess the potential for flavonoids to activate ROS pathways in LN229 cells, and A fluorescence Caspase-3/7 assay was utilised to assess the ability of the selected flavonoids to activate apoptosis in LN229 cells.

4.6.1 Intracellular toxicity of the flavonoids in LN 229 cells

There were 8 flavonoids were screened for their intracellular toxicity within LN229 cells, and the concentration range was 0.001-100 μM (a 6-fold log-concentration range). The data was reported as IC50. The lowest IC50 was for harmine (336.3 ± 2.52 μM), the relatively high IC50 were for 7-methoxyflavanone (968.2 ± 2.98 μM) and 4-hydroxy-3-methoxycinnamaldehyde (641.2 ± 2.80 μM). The demonstrated minimal toxicities of the other four flavonoids- rotenone, trihydroxyethylrutin, 5-methoxyflavone and 6-hydroxyflavanone were up to 1000 μM. Apparently, this is not the expected results, because for the studied human cell lines, they will be toxic. However, the higher tolerance of flavonoids of LN 229 cells compared to other cell lines makes it different.

The cellular toxicity of harmine was tested towards two human cancer cell lines, namely, MCF7 breast cancer and HCT116 colon cancer [527]. Furthermore, the IC50 of harmine for them were 1.3±0.2 μM and 0.70±0.03 μM [527], respectively. It was clear that harmine was toxic to these cell lines and these cell lines could be thought as relatively sensitive.

Furthermore, the IC50 of 4-hydroxy-3-methoxycinnamaldehyde for A-549 cell line (adenocarcinomic human alveolar basal epithelial cells) was between 1.3 and 8.0 μM [528], Additionally, the IC50 of 7-aminoflavone was tested towards four human cancer cell lines,

including HL-60 (57.2 ± 2.0 μM), NALM-6 (54.5 ± 2.2 μM), WM115 (90.6 ± 5.4 μM) and COLO205 (73.1 ± 4.6 μM) (IC50 ± SD) [529]. The IC of rotenone for Hela and MCF-7 cell lines were 0.2 ± 0.1, 0.4 ± 0.1 μM, respectively[530]. Furthermore, the IC of 5-methoxyflavone for U937 and MOL-4 cell lines [531] were 46.70 ± 1.60, 26.39 ± 2.22 μM, respectively.

4.6.2 Intracellular accumulation of H33342 and mitoxantrone towards LN 229 cells in the presence of flavonoids

The BCRP is a significant ATP efflux transporter that use ATP as an energy source to remove xenobiotics from the cells [532]. The overexpression of BCRP within cancer cells is common due to the MDR phenomenon. The BCRP inhibitors target BCRP, might effectively impede its efflux function, thereby leading to enhanced drug accumulation within cancer cells [533]. Multiple flavonoid compounds have been discovered to show inhibitory properties against BCRP, such as the flavones retusin and ayanin [533]. Therefore, the design for this accumulation assay is to assess the inhibitory ability of the BCRP of selected flavonoids within glioblastomas cells.

To assess the efflux function of flavonoids as BCRP inhibitors, the fluorescent BCRP probe substrates, H33342 and mitoxantrone, were used. The results showed different responses over the gradient concentration range 1-100 μM of flavonoids: 5-methoxyflavone showed the greatest increase (1.46-fold) in mitoxantrone intracellular accumulation while KO143 was 1.27-fold increase, rotenone and trihydroxyethylrutin showed higher percentage increase (1.36-1.38-fold) in H33342 intracellular accumulation-which are similar to Ko143 (1.34-fold). Thereafter, harmine and 7-aminoflavone (1.31-1.33-fold) also determined as higher accumulation increase than KO 143.

5-Methoxyflavone has been recognised as a potential chemical with favourable biological activity and selectivity towards DNA pol-β in various *in vitro* Alzheimer's disease models [534]. The evaluation of *in vivo* assays, particularly the assessment of brain uptake of 5-methoxyflavone, is promising to promote the development of therapy options for Alzheimer's disease [534].

As a major P-gp-mediated efflux pump modifier, rotenone demonstrated the most potent inhibitory effects on cell proliferation in both the L5178 and MDA-MB-231 cell lines [535].

It was found that the administration of rotenone resulted in a proportional rise in the fluorescence activity ratio (FAR) and a much greater accumulation of the drug compared to the verapamil control in lymphoma cells of mice [535]. The fluorescence accumulation ratio (FAR) is a quantitative metric used to assess the cellular uptake of rhodamine 123, a fluorescent dye.

Rutin exhibits non-selective inhibition of P-GP and BCRP pumps in breast cancer [536], thus, the inhibition effects of trihydroxyethylrutin on BCRP also was tested.

The inhibitory effect of harmine on breast cancer resistance protein (BCRP) was observed in a study utilising MDA-MB-231 cells [537], a breast cancer cell line known for its elevated BCRP expression levels. Harmine significantly diminishes the resistance mediated by BCRP to anticancer drugs such as mitoxantrone and camptothecin [537]. Given that this compound did not demonstrate inhibition of P-gp overexpressing cells, it appears that its effect on multidrug-resistant (MDR) cells is specific to BCRP [537].

In conclusion, among these 8 flavonoids, there are 5 flavonoids showed good modulation effects on BCRP, the overall order to modulation effects (Figure 4.3, Figure 4.4) being: 5-methoxyflavone > trihydroxyethylrutin > rotenone > 7-aminoflavone > harmine. 5-Methoxyflavone showed the best performance in modulating functions of BCRP towards LN 229 cells.

4.6.3 Inhibition of cellular migration towards LN 229 cells in the presence of flavonoids

Harmine, rotenone and 7-methoxyflavanone demonstrated inhibition effects on cellular migration of LN 229 cells, and these 3 drugs showed more than 50% inhibition of migration at 50 μM concentration (Figure 4.5). The percentage of closure of harmine and rotenone are both under 10%, namely, 7.69% and 3.88%, respectively. Meanwhile, the percentage of closure of 7-methoxyflavanone is 26.8%.

According to recent research findings, harmine has been found to exhibit inhibitory effects on BCRP, resulting in a reduction in resistance to the anticancer medications Mitoxantrone and camptothecin in MDA-MB-231 cells [538]. The study conducted by Wink et al. shown that harmine effectively inhibited the activity of telomerase in MCF-7 cells [538].

Furthermore, it was observed that harmine exhibited inhibitory effects on the growth and migration of breast cancer cells. This was evident both *in vitro*, using MDA-MB-231 and MCF-7 cells, and *in vivo*, in an MCF-7 xenograft mice model [538], and in BT549 (breast cancer) cell line [539].

Rotenone was found to show inhibition effects on BCRP homodimer [540]. However, there is no further research specific for rotenone and BCRP.

4.6.4 Ability of harmine, rotenone and 7-methoxyflavanone to induce ROS production

There exists empirical evidence suggesting that flavonoids have the capacity to stimulate cells to generate an excessive amount of ROS, resulting in detrimental effects on cell adhesion molecules (CAM) (catechins and naringenin), lipids, and proteins associated with cancer cells [541]. Consequently, this phenomenon triggers cell apoptosis and autophagy. There is existing evidence suggesting that flavonoids (catechins and naringenin) possess the ability to impede the proliferation of colon cancer cells by triggering cell death via ROS in a ROS-dependent mechanism [541]. This character of flavonoids is not limited in one type of cancer. Additionally, flavonoids exhibit a selective reduction in the viability of cancer cells while demonstrating no detrimental effects on normal cells. The anticancer properties of apigenin, luteolin, and myricetin are attributed to their ability to modulate ROS signalling pathways [542]. The activation of the extrinsic apoptosis pathway occurs when flavonoids effectively eliminate ROS within ovarian cancer cells [542]. Meanwhile, the presence of activated cancer cells leads to the formation of endogenous ROS, which subsequently triggers the activation of the intrinsic apoptotic pathway [542].

According to the assessment of the impacts of selected flavonoids on the increasing intracellular ROS, rotenone 100 μM showed the statistically significant in ROS production when compared to the untreated group (269.26 ± 41.82% of the untreated group).

A quantitative relationship between the induction of apoptosis by rotenone and the formation of mitochondrial ROS using HL-60 cells (human promyelocytic leukaemia cell line) by rotenone was established [543]. This discovery not only validated the involvement of rotenone-induced mitochondrial ROS in the process of apoptosis, but also

demonstrated that rotenone can cause apoptosis by augmenting the generation of mitochondrial ROS [543]. Furthermore, rotenone was discovered that increasing the level of intracellular ROS, and inhibiting CI to decrease the proliferation and migration of LoVo and MDST8 (The human colourectal cancer) cell lines [544].

4.6.5 Ability of harmine, rotenone and 7-methoxyflavanone to activate caspase-3/7 pathways

Apoptosis is a regulated mechanism of cell death that is facilitated by cascades of caspase-dependent proteolytic cleavage [545]. The deregulation of apoptosis is a pivotal factor in the facilitation of carcinogenesis and also impedes the efficacy of chemotherapy. The prevailing consensus in the scientific community suggests that the lack of apoptotic cell death plays a substantial role in the progression of cancer [545]. In addition, apart from their proven functional involvement in the process of apoptotic cell death, caspases have been discovered to have increasingly significant roles in other biological processes including cell proliferation, differentiation, tissue homeostasis, and immunological modulation [546]. The apoptotic caspases can be categorised into two discrete groups: the apical caspases, encompassing caspase-2, -8, -9, and -10, and the effector caspases, comprising caspase-3, -7, and -6 [545].

Apoptosis involves the cleavage and activation of executioner caspases-3 and -7, resulting in substantial intracellular proteolysis, impairment of cellular processes, and non-inflammatory demise of cells [547]. The activation of Caspase-3/7 is commonly regarded as the definitive molecular indicator for apoptotic cell death [547]. Numerous *in vitro* investigations on the flavonoid myricetin have demonstrated that it has a cytotoxic effect on cancer cells, including those from the colon, oesophagus, and breast, as well as leukaemia and melanoma cells [548]. The findings indicates that increased production of caspase-9 and caspase-3 levels has resulted in the activation of the mitochondrial apoptosis pathway [548]. Previous research has indicated that, pectolinaringenin (a flavonoid compound) inhibits the growth of human gastric cancer cells via modulating the PI3K/Akt/mTOR pathway, causing G2/M arrest, apoptosis, and autophagy [548]. Therefore, the impacts of flavonoids' participation on the process of apoptosis and migration of cancer cells cannot be ignored.

The fluorescent compound N-Ac-DEVD-N'-MC-R110, which is a substrate for active caspase-3/7, was employed in this study because to its capacity to generate a detectable signal following cleavage by caspase enzymes. Harmine, rotenone and 7-methoxyflavanone were assessed for the impact on the cleavage of caspase-3/7 pathway for the apoptosis at 10 and 100 μM (Figure 4.7). Harmine at 100 μM showed 109.62± 4.09 %-fold in caspase activity compared to the untreated LN 229 cells. This is the only drug demonstrated statistically significance ($P \leqslant 0.001$).

The experimental results revealed that a significant increase in harmine concentration led to the activation of apoptosis through the facilitation of cleaved-caspase 3 and cleaved-caspase 9 aggregation in MGC-803 and SGC-7901 (human gastric cancer) cell lines [549]. Additionally, harmine demonstrated efficacy in inducing autophagy in cellular systems [549]. Furthermore, harmine was found its ability to induce the activation of caspase-3/7 and caspase 9, which induces the apoptosis in neuroblastoma (NB) cell lines [550].

In addition, harmine hydrochloride (Har-hc), a derivative from harmine, was discovered its inhibition effects on the proliferation and migration of C6, U87, U373 (the glioblastoma) cell lines [551].

Harmine exhibited an anti-proliferative impact on HepG2 (human hepatocellular carcinoma) cells through the induction of apoptosis, the proliferation of HepG2 cells was dose-dependently reduced by harmine [552]. The apoptotic process was mediated by mitochondrial signalling mechanisms. The induction of programmed cell death in HepG2 cells was found to be correlated with the activation of caspase-3 and caspase-9 [552].

4.7 Conclusion

As an ABC efflux transporter, BCRP plays an important role in the phenomenon of MDR in cancer cells. The overexpression of BCRP will cause the lower intracellular concentration of anticancer agents, and the chemotherapy will be worse than expected. In this research, 8 flavonoid compounds were screened in LN229 (human glioblastoma) cells for their cytotoxicity, ability to modulate the efflux function, inhibit the migration of cancer cells and the regulation for intracellular ROS and impacts on the process of apoptosis.

According to the outcomes of the experiments, there were 2 promising flavonoids: rotenone and harmine. Both have proved that their inhibition effects on LN229 cells, ability to regulate BCRP efflux function, induce ROS level increasing and the apoptosis. Based on the results, they both have inhibition effects on GBM cell migration, and Rotenone showed over 2- fold ROS detection compared to the untreated GBM cells; Harmine indicated that the activation of caspase-3/7- the indicator of apoptosis, which showed its potential.

This chapter stresses the potentials of these 2 flavonoids in pro-oxidant process and the ability to promote cancer cell death pathways. In the future, these 2 flavonoids can be utilised to explore their effects of permeability on simulated BBB model and the following impacts.

Chapter 5
Conclusion and future works

5.1 Conclusion

As a world leading cause of death, cancer is a threaten of people's health. The research for the treatment of cancer is still the focus nowadays. This study is to improve the treatment of incurable cancers by investigating natural drugs- flavonoids and improving the treatment of tyrosine kinase inhibitors (TKIs).

The difficulty of curing brain cancer makes it a research-worthy problem. The main obstacle of the treatment of brain cancer is the BBB, which prevents the entry of most chemotherapeutic drugs. BCRP is an efflux transporter protein located on the BBB. The inhibition of BCRP can increase the concentrations of chemotherapeutic drugs inside the brain crossing the BBB. The selections of BCRP inhibitors are difficult, few promising drugs were excluded from the current study of BCRP inhibitors because of their toxicity. Flavonoids were utilised in this study, because its features as natural drugs existed in the world and relatively low cellular toxicity. In this section, a glioblastomas cell line- LN 229 cell line was utilised.

Tyrosine kinase inhibitors (TKIs) is utilised in the therapy of several cancers, such as non-small cell lung cancer (NSCLC) and gastrointestinal stromal tumours (GIST) and chronic myeloid leukaemia (CML). Gefitinib and Imatinib were selected to conduct the PK modelling in this study because there is enough clinical data to develop a virtual population model. The foundation of these two PK studies in this research is the developed Chinese cancer population group model. The ethnicities differences between Caucasian and Asian population were noticed and the different levels of CYP 2D6 phenotypes caused by ethnicities were investigated to acquire better clinical regimes for Asian people, thus, this research focus on Chinese population at first and the other Asian populations' therapies can be optimised in the future. The therapeutic drug monitoring (TDM) strategy was also investigated for adjusting the imatinib plasma level to get better clinical therapeutic outcomes. Using the true standard framework TDM can enhance the suitability of dosing regimens for different patient populations.

In Chapter 2, a virtual Chinese Cancer population group was developed and validated using the Simcyp Simulator, and the impact of CYP 2D6 polymorphism and CYP 2D6 inhibition (by bupropion) were assessed using this model. It is noticed that two most

prominent CYP 2D6 phenotypes within the Chinese population, namely EM and IM, a dosage escalation to 500 mg administered once daily would more effectively achieve the desired target trough concentration.

In Chapter 3, virtual clinical studies were used in a developed virtual Chinese cancer population group and Caucasian cancer population group. TDM can effectively reduce the cost of clinical application of imatinib and optimise the imatinib plasma concentrations for Chinese cancer population. Based on the TDM strategy, we observe whether the changes are beneficial to the maintenance of optimal plasma imatinib levels in both populations. Cim was utilised as the specific imatinib pharmacokinetic indicator, which is obtained when the plasma concentration reached at the steady state of the first dose. According to the dose studies, Chinese cancer patients need lower imatinib doses than Caucasian patients, this might be attributed to the differences in both body weight and body surface area. The therapeutic window of C_{min} is 750-1500 ng/mL, after the dose adjustment of TDM, the patients whose previous C_{min} are 550-650 or 650-750 ng/mL, can target into the effective therapeutic range, no matter they are Caucasian or Chinese cancer patients. The other concentration range of these two populations get better outcomes as well, but apparently, Chinese cancer population received more obvious therapeutic range than Caucasian patients.

In Chapter 4, 8 flavonoid compounds were examined and screened for their cytotoxicity, their modulating functions as BCRP inhibitor, their inhibition effects on human glioblastomas migration and their impacts towards LN 229 cells. It is worthwhile mentioning that their activation of apoptosis through ROS level changes and caspase-3/7 pathways, helps us to select flavonoids for the future works. According to the results of the series of experiments, 2 flavonoids- harmine and rotenone, were selected as potential anticancer agents for further research.

In the end, 2 candidate flavonoid compounds- harmine and rotenone are selected as promising BCRP modulators towards LN 229 cells. The inhibition effects on the human glioblastoma's cells' migration and pro-oxidant effects to promote apoptosis process are obvious. Therefore, the combination medication including these 2 drugs can be evaluated within LN 229 cells for the future studies.

5.2 Future works

There are more flavonoid compounds can be assessed. Apart from BCRP modulating function, the modulation effects on other ABC transporters can also be considered, such as P-gp and MRP. The performance of modulating function of these unexplored flavonoids in LN 229 cell line associated with P-gp and MRP can be observed. Additionally, the combination medication including flavonoids can be explored as well.

For the future works, there are 3 directions I would like to explore.

Firstly, the utilisation of the High-Performance Liquid Chromatography (HPLC) technique for the evaluation of BCRP modulator- flavonoids (harmine, rotenone and other flavonoids) in an in-vitro setting can also be explored [553]. This method enables the qualitative and quantitative examination of the flavonoids present in the sample, providing information on both the identity of the components and their respective concentrations. The identified concentration of flavonoids can be utilised in the developed BBB model.

Secondly, Western Blot analysis to assess alterations in the protein expression of BCRP can be examined [554]. Additionally, LN 229 cells can be subjected to modulators for a duration of 24 hours, and alterations in protein expression can be evaluated through western blotting to examine the influence of these modulators on the protein expression of BCRP. Consequently, any changes in the expression of BCRP (either upregulation or downregulation) can provide insights into the enhanced permeability of anticancer drugs across brain cells.

Thirdly, developing a BBB model with LN 229 cell line, the aim of this is to assess the effects of glioblastomas cells on the integrity of an *in vitro* co-culture BBB model. The effects of flavonoids on the permeability of BBB model can also be included. There are a few different *in vitro* BBB models, the primary considerations for model selection encompass the research objectives. In instances when monolayer or co-culture models are employed, which typically require 3-4 days to attain a stable TEER value and are very straightforward to construct, they might be utilised [555].

References:

1. Vineis, P. and C.P. Wild, *Global cancer patterns: causes and prevention.* The Lancet, 2014. **383**(9916): p. 549-557.

2. Deo, S.V.S., J. Sharma, and S. Kumar, *GLOBOCAN 2020 Report on Global Cancer Burden: Challenges and Opportunities for Surgical Oncologists.* Annals of Surgical Oncology, 2022. **29**(11): p. 6497-6500.

3. Sung, H., et al., *Global Cancer Statistics 2020: GLOBOCAN Estimates of Incidence and Mortality Worldwide for 36 Cancers in 185 Countries.* CA: A Cancer Journal for Clinicians, 2021. **71**(3): p. 209-249.

4. Pratesi, G., *Cancer Biology, 4th ed., Ruddon, R.W. (ed.), Oxford University Press, Oxford, 2007, ISBN:978-0-19-517543-1.* Surgical Oncology-oxford, 2007. **16**: p. 143.

5. Danaei, G., et al., *Causes of cancer in the world: comparative risk assessment of nine behavioural and environmental risk factors.* The lancet, 2005. **366**(9499): p. 1784-1793.

6. Ames, B.N., L.S. Gold, and W.C. Willett, *The causes and prevention of cancer.* Proceedings of the National Academy of Sciences, 1995. **92**(12): p. 5258-5265.

7. Loeb, L.A., K.R. Loeb, and J.P. Anderson, *Multiple mutations and cancer.* Proceedings of the National Academy of Sciences, 2003. **100**(3): p. 776-781.

8. Nazemi, M. and E. Rainero, *Cross-talk between the tumor microenvironment, extracellular matrix, and cell metabolism in cancer.* Frontiers in oncology, 2020. **10**: p. 239.

9. Spano, D. and M. Zollo, *Tumor microenvironment: a main actor in the metastasis process.* Clinical & Experimental Metastasis, 2012. **29**(4): p. 381-395.

10. Xi, Y. and P. Xu, *Global colorectal cancer burden in 2020 and projections to 2040.* Translational oncology, 2021. **14**(10): p. 101174.

11. Grass, G.D., N. Krishna, and S. Kim, *The immune mechanisms of abscopal effect in radiation therapy.* Current problems in cancer, 2016. **40**(1): p. 10-24.

12. Wang, J., K. Lei, and F. Han, *Tumor microenvironment: recent advances in various cancer treatments.* Eur Rev Med Pharmacol Sci, 2018. **22**(12): p. 3855-3864.

13. De Ruysscher, D., et al., *Radiotherapy toxicity.* Nature Reviews Disease Primers, 2019. **5**(1): p. 13.

14. Campbell, C., et al., *Are there ethnic and religious variations in uptake of bowel cancer screening? A retrospective cohort study among 1.7 million people in Scotland.* BMJ open, 2020. **10**(10): p. e037011.

15. Møller, H., et al., *Short-term breast cancer survival in relation to ethnicity, stage, grade and receptor status: national cohort study in England.* British journal of cancer, 2016. **115**(11): p. 1408-1415.

16. Delon, C., et al., *Differences in cancer incidence by broad ethnic group in England, 2013–2017.* British Journal of Cancer, 2022. **126**(12): p. 1765-1773.

17. Nenclares, P. and K. Harrington, *The biology of cancer.* Medicine, 2020. **48**(2): p. 67-72.

18. Ackerman, A. and J. Mones, *Solar (actinic) keratosis is squamous cell carcinoma.* British Journal of Dermatology, 2006. **155**(1): p. 9-22.

19. Pizzamiglio, S., et al., *Expression of iron-related proteins differentiate non-cancerous and cancerous breast tumors.* International journal of molecular sciences, 2017. **18**(2): p. 410.

20. Boutry, J., et al., *The evolution and ecology of benign tumors.* Biochimica et Biophysica Acta (BBA)-Reviews on Cancer, 2022. **1877**(1): p. 188643.

21. Macchiarini, P., *Primary tracheal tumours.* The lancet oncology, 2006. **7**(1): p. 83-91.

22. Jass, J.R. and L.H. Sobin, *Histological typing of intestinal tumours*. 2012: Springer Science & Business Media.

23. Datta, S. and E.L. Davies, *Benign breast disease.* Surgery (Oxford), 2013. **31**(1): p. 22-26.

24. Van Goethem, J., et al., *Spinal tumors.* European Journal of Radiology, 2004. **50**(2): p. 159-176.

25. Peate, I., *Understanding cancer.* British Journal of Healthcare Assistants, 2018. **12**(7): p. 350-355.

26. Visvader, J.E., *Cells of origin in cancer.* Nature, 2011. **469**(7330): p. 314-322.

27. Clark, W.H., *Tumour progression and the nature of cancer.* British Journal of Cancer, 1991. **64**(4): p. 631-644.

28. Ohgaki, H. and P. Kleihues, *The Definition of Primary and Secondary GlioblastomaDefinition of Primary and Secondary Glioblastomas.* Clinical cancer research, 2013. **19**(4): p. 764-772.

29. Ansieau, S., et al., *Early origin of cancer metastases: dissemination and evolution of premalignant cells.* Cell cycle, 2008. **7**(23): p. 3659-3663.

30. Pankiewicz, W., et al., *Immunohistochemical markers of cancerogenesis in the lung.* Folia Histochemica et cytobiologica, 2007. **45**(2): p. 65-74.

31. Christopherson, W.M., *Dysplasia, carcinoma in situ, and microinvasive carcinoma of the uterine cervix.* Human Pathology, 1977. **8**(5): p. 489-501.

32. McMullen, E.R., N.A. Zoumberos, and C.G. Kleer, *Metaplastic Breast Carcinoma: Update on Histopathology and Molecular Alterations.* Archives of Pathology & Laboratory Medicine, 2019. **143**(12): p. 1492-1496.

33. Quinlan, J.M., et al., *Epithelial metaplasia and the development of cancer.* Biochimica et Biophysica Acta (BBA) - Reviews on Cancer, 2007. **1776**(1): p. 10-21.

34. Ferlito, A., et al., *Squamous epithelial changes of the larynx: Diagnosis and therapy.* Head & Neck, 2012. **34**(12): p. 1810-1816.

35. Sobin, L.H., *The international histological classification of tumours.* Bull World Health Organ, 1981. **59**(6): p. 813-9.

36. Sell, S., *Stem cell origin of cancer and differentiation therapy.* Critical reviews in oncology/hematology, 2004. **51**(1): p. 1-28.

37. Lobo, N.A., et al., *The biology of cancer stem cells.* Annu. Rev. Cell Dev. Biol., 2007. **23**: p. 675-699.

38. Ruddon, R.W., *Cancer biology*. 2007: Oxford University Press.

39. Ilic, I. and M. Ilic, *International patterns and trends in the brain cancer incidence and mortality: An observational study based on the global burden of disease.* Heliyon, 2023.

40. Wanis, H.A., et al., *The Influence of Ethnicity on Survival from Malignant Primary Brain Tumours in England: A Population-Based Cohort Study.* Cancers, 2023. **15**(5): p. 1464.

41. Tandel, G.S., et al., *A review on a deep learning perspective in brain cancer classification.* Cancers, 2019. **11**(1): p. 111.

42. Huttner, A., *Overview of primary brain tumors: pathologic classification, epidemiology, molecular biology, and prognostic markers.* Hematology/oncology clinics of North America, 2012. **26**(4): p. 715-732.

43. Behin, A., et al., *Primary brain tumours in adults.* The Lancet, 2003. **361**(9354): p. 323-331.

44. Abbott, N.J., et al., *Structure and function of the blood–brain barrier.* Neurobiology of Disease, 2010. **37**(1): p. 13-25.

45. Kadry, H., B. Noorani, and L. Cucullo, *A blood–brain barrier overview on structure, function, impairment, and biomarkers of integrity.* Fluids and Barriers of the CNS, 2020. **17**(1): p. 69.

46. Lesniak, M.S. and H. Brem, *Targeted therapy for brain tumours.* Nature reviews Drug discovery, 2004. **3**(6): p. 499-508.

47. Gavrilovic, I.T. and J.B. Posner, *Brain metastases: epidemiology and pathophysiology.* Journal of neuro-oncology, 2005. **75**: p. 5-14.

48. Wang, S., et al., *Brain tumors*, in *Pediatric Neuroimaging: Cases and Illustrations*. 2022, Springer. p. 21-86.

49. Vargo, M.M., *Brain tumors and metastases.* Physical Medicine and Rehabilitation Clinics, 2017. **28**(1): p. 115-141.

50. Bai, R.-Y., V. Staedtke, and G.J. Riggins, *Molecular targeting of glioblastoma: drug discovery and therapies.* Trends in molecular medicine, 2011. **17**(6): p. 301-312.

51. Mishra, V. and P. Kesharwani, *Dendrimer technologies for brain tumor.* Drug discovery today, 2016. **21**(5): p. 766-778.

52. Ramirez, Y.P., et al., *Glioblastoma multiforme therapy and mechanisms of resistance.* Pharmaceuticals, 2013. **6**(12): p. 1475-1506.

53. Wolf, K.J., et al., *Dissecting and rebuilding the glioblastoma microenvironment with engineered materials.* Nature Reviews Materials, 2019. **4**(10): p. 651-668.

54. Landis, C.J., et al., *The pro-tumorigenic effects of metabolic alterations in glioblastoma including brain tumor initiating cells.* Biochimica et Biophysica Acta (BBA)-Reviews on Cancer, 2018. **1869**(2): p. 175-188.

55. Arnold, L.M., J.C. DeWitt, and A.A. Thomas, *Tumors of the nervous system*, in *Neurobiology of Brain Disorders*. 2023, Elsevier. p. 203-228.

56. Dorsey, J.F., et al., *Cancer of the central nervous system*, in *Abeloff's clinical oncology*. 2020, Elsevier. p. 906-967. e12.

57. Pollo, B., *Neuropathological diagnosis of brain tumours.* Neurological Sciences, 2011. **32**(2): p. 209-211.

58. Chandana, S.R., et al., *Primary brain tumors in adults.* American family physician, 2008. **77**(10): p. 1423.

59. Koo, Y.-E.L., et al., *Brain cancer diagnosis and therapy with nanoplatforms.* Advanced Drug Delivery Reviews, 2006. **58**(14): p. 1556-1577.

60. Bhargava, R., et al., *Contrast-enhanced Magnetic Resonance Imaging in Pediatric Patients: Review and Recommendations for Current Practice.* Magnetic Resonance Insights, 2013. **6**: p. MRI.S12561.

61. Abd-Ellah, M.K., et al., *A review on brain tumor diagnosis from MRI images: Practical implications, key achievements, and lessons learned.* Magnetic Resonance Imaging, 2019. **61**: p. 300-318.

62. Neugut, A.I., et al., *Magnetic Resonance Imaging‐Based Screening for Asymptomatic Brain Tumors: A Review.* The Oncologist, 2018. **24**(3): p. 375-384.

63. Salskov, A., et al., *FLT: Measuring Tumor Cell Proliferation In Vivo With Positron Emission Tomography and 3′-Deoxy-3′-[18F]Fluorothymidine.* Seminars in Nuclear Medicine, 2007. **37**(6): p. 429-439.

64. Cohen, E.E.W., et al., *American Cancer Society Head and Neck Cancer Survivorship Care Guideline.* CA: A Cancer Journal for Clinicians, 2016. **66**(3): p. 203-239.

65. Walker, B.C. and S. Mittal, *Antitumor activity of curcumin in glioblastoma.* International journal of molecular sciences, 2020. **21**(24): p. 9435.

66. Hong, X., K. Chedid, and S.N. Kalkanis, *Glioblastoma cell line-derived spheres in serum‐containing medium versus serum-free medium: A comparison of cancer stem cell properties.* Int J Oncol, 2012. **41**(5): p. 1693-1700.

67. Li, H., et al., *Differences in protein expression between the U251 and U87 cell lines.* Turk Neurosurg, 2017. **27**(6): p. 894-903.

68. Diao, W., et al., *Behaviors of Glioblastoma Cells in in Vitro Microenvironments.* Sci Rep, 2019. **9**(1): p. 85.

69. Stanković, T., et al., *In vitro biomimetic models for glioblastoma-a promising tool for drug response studies.* Drug Resistance Updates, 2021. **55**: p. 100753.

70. Ludwig, P.E., V. Reddy, and M. Varacallo, *Neuroanatomy, central nervous system (CNS).* 2017.

71. Alajangi, H.K., et al., *Blood–brain barrier: emerging trends on transport models and new-age strategies for therapeutics intervention against neurological disorders.* Molecular Brain, 2022. **15**(1): p. 1-28.

72. Thau, L., V. Reddy, and P. Singh, *Anatomy, central nervous system.* 2019.

73. Liang, C., et al., *Strategies for interface issues and challenges of neural electrodes.* Nanoscale, 2022. **14**(9): p. 3346-3366.

74. Abbott, N.J., et al., *Structure and function of the blood–brain barrier.* Neurobiology of disease, 2010. **37**(1): p. 13-25.

75. Hawkins, B.T. and T.P. Davis, *The blood-brain barrier/neurovascular unit in health and disease.* Pharmacological reviews, 2005. **57**(2): p. 173-185.

76. Smith, B.C., et al., *Targetability of the neurovascular unit in inflammatory diseases of the central nervous system.* Immunological Reviews, 2022. **311**(1): p. 39-49.

77. Kealy, J., C. Greene, and M. Campbell, *Blood-brain barrier regulation in psychiatric disorders.* Neuroscience Letters, 2020. **726**: p. 133664.

78. Singh, A. and C. Vellapandian, *Structure of the Blood Brain Barrier and the Role of Transporters in the movement of substrates across the barriers.* Qeios, 2022.

79. Krizbai, I. and M. Deli, *SIGNALLING PATHWAYS REGULATING THE TIGHT JUNCTION.* Cellular and molecular biology, 2003. **49**(1): p. 23-31.

80. Ribatti, D., et al., *Development of the blood‐brain barrier: A historical point of view.* The Anatomical Record Part B: The New Anatomist: An Official Publication of the American Association of Anatomists, 2006. **289**(1): p. 3-8.

81. Travis, A.S., *Science as receptor of technology: Paul Ehrlich and the synthetic dyestuffs industry.* Science in context, 1989. **3**(2): p. 383-408.

82. Tschirgi, R. *Protein complexes and the impermeability of the blood-brain barrier to dyes*. in *American Journal of Physiology*. 1950. AMER PHYSIOLOGICAL SOC 9650 ROCKVILLE PIKE, BETHESDA, MD 20814.

83. Schafer, D., *The Blood-Brain Barrier in Acute Liver Failure*, in *Advances in Hepatic Encephalopathy and Urea Cycle Diseases*. 1984, Karger Publishers. p. 232-239.

84. McConnell, H., et al., *Cerebrospinal fluid dynamics.* Cerebrospinal fluid in neurology and psychiatry, 1994: p. 5-33.

85. Mallard, C., C.J. Ek, and Z.S. Vexler, *The myth of the immature barrier systems in the developing brain: role in perinatal brain injury.* The Journal of physiology, 2018. **596**(23): p. 5655-5664.

86. Davson, H., *History of the blood-brain barrier concept.* Implications of the Blood-Brain Barrier and Its Manipulation: Volume 1 Basic Science Aspects, 1989: p. 27-52.

87. Kadry, H., B. Noorani, and L. Cucullo, *A blood–brain barrier overview on structure, function, impairment, and biomarkers of integrity.* Fluids and Barriers of the CNS, 2020. **17**(1): p. 1-24.

88. Sá-Pereira, I., D. Brites, and M.A. Brito, *Neurovascular unit: a focus on pericytes.* Molecular neurobiology, 2012. **45**: p. 327-347.

89. Murakami, K., et al., *The development of a new mouse model of global ischemia: focus on the relationships between ischemia duration, anesthesia, cerebral vasculature, and neuronal injury following global ischemia in mice.* Brain research, 1998. **780**(2): p. 304-310.

90. CM de Lange, E., *The physiological characteristics and transcytosis mechanisms of the blood-brain barrier (BBB).* Current pharmaceutical biotechnology, 2012. **13**(12): p. 2319-2327.

91. Soria, F.N., et al., *Current techniques for investigating the brain extracellular space.* Frontiers in Neuroscience, 2020. **14**: p. 570750.

92. Kaplan, L., B.W. Chow, and C. Gu, *Neuronal regulation of the blood–brain barrier and neurovascular coupling.* Nature Reviews Neuroscience, 2020. **21**(8): p. 416-432.

93. Crichton, R.R., D.T. Dexter, and R.J. Ward, *Brain iron metabolism and its perturbation in neurological diseases*. 2012: Springer.

94. Zhang, W., et al., *The blood brain barrier in cerebral ischemic injury–Disruption and repair.* Brain Hemorrhages, 2020. **1**(1): p. 34-53.

95. Otani, T. and M. Furuse, *Tight junction structure and function revisited.* Trends in cell biology, 2020. **30**(10): p. 805-817.

96. Heiskala, M., P.A. Peterson, and Y. Yang, *The roles of claudin superfamily proteins in paracellular transport.* Traffic, 2001. **2**(2): p. 92-98.

97. Bazzoni, G. and E. Dejana, *Endothelial cell-to-cell junctions: molecular organization and role in vascular homeostasis.* Physiological reviews, 2004. **84**(3): p. 869-901.

98. Abbott, N.J., *Blood–brain barrier structure and function and the challenges for CNS drug delivery.* Journal of inherited metabolic disease, 2013. **36**: p. 437-449.

99. Tajes, M., et al., *The blood-brain barrier: Structure, function and therapeutic approaches to cross it.* Molecular Membrane Biology, 2014. **31**(5): p. 152-167.

100. Zeiadeh, I., A. Najjar, and R. Karaman, *Strategies for enhancing the permeation of CNS-active drugs through the blood-brain barrier: a review.* Molecules, 2018. **23**(6): p. 1289.

101. Tsuji, A. and I. Tamai, *Carrier-mediated or specialized transport of drugs across the blood–brain barrier.* Advanced Drug Delivery Reviews, 1999. **36**(2): p. 277-290.

102. Miller, D.S., *Regulation of ABC transporters blood–brain barrier: the good, the bad, and the ugly.* Advances in cancer research, 2015. **125**: p. 43-70.

103. Zhang, Y. and W.M. Pardridge, *Rapid transferrin efflux from brain to blood across the blood–brain barrier.* Journal of neurochemistry, 2001. **76**(5): p. 1597-1600.

104. Schlachetzki, F., C. Zhu, and W.M. Pardridge, *Expression of the neonatal Fc receptor (FcRn) at the blood–brain barrier.* Journal of neurochemistry, 2002. **81**(1): p. 203-206.

105. Alam, M.I., et al., *Strategy for effective brain drug delivery.* European Journal of Pharmaceutical Sciences, 2010. **40**(5): p. 385-403.

106. Wang, Y., et al., *Protection against acute cerebral ischemia/reperfusion injury by QiShenYiQi via neuroinflammatory network mobilization.* Biomedicine & Pharmacotherapy, 2020. **125**: p. 109945.

107. Benet, L.Z., et al., *BDDCS, the Rule of 5 and drugability.* Adv Drug Deliv Rev, 2016. **101**: p. 89-98.

108. Mikitsh, J.L. and A.M. Chacko, *Pathways for small molecule delivery to the central nervous system across the blood-brain barrier.* Perspect Medicin Chem, 2014. **6**: p. 11-24.

109. Curley, S.M. and N.C. Cady, *Biologically-Derived Nanomaterials for Targeted Therapeutic Delivery to the Brain.* Science Progress, 2018. **101**(3): p. 273-292.

110. Pandit, R., L. Chen, and J. Götz, *The blood-brain barrier: Physiology and strategies for drug delivery.* Advanced Drug Delivery Reviews, 2020. **165-166**: p. 1-14.

111. Khawli, L.A. and S. Prabhu, *Drug Delivery across the Blood–Brain Barrier.* Molecular Pharmaceutics, 2013. **10**(5): p. 1471-1472.

112. Dong, X., *Current Strategies for Brain Drug Delivery.* Theranostics, 2018. **8**(6): p. 1481-1493.

113. Wu, D., et al., *The blood–brain barrier: structure, regulation, and drug delivery.* Signal Transduction and Targeted Therapy, 2023. **8**(1): p. 217.

114. Redzic, Z., *Molecular biology of the blood-brain and the blood-cerebrospinal fluid barriers: similarities and differences.* Fluids and Barriers of the CNS, 2011. **8**(1): p. 3.

115. Al Rihani, S.B., et al., *Disease-Induced Modulation of Drug Transporters at the Blood-Brain Barrier Level.* Int J Mol Sci, 2021. **22**(7).

116. Broehan, G., et al., *Functional analysis of the ATP-binding cassette (ABC) transporter gene family of Tribolium castaneum.* BMC genomics, 2013. **14**: p. 1-19.

117. Xiong, J., et al., *Tracing the structural evolution of eukaryotic ATP binding cassette transporter superfamily.* Scientific reports, 2015. **5**(1): p. 1-15.

118. Jones, P.M. and A.M. George, *The Switch and Reciprocating Models for the Function of ABC Multidrug Exporters: Perspectives on Recent Research.* International Journal of Molecular Sciences, 2023. **24**(3): p. 2624.

119. Esquivel, B.D., et al., *Characterization of the efflux capability and substrate specificity of Aspergillus fumigatus PDR5-like ABC transporters expressed in Saccharomyces cerevisiae.* MBio, 2020. **11**(2): p. e00338-20.

120. Linton, K.J., *Structure and function of ABC transporters.* Physiology, 2007. **22**(2): p. 122-130.

121. Srikant, S., *Evolutionary history of ATP‐binding cassette proteins.* FEBS letters, 2020. **594**(23): p. 3882-3897.

122. Eckenstaler, R. and R.A. Benndorf, *3D structure of the transporter ABCG2—What's new?* British journal of pharmacology, 2020. **177**(7): p. 1485-1496.

123. Farkas, B., et al., *Discovering the chloride pathway in the CFTR channel.* Cellular and Molecular Life Sciences, 2020. **77**: p. 765-778.

124. Gottesman, M.M. and S.V. Ambudkar, *Overview: ABC transporters and human disease.* Journal of bioenergetics and biomembranes, 2001. **33**: p. 453-458.

125. Borowski, E., M.M. Bontemps-Gracz, and A. Piwkowska, *Strategies for overcoming ABC-transporters-mediated multidrug resistance (MDR) of tumor cells.* Acta Biochimica Polonica, 2005. **52**(3): p. 609-627.

126. Juliano, R.L. and V. Ling, *A surface glycoprotein modulating drug permeability in Chinese hamster ovary cell mutants.* Biochimica et Biophysica Acta (BBA) - Biomembranes, 1976. **455**(1): p. 152-162.

127. Prachayasittikul, V. and V. Prachayasittikul, *P-glycoprotein transporter in drug development.* Excli j, 2016. **15**: p. 113-8.

128. Abdullahi, W., T.P. Davis, and P.T. Ronaldson, *Functional Expression of P-glycoprotein and Organic Anion Transporting Polypeptides at the Blood-Brain Barrier: Understanding Transport Mechanisms for Improved CNS Drug Delivery?* The AAPS Journal, 2017. **19**(4): p. 931-939.

129. Stouch, T.R. and O. Gudmundsson, *Progress in understanding the structure–activity relationships of P-glycoprotein.* Advanced Drug Delivery Reviews, 2002. **54**(3): p. 315-328.

130. Mirzaei, S., et al., *Advances in understanding the role of P-gp in doxorubicin resistance: Molecular pathways, therapeutic strategies, and prospects.* Drug Discovery Today, 2022. **27**(2): p. 436-455.

131. El-Shimy, I.A., et al., *Targeting host cell proteases as a potential treatment strategy to limit the spread of SARS-CoV-2 in the respiratory tract.* Pharmacology Research & Perspectives, 2021. **9**(1): p. e00698.

132. Sodani, K., et al., *Multidrug resistance associated proteins in multidrug resistance.* Chin J Cancer, 2012. **31**(2): p. 58-72.

133. Choudhuri, S. and C.D. Klaassen, *Structure, function, expression, genomic organization, and single nucleotide polymorphisms of human ABCB1 (MDR1), ABCC (MRP), and ABCG2 (BCRP) efflux transporters.* Int J Toxicol, 2006. **25**(4): p. 231-59.

134. Thomas, C. and R. Tampé, *Multifaceted structures and mechanisms of ABC transport systems in health and disease.* Current Opinion in Structural Biology, 2018. **51**: p. 116-128.

135. Zhang, Y.-K., et al., *Multidrug Resistance Proteins (MRPs) and Cancer Therapy.* The AAPS Journal, 2015. **17**(4): p. 802-812.

136. Cole, S.P.C., *Multidrug Resistance Protein 1 (MRP1, ABCC1), a “Multitasking” ATP-binding Cassette (ABC) Transporter *.* Journal of Biological Chemistry, 2014. **289**(45): p. 30880-30888.

137. van de Ven, R., et al., *ABC drug transporters and immunity: novel therapeutic targets in autoimmunity and cancer.* Journal of Leukocyte Biology, 2009. **86**(5): p. 1075-1087.

138. Ji, L., et al., *Nrf2 Pathway Regulates Multidrug-Resistance-Associated Protein 1 in Small Cell Lung Cancer.* PLOS ONE, 2013. **8**(5): p. e63404.

139. Nakanishi, T. and D.D. Ross, *Breast cancer resistance protein (BCRP/ABCG2): its role in multidrug resistance and regulation of its gene expression.* Chinese journal of cancer, 2012. **31**(2): p. 73.

140. Schinkel, A.H. and J.W. Jonker, *Mammalian drug efflux transporters of the ATP binding cassette (ABC) family: an overview.* Advanced drug delivery reviews, 2012. **64**: p. 138-153.

141. Juan-Carlos, P.-D.M., et al., *ABC transporter superfamily. An updated overview, relevance in cancer multidrug resistance and perspectives with personalized medicine.* Molecular biology reports, 2021. **48**(2): p. 1883-1901.

142. Breedveld, P., J.H. Beijnen, and J.H. Schellens, *Use of P-glycoprotein and BCRP inhibitors to improve oral bioavailability and CNS penetration of anticancer drugs.* Trends in pharmacological sciences, 2006. **27**(1): p. 17-24.

143. Zappe, K. and M. Cichna-Markl, *Aberrant DNA methylation of ABC transporters in cancer.* Cells, 2020. **9**(10): p. 2281.

144. Vaidya, F.U., et al., *Molecular and cellular paradigms of multidrug resistance in cancer.* Cancer reports, 2022. **5**(12): p. e1291.

145. Chen, Q., et al., *The amino terminus of the human multidrug resistance transporter ABCC1 has a U-shaped folding with a gating function.* Journal of Biological Chemistry, 2006. **281**(41): p. 31152-31163.

146. Gupta, V.K., Y. Bhalla, and V. Jaitak, *Impact of ABC transporters, glutathione conjugates in MDR and their modulation by flavonoids: an overview.* Medicinal Chemistry Research, 2014. **23**(1): p. 1-15.

147. Huls, M., F.G. Russel, and R. Masereeuw, *The role of ATP binding cassette transporters in tissue defense and organ regeneration.* Journal of Pharmacology and Experimental Therapeutics, 2009. **328**(1): p. 3-9.

148. Jonker, J.W., et al., *The breast cancer resistance protein protects against a major chlorophyll-derived dietary phototoxin and protoporphyria.* Proceedings of the National Academy of Sciences, 2002. **99**(24): p. 15649-15654.

149. Chen, L., et al., *Development of precision medicine approaches based on inter-individual variability of BCRP/ABCG2.* Acta Pharmaceutica Sinica B, 2019. **9**(4): p. 659-674.

150. Ni, Z., et al., *Structure and function of the human breast cancer resistance protein (BCRP/ABCG2).* Current drug metabolism, 2010. **11**(7): p. 603-617.

151. Gomez-Zepeda, D., et al., *ABC Transporters at the Blood-Brain Interfaces, Their Study Models, and Drug Delivery Implications in Gliomas.* Pharmaceutics, 2019. **12**(1).

152. Amawi, H., et al., *ABC transporter-mediated multidrug-resistant cancer.* Drug Transporters in Drug Disposition, Effects and Toxicity, 2019: p. 549-580.

153. Srivalli, K.M.R. and P. Lakshmi, *Overview of P-glycoprotein inhibitors: a rational outlook.* Brazilian Journal of Pharmaceutical Sciences, 2012. **48**: p. 353-367.

154. Nguyen, T.-T.-L., V.-A. Duong, and H.-J. Maeng, *Pharmaceutical formulations with P-glycoprotein inhibitory effect as promising approaches for enhancing oral drug absorption and bioavailability.* Pharmaceutics, 2021. **13**(7): p. 1103.

155. Katrajkar, K., et al., *Shedding light on interaction of so called inactive ingredients (excipients) with permeability-glycoprotein.* Journal of Drug Delivery Science and Technology, 2019. **52**: p. 531-552.

156. Mao, Q. and J.D. Unadkat, *Role of the breast cancer resistance protein (BCRP/ABCG2) in drug transport—an update.* The AAPS journal, 2015. **17**: p. 65-82.

157. Shukla, S., C.-P. Wu, and S.V. Ambudkar, *Development of inhibitors of ATP-binding cassette drug transporters–present status and challenges.* Expert opinion on drug metabolism & toxicology, 2008. **4**(2): p. 205-223.

158. Chong, T.C., et al., *Characterization of a Potent, Selective, and Safe Inhibitor, Ac15(Az8)2, in Reversing Multidrug Resistance Mediated by Breast Cancer Resistance Protein (BCRP/ABCG2).* International Journal of Molecular Sciences, 2022. **23**(21): p. 13261.

159. Boonnop, R., et al., *Black ginger extract and its active compound, 5,7-dimethoxyflavone, increase intestinal drug absorption via efflux drug transporter inhibitions.* Drug Metabolism and Pharmacokinetics, 2023. **50**: p. 100500.

160. Dias, M.C., D.C.G.A. Pinto, and A.M.S. Silva, *Plant Flavonoids: Chemical Characteristics and Biological Activity.* Molecules, 2021. **26**(17): p. 5377.

161. Morris, M.E. and S. Zhang, *Flavonoid–drug interactions: Effects of flavonoids on ABC transporters.* Life Sciences, 2006. **78**(18): p. 2116-2130.

162. Bertelli, A., et al., *Polyphenols: From Theory to Practice.* Foods, 2021. **10**(11): p. 2595.

163. Sankari, S.L., et al., *Flavonoids - Clinical effects and applications in dentistry: A review.* J Pharm Bioallied Sci, 2014. **6**(Suppl 1): p. S26-9.

164. Jubaidi, F.F., et al., *The Potential Role of Flavonoids in Ameliorating Diabetic Cardiomyopathy via Alleviation of Cardiac Oxidative Stress, Inflammation and Apoptosis.* International Journal of Molecular Sciences, 2021. **22**(10): p. 5094.

165. Khan, J., et al., *Dietary Flavonoids: Cardioprotective Potential with Antioxidant Effects and Their Pharmacokinetic, Toxicological and Therapeutic Concerns.* Molecules, 2021. **26**(13): p. 4021.

166. Aoi, W., M. Iwasa, and Y. Marunaka, *Metabolic functions of flavonoids: From human epidemiology to molecular mechanism.* Neuropeptides, 2021. **88**: p. 102163.

167. Ben Mrid, R., et al., *Secondary metabolites as biostimulant and bioprotectant agents: A review.* Science of The Total Environment, 2021. **777**: p. 146204.

168. Panche, A.N., A.D. Diwan, and S.R. Chandra, *Flavonoids: an overview.* Journal of nutritional science, 2016. **5**: p. e47.

169. Singla, R.K., et al., *Natural Polyphenols: Chemical Classification, Definition of Classes, Subcategories, and Structures.* Journal of AOAC INTERNATIONAL, 2019. **102**(5): p. 1397-1400.

170. Lien, D.T.P., P.T.B. Tram, and H. Toan, *Antioxidant properties of food natural phenolic compounds–A review.* Innov. Food Res, 2016. **2**: p. 1-5.

171. Hussain, T., et al., *Flavonoids and type 2 diabetes: Evidence of efficacy in clinical and animal studies and delivery strategies to enhance their therapeutic efficacy.* Pharmacological research, 2020. **152**: p. 104629.

172. An, P., *diwan Ad, chandra Sr. Flavonoids: an overview.* Journal of nutritional science, 2016. **5**: p. e47.

173. McDougall, G.J., et al., *Assessing potential bioavailability of raspberry anthocyanins using an in vitro digestion system.* Journal of agricultural and food chemistry, 2005. **53**(15): p. 5896-5904.

174. Langeh, U., et al., *Drug-herb combination therapy in cancer management.* Molecular Biology Reports, 2022. **49**(11): p. 11009-11024.

175. Karak, P., *Biological activities of flavonoids: an overview.* Int. J. Pharm. Sci. Res, 2019. **10**(4): p. 1567-1574.

176. Veberic, R., et al., *Anthocyanin composition of different wild and cultivated berry species.* LWT-Food Science and Technology, 2015. **60**(1): p. 509-517.

177. Tzanova, M., et al., *Selectivity of current extraction techniques for flavonoids from plant materials.* Processes, 2020. **8**(10): p. 1222.

178. Maaliki, D., et al., *Flavonoids in hypertension: a brief review of the underlying mechanisms.* Current Opinion in Pharmacology, 2019. **45**: p. 57-65.

179. Nkembo, A.T., *Flavonoids' Classification and Their Applications as Nutraceuticals.* Flavonoids and Anti-Aging: The Role of Transcription Factor Nuclear Erythroid 2-Related Factor2, 2023.

180. Agrawal, A., *Pharmacological activities of flavonoids: a review.* Int. J. Pharm. Sci. Nanotechnol, 2011. **4**(2): p. 1394-1398.

181. Panche, A.N., A.D. Diwan, and S.R. Chandra, *Flavonoids: an overview.* J Nutr Sci, 2016. **5**: p. e47.

182. Banjarnahor, S.D. and N. Artanti, *Antioxidant properties of flavonoids.* Medical Journal of Indonesia, 2014. **23**(4): p. 239-44.

183. Manthey, J.A., *Biological properties of flavonoids pertaining to inflammation.* Microcirculation, 2000. **7**(sup1): p. S29-S34.

184. Hodgson, J.M. and K.D. Croft, *Tea flavonoids and cardiovascular health.* Molecular aspects of medicine, 2010. **31**(6): p. 495-502.

185. Clere, N., et al., *Anticancer properties of flavonoids: roles in various stages of carcinogenesis.* Cardiovascular & Hematological Agents in Medicinal Chemistry (Formerly Current Medicinal Chemistry-Cardiovascular & Hematological Agents), 2011. **9**(2): p. 62-77.

186. Ninfali, P., et al., *Antiviral properties of flavonoids and delivery strategies.* Nutrients, 2020. **12**(9): p. 2534.

187. Alvesalo, J., et al., *Inhibitory effect of dietary phenolic compounds on Chlamydia pneumoniae in cell cultures.* Biochemical Pharmacology, 2006. **71**(6): p. 735-741.

188. Calderone, V., et al., *Vasorelaxing effects of flavonoids: investigation on the possible involvement of potassium channels.* Naunyn-Schmiedeberg's Archives of Pharmacology, 2004. **370**(4): p. 290-298.

189. Duthie, G.G., S.J. Duthie, and J.A.M. Kyle, *Plant polyphenols in cancer and heart disease: implications as nutritional antioxidants.* Nutrition Research Reviews, 2000. **13**(1): p. 79-106.

190. Valko, M., et al., *Free radicals, metals and antioxidants in oxidative stress-induced cancer.* Chemico-biological interactions, 2006. **160**(1): p. 1-40.

191. Rahimi, R., et al., *A review on the role of antioxidants in the management of diabetes and its complications.* Biomedicine & Pharmacotherapy, 2005. **59**(7): p. 365-373.

192. Magalingam, K.B., A.K. Radhakrishnan, and N. Haleagrahara, *Protective mechanisms of flavonoids in Parkinson's disease.* Oxidative medicine and cellular longevity, 2015. **2015**.

193. Amic, D., et al., *SAR and QSAR of the antioxidant activity of flavonoids.* Current medicinal chemistry, 2007. **14**(7): p. 827-845.

194. Shen, N., et al., *Plant flavonoids: Classification, distribution, biosynthesis, and antioxidant activity.* Food Chemistry, 2022. **383**: p. 132531.

195. Pisoschi, A.M., et al., *Oxidative stress mitigation by antioxidants-an overview on their chemistry and influences on health status.* European Journal of Medicinal Chemistry, 2021. **209**: p. 112891.

196. Anandan, R. and P. Subramanian, *Renal protective effect of hesperidin on gentamicin-induced acute nephrotoxicity in male Wistar albino rats.* Redox Report, 2012. **17**(5): p. 219-226.

197. Sesso, H.D., et al., *Flavonoid intake and the risk of cardiovascular disease in women.* The American journal of clinical nutrition, 2003. **77**(6): p. 1400-1408.

198. Vidavalur, R., et al., *Significance of wine and resveratrol in cardiovascular disease: French paradox revisited.* Experimental & Clinical Cardiology, 2006. **11**(3): p. 217.

199. Zhang, C., et al., *Tea consumption and risk of cardiovascular outcomes and total mortality: a systematic review and meta-analysis of prospective observational studies.* European journal of epidemiology, 2015. **30**: p. 103-113.

200. Busch, C., et al., *Epigenetic activities of flavonoids in the prevention and treatment of cancer.* Clinical epigenetics, 2015. **7**(1): p. 1-18.

201. Cordenunsi, B.R., et al., *Effects of temperature on the chemical composition and antioxidant activity of three strawberry cultivars.* Food chemistry, 2005. **91**(1): p. 113-121.

202. Duthie, S.J., et al., *The effects of cranberry juice consumption on antioxidant status and biomarkers relating to heart disease and cancer in healthy human volunteers.* European Journal of Nutrition, 2006. **45**(2): p. 113-122.

203. Surai, P.F., *Silymarin as a natural antioxidant: an overview of the current evidence and perspectives.* Antioxidants, 2015. **4**(1): p. 204-247.

204. Ciumărnean, L., et al., *The effects of flavonoids in cardiovascular diseases.* Molecules, 2020. **25**(18): p. 4320.

205. Ramirez-Sanchez, I., et al., *(−)-Epicatechin activation of endothelial cell endothelial nitric oxide synthase, nitric oxide, and related signaling pathways.* Hypertension, 2010. **55**(6): p. 1398-1405.

206. Mishra, S. and D.A. Kass, *Cellular and molecular pathobiology of heart failure with preserved ejection fraction.* Nature Reviews Cardiology, 2021. **18**(6): p. 400-423.

207. Toh, J., et al., *Flavonoids from fruit and vegetables: a focus on cardiovascular risk factors.* Current atherosclerosis reports, 2013. **15**: p. 1-7.

208. Levine, A.B., D. Punihaole, and T.B. Levine, *Characterization of the role of nitric oxide and its clinical applications.* Cardiology, 2012. **122**(1): p. 55-68.

209. Salvamani, S., et al., *Antiartherosclerotic effects of plant flavonoids.* BioMed research international, 2014. **2014**.

210. Wang, J., et al., *Green synthesis, characterization and anti-atherosclerotic properties of vanadium nanoparticles.* Inorganic Chemistry Communications, 2022. **146**: p. 110092.

211. Tijburg, L., et al., *Tea flavonoids and cardiovascular diseases: a review.* Critical Reviews in Food Science & Nutrition, 1997. **37**(8): p. 771-785.

212. Tunon, M., et al., *Potential of flavonoids as anti-inflammatory agents: modulation of pro-inflammatory gene expression and signal transduction pathways.* Current drug metabolism, 2009. **10**(3): p. 256-271.

213. Arct, J. and K. Pytkowska, *Flavonoids as components of biologically active cosmeceuticals.* Clinics in dermatology, 2008. **26**(4): p. 347-357.

214. Shukla, R., et al., *Role of flavonoids in management of inflammatory disorders*, in *Bioactive Food as Dietary Interventions for Arthritis and Related Inflammatory Diseases*. 2019, Elsevier. p. 293-322.

215. Maleki, S.J., J.F. Crespo, and B. Cabanillas, *Anti-inflammatory effects of flavonoids.* Food chemistry, 2019. **299**: p. 125124.

216. Tanaka, T., *Flavonoids for allergic diseases: present evidence and future perspective.* Current pharmaceutical design, 2014. **20**(6): p. 879-885.

217. Agnihotri, S., S. Wakode, and A. Agnihotri, *An overview on anti-inflammatory properties and chemo-profiles of plants used in traditional medicine.* 2010.

218. Shrivastava, A., J.K. Gupta, and M.K. Goyal, *Flavonoids and antiepileptic drugs: a comprehensive review on their neuroprotective potentials.* J Med Pharm Allied Sci, 2022. **11**: p. 4179-86.

219. Anjum, A., et al., *Spinal cord injury: pathophysiology, multimolecular interactions, and underlying recovery mechanisms.* International journal of molecular sciences, 2020. **21**(20): p. 7533.

220. Pathak, N., et al., *Neurodegenerative Disorders of Alzheimer, Parkinsonism, Amyotrophic Lateral Sclerosis and Multiple Sclerosis: An Early Diagnostic Approach for Precision Treatment.* Metabolic Brain Disease, 2022. **37**(1): p. 67-104.

221. Simunkova, M., et al., *Management of oxidative stress and other pathologies in Alzheimer's disease.* Archives of Toxicology, 2019. **93**(9): p. 2491-2513.

222. Teixeira, J.P., et al. *Future Therapeutic Perspectives into the Alzheimer's Disease Targeting the Oxidative Stress Hypothesis*. Molecules, 2019. **24**, DOI: 10.3390/molecules24234410.

223. Williams, R.J. and J.P.E. Spencer, *Flavonoids, cognition, and dementia: Actions, mechanisms, and potential therapeutic utility for Alzheimer disease.* Free Radical Biology and Medicine, 2012. **52**(1): p. 35-45.

224. Jung, U.J. and S.R. Kim, *Beneficial Effects of Flavonoids Against Parkinson's Disease.* Journal of Medicinal Food, 2018. **21**(5): p. 421-432.

225. Maher, P. *The Potential of Flavonoids for the Treatment of Neurodegenerative Diseases*. International Journal of Molecular Sciences, 2019. **20**, DOI: 10.3390/ijms20123056.

226. Aryal, S., et al. *The Pathology of Parkinson's Disease and Potential Benefit of Dietary Polyphenols*. Molecules, 2020. **25**, DOI: 10.3390/molecules25194382.

227. Tayab, M.A., et al., *Targeting neuroinflammation by polyphenols: A promising therapeutic approach against inflammation-associated depression.* Biomedicine & Pharmacotherapy, 2022. **147**: p. 112668.

228. Sindhu, R.K., et al., *Impacting the Remedial Potential of Nano Delivery-Based Flavonoids for Breast Cancer Treatment.* Molecules, 2021. **26**(17): p. 5163.

229. Nguyen, T.T.M., G. Gillet, and N. Popgeorgiev, *Caspases in the developing central nervous system: Apoptosis and beyond.* Frontiers in Cell and Developmental Biology, 2021. **9**: p. 702404.

230. Mitra, S., et al., *Impact of ROS Generated by Chemical, Physical, and Plasma Techniques on Cancer Attenuation.* Cancers, 2019. **11**(7): p. 1030.

231. Redza-Dutordoir, M. and D.A. Averill-Bates, *Activation of apoptosis signalling pathways by reactive oxygen species.* Biochimica et Biophysica Acta (BBA) - Molecular Cell Research, 2016. **1863**(12): p. 2977-2992.

232. Kopustinskiene, D.M., et al., *Flavonoids as Anticancer Agents.* Nutrients, 2020. **12**(2).

233. Simunkova, M., et al., *Antioxidant vs. Prooxidant Properties of the Flavonoid, Kaempferol, in the Presence of Cu(II) Ions: A ROS-Scavenging Activity, Fenton Reaction and DNA Damage Study.* Int J Mol Sci, 2021. **22**(4).

234. To, K.K., et al., *Reversal of multidrug resistance by Marsdenia tenacissima and its main active ingredients polyoxypregnanes.* Journal of ethnopharmacology, 2017. **203**: p. 110-119.

235. Teng, H., et al., *The role of dietary flavonoids for modulation of ATP binding cassette transporter mediated multidrug resistance.* eFood, 2021. **2**(5): p. 234-246.

236. Bansal, T., et al., *Emerging significance of flavonoids as P-glycoprotein inhibitors in cancer chemotherapy.* Journal of pharmacy & pharmaceutical sciences, 2009. **12**(1): p. 46-78.

237. Sobhani, M., et al., *Immunomodulatory; anti-inflammatory/antioxidant effects of polyphenols: A comparative review on the parental compounds and their metabolites.* Food Reviews International, 2021. **37**(8): p. 759-811.

238. Shapiro, A.B. and V. Ling, *Positively cooperative sites for drug transport by P-glycoprotein with distinct drug specificities.* European Journal of Biochemistry, 1997. **250**(1): p. 130-137.

239. Gupta, V.K., Y. Bhalla, and V. Jaitak, *Impact of ABC transporters, glutathione conjugates in MDR and their modulation by flavonoids: an overview.* Medicinal Chemistry Research, 2014. **23**: p. 1-15.

240. Zhang, L., et al., *Mechanistic study on the intestinal absorption and disposition of baicalein.* European Journal of Pharmaceutical Sciences, 2007. **31**(3-4): p. 221-231.

241. Straehla, J.P. and K.E. Warren, *Pharmacokinetic Principles and Their Application to Central Nervous System Tumors.* Pharmaceutics, 2020. **12**(10).

242. Utembe, W., et al., *Current Approaches and Techniques in Physiologically Based Pharmacokinetic (PBPK) Modelling of Nanomaterials.* Nanomaterials, 2020. **10**(7): p. 1267.

243. Willmann, S., et al., *PK-Sim®: a physiologically based pharmacokinetic 'whole-body'model.* Biosilico, 2003. **1**(4): p. 121-124.

244. Deepika, D. and V. Kumar, *The Role of "Physiologically Based Pharmacokinetic Model (PBPK)" New Approach Methodology (NAM) in Pharmaceuticals and Environmental Chemical Risk Assessment.* Int J Environ Res Public Health, 2023. **20**(4).

245. Rowland, M. and T.N. Tozer, *Clinical pharmacokinetics and pharmacodynamics : concepts and applications*. 4th ed. ed. 2011: Wolters Kluwer.

246. Rosina, A., A. Mathew, and O. Mohammed, *CONVENTIONAL Vs CONTROLLED DRUG DELIVERY SYSTEMS*. 2018.

247. Mukherjee, B., *Fundamentals of Pharmacokinetics*, in *Pharmacokinetics: Basics to Applications*. 2022, Springer. p. 1-20.

248. Peters, S.A. and H. Dolgos, *Requirements to Establishing Confidence in Physiologically Based Pharmacokinetic (PBPK) Models and Overcoming Some of the Challenges to Meeting Them.* Clinical Pharmacokinetics, 2019. **58**(11): p. 1355-1371.

249. Jamei, M., et al., *The Simcyp Population Based Simulator: Architecture, Implementation, and Quality Assurance.* In Silico Pharmacology, 2013. **1**(1): p. 9.

250. Fan, J. and I.A.M. de Lannoy, *Pharmacokinetics.* Biochemical Pharmacology, 2014. **87**(1): p. 93-120.

251. Perry, C., et al., *Utilization of Physiologically Based Pharmacokinetic Modeling in Clinical Pharmacology and Therapeutics: an Overview.* Current Pharmacology Reports, 2020. **6**(3): p. 71-84.

252. Rostami‐Hodjegan, A., *Reverse translation in PBPK and QSP: going backwards in order to go forward with confidence.* Clinical Pharmacology & Therapeutics, 2018. **103**(2): p. 224-232.

253. Manallack, D.T., et al., *The significance of acid/base properties in drug discovery.* Chemical Society Reviews, 2013. **42**(2): p. 485-496.

254. Riviere, J.E., *Absorption, distribution, metabolism, and elimination.* Veterinary pharmacology and therapeutics, 2009. **9**.

255. Gaohua, L., et al., *Development of a permeability-limited model of the human brain and cerebrospinal fluid (CSF) to integrate known physiological and biological knowledge: Estimating time varying CSF drug concentrations and their variability using in vitro data.* Drug metabolism and pharmacokinetics, 2016. **31**(3): p. 224-233.

256. Shitara, Y., *Clinical importance of OATP1B1 and OATP1B3 in drug–drug interactions.* Drug metabolism and pharmacokinetics, 2011. **26**(3): p. 220-227.

257. Zhuang, X. and C. Lu, *PBPK modeling and simulation in drug research and development.* Acta Pharmaceutica Sinica B, 2016. **6**(5): p. 430-440.

258. Tsamandouras, N., A. Rostami‐Hodjegan, and L. Aarons, *Combining the 'bottom up' and 'top down' approaches in pharmacokinetic modelling: fitting PBPK models to observed clinical data.* British journal of clinical pharmacology, 2015. **79**(1): p. 48-55.

259. Mannhold, R., H. Kubinyi, and G. Folkers, *Pharmacokinetics and metabolism in drug design*. Vol. 51. 2012: John Wiley & Sons.

260. Waters, L.J., Y. Shahzad, and J. Stephenson, *Modelling skin permeability with micellar liquid chromatography.* European Journal of Pharmaceutical Sciences, 2013. **50**(3-4): p. 335-340.

261. Kuepfer, L., et al., *Applied Concepts in PBPK Modeling: How to Build a PBPK/PD Model.* CPT: Pharmacometrics & Systems Pharmacology, 2016. **5**(10): p. 516-531.

262. Abouir, K., et al., *Reviewing Data Integrated for PBPK Model Development to Predict Metabolic Drug-Drug Interactions: Shifting Perspectives and Emerging Trends.* Frontiers in Pharmacology, 2021. **12**.

263. Carlander, U., et al., *Toward a general physiologically-based pharmacokinetic model for intravenously injected nanoparticles.* International journal of nanomedicine, 2016. **11**: p. 625.

264. Kuepfer, L., et al., *Applied concepts in PBPK modeling: how to build a PBPK/PD model.* CPT: pharmacometrics & systems pharmacology, 2016. **5**(10): p. 516-531.

265. Balhara, A., S. Kale, and S. Singh, *Physiologically Based Pharmacokinetic (PBPK) Modelling*, in *Computer Aided Pharmaceutics and Drug Delivery: An Application Guide for Students and Researchers of Pharmaceutical Sciences*, V.A. Saharan, Editor. 2022, Springer Nature Singapore: Singapore. p. 255-284.

266. Templeton, I., et al., *Quantitative Prediction of Drug–Drug Interactions Involving Inhibitory Metabolites in Drug Development: How Can Physiologically Based Pharmacokinetic Modeling Help?* CPT: Pharmacometrics & Systems Pharmacology, 2016. **5**(10): p. 505-515.

267. Tsiros, P., et al., *Population pharmacokinetic reanalysis of a Diazepam PBPK model: a comparison of Stan and GNU MCSim.* Journal of Pharmacokinetics and Pharmacodynamics, 2019. **46**.

268. Gill, J., et al., *Comparing the applications of machine learning, PBPK, and population pharmacokinetic models in pharmacokinetic drug–drug interaction prediction.* CPT: Pharmacometrics & Systems Pharmacology, 2022. **11**(12): p. 1560-1568.

269. Tylutki, Z., S. Polak, and B. Wiśniowska, *Top-down, Bottom-up and Middle-out Strategies for Drug Cardiac Safety Assessment via Modeling and Simulations.* Current Pharmacology Reports, 2016. **2**(4): p. 171-177.

270. Tsamandouras, N., A. Rostami-Hodjegan, and L. Aarons, *Combining the 'bottom up' and 'top down' approaches in pharmacokinetic modelling: fitting PBPK models to observed clinical data.* British Journal of Clinical Pharmacology, 2015. **79**(1): p. 48-55.

271. Arvanitis, C.D., et al., *Mechanisms of enhanced drug delivery in brain metastases with focused ultrasound-induced blood–tumor barrier disruption.* Proceedings of the National Academy of Sciences, 2018. **115**(37): p. E8717-E8726.

272. Luzon, E., et al., *Physiologically based pharmacokinetic modeling in regulatory decision-making at the European Medicines Agency.* Clinical Pharmacology & Therapeutics, 2017. **102**(1): p. 98-105.

273. Wagner, C., et al., *Application of Physiologically Based Pharmacokinetic (PBPK) Modeling to Support Dose Selection: Report of an FDA Public Workshop on PBPK.* CPT: Pharmacometrics & Systems Pharmacology, 2015. **4**(4): p. 226-230.

274. Jones, H., et al., *Physiologically based pharmacokinetic modeling in drug discovery and development: A pharmaceutical industry perspective.* Clinical Pharmacology & Therapeutics, 2015. **97**(3): p. 247-262.

275. Touma, J.A., A.J. McLachlan, and A.S. Gross, *The role of ethnicity in personalized dosing of small molecule tyrosine kinase inhibitors used in oncology.* Translational Cancer Research, 2017: p. S1558-S1591.

276. Xu, Z.-Y. and J.-L. Li, *Comparative review of drug–drug interactions with epidermal growth factor receptor tyrosine kinase inhibitors for the treatment of non-small-cell lung cancer.* OncoTargets and Therapy, 2019. **12**(null): p. 5467-5484.

277. Wedagedera, J.R., et al., *Population PBPK modeling using parametric and nonparametric methods of the Simcyp Simulator, and Bayesian samplers.* CPT: Pharmacometrics & Systems Pharmacology, 2022. **11**(6): p. 755-765.

278. Sung, J.H., et al., *Using physiologically-based pharmacokinetic-guided "body-on-a-chip" systems to predict mammalian response to drug and chemical exposure.* Experimental biology and medicine, 2014. **239**(9): p. 1225-1239.

279. Ezuruike, U., et al., *Guide to development of compound files for PBPK modeling in the Simcyp population‐based simulator.* CPT: Pharmacometrics & Systems Pharmacology, 2022. **11**(7): p. 805-821.

280. El‐Khateeb, E., et al., *Physiological‐based pharmacokinetic modeling trends in pharmaceutical drug development over the last 20‐years; in‐depth analysis of applications, organizations, and platforms.* Biopharmaceutics & Drug Disposition, 2021. **42**(4): p. 107-117.

281. Jabir, R.S., et al., *Plasma alpha-1-acid glycoprotein as a potential predictive biomarker for non-haematological adverse events of docetaxel in breast cancer patients.* Biomarkers, 2018. **23**(2): p. 142-146.

282. Jones, H. and K. Rowland‐Yeo, *Basic concepts in physiologically based pharmacokinetic modeling in drug discovery and development.* CPT: pharmacometrics & systems pharmacology, 2013. **2**(8): p. 1-12.

283. El-Khateeb, E., et al., *Physiological-based pharmacokinetic modeling trends in pharmaceutical drug development over the last 20-years; in-depth analysis of applications, organizations, and platforms.* Biopharmaceutics & Drug Disposition, 2021. **42**(4): p. 107-117.

284. Jemal, A., et al., *Cancer statistics, 2002.* CA Cancer J Clin, 2002. **52**(1): p. 23-47.

285. Duma, N., R. Santana-Davila, and J.R. Molina, *Non–Small Cell Lung Cancer: Epidemiology, Screening, Diagnosis, and Treatment.* Mayo Clinic Proceedings, 2019. **94**(8): p. 1623-1640.

286. Beadsmoore, C.J. and N.J. Screaton, *Classification, staging and prognosis of lung cancer.* European Journal of Radiology, 2003. **45**(1): p. 8-17.

287. Saito, S., et al., *Current status of research and treatment for non-small cell lung cancer in never-smoking females.* Cancer biology & therapy, 2017. **18**(6): p. 359-368.

288. Zarogoulidis, K., et al., *Treatment of non-small cell lung cancer (NSCLC).* Journal of thoracic disease, 2013. **5 Suppl 4**(Suppl 4): p. S389-S396.

289. Brambilla, E. and A. Gazdar, *Pathogenesis of lung cancer signalling pathways: roadmap for therapies.* European Respiratory Journal, 2009. **33**(6): p. 1485.

290. Myers, D.J. and J.M. Wallen, *Lung adenocarcinoma.* StatPearls [Internet], 2021.

291. Minna, J.D., J.A. Roth, and A.F. Gazdar, *Focus on lung cancer.* Cancer cell, 2002. **1**(1): p. 49-52.

292. Pikor, L.A., et al., *Genetic alterations defining NSCLC subtypes and their therapeutic implications.* Lung Cancer, 2013. **82**(2): p. 179-189.

293. Gold, K.A., et al., *Personalizing lung cancer prevention through a reverse migration strategy.* Topics in current chemistry, 2013. **329**: p. 221-240.

294. Yu, K.-H., et al., *Classifying non-small cell lung cancer types and transcriptomic subtypes using convolutional neural networks.* Journal of the American Medical Informatics Association, 2020. **27**(5): p. 757-769.

295. Goldstraw, P., et al., *The IASLC lung cancer staging project: proposals for revision of the TNM stage groupings in the forthcoming (eighth) edition of the TNM classification for lung cancer.* 2016. **11**(1): p. 39-51.

296. Chen, W., et al., *Cancer statistics in China, 2015.* 2016. **66**(2): p. 115-132.

297. Martín-Sánchez, J.C., et al., *Projections in breast and lung cancer mortality among women: a Bayesian analysis of 52 countries worldwide.* 2018. **78**(15): p. 4436-4442.

298. Rajaram, P., et al., *Epidermal growth factor receptor: Role in human cancer.* Indian J Dent Res, 2017. **28**(6): p. 687-694.

299. Mitsudomi, T. and Y. Yatabe, *Epidermal growth factor receptor in relation to tumor development: EGFR gene and cancer.* Febs j, 2010. **277**(2): p. 301-8.

300. Wieduwilt, M.J. and M.M. Moasser, *The epidermal growth factor receptor family: biology driving targeted therapeutics.* Cellular and molecular life sciences : CMLS, 2008. **65**(10): p. 1566-1584.

301. Scaltriti, M. and J. Baselga, *The Epidermal Growth Factor Receptor Pathway: A Model for Targeted Therapy.* Clinical Cancer Research, 2006. **12**(18): p. 5268-5272.

302. Okabe, T., et al., *Differential constitutive activation of the epidermal growth factor receptor in non–small cell lung cancer cells bearing EGFR gene mutation and amplification.* Cancer research, 2007. **67**(5): p. 2046-2053.

303. Shigematsu, H., et al., *Clinical and biological features associated with epidermal growth factor receptor gene mutations in lung cancers.* Journal of the National Cancer Institute, 2005. **97**(5): p. 339-346.

304. Lin, Y., X. Wang, and H. Jin, *EGFR-TKI resistance in NSCLC patients: mechanisms and strategies.* Am J Cancer Res, 2014. **4**(5): p. 411-35.

305. Masood, A., R.K. Kancha, and J. Subramanian, *Epidermal growth factor receptor (EGFR) tyrosine kinase inhibitors in non-small cell lung cancer harboring uncommon EGFR mutations: Focus on afatinib.* Seminars in Oncology, 2019. **46**(3): p. 271-283.

306. Gridelli, C., et al., *Gefitinib as first-line treatment for patients with advanced non-small-cell lung cancer with activating epidermal growth factor receptor mutation: Review of the evidence.* Lung Cancer, 2011. **71**(3): p. 249-57.

307. Lynch, T.J., et al., *Activating mutations in the epidermal growth factor receptor underlying responsiveness of non-small-cell lung cancer to gefitinib.* N Engl J Med, 2004. **350**(21): p. 2129-39.

308. K. P, S.H., et al., *Antioxidant activity of erlotinib and gefitinib: theoretical and experimental insights.* Free Radical Research, 2022: p. 1-13.

309. Timmers, L., et al., *Adherence, exposure and patients' experiences with the use of erlotinib in non-small cell lung cancer.* Journal of cancer research and clinical oncology, 2015. **141**(8): p. 1481-1491.

310. Yang, S.-C., et al., *Health-related quality of life after first-line anti-cancer treatments for advanced non-small cell lung cancer in clinical practice.* Quality of Life Research, 2016. **25**(6): p. 1441-1449.

311. Wu, Y.-L., et al., *Tumor response and health-related quality of life in clinically selected patients from Asia with advanced non-small-cell lung cancer treated with first-line gefitinib: post hoc analyses from the IPASS study.* Lung cancer, 2013. **81**(2): p. 280-287.

312. Ranson, M., et al., *A phase I dose-escalation and bioavailability study of oral and intravenous formulations of erlotinib (Tarceva®, OSI-774) in patients with advanced solid tumors of epithelial origin.* Cancer Chemotherapy and Pharmacology, 2010. **66**(1): p. 53-58.

313. Swaisland, H.C., et al., *Single-dose clinical pharmacokinetic studies of gefitinib.* 2005. **44**(11): p. 1165-1177.

314. Wilson, C.G., et al., *Do gastrointestinal transit parameters influence the pharmacokinetics of gefitinib?* International Journal of Pharmaceutics, 2009. **376**(1): p. 7-12.

315. van Erp, N.P., H. Gelderblom, and H.J. Guchelaar, *Clinical pharmacokinetics of tyrosine kinase inhibitors.* Cancer Treat Rev, 2009. **35**(8): p. 692-706.

316. Swaisland, H.C., et al., *Exploring the relationship between expression of cytochrome P450 enzymes and gefitinib pharmacokinetics.* Clin Pharmacokinet, 2006. **45**(6): p. 633-44.

317. Li, J., et al., *Differential metabolism of gefitinib and erlotinib by human cytochrome P450 enzymes.* Clin Cancer Res, 2007. **13**(12): p. 3731-7.

318. Chen, Y., et al., *Physiologically Based Pharmacokinetic Modeling to Evaluate the Systemic Exposure of Gefitinib in CYP2D6 Ultrarapid Metabolizers and Extensive Metabolizers.* J Clin Pharmacol, 2018. **58**(4): p. 485-493.

319. Li, J., et al., *Binding of gefitinib, an inhibitor of epidermal growth factor receptor-tyrosine kinase, to plasma proteins and blood cells: in vitro and in cancer patients.* Investigational New Drugs, 2006. **24**(4): p. 291-297.

320. Yu, H., et al., *Practical Guidelines for Therapeutic Drug Monitoring of Anticancer Tyrosine Kinase Inhibitors: Focus on the Pharmacokinetic Targets.* Clinical Pharmacokinetics, 2014. **53**(4): p. 305-325.

321. Zhao, Y.-Y., et al., *The relationship between drug exposure and clinical outcomes of non-small cell lung cancer patients treated with gefitinib.* 2011. **28**(3): p. 697-702.

322. Yeo, W.-L., et al., *Erlotinib at a dose of 25 mg daily for non-small cell lung cancers with EGFR mutations.* 2010. **5**(7): p. 1048-1053.

323. Rowland, A., et al., *Kinase inhibitor pharmacokinetics: comprehensive summary and roadmap for addressing inter-individual variability in exposure.* Expert Opinion on Drug Metabolism & Toxicology, 2017. **13**(1): p. 31-49.

324. Scheffler, M., et al., *Clinical Pharmacokinetics of Tyrosine Kinase Inhibitors.* Clinical Pharmacokinetics, 2011. **50**(6): p. 371-403.

325. Polasek, T.M., et al., *Perpetrators of pharmacokinetic drug-drug interactions arising from altered cytochrome P450 activity: a criteria-based assessment.* Br J Clin Pharmacol, 2011. **71**(5): p. 727-36.

326. Sung, M.R., et al., *Effects of Ethnicity on Outcomes of Patients With EGFR Mutation-Positive NSCLC Treated With EGFR Tyrosine Kinase Inhibitors and Surgical Resection.* JTO Clin Res Rep, 2022. **3**(2): p. 100259.

327. Gibson, A.J.W., et al., *Impact of Asian ethnicity on outcome in metastatic EGFR-mutant non–small cell lung cancer.* Asia-Pacific Journal of Clinical Oncology, 2019. **15**(6): p. 343-352.

328. Zhang, Q., et al., *Comparison of the characteristics of uncommon epidermal growth factor receptor (EGFR) mutations and EGFR‑tyrosine kinase inhibitor treatment in patients with non‑small cell lung cancer from different ethnic groups.* Exp Ther Med, 2020. **19**(6): p. 3513-3520.

329. Cheeti, S., et al., *A physiologically based pharmacokinetic (PBPK) approach to evaluate pharmacokinetics in patients with cancer.* 2013. **34**(3): p. 141-154.

330. Launay-Vacher, V., et al., *Prevalence of renal insufficiency in cancer patients and implications for anticancer drug management: the renal insufficiency and anticancer medications (IRMA) study.* 2007. **110**(6): p. 1376-1384.

331. Barter, Z.E., et al., *Covariation of human microsomal protein per gram of liver with age: absence of influence of operator and sample storage may justify interlaboratory data pooling.* 2008. **36**(12): p. 2405-2409.

332. Barter, Z.E., G.T. Tucker, and K. Rowland-Yeo, *Differences in cytochrome p450-mediated pharmacokinetics between chinese and caucasian populations predicted by mechanistic physiologically based pharmacokinetic modelling.* Clin Pharmacokinet, 2013. **52**(12): p. 1085-100.

333. Barter, Z., K. Yeo, and G. Tucker, *Prediction of Differences in Pharmacokinetics between Chinese and Caucasian Populations using a Mechanistic Physiologically-Based Pharmacokinetic Model*. 2011.

334. Chen, Y., et al., *Physiologically Based Pharmacokinetic Modeling to Evaluate the Systemic Exposure of Gefitinib in CYP2D6 Ultrarapid Metabolizers and Extensive Metabolizers.* 2018. **58**(4): p. 485-493.

335. Ting, S. and S. Schug, *The pharmacogenomics of pain management: prospects for personalized medicine.* J Pain Res, 2016. **9**: p. 49-56.

336. Bradford, L.D.J.P., *CYP2D6 allele frequency in European Caucasians, Asians, Africans and their descendants.* 2002. **3**(2): p. 229-243.

337. Yuan, Y., et al. *Critical appraisal of the role of gefitinib in the management of locally advanced or metastatic non-small cell lung cancer*. OncoTargets and therapy, 2014. **7**, 841-852 DOI: 10.2147/ott.s34124.

338. Hirte, H.W., *Profile of erlotinib and its potential in the treatment of advanced ovarian carcinoma.* Onco Targets Ther, 2013. **6**: p. 427-35.

339. Swaisland, H.C., et al., *Pharmacokinetic drug interactions of gefitinib with rifampicin, itraconazole and metoprolol.* Clin Pharmacokinet, 2005. **44**(10): p. 1067-81.

340. Swaisland, H., et al., *Pharmacokinetics and tolerability of the orally active selective epidermal growth factor receptor tyrosine kinase inhibitor ZD1839 in healthy volunteers.* Clin Pharmacokinet, 2001. **40**(4): p. 297-306.

341. Wright, J.G., et al., *Estimation of glomerular filtration rate in cancer patients.* Br J Cancer, 2001. **84**(4): p. 452-9.

342. Cheng, Y., et al., *A novel nomogram to predict the reliability of estimated glomerular filtration rate formulae in oncology patients.* BMC Cancer, 2020. **20**(1): p. 530.

343. Tong, Y., et al., *Evaluation of Serological Indicators and Glomerular Filtration Rate Equations in Chinese Cancer Patients.* Medical science monitor : international medical journal of experimental and clinical research, 2017. **23**: p. 2949-2960.

344. Dai, D.-M., et al., *Difference in hematocrit and plasma albumin levels as an additional biomarker in the diagnosis of infectious disease.* Archives of medical science : AMS, 2019. **16**(3): p. 522-530.

345. Cao, Y., et al., *The value of haematological parameters and serum tumour markers for predicting KRAS mutations in 784 Chinese colorectal cancer patients: a retrospective analysis.* BMC Cancer, 2020. **20**(1): p. 1099.

346. Shi, K., et al., *Clinical characteristics of malignant melanoma in central China and predictors of metastasis.* Oncol Lett, 2020. **19**(2): p. 1452-1464.

347. Wang, X., et al., *Changes of serum albumin level and systemic inflammatory response in inoperable non-small cell lung cancer patients after chemotherapy.* 2014. **10**(4): p. 1019-1023.

348. Yang, Y., et al., *Renal Function and All-Cause Mortality Risk Among Cancer Patients.* 2016. **95**(20): p. e3728.

349. Wang, F., et al., *Alpha-1-acid glycoprotein as potential predictive biomarker of docetaxel adverse effects in breast cancer patients.* 2017. **26**(12): p. 895-899.

350. Hashimoto, S., et al., *α1-Acid glycoprotein fucosylation as a marker of carcinoma progression and prognosis.* 2004. **101**(12): p. 2825-2836.

351. Matsuura, H. and S. Nakazawa, *Prognostic significance of serum alpha 1-acid glycoprotein in patients with glioblastoma multiforme: a preliminary communication.* 1985. **48**(8): p. 835-837.

352. Zhang, Z., et al., *Dual blockade of EGFR and VEGFR pathways: Results from a pilot study evaluating apatinib plus gefitinib as a first-line treatment for advanced EGFR-mutant non-small cell lung cancer.* Clinical and translational medicine, 2020. **10**(2): p. e33.

353. Ma, Y., et al., *The analysis of pharmacokinetic and pharmacogenomic impact on gefitinib efficacy in advanced non-small cell lung cancer patients: results from a prospective cohort study.* Ann Transl Med, 2019. **7**(24): p. 806.

354. Zhao, J., et al., *Cerebrospinal Fluid Concentrations of Gefitinib in Patients With Lung Adenocarcinoma.* Clinical Lung Cancer, 2013. **14**(2): p. 188-193.

355. Xu, Z.-Y. and J.-L. Li, *Comparative review of drug-drug interactions with epidermal growth factor receptor tyrosine kinase inhibitors for the treatment of non-small-cell lung cancer.* OncoTargets and therapy, 2019. **12**: p. 5467-5484.

356. Chhun, S., et al., *Gefitinib-phenytoin interaction is not correlated with the C-erythromycin breath test in healthy male volunteers.* Br J Clin Pharmacol, 2009. **68**(2): p. 226-37.

357. Agency, E.M., *Iressa (gefitinib) Summary of Product Characteristics*. 2017.

358. Edginton, A.N., W. Schmitt, and S. Willmann, *Development and evaluation of a generic physiologically based pharmacokinetic model for children.* Clin Pharmacokinet, 2006. **45**(10): p. 1013-34.

359. Ginsberg, G., et al., *Physiologically based pharmacokinetic (PBPK) modeling of caffeine and theophylline in neonates and adults: implications for assessing children's risks from environmental agents.* J Toxicol Environ Health A, 2004. **67**(4): p. 297-329.

360. Parrott, N., et al., *Development of a physiologically based model for oseltamivir and simulation of pharmacokinetics in neonates and infants.* Clin Pharmacokinet, 2011. **50**(9): p. 613-23.

361. U.S. Food and Drug Administration. *Summary Minutes of the Advisory Committee for Pharmaceutical Science and Clinical Pharmacology*. 2012 [cited 2018 29th May]; Available from: https://wayback.archive-it.org/7993/20170403224110/https://www.fda.gov/AdvisoryCommittees/CommitteesMeetingMaterials/Drugs/AdvisoryCommitteeforPharmaceuticalScienceandClinicalPharmacology/ucm286697.htm.

362. Almurjan, A., H. Macfarlane, and R.K.S. Badhan, *Precision dosing-based optimisation of paroxetine during pregnancy for poor and ultrarapid CYP2D6 metabolisers: a virtual clinical trial pharmacokinetics study.* Journal of Pharmacy and Pharmacology. **n/a**(n/a).

363. Olafuyi, O. and R.K.S. Badhan, *Dose Optimization of Chloroquine by Pharmacokinetic Modeling During Pregnancy for the Treatment of Zika Virus Infection.* J Pharm Sci, 2019. **108**(1): p. 661-673.

364. Segura, M., et al., *Quantitative determination of paroxetine and its 4-hydroxy-3-methoxy metabolite in plasma by high-performance liquid chromatography/electrospray ion trap mass spectrometry: application to pharmacokinetic studies.* Rapid Commun Mass Spectrom, 2003. **17**(13): p. 1455-61.

365. Yasui-Furukori, N., et al., *Terbinafine increases the plasma concentration of paroxetine after a single oral administration of paroxetine in healthy subjects.* Eur J Clin Pharmacol, 2007. **63**(1): p. 51-6.

366. Massaroti, P., et al., *Validation of a selective method for determination of paroxetine in human plasma by LC-MS/MS.* J Pharm Pharm Sci, 2005. **8**(2): p. 340-7.

367. Segura, M., et al., *Contribution of cytochrome P450 2D6 to 3,4-methylenedioxymethamphetamine disposition in humans - Use of paroxetine as a metabolic inhibitor probe.* Clinical Pharmacokinetics, 2005. **44**(6): p. 649-660.

368. Swaisland, H.C., et al., *Pharmacokinetic drug interactions of gefitinib with rifampicin, itraconazole and metoprolol.* Clinical pharmacokinetics, 2005. **44**: p. 1067-1081.

369. Swaisland, H.C., et al., *Single-dose clinical pharmacokinetic studies of gefitinib.* Clinical pharmacokinetics, 2005. **44**: p. 1165-1177.

370. Swaisland, H., et al., *Pharmacokinetics and tolerability of the orally active selective epidermal growth factor receptor tyrosine kinase inhibitor ZD1839 in healthy volunteers.* Clinical pharmacokinetics, 2001. **40**: p. 297-306.

371. Zhang, Z., et al., *Dual blockade of EGFR and VEGFR pathways: Results from a pilot study evaluating apatinib plus gefitinib as a first-line treatment for advanced EGFR-mutant non-small cell lung cancer.* Clinical and translational medicine, 2020. **10**(2): p. e33.

372. Cheng, Y., et al., *A novel nomogram to predict the reliability of estimated glomerular filtration rate formulae in oncology patients.* BMC cancer, 2020. **20**(1): p. 1-9.

373. Tong, Y., et al., *Evaluation of serological indicators and glomerular filtration rate equations in chinese cancer patients.* Medical Science Monitor: International Medical Journal of Experimental and Clinical Research, 2017. **23**: p. 2949.

374. Dai, D.-M., et al., *Difference in hematocrit and plasma albumin levels as an additional biomarker in the diagnosis of infectious disease.* Archives of Medical Science, 2019. **16**(3): p. 522-530.

375. Cao, Y., et al., *The value of haematological parameters and serum tumour markers for predicting KRAS mutations in 784 Chinese colorectal cancer patients: a retrospective analysis.* BMC cancer, 2020. **20**: p. 1-9.

376. Shi, K., et al., *Clinical characteristics of malignant melanoma in central China and predictors of metastasis.* Oncology Letters, 2020. **19**(2): p. 1452-1464.

377. Wang, X., et al., *Changes of serum albumin level and systemic inflammatory response in inoperable non-small cell lung cancer patients after chemotherapy.* Journal of cancer research and therapeutics, 2014. **10**(4): p. 1019-1023.

378. Yang, Y., et al., *Renal function and all-cause mortality risk among cancer patients.* Medicine, 2016. **95**(20).

379. Salim, J.R., et al., *ALPHA-1-ACID GLYCOPROTEIN, A POTENTIAL PREDICTIVE BIOMARKER OF DOCETAXEL ADVERSE EFFECTS IN MALAYSIAN BREAST CANCER PATIENTS.*

380. Hashimoto, S., et al., *α1-Acid glycoprotein fucosylation as a marker of carcinoma progression and prognosis.* Cancer: Interdisciplinary International Journal of the American Cancer Society, 2004. **101**(12): p. 2825-2836.

381. Matsuura, H. and S. Nakazawa, *Prognostic significance of serum alpha 1-acid glycoprotein in patients with glioblastoma multiforme: a preliminary communication.* Journal of Neurology, Neurosurgery & Psychiatry, 1985. **48**(8): p. 835-837.

382. Ma, Y., et al., *The analysis of pharmacokinetic and pharmacogenomic impact on gefitinib efficacy in advanced non-small cell lung cancer patients: results from a prospective cohort study.* Annals of translational medicine, 2019. **7**(24).

383. Liu, Y.-T., et al., *Survival of patients with advanced lung adenocarcinoma before and after approved use of gefitinib in China.* 2015. **6**(5): p. 636-642.

384. Kim, E.S., et al., *Gefitinib versus docetaxel in previously treated non-small-cell lung cancer (INTEREST): a randomised phase III trial.* 2008. **372**(9652): p. 1809-1818.

385. Maemondo, M., et al., *Gefitinib or chemotherapy for non–small-cell lung cancer with mutated EGFR.* 2010. **362**(25): p. 2380-2388.

386. van Dyk, M. and A.J.T.C.R. Rowland, *Physiologically-based pharmacokinetic modeling as an approach to evaluate the effect of covariates and drug-drug interactions on variability in epidermal growth factor receptor kinase inhibitor exposure.* 2017, 2017: p. S1600-S1612.

387. Zhang, H., et al., *Association of Variability and Pharmacogenomics With Bioequivalence of Gefitinib in Healthy Male Subjects.* 2018. **9**(849).

388. Bergman, E., et al., *Pharmacokinetics of gefitinib in humans: the influence of gastrointestinal factors.* Int J Pharm, 2007. **341**(1-2): p. 134-42.

389. Herbst, R.S., et al., *Selective oral epidermal growth factor receptor tyrosine kinase inhibitor ZD1839 is generally well-tolerated and has activity in non-small-cell lung cancer and other solid tumors: results of a phase I trial.* J Clin Oncol, 2002. **20**(18): p. 3815-25.

390. Karalis, V., M. Symillides, and P. Macheras, *Bioequivalence of highly variable drugs: a comparison of the newly proposed regulatory approaches by FDA and EMA.* Pharm Res, 2012. **29**(4): p. 1066-77.

391. Ranson, M., et al., *ZD1839, a selective oral epidermal growth factor receptor-tyrosine kinase inhibitor, is well tolerated and active in patients with solid, malignant tumors: results of a phase I trial.* J Clin Oncol, 2002. **20**(9): p. 2240-50.

392. Nakagawa, K., et al., *Phase I pharmacokinetic trial of the selective oral epidermal growth factor receptor tyrosine kinase inhibitor gefitinib ('Iressa', ZD1839) in Japanese patients with solid malignant tumors.* Ann Oncol, 2003. **14**(6): p. 922-30.

393. Nussbaumer, S., et al., *Analysis of anticancer drugs: a review.* 2011. **85**(5): p. 2265-2289.

394. Bardelmeijer, H.A., et al., *The oral route for the administration of cytotoxic drugs: strategies to increase the efficiency and consistency of drug delivery.* 2000. **18**(3): p. 231-241.

395. Baselga, J., et al., *Phase I safety, pharmacokinetic, and pharmacodynamic trial of ZD1839, a selective oral epidermal growth factor receptor tyrosine kinase inhibitor, in patients with five selected solid tumor types.* Journal of clinical oncology, 2002. **20**(21): p. 4292-4302.

396. Herbst, R.S., et al., *Selective oral epidermal growth factor receptor tyrosine kinase inhibitor ZD1839 is generally well-tolerated and has activity in non–small-cell lung cancer and other solid tumors: Results of a phase I trial.* Journal of Clinical Oncology, 2002. **20**(18): p. 3815-3825.

397. Suzumura, T., et al., *Reduced CYP2D6 function is associated with gefitinib-induced rash in patients with non-small cell lung cancer.* BMC cancer, 2012. **12**: p. 568-568.

398. Nakamura, Y., et al., *Pharmacokinetics of Gefitinib Predicts Antitumor Activity for Advanced Non-small Cell Lung Cancer.* Journal of Thoracic Oncology, 2010. **5**(9): p. 1404-1409.

399. CDER, *Clinical Pharmacolgy Review (Iressa)*, C.f.D.E.a. Research, Editor. 2014, U.S. Food and Drug Administration: USA.

400. Hicks, J.K., J.J. Swen, and A. Gaedigk, *Challenges in CYP2D6 phenotype assignment from genotype data: a critical assessment and call for standardization.* Curr Drug Metab, 2014. **15**(2): p. 218-32.

401. A, L.L., et al., *Interethnic variability of CYP2D6 alleles and of predicted and measured metabolic phenotypes across world populations.* Expert Opin Drug Metab Toxicol, 2014. **10**(11): p. 1569-83.

402. Zhang, L., et al., *Gefitinib versus placebo as maintenance therapy in patients with locally advanced or metastatic non-small-cell lung cancer (INFORM; C-TONG 0804): a multicentre, double-blind randomised phase 3 trial.* 2012. **13**(5): p. 466-475.

403. Lynch, T.J., et al., *Activating mutations in the epidermal growth factor receptor underlying responsiveness of non–small-cell lung cancer to gefitinib.* 2004. **350**(21): p. 2129-2139.

404. Natale, R.B., et al., *Vandetanib versus gefitinib in patients with advanced non–small-cell lung cancer: results from a two-part, double-blind, randomized phase II study.* 2009. **27**(15): p. 2523-2529.

405. Fukuoka, M., et al., *Multi-institutional randomized phase II trial of gefitinib for previously treated patients with advanced non–small-cell lung cancer.* Journal of clinical oncology, 2003. **21**(12): p. 2237-2246.

406. Kris, M.G., et al., *Efficacy of gefitinib, an inhibitor of the epidermal growth factor receptor tyrosine kinase, in symptomatic patients with non–small cell lung cancer: a randomized trial.* Jama, 2003. **290**(16): p. 2149-2158.

407. Pottier, C., et al., *Tyrosine Kinase Inhibitors in Cancer: Breakthrough and Challenges of Targeted Therapy.* Cancers, 2020. **12**(3): p. 731.

408. Clarke, W.A., et al., *Therapeutic drug monitoring in oncology: International Association of Therapeutic Drug Monitoring and Clinical Toxicology consensus guidelines for imatinib therapy.* Eur J Cancer, 2021. **157**: p. 428-440.

409. Buclin, T., et al., *The Steps to Therapeutic Drug Monitoring: A Structured Approach Illustrated With Imatinib.* Front Pharmacol, 2020. **11**: p. 177.

410. Zuidema, S., et al., *Optimizing the dose in patients treated with imatinib as first line treatment for gastrointestinal stromal tumours: A cost‐effectiveness study.* 2019. **85**(9): p. 1994-2001.

411. Gotta, V., et al., *Clinical usefulness of therapeutic concentration monitoring for imatinib dosage individualization: results from a randomized controlled trial.* Cancer Chemotherapy and Pharmacology, 2014. **74**(6): p. 1307-1319.

412. Vener, C., et al., *First-line imatinib vs second- and third-generation TKIs for chronic-phase CML: a systematic review and meta-analysis.* Blood advances, 2020. **4**(12): p. 2723-2735.

413. Al Hamad, M., *Contribution of BCR-ABL molecular variants and leukemic stem cells in response and resistance to tyrosine kinase inhibitors: a review [version 2; peer review: 2 approved].* F1000Research, 2022. **10**(1288).

414. Liu, J., et al., *Mutations in the BCR‐ABL1 kinase domain in patients with chronic myeloid leukaemia treated with TKIs or at diagnosis.* Oncol Lett, 2020. **20**(2): p. 1071-1076.

415. Soverini, S., R. Bassan, and T. Lion, *Treatment and monitoring of Philadelphia chromosome-positive leukemia patients: recent advances and remaining challenges.* Journal of Hematology & Oncology, 2019. **12**(1): p. 39.

416. Riether, C., C.M. Schürch, and A.F. Ochsenbein, *Regulation of hematopoietic and leukemic stem cells by the immune system.* Cell Death & Differentiation, 2015. **22**(2): p. 187-198.

417. Zhang, X., et al., *The NH₂-Terminal Coiled-Coil Domain and Tyrosine 177 Play Important Roles in Induction of a Myeloproliferative Disease in Mice by Bcr-Abl.* Molecular and Cellular Biology, 2001. **21**(3): p. 840-853.

418. Mu, H., et al., *Combination Therapies in Chronic Myeloid Leukemia for Potential Treatment-Free Remission: Focus on Leukemia Stem Cells and Immune Modulation.* Frontiers in Oncology, 2021. **11**.

419. Iqbal, N. and N. Iqbal, *Imatinib: a breakthrough of targeted therapy in cancer.* Chemotherapy research and practice, 2014. **2014**: p. 357027-357027.

420. Rubin, B.P., M.C. Heinrich, and C.L. Corless, *Gastrointestinal stromal tumour.* The Lancet, 2007. **369**(9574): p. 1731-1741.

421. Kelly, C.M., L. Gutierrez Sainz, and P. Chi, *The management of metastatic GIST: current standard and investigational therapeutics.* Journal of Hematology & Oncology, 2021. **14**(1): p. 2.

422. Søreide, K., et al., *Global epidemiology of gastrointestinal stromal tumours (GIST): a systematic review of population-based cohort studies.* 2016. **40**: p. 39-46.

423. Chiang, N.-J., et al., *The epidemiology of gastrointestinal stromal tumors in Taiwan, 1998–2008: a nation-wide cancer registry-based study.* 2014. **14**(1): p. 1-9.

424. Nomura, E., A. Ioka, and H.J.J.j.o.c.o. Tsukuma, *Incidence of soft tissue sarcoma focusing on gastrointestinal stromal sarcoma in Osaka, Japan, during 1978–2007.* 2013. **43**(8): p. 841-845.

425. Xu, L., et al., *Incidence of gastrointestinal stromal tumor in Chinese urban population: A national population-based study.* Cancer Med, 2021. **10**(2): p. 737-744.

426. Gelderblom, H., et al., *Imatinib in combination with phosphoinositol kinase inhibitor buparlisib in patients with gastrointestinal stromal tumour who failed prior therapy*

with imatinib and sunitinib: a Phase 1b, multicentre study. British Journal of Cancer, 2020. **122**(8): p. 1158-1165.

427. Zuidema, S., et al., *Optimizing the dose in patients treated with imatinib as first line treatment for gastrointestinal stromal tumours: A cost-effectiveness study.* British Journal of Clinical Pharmacology, 2019. **85**(9): p. 1994-2001.

428. Søreide, K., et al., *Global epidemiology of gastrointestinal stromal tumours (GIST): A systematic review of population-based cohort studies.* Cancer Epidemiology, 2016. **40**: p. 39-46.

429. Akahoshi, K., et al., *Current clinical management of gastrointestinal stromal tumor.* World J Gastroenterol, 2018. **24**(26): p. 2806-2817.

430. Joensuu, H., *Gastrointestinal stromal tumor (GIST).* Annals of Oncology, 2006. **17**: p. x280-x286.

431. Joensuu, H., et al., *Risk of recurrence of gastrointestinal stromal tumour after surgery: an analysis of pooled population-based cohorts.* 2012. **13**(3): p. 265-274.

432. Guerin, A., et al., *The economic burden of gastrointestinal stromal tumor (GIST) recurrence in patients who have received adjuvant imatinib therapy.* 2015. **18**(3): p. 241-248.

433. Hochhaus, A., et al., *Long-Term Outcomes of Imatinib Treatment for Chronic Myeloid Leukemia.* New England Journal of Medicine, 2017. **376**(10): p. 917-927.

434. Soverini, S., et al., *Best Practices in Chronic Myeloid Leukemia Monitoring and Management.* Oncologist, 2016. **21**(5): p. 626-33.

435. Hochhaus, A., et al., *Six-year follow-up of patients receiving imatinib for the first-line treatment of chronic myeloid leukemia.* Leukemia, 2009. **23**(6): p. 1054-61.

436. Kantarjian, H.M., et al., *Nilotinib versus imatinib for the treatment of patients with newly diagnosed chronic phase, Philadelphia chromosome-positive, chronic myeloid leukaemia: 24-month minimum follow-up of the phase 3 randomised ENESTnd trial.* Lancet Oncol, 2011. **12**(9): p. 841-51.

437. Bixby, D. and M. Talpaz, *Mechanisms of resistance to tyrosine kinase inhibitors in chronic myeloid leukemia and recent therapeutic strategies to overcome resistance.* Hematology Am Soc Hematol Educ Program, 2009: p. 461-76.

438. Kantarjian, H.M., et al., *Efficacy of imatinib dose escalation in patients with chronic myeloid leukemia in chronic phase.* Cancer, 2009. **115**(3): p. 551-60.

439. White, D.L., et al., *Chronic phase chronic myeloid leukemia patients with low OCT-1 activity randomized to high-dose imatinib achieve better responses and have lower failure rates than those randomized to standard-dose imatinib.* Haematologica, 2012. **97**(6): p. 907-14.

440. Baccarani, M., et al., *Comparison of imatinib 400 mg and 800 mg daily in the front-line treatment of high-risk, Philadelphia-positive chronic myeloid leukemia: a European LeukemiaNet Study.* Blood, 2009. **113**(19): p. 4497-4504.

441. Demetri, G.D., et al., *Efficacy and safety of imatinib mesylate in advanced gastrointestinal stromal tumors.* N Engl J Med, 2002. **347**(7): p. 472-80.

442. Demetri, G., et al., *Management of patients with gastrointestinal stromal tumor (GIST)–update of the NCCN clinical practice guidelines.* 2007. **5**(suppl 2): p. S1-29.

443. Gschwind, H., et al., *Metabolism and disposition of Gleevec™(STI571) in healthy volunteers.* 2001. **33**(1): p. 217.

444. Peng, B., et al., *Absolute bioavailability of imatinib (Glivec) orally versus intravenous infusion.* J Clin Pharmacol, 2004. **44**(2): p. 158-62.

445. Peng, B., et al., *Pharmacokinetics and pharmacodynamics of imatinib in a phase I trial with chronic myeloid leukemia patients.* J Clin Oncol, 2004. **22**(5): p. 935-42.

446. Dagher, R., et al., *Approval summary: imatinib mesylate in the treatment of metastatic and/or unresectable malignant gastrointestinal stromal tumors.* 2002. **8**(10): p. 3034-3038.

447. Druker, B.J., et al., *Effects of a selective inhibitor of the Abl tyrosine kinase on the growth of Bcr–Abl positive cells.* 1996. **2**(5): p. 561-566.

448. Arellano, C., et al., *Determination of unbound fraction of imatinib and N-desmethyl imatinib, validation of an UPLC-MS/MS assay and ultrafiltration method.* J Chromatogr B Analyt Technol Biomed Life Sci, 2012. **907**: p. 94-100.

449. Khan, M.S., D.T. Barratt, and A.A. Somogyi, *Impact of CYP2C8*3 polymorphism on in vitro metabolism of imatinib to N-desmethyl imatinib.* Xenobiotica, 2016. **46**(3): p. 278-87.

450. Filppula, A.M., et al., *Autoinhibition of CYP3A4 leads to important role of CYP2C8 in imatinib metabolism: variability in CYP2C8 activity may alter plasma concentrations and response.* 2013. **41**(1): p. 50-59.

451. Nebot, N., et al., *Participation of CYP2C8 and CYP3A4 in the N-demethylation of imatinib in human hepatic microsomes.* 2010. **161**(5): p. 1059-1069.

452. Filppula, A.M., et al., *Potent mechanism-based inhibition of CYP3A4 by imatinib explains its liability to interact with CYP3A4 substrates.* 2012. **165**(8): p. 2787-2798.

453. Rochat, B., et al., *In vitro biotransformation of imatinib by the tumor expressed CYP1A1 and CYP1B1.* Biopharm Drug Dispos, 2008. **29**(2): p. 103-18.

454. Barratt, D.T., et al., *CYP2C8 Genotype Significantly Alters Imatinib Metabolism in Chronic Myeloid Leukaemia Patients.* Clin Pharmacokinet, 2017. **56**(8): p. 977-985.

455. Larson, R.A., et al., *Imatinib pharmacokinetics and its correlation with response and safety in chronic-phase chronic myeloid leukemia: a subanalysis of the IRIS study.* Blood, 2008. **111**(8): p. 4022-8.

456. Li, J., et al., *Chinese consensus guidelines for diagnosis and management of gastrointestinal stromal tumor.* Chinese journal of cancer research = Chung-kuo yen cheng yen chiu, 2017. **29**(4): p. 281-293.

457. Zalcberg, J.R., et al., *Outcome of patients with advanced gastro-intestinal stromal tumours crossing over to a daily imatinib dose of 800 mg after progression on 400 mg.* European Journal of Cancer, 2005. **41**(12): p. 1751-1757.

458. Blanke, C.D., et al., *Phase III randomized, intergroup trial assessing imatinib mesylate at two dose levels in patients with unresectable or metastatic gastrointestinal stromal tumors expressing the kit receptor tyrosine kinase: S0033.* 2008. **26**(4): p. 626-632.

459. Li, J. and L. Shen, *The current status of and prospects in research regarding gastrointestinal stromal tumors in China.* 2020. **126**(S9): p. 2048-2053.

460. Li, J., et al., *Efficacy of imatinib dose escalation in Chinese gastrointestinal stromal tumor patients.* World journal of gastroenterology, 2012. **18**(7): p. 698-703.

461. Joensuu, H., J.C. Trent, and P.J.C.t.r. Reichardt, *Practical management of tyrosine kinase inhibitor-associated side effects in GIST.* 2011. **37**(1): p. 75-88.

462. Picard, S., et al., *Trough imatinib plasma levels are associated with both cytogenetic and molecular responses to standard-dose imatinib in chronic myeloid leukemia.* 2007. **109**(8): p. 3496-3499.

463. Demetri, G.D., et al., *Imatinib plasma levels are correlated with clinical benefit in patients with unresectable/metastatic gastrointestinal stromal tumors.* 2009. **27**(19): p. 3141-3147.

464. Cortes, J., et al., *Pharmacokinetic/pharmacodynamic correlation and blood-level testing in imatinib therapy for chronic myeloid leukemia.* 2009. **23**(9): p. 1537-1544.

465. Gao, B., et al., *Evidence for therapeutic drug monitoring of targeted anticancer therapies.* 2012. **30**(32): p. 4017-4025.

466. Gotta, V., et al., *Systematic review of population pharmacokinetic analyses of imatinib and relationships with treatment outcomes.* 2013. **35**(2): p. 150-167.

467. Roychowdhury, S. and M. Talpaz, *Managing resistance in chronic myeloid leukemia.* Blood Rev, 2011. **25**(6): p. 279-90.

468. Clarke, W.A., et al., *Therapeutic drug monitoring in oncology: International Association of Therapeutic Drug Monitoring and Clinical Toxicology consensus guidelines for imatinib therapy.* European Journal of Cancer, 2021. **157**: p. 428-440.

469. Bouchet, S., et al., *Relationship between imatinib trough concentration and outcomes in the treatment of advanced gastrointestinal stromal tumours in a real-life setting.* European Journal of Cancer, 2016. **57**: p. 31-38.

470. García-Ferrer, M., et al., *Utility of Therapeutic Drug Monitoring of Imatinib, Nilotinib, and Dasatinib in Chronic Myeloid Leukemia: A Systematic Review and Meta-analysis.* Clinical Therapeutics, 2019. **41**(12): p. 2558-2570.e7.

471. Jack, R.H., E.A. Davies, and H. Møller, *Prostate cancer incidence, stage at diagnosis, treatment and survival in ethnic groups in South-East England.* BJU international, 2010. **105**(9): p. 1226-1230.

472. Zhu, Y. and S.X. Qian, *Clinical efficacy and safety of imatinib in the management of Ph(+) chronic myeloid or acute lymphoblastic leukemia in Chinese patients.* Onco Targets Ther, 2014. **7**: p. 395-404.

473. Yu, H. and R.K. Singh Badhan, *The Pharmacokinetics of Gefitinib in a Chinese Cancer Population Group: A Virtual Clinical Trials Population Study.* J Pharm Sci, 2021. **110**(10): p. 3507-3519.

474. Adiwidjaja, J., A.V. Boddy, and A.J. McLachlan, *Implementation of a Physiologically Based Pharmacokinetic Modeling Approach to Guide Optimal Dosing Regimens for Imatinib and Potential Drug Interactions in Paediatrics.* Front Pharmacol, 2019. **10**: p. 1672.

475. Petain, A., et al., *Population pharmacokinetics and pharmacogenetics of imatinib in children and adults.* Clin Cancer Res, 2008. **14**(21): p. 7102-9.

476. Eechoute, K., et al., *A long-term prospective population pharmacokinetic study on imatinib plasma concentrations in GIST patients.* Clinical Cancer Research, 2012. **18**(20): p. 5780-5787.

477. Renard, D., et al., *Pharmacokinetic interactions among imatinib, bosentan and sildenafil, and their clinical implications in severe pulmonary arterial hypertension.* British Journal of Clinical Pharmacology, 2015. **80**(1): p. 75-85.

478. Yu, H. and R.K. Singh Badhan, *The pharmacokinetics of gefitinib in a Chinese Cancer population group: a virtual clinical trials population study.* J Pharm Sci, 2021.

479. Xia, Y., et al., *Correlations between imatinib plasma trough concentration and adverse reactions in Chinese patients with gastrointestinal stromal tumors.* Cancer, 2020. **126 Suppl 9**(S9): p. 2054-2061.

480. Wu, X., et al., *Relative Factors Analysis of Imatinib Trough Concentration in Chinese Patients with Gastrointestinal Stromal Tumor.* Chemotherapy, 2018. **63**(6): p. 301-307.

481. Zhong, J.S., et al., *Correlation between imatinib trough concentration and efficacy in Chinese chronic myelocytic leukemia patients.* Acta Haematol, 2012. **127**(4): p. 221-7.

482. Zhang, Q., et al., *Association of Imatinib Plasma Concentration and Single-nucleotide Polymorphisms with Adverse Drug Reactions in Patients with Gastrointestinal Stromal Tumors.* Mol Cancer Ther, 2018. **17**(12): p. 2780-2787.

483. Ijzerman, N.S., et al., *Therapeutic drug monitoring of imatinib in patients with gastrointestinal stromal tumours – Results from daily clinical practice.* European Journal of Cancer, 2020. **136**: p. 140-148.

484. Lankheet, N.A., et al., *Optimizing the dose in cancer patients treated with imatinib, sunitinib and pazopanib.* 2017. **83**(10): p. 2195-2204.

485. Lankheet, N.A., et al., *Plasma concentrations of tyrosine kinase inhibitors imatinib, erlotinib, and sunitinib in routine clinical outpatient cancer care.* 2014. **36**(3): p. 326-334.

486. Farag, S., et al., *Imatinib pharmacokinetics in a large observational cohort of gastrointestinal stromal tumour patients.* 2017. **56**(3): p. 287-292.

487. Parrott, N., et al., *Development of a physiologically based model for oseltamivir and simulation of pharmacokinetics in neonates and infants.* Clinical pharmacokinetics, 2011. **50**(9): p. 613-623.

488. Ginsberg, G., et al., *Physiologically based pharmacokinetic (PBPK) modeling of caffeine and theophylline in neonates and adults: implications for assessing children's risks from environmental agents.* Journal of Toxicology and Environmental Health, Part A, 2004. **67**(4): p. 297-329.

489. Food, U. and D. Administration, *Summary minutes of the advisory committee for pharmaceutical science and clinical pharmacology*. 2012, FDA, Silver Spring, MD.

490. Olafuyi, O. and R.K. Badhan, *Dose optimization of chloroquine by pharmacokinetic modeling during pregnancy for the treatment of Zika virus infection.* Journal of pharmaceutical sciences, 2019. **108**(1): p. 661-673.

491. Almurjan, A., H. Macfarlane, and R.K.S. Badhan, *The application of precision dosing in the use of sertraline throughout pregnancy for poor and ultrarapid metabolizer CYP 2C19 subjects: A virtual clinical trial pharmacokinetics study.* Biopharmaceutics & Drug Disposition. **n/a**(n/a).

492. Poulin, P. and F.P.J.J.o.p.s. Theil, *Development of a novel method for predicting human volume of distribution at steady‐state of basic drugs and comparative assessment with existing methods.* 2009. **98**(12): p. 4941-4961.

493. Obach, R.S., et al., *The prediction of human pharmacokinetic parameters from preclinical and in vitro metabolism data.* 1997. **283**(1): p. 46-58.

494. Sheiner, L.B. and S.L. Beal, *Some Suggestions for Measuring Predictive Performance.* Journal of Pharmacokinetics and Biopharmaceutics, 1981. **9**(4): p. 503-512.

495. Edginton, A.N., W. Schmitt, and S.J.C.p. Willmann, *Development and evaluation of a generic physiologically based pharmacokinetic model for children.* 2006. **45**(10): p. 1013-1034.

496. Gambacorti-Passerini, C., et al., *Multicenter independent assessment of outcomes in chronic myeloid leukemia patients treated with imatinib.* 2011. **103**(7): p. 553-561.

497. Liegl-Atzwanger, B., J.A. Fletcher, and C.D.M. Fletcher, *Gastrointestinal stromal tumors.* Virchows Archiv, 2010. **456**(2): p. 111-127.

498. Sorour, M.A., et al., *Gastrointestinal stromal tumors (GIST) related emergencies.* Int J Surg, 2014. **12**(4): p. 269-80.

499. Picard, S., et al., *Trough imatinib plasma levels are associated with both cytogenetic and molecular responses to standard-dose imatinib in chronic myeloid leukemia.* Blood, 2007. **109**(8): p. 3496-3499.

500. Yu, H., et al., *Practical guidelines for therapeutic drug monitoring of anticancer tyrosine kinase inhibitors: focus on the pharmacokinetic targets.* Clin Pharmacokinet, 2014. **53**(4): p. 305-25.

501. Nikolova, Z., et al., *Bioequivalence, safety, and tolerability of imatinib tablets compared with capsules.* Cancer Chemother Pharmacol, 2004. **53**(5): p. 433-8.

502. Chen, Y., et al., *Factors Influencing the Steady-State Plasma Concentration of Imatinib Mesylate in Patients With Gastrointestinal Stromal Tumors and Chronic Myeloid Leukemia.* Front Pharmacol, 2020. **11**: p. 569843.

503. Zhang, Q., et al., *Association of Imatinib Plasma Concentration and Single-nucleotide Polymorphisms with Adverse Drug Reactions in Patients with Gastrointestinal Stromal Tumors.* Molecular Cancer Therapeutics, 2018. **17**(12): p. 2780-2787.

504. O'hare, T., et al., *Pushing the limits of targeted therapy in chronic myeloid leukaemia.* Nature reviews Cancer, 2012. **12**(8): p. 513-526.

505. Gotta, V., et al., *Large-scale imatinib dose–concentration–effect study in CML patients under routine care conditions.* Leukemia Research, 2014. **38**(7): p. 764-772.

506. Kobayashi, S., et al., *Efficacy of low-dose imatinib in chronic-phase chronic myelogenous leukemia patients.* Ann Hematol, 2009. **88**(4): p. 311-5.

507. Park, S.J., et al., *Reduced dose of imatinib for patients with chronic myeloid leukemia and low body surface area.* Acta Haematol, 2007. **118**(4): p. 219-21.

508. Horikoshi, A., K. Takei, and S.J.L.r. Sawada, *Relationship between daily dose of imatinib per square meter and its plasma concentration in patients with chronic-phase chronic myeloid leukemia (CML).* 2006. **31**(4): p. 574-575.

509. Horikoshi, A., K. Takei, and S. Sawada, *Effects of lower dose of imatinib to CML patients.* Leuk Res, 2003. **27**(12): p. 1167.

510. Miyazawa, K., et al., *Thrombocytopenia induced by imatinib mesylate (Glivec) in patients with chronic myelogenous leukemia: is 400 mg daily of imatinib mesylate an optimal starting dose for Japanese patients?* 2003. **77**(1): p. 93.

511. Wang, Y., et al., *Effects of imatinib (Glivec) on the pharmacokinetics of metoprolol, a CYP2D6 substrate, in Chinese patients with chronic myelogenous leukaemia.* 2008. **65**(6): p. 885-892.

512. Singh, N., et al., *Drug monitoring of imatinib levels in patients undergoing therapy for chronic myeloid leukaemia: comparing plasma levels of responders and non-responders.* Eur J Clin Pharmacol, 2009. **65**(6): p. 545-9.

513. Lee, W.J., et al., *Clinical and histopathologic analysis of 46 cases of cutaneous adverse reactions to imatinib.* 2016. **55**(5): p. e268-e274.

514. Pretel-Irazabal, M., A. Tuneu-Valls, and N.J.A.D.-S. Ormaechea-Pérez, *Adverse skin effects of imatinib, a tyrosine kinase inhibitor.* 2014. **105**(7): p. 655-662.

515. Huang, W., et al., *Therapeutic drug monitoring-based dose optimization for imatinib-associated serious cutaneous reactions in a patient with gastrointestinal stromal tumours: A case report.* 2020. **45**(4): p. 856-862.

516. Yoon, S., et al., *Imatinib plasma monitoring-guided dose modification for managing imatinib-related toxicities in gastrointestinal stromal tumor patients.* 2013. **28**(8): p. 1248-1252.

517. Conti, R.M., et al., *The cost-effectiveness of therapeutic drug monitoring for the prescription drug-based treatment of chronic myeloid leukemia.* 2021. **27**(8): p. 1077-1085.

518. Grochans, S., et al., *Epidemiology of Glioblastoma Multiforme–Literature Review.* Cancers, 2022. **14**(10): p. 2412.

519. Ou, A., W.K.A. Yung, and N. Majd, *Molecular Mechanisms of Treatment Resistance in Glioblastoma.* International Journal of Molecular Sciences, 2021. **22**(1): p. 351.

520. Fan, J., et al., *ABC transporters affects tumor immune microenvironment to regulate cancer immunotherapy and multidrug resistance.* Drug Resistance Updates, 2023. **66**: p. 100905.

521. Fan, X., et al., *Evaluation of inhibitory effects of flavonoids on breast cancer resistance protein (BCRP): From library screening to biological evaluation to structure-activity relationship.* Toxicology in Vitro, 2019. **61**: p. 104642.

522. Staud, F. and P. Pavek, *Breast cancer resistance protein (BCRP/ABCG2).* The International Journal of Biochemistry & Cell Biology, 2005. **37**(4): p. 720-725.

523. Armento, A., et al., *Molecular mechanisms of glioma cell motility.* Exon Publications, 2017: p. 73-93.

524. Rosén, E., et al., *Inference of glioblastoma migration and proliferation rates using single time-point images.* Communications Biology, 2023. **6**(1): p. 402.

525. Bahar, E. and H. Yoon, *Modeling and Predicting the Cell Migration Properties from Scratch Wound Healing Assay on Cisplatin-Resistant Ovarian Cancer Cell Lines Using Artificial Neural Network.* Healthcare, 2021. **9**(7): p. 911.

526. Singer, E., et al., *Reactive oxygen species-mediated therapeutic response and resistance in glioblastoma.* Cell Death & Disease, 2015. **6**(1): p. e1601-e1601.

527. Filali, I., et al., *Synthesis of New Harmine Isoxazoles and Evaluation of their Potential Anti-Alzheimer, Anti-inflammatory, and Anticancer Activities.* Med Chem, 2016. **12**(2): p. 184-90.

528. Chan, E.W.C. and S.K. Wong, *Phytochemistry and pharmacology of ornamental gingers, Hedychium coronarium and Alpinia purpurata: a review.* Journal of Integrative Medicine, 2015. **13**(6): p. 368-379.

529. Mucha, P., et al., *Cytotoxic effect, generation of reactive oxygen/nitrogen species and electrochemical properties of Cu(ii) complexes in comparison to half-sandwich complexes of Ru(ii) with aminochromone derivatives.* RSC Adv, 2019. **9**(55): p. 31943-31952.

530. Srivastava, P. and D. Panda, *Rotenone inhibits mammalian cell proliferation by inhibiting microtubule assembly through tubulin binding.* The FEBS Journal, 2007. **274**(18): p. 4788-4801.

531. Wudtiwai, B., et al., *Methoxyflavone derivatives modulate the effect of TRAIL-induced apoptosis in human leukemic cell lines.* Journal of Hematology & Oncology, 2011. **4**: p. 1-11.

532. Deng, F., et al., *Novel inhibitors of breast cancer resistance protein (BCRP, ABCG2) among marketed drugs.* European Journal of Pharmaceutical Sciences, 2023. **181**: p. 106362.

533. Pick, A., et al., *Structure–activity relationships of flavonoids as inhibitors of breast cancer resistance protein (BCRP).* Bioorganic & Medicinal Chemistry, 2011. **19**(6): p. 2090-2102.

534. Chen, Z., et al., *Synthesis of 11C-labeled DNA polymerase-β inhibitor 5-methoxyflavone and PET/CT imaging thereof.* Nuclear Medicine and Biology, 2019. **78-79**: p. 17-22.

535. Molnar, J., *In vitro search for synergy between flavonoids and epirubicin on multidrug-resistant cancer cells.* In vivo, 2005. **19**(2): p. 367-374.

536. Dong, K.F., et al., *Mechanism of Astragalus membranaceus in the treatment of laryngeal cancer based on gene co-expression network and molecular docking.* Scientific Reports, 2020. **10**(1): p. 11184.

537. Kanoujia, J., et al., *Recent advances in BCRP-induced breast cancer resistance treatment with marine-based natural products.* IUBMB Life. **n/a**(n/a).

538. Hu, X., et al., *Discovery of β-carboline-(phenylsulfonyl)furoxan hybrids as potential anti-breast cancer agents.* Bioorganic & Medicinal Chemistry Letters, 2021. **40**: p. 127952.

539. Nafie, E., et al., *Harmine inhibits breast cancer cell migration and invasion by inducing the degradation of Twist1.* PLOS ONE, 2021. **16**(2): p. e0247652.

540. Domínguez, C.J., et al., *Acute regulation of apical ABC transporters in the gut. Potential influence on drug bioavailability.* Pharmacological Research, 2021. **163**: p. 105251.

541. Dükel, M., Z. Tavsan, and H.A. Kayali, *Flavonoids regulate cell death-related cellular signaling via ROS in human colon cancer cells.* Process Biochemistry, 2021. **101**: p. 11-25.

542. Tavsan, Z. and H.A. Kayali, *Flavonoids showed anticancer effects on the ovarian cancer cells: Involvement of reactive oxygen species, apoptosis, cell cycle and invasion.* Biomedicine & Pharmacotherapy, 2019. **116**: p. 109004.

543. Li, N., et al., *Mitochondrial Complex I Inhibitor Rotenone Induces Apoptosis through Enhancing Mitochondrial Reactive Oxygen Species Production *.* Journal of Biological Chemistry, 2003. **278**(10): p. 8516-8525.

544. Bastin, J., et al., *Downregulation of mitochondrial complex I induces ROS production in colorectal cancer subtypes that differently controls migration.* Journal of Translational Medicine, 2023. **21**(1): p. 522.

545. McComb, S., et al., *Efficient apoptosis requires feedback amplification of upstream apoptotic signals by effector caspase-3 or -7.* Science Advances, 2019. **5**(7): p. eaau9433.

546. Keller, N., et al., *Caspase-8 function, and phosphorylation, in cell migration.* Seminars in Cell & Developmental Biology, 2018. **82**: p. 105-117.

547. McKenzie, B.A., et al., *Activation of the executioner caspases-3 and -7 promotes microglial pyroptosis in models of multiple sclerosis.* Journal of Neuroinflammation, 2020. **17**(1): p. 253.

548. Vetrivel, P., et al., *Function of flavonoids on different types of programmed cell death and its mechanism: a review.* Journal of Biomedical Research, 2019. **33**(6): p. 363.

549. Li, C., et al., *Anticancer activities of harmine by inducing a pro-death autophagy and apoptosis in human gastric cancer cells.* Phytomedicine, 2017. **28**: p. 10-18.

550. Uhl, K.L., et al., *Harmine, a dual-specificity tyrosine phosphorylation-regulated kinase (DYRK) inhibitor induces caspase-mediated apoptosis in neuroblastoma.* Cancer Cell International, 2018. **18**(1): p. 82.

551. Liu, H., et al., *Harmine hydrochloride inhibits Akt phosphorylation and depletes the pool of cancer stem-like cells of glioblastoma.* Journal of Neuro-Oncology, 2013. **112**(1): p. 39-48.

552. Cao, M.-R., et al., *Harmine induces apoptosis in HepG2 cells via mitochondrial signaling pathway.* Hepatobiliary & Pancreatic Diseases International, 2011. **10**(6): p. 599-604.

553. Kartal, M., M.L. Altun, and S. Kurucu, *HPLC method for the analysis of harmol, harmalol, harmine and harmaline in the seeds of Peganum harmala L.* J Pharm Biomed Anal, 2003. **31**(2): p. 263-9.

554. Mahmood, T. and P.C. Yang, *Western blot: technique, theory, and trouble shooting.* N Am J Med Sci, 2012. **4**(9): p. 429-34.

555. Bagchi, S., et al., *In-vitro blood-brain barrier models for drug screening and permeation studies: an overview.* Drug Design, Development and Therapy, 2019. **13**: p. 3591-3605.

Appendix A

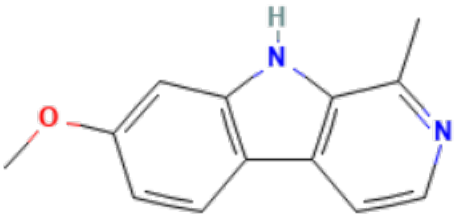

Harmine

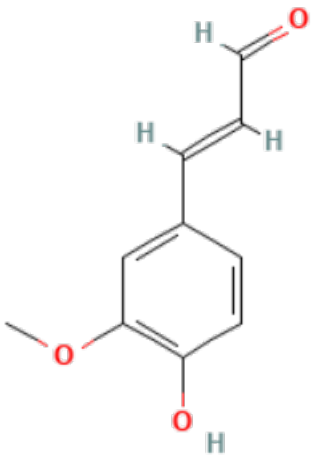

4-Hydroxy-3-methoxycinnamaldehyde

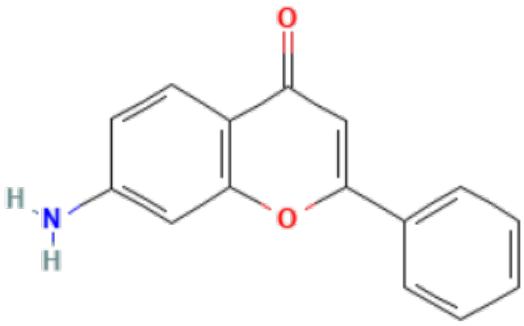

7-Aminoflavone

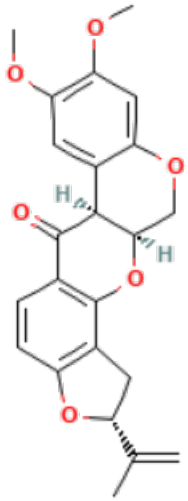

Rotenone

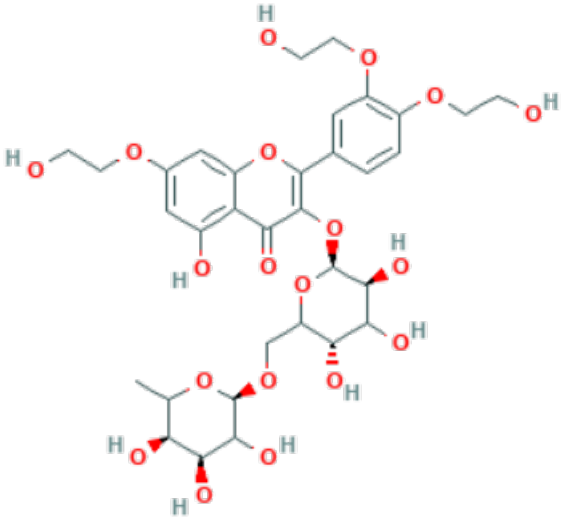

Trihydroxyethylrutin

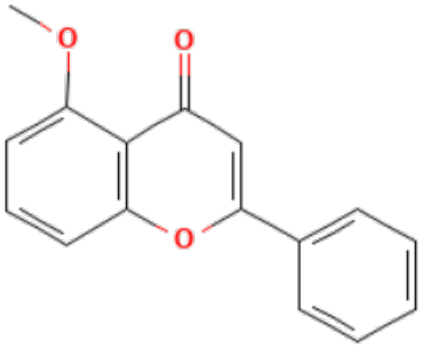

5-Methoxyflavone

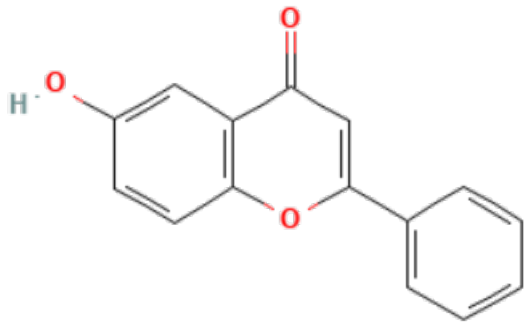

6-Hydroxyflavanone

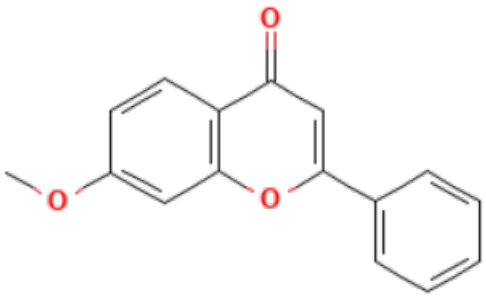

7-Methoxyflavanone

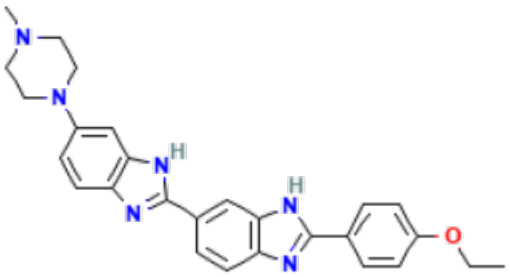

H33342

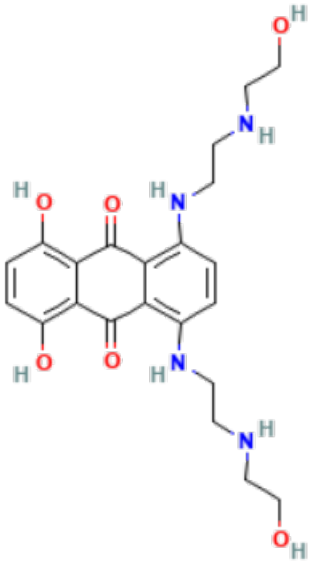

Mitoxantrone